Smart Multifunctional Composite Materials for Improvement of Structural and Non-Structural Properties

Pinto, Fulvio

Award date:
2013

Awarding institution:
University of Bath

Smart Multifunctional composite materials for improvement of structural and non-structural properties

Fulvio Pinto

Thesis submitted as partial fulfilment for
the degree of Doctor of Philosophy

University of Bath

Department of Mechanical Engineering

March 2013

Signature of Author . . . . Fulvio Pinto

.

COPYRIGHT

.

Per aspera ad astra
"To the stars through difficulties"
Lucius Annaeus Seneca, Hercules Furens, act II, v. 437

.

Acknowledgments

First and foremost, I would like to express my sincere gratitude to my supervisor, Dr Michele Meo, for the invaluable guidance and especially patience during my PhD study and research. It is thank to him that I grew as a researcher and a person. I am sure that this project would not have been possible without his support and encouragement.

My sincere thank goes also to all my office mates and the people from the University of Bath that contributed with their expertise and skills to my research. I was lucky to work with such a professional and talented group in these years. In particular, I would like to thank Ettore Barbieri, Umberto Polimeno, Simon Pickering, Tiemen Postma, Francesco Amerini, Stefano Angioni, Amit Visrolia, Gian-Piero Malfense Fierro, Mikael Amura and Diego Colombara.
A special thank goes to Francesco Ciampa, who as a good friend, was always willing to help and give his best suggestions. It would have been a lonely office without him.

I would like to thank my parents, Clara and Fernando, for being a continuous source of inspiration and love. I hope that one day I will succeed to become a great person as they are.

Last but not the least, I dedicate this thesis to the love of my life, Milena, for her unconditional love and support that gave me the strength to overcome the toughest moments. I know, at times, I can be particularly trying. Thank you.

Abstract

The principal aim of this thesis is to analyse the effectiveness of multifunctional smart materials as intelligent structures to improve mechanical properties and activate additional non-structural features. In order to investigate these multiple aspects, a comprehensive literature review has been presented focusing on the state of the art in multifunctional and smart materials. From this analysis, five different systems based on different designing solutions and manufacturing techniques were developed and experimentally validated.

Multiscaled composites are a typical example of multifunctional materials and are based on the addition of engineered nanoscaled reinforcement to traditional mesoscopic systems. To test the effectiveness of nanomodification, an experimental campaign has been carried out, aimed to the characterisation of a nanocomposite obtained embedding Graphene Nanoplatelets (GNPs) in the polymeric structure of Low Density Polyethylene films at difference concentrations. Nanoscaled fillers were subsequently used to manufacture a threephasic multi-scaled composite based on the inclusion of nanometric SiO_2 particles in a traditional carbon fabric/epoxy system.

Following a different approach, hybrid structures with embedded Non-Newtonian fluids have been manufactured and tested and the results showed that nonlinear viscosity can be exploited to dynamically enhance material properties during an impact event.

The possibility to intervene both on structural and non-structural properties has been investigated with another hybrid system, based on the embodiment of Shape memory Alloys (SMA) wires within a traditional unidirectional CFRP. The study of the impact properties pointed out that the superelasticity effect and the hysteretic stress/strain behaviour of the embedded wires reduce the extent of the internal delamination for samples subjected to low velocity impacts. Moreover, by exploiting the SMAs thermo-electrical properties it is possible to use the embedded metallic network as a strain sensor by measuring the electrical resistance variation and as an embedded heat source to be used for rapid thermographic damage location and evaluation.

Table of Contents

Table of Contents vi
Table of Figures ..... *iix*
1 Introduction 1
1.1 Overview 1
1.2 Outline of the Thesis 5
PART I 7
2 Composite materials: an overview 7
2.1 Role of Reinforcement and matrix 8
2.1.1 Role of the reinforcement 9
2.1.2 Role of the matrix 12
2.1.3 Lightness of composite materials 13
2.1.4 Advantages of Composite Materials 13
2.1.5 The dualism between manufacturing and design 15
3 Multifunctional Materials 18
3.1 Intelligence in materials 22
3.1.1 Primitive Intelligence 22
3.1.2 Inherent Intelligence 23
3.1.3 Human mediated intelligence 26
4 Classification of Multifunctional materials 27
4.1 Multi-structural smart materials 29
4.1.1 Zero-dimensional nanocomposites: nanoparticles based systems 32
4.1.2 Bi-dimensional nanocomposites: nanolayers based systems 35
4.1.3 Mono-dimensional nanocomposites: nanotubes and nanowires 36
4.1.4 Strengthening of nanocomposites 40
4.2 Non-structural Smart Materials 42
4.2.1 Thermo-electrical properties 43
4.2.2 Sensing and Actuation 45
4.2.3 Self-Healing Materials 56
4.2.4 Power Harvesting and Storage 58
4.3 Conclusive remarks 60
PART II: 61
Smart Nanocomposite systems for mechanical properties improvement 61

5 Biphasic graphene-based nanocomposite for mechanical properties enhancement 63
5.1 Experimental: Material preparation 65
5.2 Composite mechanical characterization 67
5.2.1 XRD Analysis: 68
5.2.2 Thermal Analysis 70
5.2.3 Dynamic Mechanical Analysis, Frequency Sweep 71
5.2.4 Mechanical Analysis, Tensile Test: 74
5.3 Discussion 82
6 Threephasic SiO_2-based nanocomposite for mechanical properties enhancement 84
6.1 Experimental: Thripasic Nanocomposite Manufacturing 86
6.1.1 Raw materials 86
6.1.2 Impregnation process 89
6.1.3 Analysis of single impregnated fabrics 93
6.1.4 Composite manufacturing 99
6.2 Composite Mechanical Characterisation 104
6.2.1 Three Point Bending Test 104
6.2.2 Tensile Test 108
6.2.3 Dynamic Mechanical Analysis 111
6.2.4 Indentation and Hardness Test 116
6.3 CNT hybridisation of nanoreinforced carbon fabric 118
6.4 Discussion 122
PART III: 125
Smart Multifunctional systems for impact properties enhancement 125
7 Multifunctional composites based on the inclusion of non-Newtonian Fluids for improved impact properties 127
7.1 Theoretical Aspects 128
7.2 Experimental: Solution Preparing 132
7.2.1 Rheological Analysis 133
7.3 Composite Mechanical Characterisation 137
7.3.2 C-Scan Analysis 150
7.3.3 Soundwaves Absorption test 152
7.4 Discussion 154
8 Multifunctional hybrid composites based on the inclusion of Shape Memory Alloys for improved impact properties 156
8.1 SMA-Composites 156
8.1.1 Theoretical Aspects 157
8.2 Experimental: Sample Manufacturing 161

8.3 Composite Mechanical Characterisation 162
8.3.1 Low-velocity impact test 162
8.4 Discussion 172
PART IV: 173
Multifunctional composites for non-structural applications 173
9 Multifunctional hybrid composite based on the inclusion of Shape Memory Alloys for SHM and NDT features 174
9.1 Experimental: SMA samples manufacturing 176
9.2 Strain Sensing Ability of SMA based hybrid composites 179
9.3 Thermographic inspection of SMA based Hybrid Composites 181
9.4 De-Ice feature for SMA-based hybrid Composites 186
9.5 Discussion 190
10 Conclusions 191
10.1 Future Works 193
10.2 PHD Activities 195

Table of Figures

Figure 1 - Original contributions of this research to multifunctional nanoscaled and smart composites 4
Figure 2 - Schematics of composite material components 8
Figure 3 - composite materials reinforcements: a) particles; b) short fibres; c) long fibres 9
Figure 4 - Sequential algorithm of the production procedure for traditional monolithic materials 16
Figure 5 - Sequential algorithm of the production procedure for traditional monolithic materials 16
Figure 6 - Schematics of the comparison between traditional materials and multifunctional smart systems: a) traditional structural and non-structural materials; b) multifunctional material with multistructural properties; b) multifunctional material with non-structural properties. 20
Figure 7 - schematic of Primitive Intelligence for Multifunctional Materials 23
Figure 8 - schematic of Inherent Intelligence for Multifunctional Materials 24
Figure 9 - Categorization of Multifunctional materials 27
Figure 10 - Surface/volume ratio for different kind of nanoreinforcements 31
Figure 11 – TEM images of spherical nanoparticles of silica; image from [20] 33
Figure 12- (left) structure of a phyllosilicate, (right) morphology of nanoclay/polymer composites: (a) conventional state, (b) partially intercalated and exfoliated state, (c) totally intercalated state, (d) totally exfoliated and dispersed state. Image taken from [29] 35
Figure 13 – Schematics of carbon nanotubes from [37]: a) clinographic view of a CNT: each concentric cylinder represents a closed layer of carbon exagons; b) schematics diagram of the helical geometric arrangement of carbon atoms 37
Figure 14 - The surface of a microscscaled carbon fibre, before and after the growth of a CNTs forest; image from [41] 38
Figure 15 - Interlaminar CNTs forest growing process: 1) CNTs are grown on the surface of the cloth; 2) superimposition of several CNTs reinforced layers to create a laminate; 3) creation of a three-dimensional multiscaled composite; image from [44] 39
Figure 16 - Schematics of the Roller techniques employed by Garcia et al. to transfer an aligned forest of CNTs from its original silicon substrate to the surface of a carbon fibre prepreg. Image taken from [45]. 40
Figure 17 - Thermoelectrical behaviour of CNTs: a) Linear behaviour of the percolation threshold of composites obtained by embedding CNTs with increasing aspect ratio and at a certain curl ratio; b) Relationship between conductivity and CNT waviness; images from [53] 43
Figure 18 – Difficulty in the modelling of thermal conductivity for CNTs based composites: a) Enhancement of thermal conductivity for composites with increasing SWCNT content (image from [58]); b) Decreasing of thermal conductivity with increasing SWCNTs content and enhancement with increasing MWCNTs; image from [59]. 45
Figure 19 - Poling mechanisms in piezoelectric materials 47
Figure 20 -Direction of the applied electrical field and displacement for: a) traditional piezoelectric materials with conventional electrodes; b) innovative piezoelectrics with interdigitatated electrodes; image from [74] 48

Figure 21 - Schematics of a Macro-fibre-Composite (MFC) piezoelectric actuator; image from Drossel et al. [77] 49
Figure 22 - Schematics of an Active Fibre Composite; image from Sarangi et al. [80] 50
Figure 23 - "SMART layer" developed by Lin and Chang [85]: a) Schematics of the SMART layer integration within a composite laminate; b) an example of a SMART layer produced during the experimental campaign illustrated in the paper.....51
Figure 24 - Integration of CNT structures for strains and damages locations in layered composites: a) disposition of a squared array (CxR) of CNTs within the laminate stack in order to provide in-plane strains and damage monitoring; b) Perpendicular distribution of short CNTs used as a sensor for out-of-plane monitoring; image from [86]. 52
Figure 25 - Relationship between Strain and Electrical Resistance variation for CNTs reinforced composites: a) experimental results obtained by Myounggu [89] and b) Song[90]. 53
Figure 26 - FBG based composites: a) schematics of the laminated composite beam used by Du et al during their experimental campaign; b) three point bending test setup to measuring the internal strain distribution of the beam; image from [95].....54
Figure 27 - FBG based smart composite structures manufactured by Takeda et al. : a) optical fibres embedded within the composite structure; b)integration of smart sensors within the upper panel of a composite fuselage; images taken from [97].....55
Figure 28 – Self-healing material developed by White and Sottos : a) schematics of the interaction between healing agent and catalyst during the propagation of a crack through an epoxy resin; b) time sequence and SEM image of a destroyed microcapsule during the healing process; images from [100]. 56
Figure 29 - Micrographs of the "bleeding composite" realised by Pang and Bond, based on the inclusion of hollow fibre containing an healing agent; images from [106]. 58
Figure 30 - Layout of the integration process required to embedd a thin-film lithium energy cell within the structure of a traditional composite laminate; image from [111] 60
Figure 31 - Layered structures of graphite. Image taken from [122].....63
Figure 32 - Graphene Nanoplatelets manufacturing process.....65
Figure 33 -a) Schematic of Compression Moulding process; b) Schematic of Blown Extrusion process; c) Schematics of randomly in plane oriented nanoparticles; d) Schematics of three-dimensional nanoparticles.....66
Figure 34 - a) SEM micrograph of the expandable graphite flake (left side) and of expanded graphite filament (right side) ; b) and c) SEM micrographs of GNP after the drying process 67
Figure 35 - XRD of graphite (a), LDPE/GNP composites (b) and effect of GNP concentration (c). Figure (d) represents the typical microstructure of the LDPE/GNP composite.....69
Figure 36 - DSC thermograms and results for LDPE and LDPE/GNP nanocomposites 70
Figure 68 - Argand-Gauss diagram of the Complex Modulus 71
Figure 37 - DMA frequency sweep curves for LDPE/GNP composites: (a) storage modulus, (b) loss modulus, (c) Tan delta 72
Figure 38 - Storage Modulus, Loss Modulus and Tan delta results at 1Hz for LDPE and LDPE/GNP composites.....73

Figure 39 - a) Stress-Strain curves for neat LDPE and composites with increasing content of GNP. The inlet shows the slopes of the curves; b) Relation between Young's modulus increasing and change in fracture mode for LDPE and LDPE/GNP composites; c) LDPE and LD 75
Figure 40 - a) Stress-Strain curves for neat LDPE in blown extrusion process; b) Stress-Strain curves for LDPE/GNP composites in blown extrusion process. The inlets show the slopes of the curves. 77
Figure 41 - Comparison between Stress-Strain curves for LDPE/GNP composites and pure LDPE in transverse direction (a) and machined direction (b); The inlets show the slopes of the curves. 79
Figure 42 - Young's modulus increase for LDPE/GNP in both transverseal and machine direction. 80
Figure 43 - a) Comparison between Halpin-Tsai modulus evaluation model and experimental data for compression moulded LDPE/GNP composites; b) Comparison between Halpin-Tsai modulus evaluation model and experimental data for blown extruded LDPE/GNP composites.....81
Figure 44 - TeXtreme fabric 86
Figure 45 - VTM264 resin film.....87
Figure 46 – TEM image of the silica nanoparticles 88
Figure 47 - Solution preparing flow chart 89
Figure 48 - fabric impregnation flow chart.....90
Figure 49 - Some of the impregnation techniques tested: (a) aerosol, (b) calendering, (c) spray, (d) roll-up 91
Figure 50 - silica percentage versus weight increase 92
Figure 51 - SEM images of neat carbon fabric sample 94
Figure 52 - SEM images of rolled-up sample.....95
Figure 53 - SEM images of fabric treated with SPI technique 96
Figure 54 - agglomerates and nanometric particles on the fibres after impregnation..97
Figure 55 – Silica XRAY mapping for (a) rolled-up sample and (b) pressured sample 98
Figure 56 - Laminates produced for mechanical characterisation 99
Figure 57 – Samples manufacturing procedure: (a) fabric used for laminates manufacturing, (b) resin film cutting 100
Figure 58 - vacuum bagging procedure: peel-ply positioning, perforated release film, breather, bag preparation, bag positioning on the tool, crinkles formation, valves positioning 101
Figure 59 - Samples under vacuum and ready for autoclave curing.....102
Figure 60 – Post-cure inspection: (a) SEM analysis of the triphasic system, (b) and (c) XRAY mapping of silicium and carbon elements 103
Figure 61 - Samples prepared for three point bending test.....104
Figure 62 - Load/displacement curves for NEAT and silica-doped samples 105
Figure 63 - Three Point Bending results: a) Bending modulus for multiscaled composite with increasing nanosilica content; b) modulus enhancement.....107
Figure 64 – Samples prepared for tensile test.....108
Figure 65 - Tabs attached on samples 108
Figure 66 - stress/strain curves for nanosilica reinforced multiscaled samples and traditional laminates 109
Figure 67 –Tensile Test results: a) Young's modulus for multiscaled composite with increasing nanosilica content; b) effect of nanosized filler on the Young's Modulus 110

Figure 69 - DMA test equipment: a) the instrumentation used for the test campaign; b) detail of the experimental setup 111
Figure 70 - DMA analysis: Storage Modulus Behaviour for silica based multiscaled nanocomposites and traditional microscaled laminates 112
Figure 71 - DMA analysis: Tan δ behaviour for silica based multiscaled nanocomposites and traditional microscaled laminates 113
Figure 72 - Tensile Test results: a) Storage Modulus and Tan delta for multiscaled composite with increasing nanosilica content; b) effect of nanosized filler on Storage Modulus and Tan delta 114
Figure 73 - Comparison between experimental results and theoretical model for tan delta depression due to increasing nanofiller content 115
Figure 74 – Storage Modulus behaviour: Comparison between SPI technique and Calendering 116
Figure 75 - a) hardness test sample; b) sample's geometry 117
Figure 76 - Hardness Test Results: a) Indent dimensions variations, b) Vickers number behaviour with increasing concentration of SiO2 nanoparticles 118
Figure 77 - schematics of the reinforcement procedure of a multiscaled hybridised fabric 119
Figure 78 - CVD results on carbon fabric: a) dry unreinforced fabric; b) CNT growing on nanosilica substrate 120
Figure 79 - CNTs growing on SiO2 substrate: 1) closeup on a large agglomerate of silica and on the entangled CNTs forest grown from it. b) Bridging of a CNT from two different silica nanoparticles 120
Figure 80 – STF based Liquid Body Armour produced by the University of Delaware and the US Army Research Laboratory 128
Figure 81 - rheology of non-Newtonian fluids 129
Figure 82 - Schematics of Shear Thinning and Shear Thickening Effect 130
Figure 83 - STF preparation 133
Figure 84 - Rheological analysis for STF at different nanoparticles concentrations: a) STF/10; b) STF/20; c) STF/25; d) comparison between the different curves 135
Figure 85 - viscosity increase with increasing nanoparticles concentration 136
Figure 86 - behaviour of thickening start shear rate with increasing nanoparticles concentration 137
Figure 87 - schematics of STF/CFRP composite preparation 137
Figure 88 - manufacturing procedure of STF/CFRP composite samples 138
Figure 89 – a) schematics of the calendering technique used for complex geometry samples; b) leading edge samples 139
Figure 90 – forced vibration signals for STF and Neat samples 140
Figure 91 - free vibration signals and results for STF and Neat samples 141
Figure 92 - Force Displacement curves from the impact test on 7nm Silica STF reinforced CFRP: a) 6J; 20J: 40J: 142
Figure 93 - Force Displacement curves for 7nm Silica STF reinforced CFRP: a) control sample; b) STF7/10; c)STF7/20; d)STF7/25 143
Figure 94 - Summary of the results for impact on STF7 reinforce samples: a) Force Peak variation at different energies and different silica concentration in STF; b) Energy absorption variation at different energies and different silica concentration in STF 144
Figure 95 - Force Displacement curves from the impact test on 14nm Silica STF reinforced CFRP: a) 6J; 20J: 40J: 146

Figure 96 - Force Displacement curves for 14nm Silica STF reinforced CFRP: a) control sample; b) STF7/15; c)STF7/25;.....146
Figure 97 - Summary of the results for impact on STF14 reinforce samples: a) Force Peak variation at different energies and different silica concentration in STF; b) Energy absorption variation at different energies and different silica concentrations in STF 147
Figure 98 - post impact image of STF reinforced sample in comparison with a traditional CFRP subjected to the same impact; a) Control sample, top surface; b) Control sample, bottom surface; c) STF reinforced CFRP top surface; d) STF reinforced CFRP bottom surface;.....148
Figure 99 - Impact test on leading edge sample: a) failure of the control sample in comparison with the nanoreinforced one; b) samples after the impact.....150
Figure 100 - C-Scan analysis of Impacted STF samples and traditional CFRP 151
Figure 101 - schematics of soundwaves absorption test 152
Figure 102 - sample preparation for sound absorption test 152
Figure 103 - recorded audio signal for different damping media: a) air; b) water; c) STF; d) comparison of the media.....154
Figure 104 - Gibbs energy variation for austenite (A) and martensite (M) phases....158
Figure 105 - lattice configuration for Martensite and Austenite in NiTi SMA 158
Figure 106 - trasformation mechanisms between Austenite and both de-twinned and twinned Martensite 159
Figure 107 - Shape memory effect (T<Mf): a) elastic deformation of twinned martensite; b) de-twinning transformation from multi-variant (twinned) martensite to single-variant (de-twinned) martensite; c) elastic transformation of de-twinned martensite ; d) elastic recovery obtained with the removal of the load; e) shape memory effect obtained applying a thermal loading ΔT, heating up the material to a T>Af 160
Figure 108 - Super-elasticity (T>Af): a) elastic deformation of Austenite; b) transformation from austenite to single-variant (de-twinned) martensite (Stress Induced Martensite); 3) elastic deformation of DTM; 4) elastic recovery after load removal; 5) super-elasticity effect due to the instability of DTM for T>Af.....160
Figure 109 - manufacturing schematic of PPS/CF SMA hybrid composite.....161
Figure 110 - data results for baseline (PPS/CF) samples: a) force displacement behaviour; b) time displacement; c) Energy absorption history 164
Figure 111 - data results for hybrid (PPS/CF+SMA) samples: a) force displacement behaviour; b) time displacement; c) Energy absorption history 165
Figure 112 - Visual inspection of impacted samples: a) PPS/CF unreinforced sample; b) PPS/CF+SMA hybrid sample 166
Figure 113 - C-Scan images for hybrid and unreinforced PPS/CF.....167
Figure 114 - Comparison between PPS/CF and hybrid composite: a) Maximum Force; b) Penetration Depth; c) Energy Absorption; d) Projected damaged Area 168
Figure 115 - variation of the elastic behaviour between PPS/CF unreinforced samples and SMA based hybrid ones 169
Figure 116 - Relationship between extent of the delamination and energy absorptio for PPS/CF and hybrid composites.....171
Figure 117 - Optical microscope image of a single NiTi wire 176
Figure 118 - Stratification layout of sample 1 (4 plies, 1 SMA wire) (a), and finished specimen (b).....177
Figure 119 - Stratification layout of sample 2 (4 plies, SMA network, 1 defect) (a), and finished specimen (b).....177

Figure 120 - Stratification layout of Sample 3 (16 plies, 2 SMA networks, 3 defects) 178
Figure 121 - Sample 3 178
Figure 122 - Single NiTi tensile behaviour: a) experimental setup; b) Stress-Strain behaviour and electrical resistance variation of NiTi wire in tensile mode 179
Figure 123 - SMA based composites Three Point Bending test: a) experimental setup; b) Flexural Load versus Flexural Extension and electrical resistance variation for SMA based composites 180
Figure 124 - Themographic inspection of SMA based composites: a) experimental setup; b) opservation time of the IR camera in the step-heating process 182
Figure 125 - Thermography images for undefective parts of sample 2 at t=3s.....183
Figure 126 - Thermography images for defective parts of sample 2 at t=3s.....183
Figure 127 - Schematics of the heat flow diffusion impeded by the PTFE patch 184
Figure 128 - Apparent temperature variation over time for damaged and undamaged areas.....184
Figure 129 - Thermal image of the apparent temperature for sample A obtained at t=3 sec with double vertically aligned NiTi wires surrounding the PFTE patch.....185
Figure 130 - a) Thermography images for multiple defective parts of Sample 3 2 (sample dimensions - 100x60 mm – are represented with the dashed line) at t=3s; b) Amplitude contrast of apparent temperature variation for PFTE1 (0.575mm) and PFTE3 (1.25)……..187
Figure 131 - Thermography image with a current of 0.5 A (a) and time histories for the “hot” and the “cold” area of the sample (b); SMArt Thermography image with a current of 1 A 188
Figure 132 - SMArt Thermography image with a current of 1 A (c) and time histories for the “hot” and the “cold” area of the sample (d).....189

1 Introduction

1.1 Overview

The rapid diffusion of composite structures during the last thirty years has highlighted the importance of controlling the specific properties of a material by designing its internal structure from the microscopic to the macroscopic scale. Indeed, because of the multiphasic nature of such materials, a complete knowledge of each of their components and their interactions is required in order to design and manufacture tailorable systems able to match costumers' needs.

Moreover, as composite materials were called to face new challenges in terms of structural and specific features requirements, their internal structure has become more and more complex, including additional engineered phases, going from nanoscaled fillers to hybrid materials, passing through nanofluids, metals and three-dimensional reinforcements.

Based on these considerations, Multifunctional composites represent the next generation of engineered materials, being able to change the way in which a structure is perceived and its role in the context of human interaction. However, because of the intrinsic complexity of their internal structures and the multidisciplinarity connected with the use of multiple phases with different chemical, physical, electronic, mechanical and (in some cases) biological properties, an exhaustive dissertation on multifunctional composites is quite complex and requires a certain level of schematisation of the different topics.

Briefly the questions that will be addressed are:

- *Is the inclusion of additional engineered phases within a material able to dynamically affect some specific features so that the composite system can be defined intelligent?*

- *What are the potentialities of such materials in terms of feature enhancement? In what kind of applications can be employed?*

In order to answer these questions, it is necessary to understand the main differences between a traditional composite laminate and these new generation materials. Indeed, although multifunctional materials made their appearance more than 20 years ago, there are only few works in literature that have dealt with the concepts of multifunctionality and intelligence in the context of material science in details. Hence, it is necessary to perform an exhaustive analysis of the state of the art present in literature in order to understand the potentialities of such systems and to obtain a clear picture of the various levels of "intelligence" and innovative features that it is possible to confer to them.

From this analysis, it is possible to identify two macro-categories of multifunctional materials that differ in the nature of their "multifunctionality":

- Multifunctional materials with improved **multistructural features**
- Multifunctional material with **non-structural features**

The first category encompasses all those systems in which the multifunctionality is given by the embodiment of an engineered phase able to enhance specific mechanical properties of the material by enabling additional reinforcement effects or dynamically activate strengthen mechanisms. These materials represent the direct evolution of the traditional microscaled CFRP and are mostly based on embedded nanostructures or hybrid phases. The second group is formed instead by materials that are able to perform actions which are not strictly connected to the load-bearing function typical of traditional materials. Features like Structural Health monitoring ability, self-healing, sensing and actuation are typical examples of characteristics of this class of materials which can also simultaneously present traditional structural properties.

Another possible classification can be made according to the nature of the additional phase included within the composite structure, so that it is possible to identify two different classes of multifunctional materials:

- **Nanoreinforced composites**: systems which are based on the embodiment of nanoscaled fillers. Nanomodification represents a reliable and solid procedure to manufacture next-gen composites because of the small quantities required to enhance several mechanical properties and modify thermo-electrical behaviour. Nanoscaled reinforcement can be under form of nanoparticles, nanoplatelets or nanotubes and are usually employed to reinforce both thermoset and thermoplastic polymers. More complex systems can be obtained by using the nanoreinforced polymers as matrices to manufacture multiscaled composites. These systems are characterised by improved properties generated from the superimposition of the nanoeffects given by the nanofillers and the traditional effects of the traditional micro-sized long fibres.

- **Hybrid composites**: these systems are manufactured including particular engineered phases within the traditional composite structure. By exploiting specific properties of such components it is possible to enable extra reinforcement mechanisms or activate non-structural features. Typical examples of hybridised components are metals, nanofluids, through-the-thickness reinforcements, optical fibres and piezoelectric materials.

Based on these considerations, is it possible to analyse these different aspects of multifunctional materials with an experimental campaign on both nanoscaled and hybridised composite aimed to the design and characterisation of five different smart engineered systems, illustrating their advantages, disadvantages and potential applications as illustrated in Figure 1.

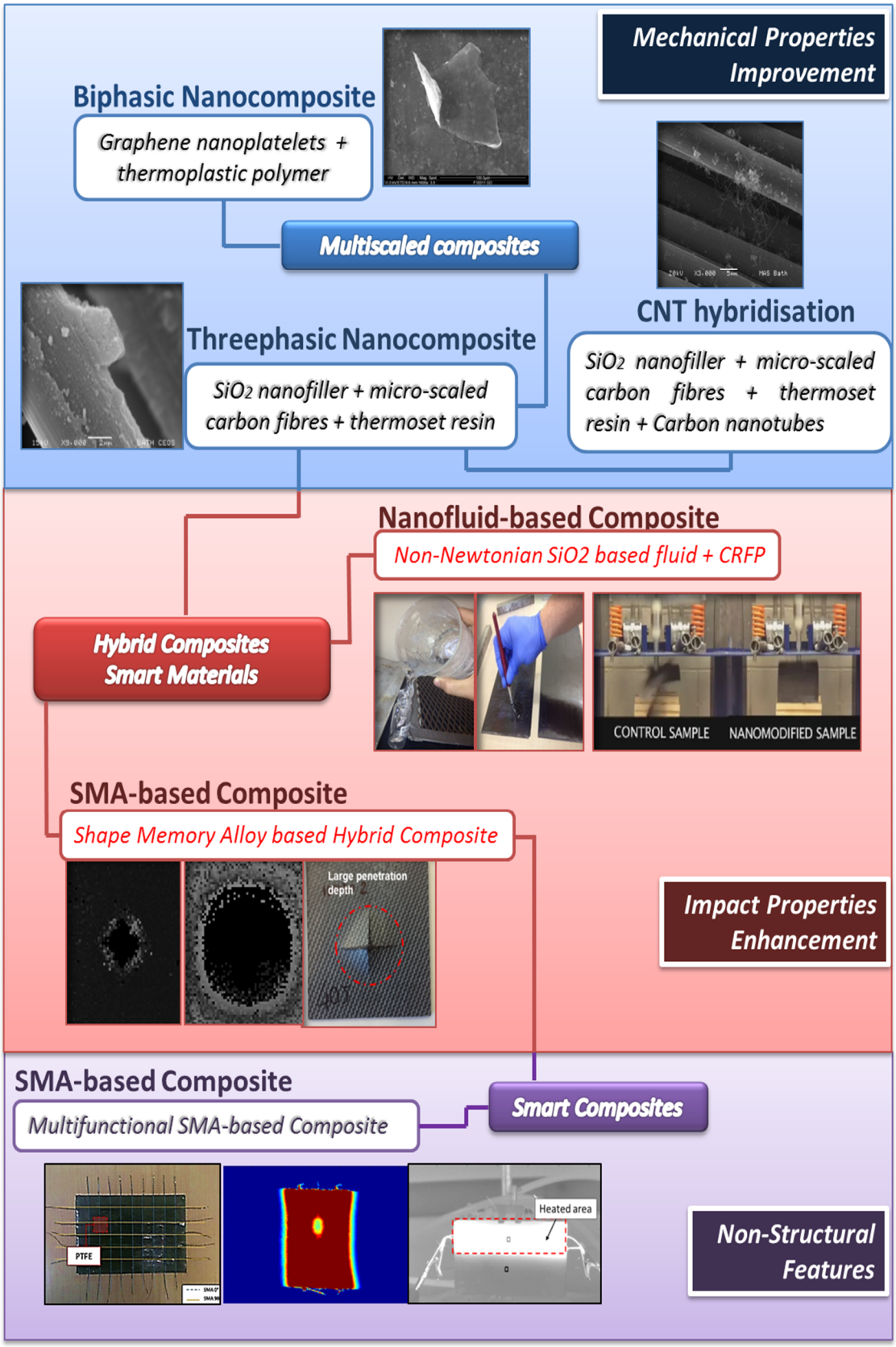

Figure 1 - Original contributions of this research to multifunctional nanoscaled and smart composites

1.2 Outline of the Thesis

The present study is focused on the analysis of the feasibility of smart multifunctional composites for structural and non-structural applications and their advantages in comparison with traditional composite laminates. The work can be briefly summarised in four main parts. The first part constitutes the preface of the research and it consists in a brief introduction on composite materials and their characteristics (Section 2), followed by a definition of structural and non-structural properties and by an exhaustive analysis of the concept of multifunctionality and intelligence in composite systems (Section 3). Section 4 illustrates what schematised in the previous section, containing an extensive and complete literature review on the most important experimental findings of the last twenty years in the field of multifunctional composites.

Part II is focused on the analysis of two different multifunctional systems, based on the inclusion of nanoscaled phases within their structures in order to improve specific mechanical properties such as stiffness and hardness. In particular, Section 5 is aimed to the complete thermo-mechanical characterisation of a nanoreinforced system obtained embedding Graphene Nano-Platelets within a thermoplastic matrix in order to measure the effect given by small amounts of nanofiller on the mechanical behaviour of thin composite nanofilms. Based on the results obtained, Section 6 analyses a more complex system in which silica nanoparticles are used to modify a traditional carbon fibres fabric to manufacture a three-phasic composite. The enhanced mechanical properties of this multiscaled structure arise from the superimposition of the microscaled reinforcement and the nanoeffects given by the nanoparticles and are investigated with a comprehensive experimental campaign.

The use of hybrid components in multifunctional composites is the main focus of Part III, which investigates the enhancement of impact properties that it is possible to achieve by exploiting dynamic properties of additional phases embedded within a traditional laminate structure. Indeed, starting from the findings of previous paragraph, Section 7 illustrates how modifying the manufacturing process of section

6.1.2 it is possible to use silica nanoparticles to realise a Non-Newtonian fluid that can be subsequently included in the laying-up sequence to form a smart composite that can actively reacts to external loads. Results from an experimental campaign demonstrate that by exploiting the nanofluid nonlinear viscosity, the material is able to respond dynamically to collisions with foreign objects, showing improved impact resistance and damping rate. A second smart system based on a similar approach is described in Section 8, which investigates the possibility to employ a different engineered phase as additional hybrid reinforcement within composite laminates. Samples obtained by embedding a network of Shape Memory Alloys wires in the stacking sequence of a traditional CFRP were subjected to low velocity impacts and the impact damages were observed via C-Scan analysis. Results showed that the superelastic behaviour of shape memory alloys can be used to increase the energy absorption rate of hybridised laminates during the impact, reducing the extent of the internal delamination.

SMA based composites can be also used to enable additional non-structural features in a composite systems, as it is illustrated in Part IV. Indeed, by exploiting the reciprocal correlation between internal resistance variation and mechanical strain, it is possible to manufacture SMA-based composites able to monitor their internal strain distribution (Section 9.2). Moreover, the same integrated SMA network can be employed as an internal heat source for thermographic analyses giving the possibility to immediately detect the presence of small internal damages by heating the sample via Joule effect and measuring the differences in the apparent temperature variation on the surface (Section 9.3). In addition, it is possible to use the wire network to increase the temperature of composite parts to avoid ice agglomeration or melt dangerous iced layers on wings or other sensible aerostructures components. Because of the low thermal diffusivity of the resin, it is possible to have a selective control of the temperature gradient, heating-up only specific areas of the part (9.4).

PART I

2 Composite materials: an overview

Going back through history it is possible to notice that every major technical and scientific revolution has been accompanied by radical transformations in the field of material science. Indeed, this had been a driving force since the innovation of smelting and casting metals in the Bronze Age, that represented a turning point in the development of human society, which for the first time was able to produce something “engineered” to be used to simplify everyday tasks such as hoes and spades (but also daggers and swords) instead of being limited by which stones could be found in the surrounding area and what could be traded. From there, the evolution of materials and manufacturing techniques has been exponential not only in terms of technical knowledge but also in terms of the understanding of the requirements needed by a material to solve certain problems, leading to the formulation of well-defined criteria for the range of applications available for every material.

The Information Technology Age started at the half of nineteenth century has not left material science untouched, although at a first analysis it could seem that the major progresses have been achieved in completely different fields such as communications and design. Indeed, there is no need to be an expert to understand that the advantages of high-tech turbines or innovative smartphone designs are completely useless without a properly engineered material able to withstand service loads and structural solicitations during the entire lifespan of the product.

On these bases, composite technology currently plays an important role in modern engineering, replacing the traditional metallic materials in several industrial applications such as aerospace, automotive and marine sector to enhance mechanical properties and reduce structural weight. The particular advantage of this kind of material is related to the possibility to “tailor” the properties of a specific part to the needs of different customers, leading to a material which is designed and

manufactured specifically for that application and avoiding the problem of "over-design".

Basically a composite can be defined as a material obtained by the combination of two or more components that differ in form or composition on a macroscopic scale and are characterised by complementary properties. The main difference with a traditional alloy is that in case of composites each constituent does not dissolve or merge completely into another phase, retaining its identity and resulting in a material characterised by better properties than the ones of the single components considered separately.

Going more in depth in this definition, a particular role among the large "composite materials" group is played by fibrous composite materials which are characterised by having a very thin and sharp macroscopic interphase between the different components of which they are made of (matrix and reinforcement), that actually acts as another phase within the material, characterised by its own properties.

2.1 Role of Reinforcement and matrix

As we mentioned earlier, structural composites are bi-phasic systems based on the multiple presence of a mainly fibrous reinforcement and a matrix in which the first behaves as the source for key structural properties while the latter serves as binder to shape the material structural identity.

In order to analyse more in depth their unique mechanical properties and fully understand where these properties come from it is important to focus our attention on the role played by each of these components within the composite structure and how they act both as a single phase and a complex system.

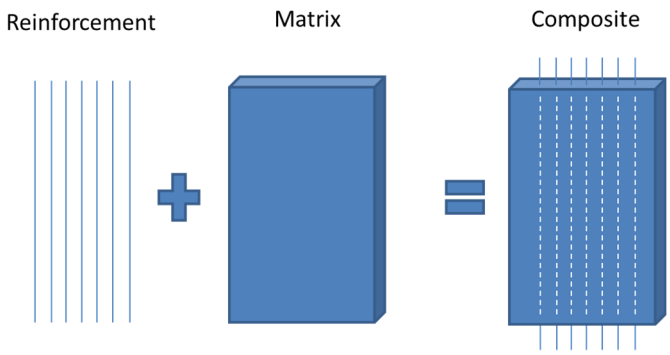

Figure 2 - Schematics of composite material components

2.1.1 Role of the reinforcement

We can define the reinforcement (or charge) as a dispersed discontinuous phase, which is embedded using a large number of techniques within the matrix.

Its functions can be summarised as follows:

- Carry the loads. In a structural composite a percentage between 70 and 90% of the loads is carried by the internal fibres
- Provide strength, stiffness, thermal stability and all the other structural properties of the composite
- Define the thermo-electrical behaviour of the material according to the typology of fibre used thus acting as a conductor or an insulator

The most common materials used as reinforcement are:

- Glass fibres
- Carbon fibres
- Ceramic fibres
- Aramid fibres (e.g. Kevlar)
- Mineral fibres (e.g. basalt)

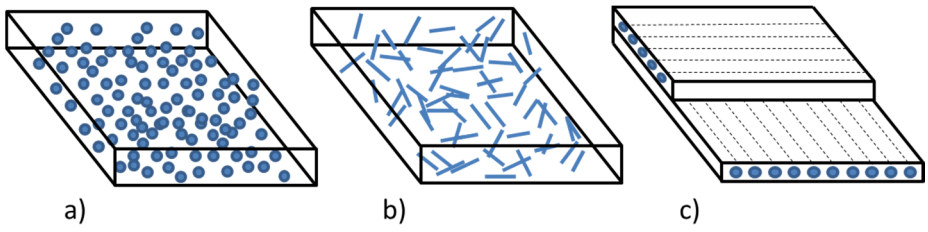

Figure 3 - composite materials reinforcements: a) particles; b) short fibres; c) long fibres

Following a different approach it is possible to categorise the different kinds of reinforcement according to their geometry:

- **Particles based composites**, such as alumina. The effectiveness of such reinforcements depends strongly on the properties of the components. Ductile particles characterised by good resilience are usually employed when the matrix is brittle in order to reach higher levels of resistance and increase the deformability of the material. On the other side, when the matrix is ductile, the reinforcements used are generally particles characterised by high levels of stiffness and strength in order to enhance resistance without affecting the toughness of the final composite. This is the case of alumina based composite in which stiff particles of aluminium oxide (Al_2O_3) are embedded in an aluminium matrix.

  This kind of composites can present a very broad range of properties according to the relative percentage of matrix and reinforcement and shows typically an isotropic behaviour.

- **Fibres based composites**, such as carbon fibres reinforced polymers (*CFRP*). They are widely used because of their good properties, in particular because of their high resistance and low weight. The main advantages of this kind of materials are the overall improved mechanical properties rising from the presence of the fibres within the matrix. Indeed, a large number of materials normally considered brittle and quite weak, present a very good set of mechanical properties when they are machined in a fibre form. Glass for example has a reported strength of 170 MPa when it is in its bulk form, but it can reach more than 3500 MPa for fibres with a diameter less of 100 μm. Same behaviour can be observed for other traditional fibrous reinforcement such as graphite and carbon. In particular, in carbon fibres, atoms are bonded together to form an aligned structure of microscopic crystals which is responsible for their high mechanical properties.

  However, while the reaction to a tensile load for fibrous composites is usually very good in terms of tensile strength and elasticity, they show a very weak behaviour when subjected to a compressive load so that they need to be embedded in a matrix. Indeed, the presence of the matrix guarantees a uniform loads distribution and protects the fibres from aggressive environments.

According to their dimensions, fibres can be catalogued as:

- *Short fibres.* Characterised by diameter of 1-10 μm and by a length-to-diameter ratio of 10-100, they can be oriented or randomly distributed within the matrix. As for the particles based composites, a random distribution of the reinforcement usually leads to isotropic materials, while when the fibres are oriented in a specific direction they present anisotropic or orthotropic behaviour.

- *Long oriented fibres.* This kind of material is characterised by having very good mechanical properties in the direction of the fibres but weak ones in the other directions where the matrix is the dominant constituent. A typical example is wood in which the cellulose fibres are embedded in the lignin matrix guaranteeing an excellent withstanding of loads in the fibres direction. Long fibres based composite are usually manufactured coupling fibres with very high strength such as glass, carbon or aramid polymers (e.g. Kevlar) with resins characterised by good ductility and lightness (1/4 of the volumetric mass of steel).

- *Laminates.* Since the presence of long fibres leads to high anisotropy, usually long fibres reinforced composite laminae are combined together to obtain a laminate in which each layer is characterised by a particular fibres orientation, resulting in a material with similar properties in different directions.
  One of the most common problems of these materials is delamination, that is the separation of one or more layers that can be compared with a punctual defect (or a microscopic crack) that propagates through a particular direction within the material. The fracture can move forward between two layers leading to their separation or perpendicularly to the fibres: the result depends on the behaviour of the fibre that can be pulled out from the matrix or can maintain its integrity keeping the two parts together, in case the crack propagates towards the interphase between the two components.

- *Sandwich*. They are obtained interposing a honeycomb-like structure or a rigid sponge between several layers of fibrous laminae, to obtain a good compensation of stiffness.

2.1.2 Role of the matrix

The matrix is a homogenous phase that plays a fundamental role within the composite carrying out several functions, which are vital for a good performance of the structure itself.

The most important functions provided can be summarised as follows:

- Keep the fibres together and provide a good transfer of the loads
- Provide stiffness and defining the shape of the structure
- Isolate the reinforcement so that each fibre can act independently in presence of a delamination or a crack
- Define the superficial roughness of the part
- Protect the reinforcement from chemical attacks and mechanical damages

Fracture methods of composites are strongly dependent on the chemical nature of the matrix so as its compatibility with the other components that form the structure.

As for the material used, matrices are usually based on polymer materials as they guarantee low density and good resilience, although their properties can be seriously affected by temperature. However, according to the requirements of the final product, a large number of materials can be used as a matrix for composites manufacturing:

- *Polymeric materials* (thermoplastic polymers such as Nylon or ABS, thermoset polymers such as Epoxy resins, polyester resins)
- *Metals* (typically aluminium, titanium and their alloys)
- *Ceramics* (usually silica carbide or alumina)

2.1.3 Lightness of composite materials

Composite materials have several advantages over metals in terms of mechanical properties in relations with their weight. This can be easily observed from the equation below, which represents the axial deformation *u* of a prismatic beam subjected to an axial load P:

$$u = \frac{PL}{AE} \ ,$$

Where L is the length of the beam, A is the cross sectional area and E is the Young's Modulus. Knowing that the mass *m* of the beam can be expressed as $m = \rho AL$, where ρ represents the density of the beam, it is possible to rewrite the expression as:

$$m = \frac{PL^2}{u} \frac{1}{E/\rho}$$

From this equation it is possible to observe that for a given deflection under a specific load, the beam characterised by the higher value of E/ρ ratio will be lighter (therefore more performant).

To measure the advantage in terms of mechanical properties we need to take in account two different parameters:

- The E/ρ ratio (defined as *specific modulus*)
- The ratio σ_{ult}/ρ between strength and density of the material (defined as *specific strength*)

The big advantage in the use of composite materials lays in the high value of both this ratios. For example, the strength of a carbon fibres/epoxy composite can be the same of steel but the specific strength of the first one is almost three times higher.

2.1.4 Advantages of Composite Materials

During the last three decades there has been an increasing use of composite structural parts in all those applications where weight is an issue and that require high performance parts.

Going into more depth, there are several advantages connected with the usage of composite materials that can be summarised as follows:

- *Lightness*. As we have explained in the previous paragraph, it is possible to manufacture composite parts with mechanical properties similar to the ones of metals (in terms of strength and stiffness) but with a reduced weight. This leads to a reduction in the fuel costs and in the emission of CO_2.

- *Fatigue*. Composites are characterised by high levels of fatigue strength. In comparison, traditional metals such as steel or aluminium alloys exhibit a level of fatigue strength around 50% of their static strength, while for composites this percentage reaches more than 90%.

- *Corrosion resistance*. Corrosion happens in traditional metals when they interact with water or air, therefore for certain applications there is the need for special coatings that can affect other mechanical properties. Since the external surface of a composite is generally polymeric, the resistance to chemical attacks of these materials is very high.

- *Design flexibility*. Since the volumetric thermal expansion coefficient of composite material is much lower than metals, it is possible to realise structures with higher levels of dimensional stability. In other words, composite parts are able to retain their shapes when exposed to thermal gradients, variations of pressure and moisture modifications. Moreover, complex parts with large curvatures can be manufactured with composite materials without using any welding, increasing process effectiveness and feasibility.

- *Multi-functionality*. The control on all the components that form the structure of a composite, gives the possibility to add different capabilities (structural or non-structural) to the material. Mechanical, thermal and electrical properties can be modified and enhanced by adding particular chemical entities that affect the behaviour of the material or completely new functions can be activated embedding additional phases, leading to the so called

"multifunctional material", which are the main topic of this work and will be explained more in detail in the next Sections.

2.1.5 The dualism between manufacturing and design

The first step of the production process for traditional parts made with monolithic metals such as aluminium alloys is the selection of the material, which is chosen from a design handbook depending on the properties required for the specific application. Afterwards, it is possible to identify the correct manufacturing technique based upon the selected material, in order to optimise the entire process and fabricate the final structure. In contrast, the use of composite materials for structural parts requires that the entire fabrication process have to be revised and innovated, leading to a more complex system in which the selection of the materials (and subsequently of their microstructures) and the identification of the manufacturing technique are two steps of the production procedure that cannot be taken separately but merge together into a continuum integrated philosophy. This difference rises because the mechanical properties of a composite material are strictly connected with its micro-structure which is determined by the manufacturing process. In other words, while for traditional monolithic parts, the selection of the manufacturing technique can affect only some of the material characteristics (elasticity, stiffness, etc…), the mechanical properties of composite materials are determined by specific factors such as fibres/matrix ratio, spatial distribution and orientation of the fibres within each ply, lamination sequence and other properties which are all a direct consequence of the manufacturing technique. Moreover, the manufacturing process imposes also several conditions for the shapes of the parts to be produced, defining geometry criteria and constrains that have to be taken in account during the production process.

Figure 4 illustrates the fabrication algorithm for a traditional mechanical part made with aluminium alloys. As it is possible to observe, in this case Design and Manufacturing represent two distinct phases of the production procedure, which are sequentially organised in a cascade arrangement.

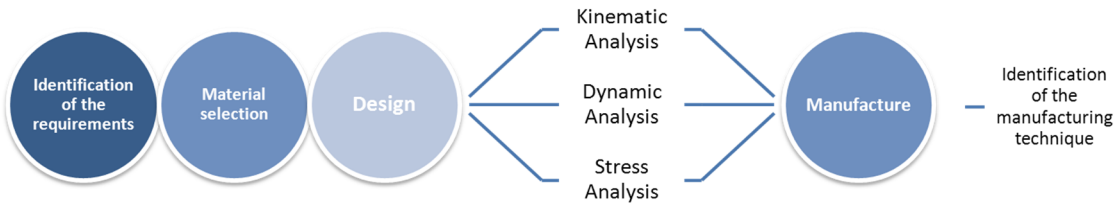

Figure 4 - Sequential algorithm of the production procedure for traditional monolithic materials

The Design step comprises different sub-steps that provide several information and specifications required for the correct fabrication of the part. In particular via the Kinematic and Dynamic analyses it is possible to evaluate velocities, accelerations and forces of the system, while the Stress Analysis provides the stress-strain behaviour of the structure and the time-dependent deformation field.

The following step is the identification of the manufacturing technique required to fabricate the final product. Of course also for traditional monolithic parts the selection of the manufacturing process will imply a modification of some material properties , such as the dimension of the grain structure for a metal during a casting process, but these modifications can be controlled and do not change the intrinsic nature of the material.

The fabrication algorithm of a composite part is represented in Figure 5 and clearly shows the differences with a traditional monolithic part production process.

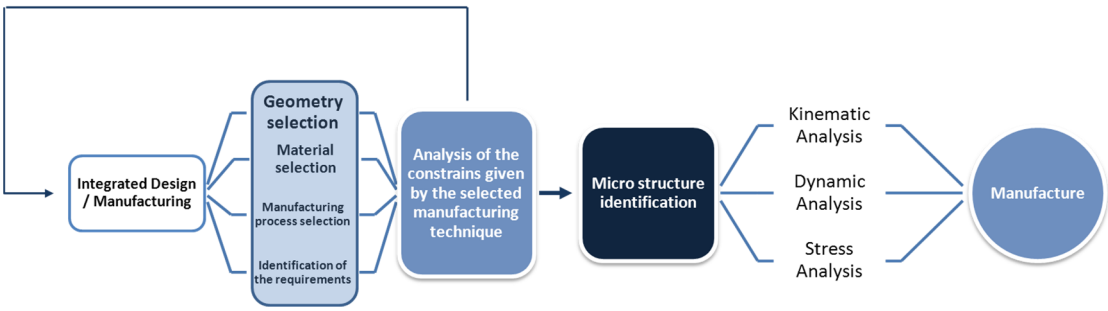

Figure 5 - Sequential algorithm of the production procedure for composite materials

In this case, Design and Manufacturing steps are integrated into an inextricably continuous process which comprises the geometry selection, the manufacturing process selection and the identification of the material, which are all based upon the

requirements needed for the final structure. At the end of this step, a comparative analysis is made between the material requirements and the constraints given by the chosen manufacturing technique and the geometries available, leading to the identification of the composite microstructure that can be used in the analytic phase.

A typical example is whether or not using continuous fibres for the realisation of a composite structure. As we have said earlier in this paragraph, the length of the fibrous reinforcement strongly determines the mechanical behaviour of the final part, affecting the loads distribution on the part itself and its final properties. Available manufacturing techniques will be different depending of the kind of fibrous reinforcement required. Indeed, while lamination or compression moulding are appropriate processes for discontinuous fibres, continuous fibres require completely different techniques such as pultrusion, filament winding or 3D preform layup. As a consequence, the final shape of the part will be determined (e.g. filament winding can produce only parts with cylindrical symmetry or compression moulding cannot produce hollow structures or parts characterised by obtuse angles) and this choice will lead to specific anisotropies (*aleotropies* or *orthotropies*) that will impart particular mechanical properties to the final composite product.

3 Multifunctional Materials

As we have said in the previous Section, the evolution of humankind has always been accompanied by important revolutions in the field of material science. Through the ages such revolutions led to new materials and new manufacturing techniques, with the primary objective of exploiting their mechanical properties in load bearing applications. Materials whose main function is to withstand particular loads and solicitations can be labelled as "structural materials" and they are generally characterised by high mechanical strength, good fatigue resistance, high thermal stability and very low chemical interactions with the environment.

Next to the structural ones, the last two centuries have seen the dawn of another category of materials which have played, and still plays, a significant role in the most important technical and scientific achievements. This new class of materials, named "*non-structural*", gather all those materials which are employed not for their structural properties but to exploit some particular characteristics that make them able to interact with the environment following different approaches rather than the typical load-bearing aspect. A good example to better understand the difference between "*structural*" and "*non-structural*" materials is silicon and its compounds. Silicon is the second most abundant element in the Earth's crust [1] and it can be found mainly in form of silicon dioxide or silicates. Through the centuries, these compounds have been used as a structural material to manufacture ceramic bricks, Portland cement, concrete and porcelain, however silicon in its amorphous form has played an important role in the technical progresses of the last two hundreds as a non-structural material. Indeed this material, obtained in its amorphous form by Berzelius in 1824 reducing potassium fluorosilicate with metallic potassium [2] has become the protagonist of the electronic and digital revolution of the twentieth century because of its electrical properties rather than mechanical ones and it is nowadays used to produce wafer in semiconductor industry, transistor, solar cells and detector.

Another typical examples of non-structural material are piezoelectric materials, discovered by the Curie brothers in 1880 and characterised by the unique property of being able to accumulate electrical charges within their structure as a response to an

applied mechanical stress [3]. These materials are currently employed in several applications such as energy transformer, sensor, actuator and for energy harvesting purposes.

Based on these considerations, the interest of researchers in the last twenty years has been aimed towards the design and manufacturing of a new generation of engineered materials, characterised by a complex interaction of different properties and features, named “multifunctional materials”. These systems, also known as “smart materials”, are by definition composites characterised by the distinctive feature of being able to detect environmental changes or external stimuli at the most optimum conditions and actively respond according to these modifications. This dynamic response rises from the embodiment of engineered phases that can activate specific mechanisms that can enhance mechanical behaviour of the material, leading to multistructural composites, or enable completely new functions to develop materials with innovative non-structural properties.

The evolution of these materials is oriented towards the creation of smart systems which have functions and capabilities far beyond the traditional structural materials and it is driven by the important concept of “environmental awareness”, that is the analysis of a material not as a single entity but as a multifunctional structure within a complex entity, investigating its relationships with the environment and the mutual reciprocity in terms of information and functions exchanged between the different phases that form its structure. Indeed, the main difference between a traditional material and a new-generation smart system can be observed in Figure 6.

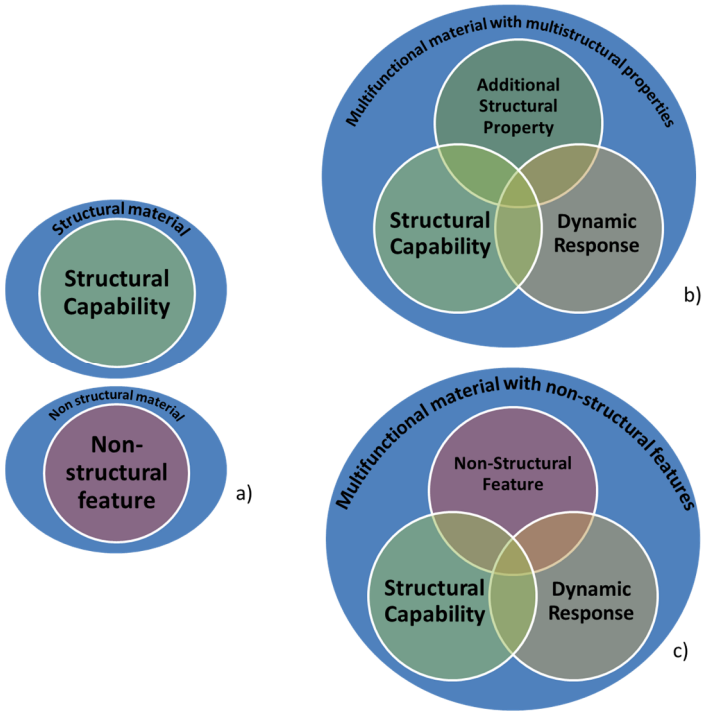

Figure 6 - Comparison between traditional materials and multifunctional smart systems: a) traditional structural and non-structural materials; b) multifunctional material with multistructural properties; c) multifunctional material with non-structural properties.

A traditional material, whether structural or non-structural, is characterised by its own properties and features which determine its field of application, its advantages and disadvantages. However, the role played by these materials within the environment is passive, as they are not able to "sense" what is around them and actively respond to stimuli or specific solicitations. A smart material on the other side is characterised by the presence of a particular ability, the "environmental interaction", which consists in a certain level of "awareness" of the material itself. Because of this peculiarity, the material is able to receive specific inputs from the outside and actively respond enabling particular structural properties or non-structural features that were latent until that moment. It is important to underline that this "awareness" is not strictly connected to the inclusion of electronic devices within the structure, although sensors embedded smart material are an important category of multifunctional composites, but it can be fulfilled also activating particular chemical reactions or embedding specific components characterised by their own structural and non-structural properties that are activated only in particular loading conditions or as a response to particular environmental changes. In other words, the concept of "intelligence" for a material is

strongly connected to the ability to activate an exchange of information with the external environment, enabling new capabilities and mechanisms to enhance the performance (structural or not) of the material itself.

A further evolution of this kind of materials requires the incorporation of at least one of the following features:

- *Sensing*. The presence of sensors embedded within the material volume or coated on the surfaces allows the material to measure the intensity of an external stimulus. Basically a sensor is a convertor able to measure physical quantities and convert the reading into a signal that can be analysed and checked by instrumentations. The information collected by such a device can be used for monitoring some specific quantities (such as strain, temperature, pressure, acceleration, etc…) or as a trigger to execute specific actions in the smart system. It is important to underline that a sensing device is not necessarily a piece of electronic equipment. Indeed, as it will be explained more in depth in the next Sections, the environmental awareness can be fulfilled also by embedding new phases within the material structure, able to respond to particular external stimuli activating new mechanisms or features.

- *Actuation*. An actuator is an electrical, hydraulic or pneumatic motion device that has the main function of giving the needed force to perform actions such as moving or excite other specific devices. Generally it is activated by an external stimulus (such as electricity) and as for sensors it can be embedded within the volume or coated on its surface.

Because of the intrinsic complexity of these systems, their realisation requires the integration of several scientific and technological competences, aiming to the definition of a new generation of materials intended for aeronautics, aerospace, and all the others industrial fields that require intelligent functions such as dynamic shock absorption, smart shape control, self-diagnosis and monitoring.

3.1 Intelligence in materials

In order to better define the smart behaviour of this new generation of smart multifunctional materials, researchers tend to take biological system as a reference. Based on these premises, in a work made in 1990 based on the study of the members of the "*Materials Technology Committee and Subcommittee in the Council for Aeronautics, Electronics and Other Advanced Technology"*, T. Takagi identified three different categories of material intelligence that can be grouped as[4]:

- *primitive intelligence*
- *inherent intelligence*
- *human mediated intelligence*

3.1.1 Primitive Intelligence

Primitive intelligence is represented by those intrinsic properties which characterise every component of a multifunctional system and constitute the bases on which the multifunctionality can be built. As it is possible to observe from Figure 7, primitive intelligence is hierarchically structured on two levels. At the first level there are three different main features (or capabilities) which illustrate the behaviour of the material. Basically, in order to be considered "smart" a system needs to have the ability to sense the external environment (or its own internal status) via specific sensors able to detect and monitor particular characteristics (sensing feature), then, using the information collected it can respond with an appropriate action (actuation feature). These operations can require the assistance of a Processing unit which coordinates the multiple functions and evaluate the correct response of the material.

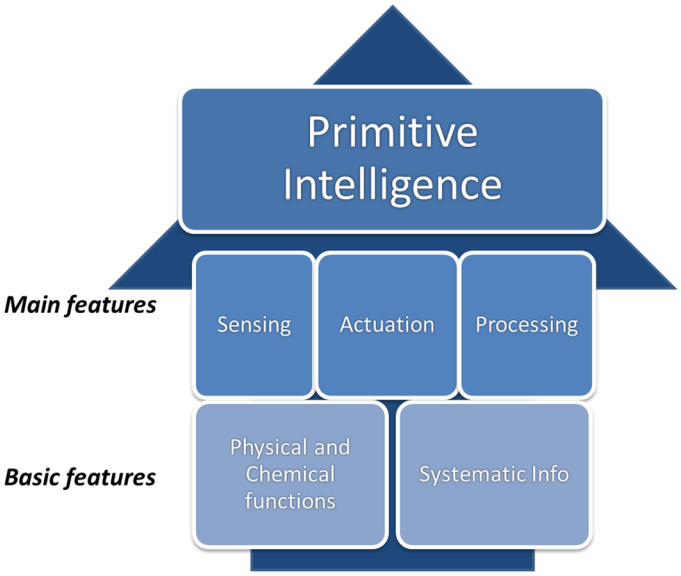

Figure 7 - schematic of Primitive Intelligence for Multifunctional Materials

Moving one level down it is possible to find the basic features, which represent the functions that are essential for a system in order to operate correctly in an active environment. Indeed, it is necessary a complete knowledge of the physical and chemical structure of the material in order to understand what are the mechanisms behind the main functions and correctly analyse the results before activating the appropriate actuation function. Moreover, there has to be a correct systematic information flow in order to orchestrate main features such as sensing, actuation and processing.

3.1.2 Inherent Intelligence

This category is probably the most important one in the analysis of the behaviour of smart multifunctional materials and it encompasses those functions and mechanisms that constitute the intelligence of the material [5]. Indeed, rather than being mediated by human interaction, inherent intelligence is represented by those features, which are based on the superimposition of all the intrinsic properties that are part of the Primitive Intelligence. As said earlier in this chapter, the correlation with biological systems comes in handy in the analysis of multifunctional materials. In this case the inherent intelligence can be related to two specific biological functions: homeostasis and time-dependency. Homeostasis can be defined as the tendency of a system to

maintain a stable and relatively constant equilibrium of interdependent properties [6] and it is easily understandable why it is a vital function for smart materials. Indeed, the ability of keeping its properties constant after severe environmental modifications or internal shocks is a key point for any multifunctional material as it leads to an extension of its service-life.

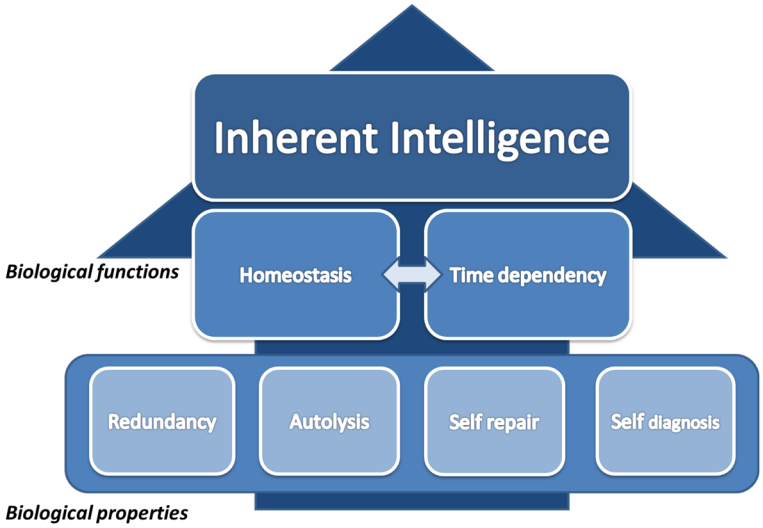

Figure 8 - schematic of Inherent Intelligence for Multifunctional Materials

Another crucial function which is strictly connected with the homeostasis is time-dependency. As said previously, the primitive functions of a smart system are basically expressed by the combination of sensors and actuators, coordinated by a processor. However, the time frame in which the system responds to an external stimulus plays an important role in the global behaviour of the material, especially when the external stimulus is a dynamic event such as an impact with foreign objects or a thermal shock. In these cases the functions that the materials must enable in order to maintain its integrity (structural and non-structural) have to be activated in a certain amount of time that is determined by a combination between sensing and actuating functions.

Going deeper in this analysis, it is possible to derive several properties which are positioned on a second level in the hierarchical scheme shown in Figure 8. These properties represent the core functions of multifunctional materials and the most important and interesting can be briefly summarised as follow:

- *Redundancy*. Biological systems are usually characterised by a certain degree of redundancy in their functions in order to activate alternative mechanisms to maintain equilibrium and extend their lifespan in critical situations. The study made by Keller and de Castro [7] represents an example of structural redundancy in multifunctional fibres reinforced polymer (FRP) beam structures. Indeed, the presence of a system of flexible bolted joints composed of high non-linear adhesives enhance structure ductility and provides alternative load paths to withstand loads in case of unexpected failures.

- *Autolysis*. A typical function of biological system is their ability to self-decompose once they are no longer needed and be reabsorbed by the environment. Several smart materials are able to mimic this capability, leading to multifunctional systems characterised by high levels of biocompatibility, usually employed in biomedical applications such as tissue engineering and regenerative medicine [8-10]. Scaffolds are smart porous systems employed in the field of biotechnology that serve as a substrate for cells seeding and as a physical support during the tissue growth. A fundamental requirement for these materials is that they must ensure total biocompatibility with the human body during the healing process, therefore intelligent material such as Poly L lactic acid (PLLA) [11], able to balance their absorption rate with the tissue growth, have been studied and developed.

- *Self-repair*. The ability of restoring damaged living material is probably one of the most important characteristics of any living organism. Several studies have been carried out during the last 15 years aimed to enable self-healing functions in smart multifunctional materials [12-14]. This topic will be discussed at greater length in Section 4.2.3.

- *Self-diagnosis*. Some biological systems are able to detect malfunctions and degradation by analysing the variation of particular properties such as temperature or the concentration of specific chemical substances. Structural

Health Monitoring (SHM) is an important function that is playing an important role in the development of multifunctional smart materials. The main concept of these innovative systems is their ability to implement a damage identification strategy enabled by the analysis of damage-sensitive features. A vast multitude of studies has been carried out during the last decade to investigate the effectiveness and the feasibility of these systems [15-17], and they will be illustrated more in depth in section 4.2.3.

3.1.3 Human mediated intelligence

During the design and the study of this new class of materials it is important to take in account the interaction between the final product and the user that will exploit its functions and capabilities from the human perspective. Moreover, since one of the most important features of these materials is their interaction with the outside, their impact on the environment in which they will be employed is a very important factor that cannot be ignored.

These properties can be summarised as follows:

- Reliability and compatibility with human life and biological system
- Optimisation of the resource in order to keep down the total cost of the material (in terms of energy and raw materials)
- Human friendliness in terms of ability to be employed in multidisciplinary context
- Ability to be manufactured by using resources without waste

4 Classification of Multifunctional materials

In the previous Section the definition of smart material has been given, together with a description of the concept of intelligence in materials. This chapter presents a more in depth analysis of the breakthroughs in the field of smart multifunctional systems with a review of the most significant achievements present in literature.

There is a large number of multifunctional smart materials that have been studied or are already on the market, however a complete classification of these systems is not easy because of the idea itself of "multifunctionality" that allows multiple features in the same material system. Basically, a rough classification can be made according to the kind of performances that the multifunctional material will feature and it is represented in Figure 9.

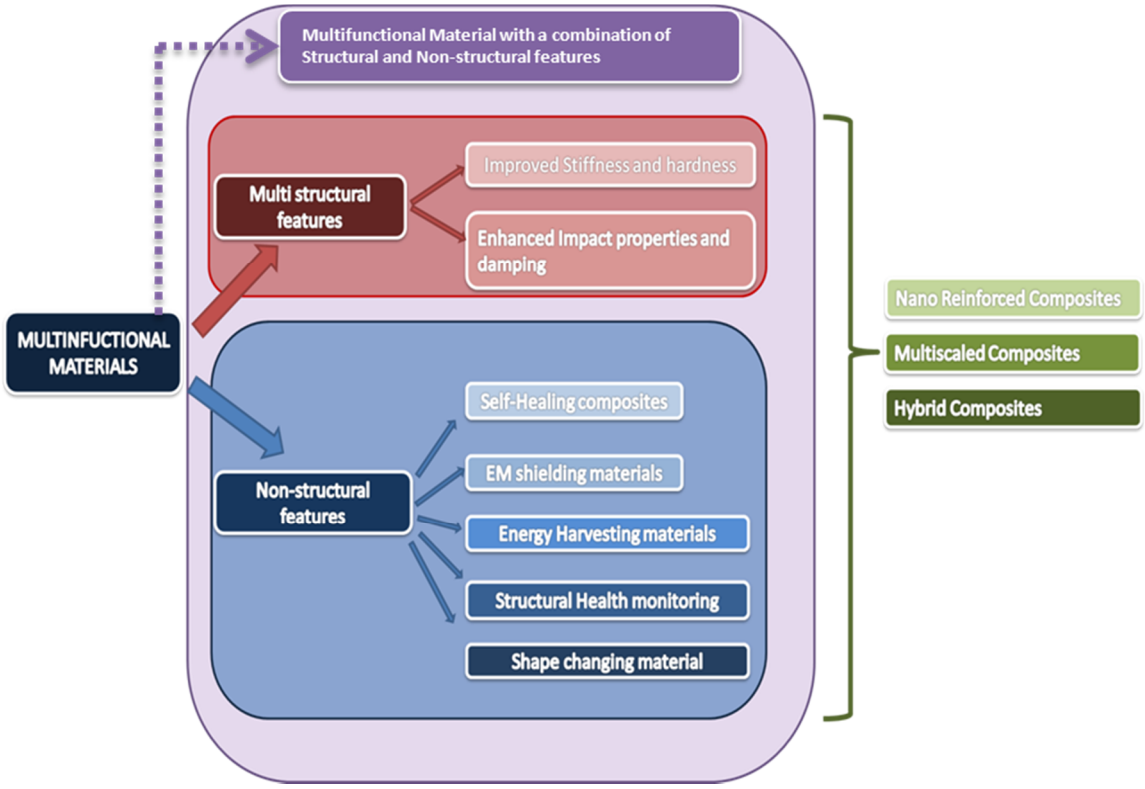

Figure 9 - Categorisation of Multifunctional materials

As it is possible to observe from the image, it is possible to identify three macrocategories of multifunctional systems:

- Systems that perform **multiple structural features**, such as nanoreinforced and multiscaled systems. These materials have the unique capability of being characterised by a multiphasic structure which is able to balance mechanical properties under different loading conditions by activating different energy dissipation mechanisms or load-bearing features

- Systems in which the multifunctionality relies in **non-structural functions**, such as self-healing, power harvesting and structural health monitoring.

- Systems that are able to activate a **combination of structural and non-structural functions** to enhance mechanical properties and enable specific features to extend product life and feasibility

Another distinction can be made according to the nature of the additional phase embedded within the multifunctional system:

- **Nano Reinforced Composites**: materials in which the additional phase is characterised by nanoscaled dimensions. These systems are widely diffused as the minimum amount of nanofiller required to modify completely mechanical, thermal and electrical behaviour of a traditional laminate is very small and does not affect the total weight of the structure. They are generally used to manufacture multi-structural systems and to enhance electrical properties.

  When the effects of these nanoscaled fillers are coupled with those generated from traditional microscaled reinforcements it is possible to obtain more complex structures like **Multi-Scaled Composites**. Usually these systems are employed for multistructural applications, however, especially in the case of CNTs based multiscaled composites, they can present non-structural features such as NDT/SHM.

- **Hybrid Composites**: systems obtained by embedding additional phases characterised by unique features and functions within the laminate structure in order to exploit those properties to modify different aspects of a material's behaviour. These systems can be aimed towards the activation of both structural and non-structural features and usually are based on the inclusion of metals, three-dimensional reinforcement, fluids, through-the-thickness reinforcements, etc. Unlike nanoscaled composites, hybrid materials are characterised by the presence of a more invasive additional phase that can affect weight or other properties.

4.1 Multi-structural smart materials

As explained in the first Section, one of the great advantages of composites over traditional monolithic materials is the possibility of tailoring their properties on the customer needs. Indeed, for traditional materials it is very difficult to obtain simultaneous improvements in different structural functions because some properties are interlinked and mutually dependent. On the contrary, because composites are characterised by a higher level of "customisability" at microscopic scale, it is possible to enhance their mechanical properties by adding specific phases within their structure in order to activate additional mechanisms and features. Since this improved mechanical behaviour arises from the superimposition of the different structural mechanisms of each phase, this class of multifunctional composites can be classified as multistructural materials.

One example of multistructural smart material is in the work made by Gibson et al [18] which investigates the effects given by the inclusion of polymeric interleaves sandwiched between composite laminae. Their results showed that the polymeric layer improves energy dissipation mechanisms, enhancing fracture toughness and damping without affecting the other properties. In other words, the presence of the extra polymeric layers is able to provide new structural features such as delamination resistance and structural vibration damping. Another example is the threephasic composite developed by Manjunatha et al [19], made embedding rubber microscopical particles within a glass fibres reinforced polymer. Their results show

that the presence of the rubber particles can increase by 300% the fatigue life of the modified composite in comparison with a conventional one.

Nanoreinforced composites are multistructural materials characterised by the presence of a nanoscaled phase embedded within a traditional CFRP. There are several works in literature that report how the inclusion of an additional nanometric phase is capable of improving multiple structural functions, especially when the nanoeffects arising from the small dimensions of the nanoreinforcements are coupled with long micrometric fibres or particles (multiscaled composites). Indeed, fibres-dominated mechanical properties are usually excellent in traditional CFRP, while matrix dominated properties are poor because they depend only on the resin which is characterised by lower mechanical properties. The inclusion of a third nanometric phase can overcome these problems, enhancing mechanical properties of matrix rich areas, without affecting fibres dominated properties.
Basically, in order to obtain a nanoscaled multifunctional composite there are two possible approaches that can be followed, according to the geometry and the chemical interactions of the nanometric reinforcements. Indeed, nanoparticles and nanoplatelets are usually embedded within a conventional matrix and then used to develop threephasic multiscaled systems, while nanotubes and nanowires can also be grown on the surface of the fibres in order to create a complex entangled network that enhances mechanical properties of the entire structure and enables different functions.

To fully understand the effects given by the inclusion of a nanoscaled phase within a conventional composite, it is important to better understand the role of nanotechnology and its impact in modern material research.
Nanotechnology can be defined as the design, creation and manufacturing of materials and systems based on phases characterized by dimensions in the range of 0,1-500 nm, which exhibit unique physical and chemical properties due to their dimensions.
Current interest in nanotechnology ranges in several industry sectors, including biotechnology, nanoelectronic and nanostructural materials, among which nanocomposites are one of the most important parts.

From a structural point of view, a nanocomposite can be defined as a material in which one of his components has at least one nanometric dimension. According to this definition, we can distinguish three different component categories:

1) **zero dimensional** (nanoparticles with *three nanometric dimensions* –such as metal and ceramic oxides)
2) **mono dimensional** (nanotubes and nanowires with *two nanometric dimensions* – such as carbon ot titanium oxide nanotubes)
3) **bi dimensional** (nanoplatelets with just *one nanometric dimension* – such as layered silicates, nanoclays and graphene)

Furthermore, from a design point of view, it is possible to distinguish two other different nanocomposites categories:

1) **biphasic composites** (polymer matrix + nanoreinforcement)
2) **triphasic composites** (polymer matrix + fibrous reinforcement + nanoreinforcement)

The specific relationship that links the structure of the nanoreinforcement with its specific properties is one of the most important morphological characteristics and can be expressed with the ratio between the surface area and the volume of the nanometric component (see Figure 10).

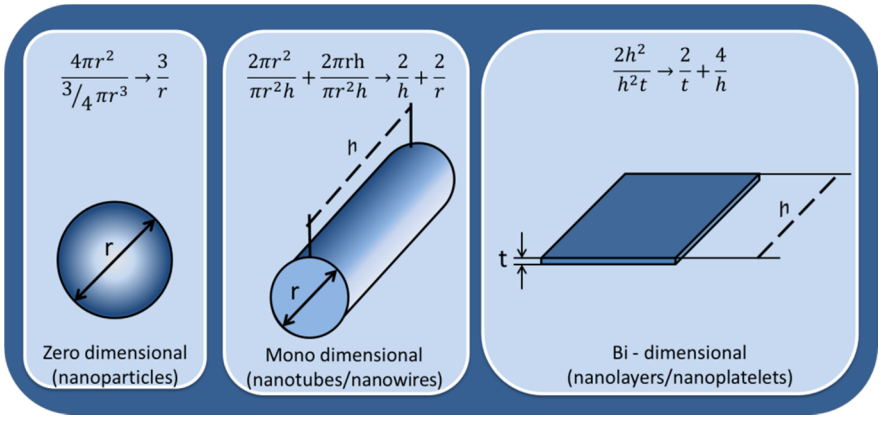

Figure 10 - Surface/volume ratio for different kind of nanoreinforcements

In particular, varying particles dimensions (or length in case of nanowires and thickness in case of nanoclays) from micrometric to nanometric scale, this ratio is

increased by several orders of magnitude. Such modification changes the nature of the interphase between reinforcement and matrix, leading to new properties, which are liable for the impressive characteristics of nanocomposites.

In order have an in-depth view of nanotechnology, it is better to analyse the different kind of nanocomposites separately, focusing on the most significant experimental results found in literature.

4.1.1 Zero-dimensional nanocomposites: nanoparticles based systems

Composites reinforced with micrometric particles are probably the materials most widely used in industry. These particles are usually added in order to increase matrix mechanical characteristics, such as elastic modulus, tensile strength and fatigue resistance. Cho et al [20] studied the behaviour of polymeric composites reinforced with spherical particles made of alumina and glass and characterised by different dimensions (from 0.5 mm to 15 nm). Results from tensile tests revealed that reducing the dimension within the micrometric range does not influence the composite Young's Modulus, however when the dimensions go down to the nanometric scale, the material properties become more sensible to the particles dimensions, showing a strong increase of the Young's Modulus and tensile strength as the dimension are reduced.

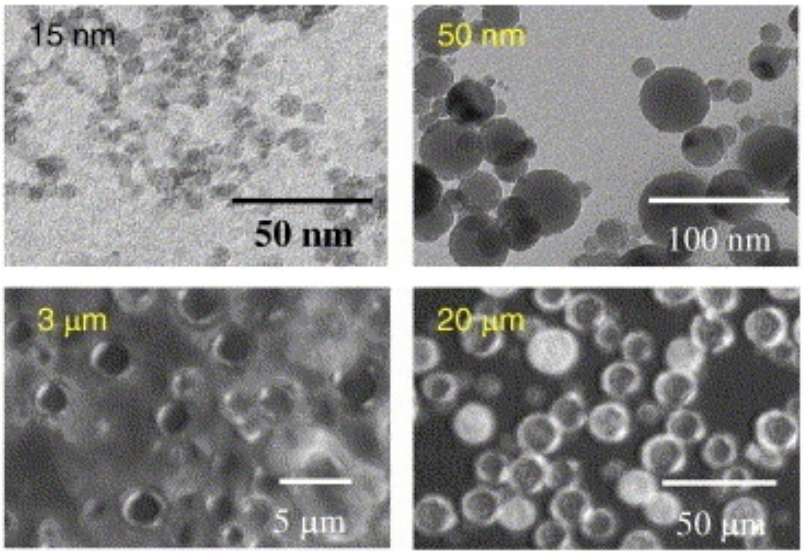

Figure 11 – TEM images of spherical nanoparticles of silica; image from [20]

The work carried out by Singh et al. [21] analyses the fracture toughness of polymeric thermoset resins doped with micron- and nanometer-sized aluminium particles. They observed that both particles size and volume fraction play an important role in the composite toughness and fracture behaviour, enhancing the mechanical response of the material when the volume fraction is increased and the particle dimensions decrease. Moreover it was noticed that the incorporation of normal aluminium weakens the composite, while after a treatment with organosilicates, fracture toughness is increased by around 100%.

Similar results have been obtained by Lopez et al. [22] which investigated the behaviour of nanocomposites obtained embedding alumina nanoparticles in a vinylester resin at different percentages. The results show a linear increase of the modulus as the percentage of nanoparticles within the composite structure is raised to higher levels. However these values remain lower than the modulus recorded for pure resin, probably because of the presence of alumina aggregates within the polymer.

Zhang et al [23] have studied the effect of nanosilica particles in epoxy based composite, analysing their mechanical behaviour at different temperatures. Results show that the presence of a homogeneously dispersed nanometric phase enhances elastic modulus, impact resistance and fracture toughness when the volume content is increased. Analytical models revealed that the nanoparticles induce an enhancement

of the local deformability around the crack tip. Moreover, it has been observed that the effect of nanosilica on the fracture behaviour is strongly influenced by the temperatures, activating different mechanisms at different test temperatures.

In order to understand more in depth the mechanisms behind these improvements, some authors studied the interactions between polymer chains and nanoparticles by using molecular dynamic simulation [24, 25]. Results show that if the polymer-nanoparticles interaction strength is higher than the polymer-polymer one, the elastic modulus is enhanced as the dimensions of the nanoparticles are reduced. Another key factor is the density of polymeric chains that surround the nanoparticles, which is strongly influenced by the nanoparticles dimensions, creating a stiff layer around the reinforcement that is able to enhance energy absorption rate.

A multiscaled hybrid system is the object of the study carried out by Vlasveld et al [26], which investigates the mechanical properties of a threephasic system obtained embedding nanoscaled mica particles in a woven glass fibres reinforced PA6 matrix. Their outcomes indicate that the nanomodification increases the matrix modulus, enhancing the matrix-dominated flexural and compressive strength by more than 40%. Similar behaviour was observed by Uddin et al [27] who reports a 40% increase of the tensile strength in the transverse direction as a result of an experimental campaign on a threephasic composite obtained modifying a conventional epoxy resin with silica nanoparticles and then using it with E-glass fibres to obtain a mulstiscaled system.

Although they are usually employed to modify the mechanical behaviour of a composite, it is important to underline that nanoparticles can be used also to enable specific non-structural functions. For instance, a unique effect of nanoparticles was observed by Naganuma e Kagawa [28] in a study carried out on nanosilica reinforced epoxy resin and it is related to the optical properties of these nanoparticles. In fact, while micrometric particles generally scatter light, reducing their dimensions to nanoscale changes their behaviour, making composites that are usually opaque transparent.

4.1.2 Bi-dimensional nanocomposites: nanolayers based systems

Nanoplatelets based nanocomposites are characterized by the presence of nanometric layers embedded within the polymeric matrix, generally based on phyllosilicates [29]. Phyllosilicates are silicates based mostly on alumina and silica organized in a layered structure. Each layer consists in a sequence of tetrahedric and octahedric nanometric silica sheets that can be dispersed within a polymer in two different ways:

- tactoids (piled silica/alumina sheets)
- intercalated/exfoliated layers (resin-separated layers)

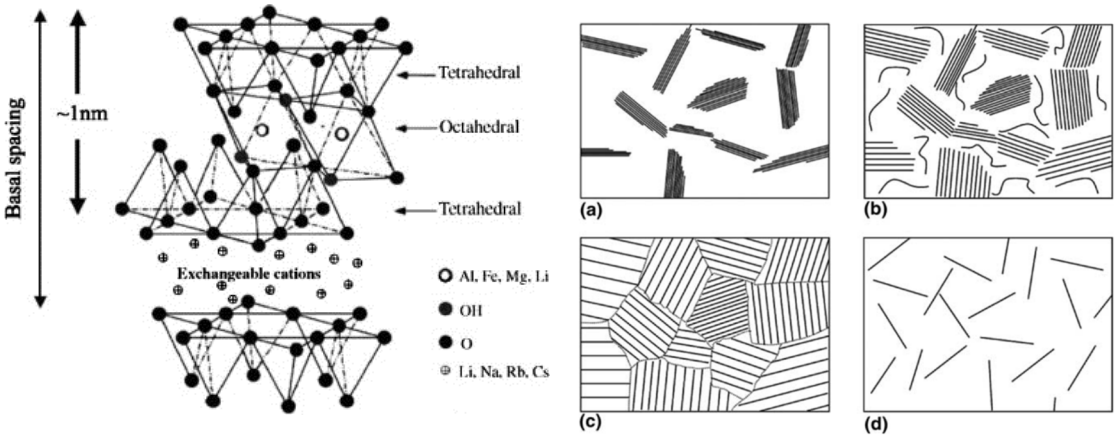

Figure 12- (left) structure of a phyllosilicate, (right) morphology of nanoclay/polymer composites: (a) conventional state, (b) partially intercalated and exfoliated state, (c) totally intercalated state, (d) totally exfoliated and dispersed state. Image taken from [29]

The main difference between these two structures is that the dispersion of tactoids in a resin will give rise to classical microcomposite, whilst using detached nanoplatelets it is possible to obtain nanocomposites.

Structures reinforced with nanoplatelets (generally montomorillonite, saponite and hectorite) have been widely investigated and the results show large enhancements of tensile strength, tenacity and impact properties [30, 31]

Okada and Usuki [32] illustrated that doping nylon6 with a small amount of montmorillonite, it is possible to improve stiffness, increase Young's Modulus (structural features) and decrease water absorption rate (non-structural feature).

A multiscaled hybrid system is the object of the study carried out by Tsai and Wu [33]. In their work they analyse the mechanical behaviour of a threephasic system obtained embedding nanoscaled organoclay in glass fibres reinforced epoxy and they observed that the presence of the nanoscaled phase enhances both tensile strength (+74%) and Young's modulus (+67%).

Another important category of bi-dimensional composites is based on the inclusion of graphene layers within the structure of traditional materials. Graphene is an allotrope of carbon made by a single planar sheet of carbon atoms densely packed in a honeycomb crystal lattice and has attracted the attention of a large number of researchers during the last years because of the exceptional properties that it is possible to confer to traditional materials once they are embedded within their structures. Since one of the experimental parts of thesis will be focused on the study of a graphene-modified composite, a more complete literature review on such multifunctional systems will be presented in Section 5.

4.1.3 Mono-dimensional nanocomposites: nanotubes and nanowires

A nanotube is a nanoscaled structure made by a sequence of atoms arranged in a long thin cylindrical structure. There are several materials that can be synthesised in form of nanotubes such as titanium oxide [34], silica [35] and silicon carbide [36], however carbon nanotubes (CNTs) became, since their discovery in 1991 [37], the leading nanostructure of a new generation of multiscaled materials, not only for their excellent mechanical properties but also for some specific non-structural features that characterise them and that can modify the behaviour of the material in which they are used as components.

Basically a CNT can be defined as a series of carbon atoms arranged in a tube-like shape formed by at least one layer of graphite.

Depending on the number of layers that forms the single CNT structure it is possible to obtain two different cateogires of nanotubes:

- single walled carbon nanotubes (SWCNT)
- multi walled carbon nanotubes (MWCNT)

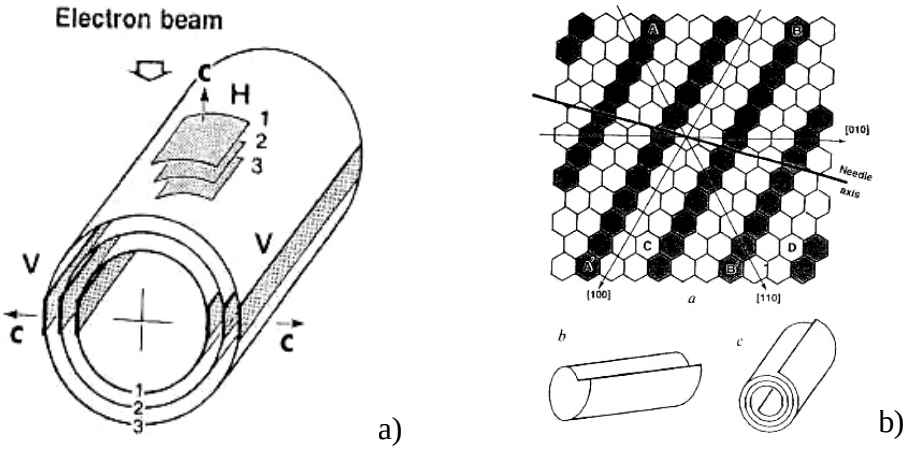

Figure 13 – Schematics of carbon nanotubes from [37]: a) clinographic view of a CNT: each concentric cylinder represents a closed layer of carbon exagons; b) schematics diagram of the helical geometric arrangement of carbon atoms

Mechanical properties of nanotubes have been under investigation since the early 90s, and they can be summarized as follows:

1) SWCNT density is 1,33-1,40 g/cm^3 (half of aluminium density)
2) SWCNT Young's modulus is comparable with diamond one (1.2 TPa)
3) Tensile strength is higher than steel (2 GPa)
4) When subjected to wide-angle deformations, SWCNTs exhibit higher plastic deformation than metals. This characteristic makes nanotubes more performant compared to traditional carbon fibres, which exhibit brittle fracture at lower strains level.

As for the manufacturing process, both nanoparticles and nanolayers based systems can be obtained by doping conventional polymeric resins in order to introduce the nanoscaled components. Nanotubes can be manufactured following the same approach with very good results in terms of mechanical properties enhancement, as reported in several works in literature.

For instance, Rajoria and Jalili [38] studied the influence of several parameters on the stiffness and damping properties of carbon nanotubes-epoxy composites. Based on the results from free and forced vibration tests, they concluded that the reinforcement

effect of MWCNTs is higher than the one for SWCNTs, showing an increase of more than 700% compared with plain epoxy resin.

Tai et al. [39] analysed nanocomposites obtained reinforcing a phenolic resin with MWCNTs and they observed an enhancement in terms of Young's Modulus and toughness. Field emission scanning electron microscope (FESEM) images show an even distribution of nanotubes within the resin and the presence of nanotubes pull-out in the proximity of the cracks. Dual walled carbon nanotubes (DWCNTs) were used by Gojny et al. [40] in order to manufacture nanoreinforced composites. Tensile tests results indicate a dramatic increase of both Young's Modulus and maximum strain for small amounts of nanoreinforcement (~0,1% wt.) and a significant improvements in terms of tenacity in comparison with normal epoxy resins.

Apart from matrix nano-modification, carbon nanotubes can be included in multiscaled composite using chemical vapour deposition (CVD) process to induce their growth on microscaled fibrous reinforcements [41].

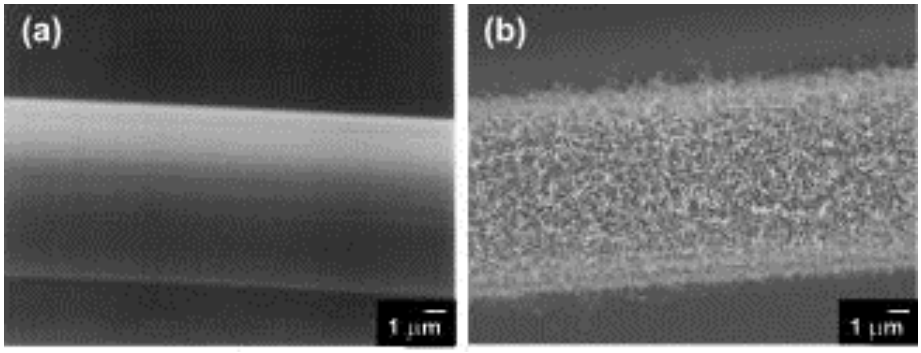

Figure 14 - The surface of a microscscaled carbon fibre, before and after the growth of a CNTs forest; image taken from [41]

An example of this procedure is in the study conducted by Sager et al [42], aimed to study the interfacial shear strength of long carbon fibres coated with carbon nanotubes with different morphologies. Results showed that randomly oriented MWCNT and aligned MWCNT are able to enhance interfacial shear strength by 71% and 11%, respectively, due to the increase in the adhesion between matrix and fibres and the strengthening of the interphase.

The fracture behaviour of CNT reinforced fibres was investigated by Hung et al [43], analysing induced fracture surfaces of damaged multiscaled nanoreinforced composites. SEM analyses demonstrate that composites fracture behaviour is strongly affected by the presence of a nanoscaled phase within the microscopic structure. Indeed, due to the exceptional mechanical properties of CNTs and the consistent increase of the total interfacial area between the different components, new energy dissipation mechanisms are activated such as CNTs/fibres joint failure and CNTs pull-out, enhancing mechanical properties of the entire system.

A different approach to improve out-of-plane properties of traditional composites using carbon nanotubes is described in the work made by Veedu et al [44] and, consists in growing interlaminar long CNTs forests (with an average length of 60 μm) via CVD on the surfaces of different layers of woven SiC fabrics in a traditional composite laminate.

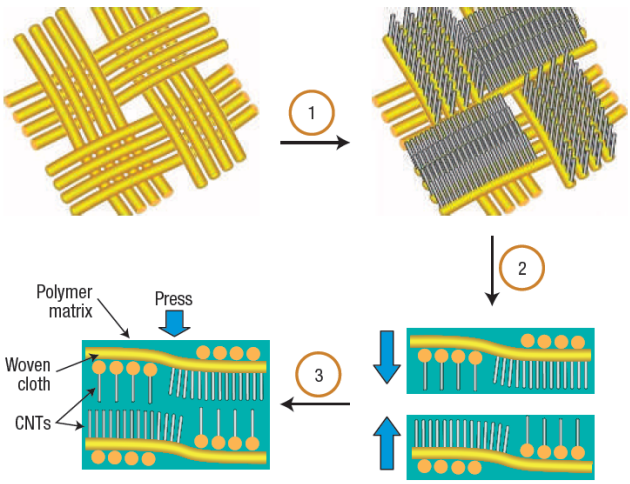

Figure 15 - Interlaminar CNTs forest growing process: 1) CNTs are grown on the surface of the cloth; 2) superimposition of several CNTs reinforced layers to create a laminate; 3) creation of a three-dimensional multiscaled composite; image from [44]

As it is possible to observe in Figure 15, the CNTs forest coated on each ply allows the fastening of stacked layers, forming a three-dimensional multiscaled composite, characterised by enhanced properties in the through-thickness direction.

Because of the great diffusion of CFRP, other authors have investigated alternative procedures to transfer CNTs forests on the surface of carbon based prepreg layers to modify interlaminar surfaces. For instance, the roller technique developed by Garcia et al [45] is able to fully transplant Vertically Aligned Carbon Nanotubes (VACNTs) from a Si substrate to the prepreg surface.

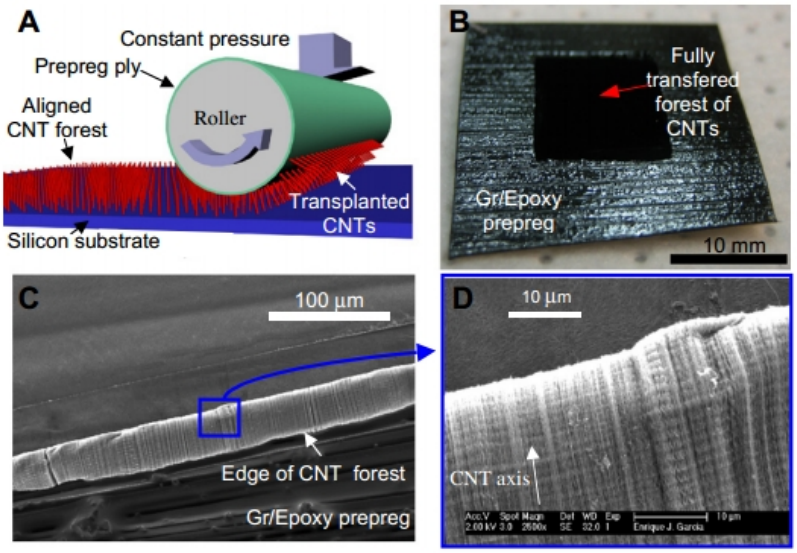

Figure 16 - Schematics of the Roller techniques employed by Garcia et al. to transfer an aligned forest of CNTs from its original silicon substrate to the surface of a carbon fibre prepreg. Image taken from [45].

SEM images showed that the CNTs forest was completely transferred on the carbon substrate without losing alignment and without any nanotubes breakage. Fracture tests indicate an increase of more than 100% in the critical energy release rate Mode I and more than 300% in mode III because of improved plastic deformation of the entire structure and crack bridging of the CNTs.

4.1.4 Strengthening of nanocomposites

As we mentioned above, the experimental results presented in the last paragraphs can be explained with the nanometric dimensions of the reinforcements. In fact, reducing the reinforcement extension leads to an increase of the surface in contact with the polymeric matrix, generating what have been called “nanoeffects” within the composite structure. The fundamental difference with microscaled reinforcement is that the reinforcement dimensions are of the same magnitude of the radius of gyration of the polymer chains that form the matrix. This relationship leads to complete new

intermolecular interactions, which are different from what usually happens in classical microreinforced composites, inducing the formation of a polymer interphase layer characterised by its own set of properties.

In brief, strengthening mechanisms in nanocomposites can be organised in two different categories:

- *in plane mechanisms* (e.g. crack pinning or bowing and crack deflection)
- *out of plane mechanisms* (e.g. immobilized polymer layers and debonding/plastic voids growth)

4.1.4.1 Crack Pinning

This effect was postulated originally by Lange in 1970 [46] and has been observed also in micro-reinforced composites [47, 48], although at lower intensity. Crack pinning effect is associated with what is called “dispersion hardening” and happens when the particles act as pinning points during cracks propagation. In these cases, the crack is stretched out, forming a secondary nonlinear source, whilst the main one stays pinned at the position where it encountered the particle. Because the energy associated to a dislocation is function of its length, a higher energy level is required for its propagation. This effect could be amplified reducing the distance between the different particles or using smaller particles as it leads to the opening of multiple nonlinear cracks, dissipating more energy.

4.1.4.2 Crack Deflection

This particular mechanism happens when the crack tip arrives in the proximities of a stiffer particle and is deflected, being forced to turn around it. The crack becomes twisted or tilted from its plane of propagation, increasing its total surface area thus absorbing more energy. In addition, the crack alters its mode of propagation from normal *mode I* to a superposition that includes contributes from *modes II* and *III* [49].

4.1.4.3 Immobilised polymer

This mechanism involves the creation of a layer of immobilised polymer between the reinforcement particles [50]. Because of their nanometric size, this layer can be

dislocated throughout the structure, creating an interphase network that strengthens the composite. However, this substructure changes the chemical properties of the material, varying the glass transition temperature and can affect other mechanical behaviour (such as storage modulus or damping).

4.1.4.4 Debonding and Plastic voids growth

The debonding mechanism is another toughening effect that is activated when particles embedded within the composite structure are debonded from the matrix. Even though this process absorb just a small amount of energy (in comparison with energies involved in matrix plastic deformation or the other mechanisms listed above), it can reduce the constrains on the crack tip, allowing a subsequent growth of voids that permits larger deformations. In other words, debonding effect does not enhance energy absorption per se, but it is able to activate secondary mechanisms that can guarantee higher energy absorption. This last effect has been pointed out as main responsible for nanocomposites toughening by Johnson et al. [51] for a nanosilica reinforced thermoset resin.

4.2 Non-structural Smart Materials

As illustrated in the previous paragraphs, another important class of multifunctional composites is constituted by all those smart materials which are characterised by a combination of structural and non-structural properties. Indeed, the features implemented in these materials can be extended to functions which are not strictly structural, but that can provide completely new abilities, enhancing their feasibility and effectiveness in several application fields. In this section the most important non-structural characteristics that have been developed for smart material systems will be presented, focusing on the most significative experimental results obtained in this field during the last decade.

4.2.1 Thermo-electrical properties

Thermal and electrical conductivities are two non-structural characteristics that are often required in a material for several applications. For instance, one of the major issues that limits the use of non-metallic materials in aeronautical applications is that they must be characterised by an electrical conductivity higher than 10^{-6} siemens. Indeed, since polymer-based composites are usually insulants, they can be charged electrostatically when the structure is subjected to lightning strikes, increasing the possibility of damages and critical failures. One possible solution to this problem is to reinforce composite systems with metallic wires, enhancing shielding properties. However, since this process increases total weight of the structure and adds complexity to the maintenance process [52], researchers' interest is now oriented towards multifunctional composite solutions with enhanced thermo-electrical properties.

Carbon nanotubes technology offers a valid alternative to traditional metallic materials, due to the small percentage of CNTs required to modify the electrical behaviour. This quantity, called percolation threshold, represents the percentage of nanotubes required to create a conductive network equally distributed all over the material and it is strongly dependent on CNT aspect ratio and shape, as demonstrated by Li et al [53] and shown in Figure 17.

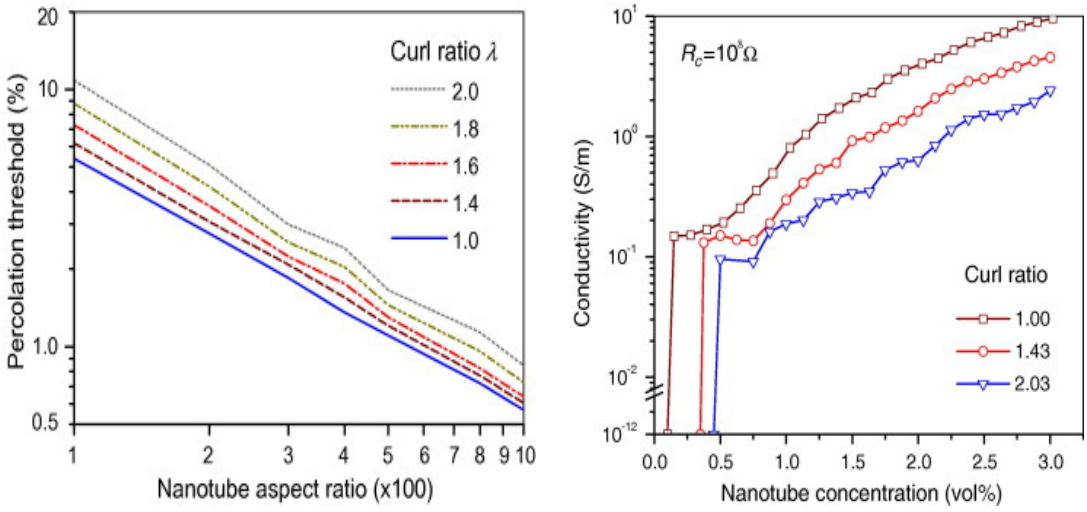

Figure 17 - Thermoelectrical behaviour of CNTs: a) Linear behaviour of the percolation threshold of composites obtained by embedding CNTs with increasing aspect ratio and at a certain curl ratio; b) Relationship between conductivity and nanotubes concentration for different waviness; images from [53]

Sandler et al [54] have analysed the electrical behaviour of epoxy based composites reinforced with catalytically grown nanotubes and concluded that a concentration between 0.0025 and 1 % wt. is enough to increase electrical conductivity by four orders of magnitude (two orders of magnitude between 0.0025 and 0.005% wt.), without affecting mechanical properties. The effects of the different manufacturing techniques have been investigated by Grimes et al [55], who analysed the electrical properties of nanoscaled composite reinforced with untreated and graphitised MWCNTs. Their results indicate that when the tubes are not subjected to any high temperature process during the manufacturing, the presence of residual catalyst particles within the nanotube core increases by 3.5 times the electrical conductivity of the nanostructure.

Even though the percolation threshold for CNTs based composites is very low, it is important to analyse the possible undesirable effects on material processability that can rise from the inclusion of such a nanoscaled phase. Hu et al [56] have analysed the relationship between electrical properties and rheological behaviour of Polyethylene terephthalate (PET)/MWCNT composites. They observed that, while a concentration of 0.6 % wt. was high enough to modify the rheological properties of the material from a liquid to a solid-like viscous fluid, the transition insulant/conductor happened for concentrations higher (0.9 % wt.) than those observed by previous authors. This difference can be explained with the lower CNTs density required to impair the movements of PET chains, in relation with the higher one needed to reach the percolation threshold and reduces the manufacturing techniques available for this kind of materials (e.g. extrusion).

Another important effect that rises from the inclusion of CNTs is the modification of the thermal characteristic of a composite system. However, unlike electrical conductivity, thermal conductivity increases almost linearly with the increasing of CNTs concentration, as observed by Shenogina [57], therefore it is not possible to identify a true “thermal percolation” as for the electrical behaviour. An experimental campaign conducted by Biercuk et al [58] on sample loaded with 1% wt. of SWCNTs showed an increase of 70% in thermal conductivity, while Moisala et al [59] observed

higher enhancements for MWCNTs and a decrease for SWCNT based composites. These results, shown in Figure 18, indicate that the thermal behaviour of CNTs rises from a superimpositions of several effects, therefore it has to be analysed carefully in order to fully understand the different mechanisms behind it.

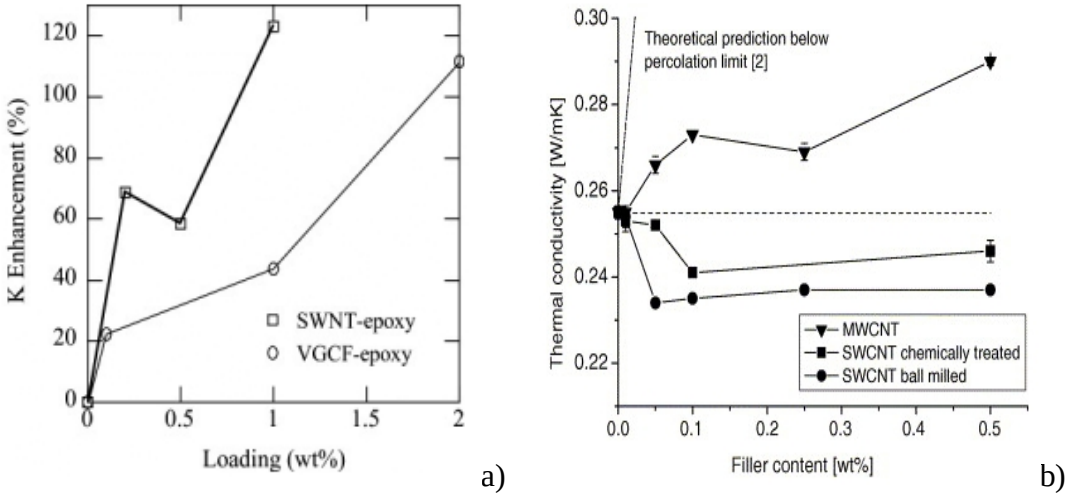

a) b)

Figure 18 – Difficulty in the modelling of thermal conductivity for CNTs based composites: a) Enhancement of thermal conductivity for composites with increasing SWCNT content (image from [58]); b) Decreasing of thermal conductivity with increasing SWCNTs content and enhancement with increasing MWCNTs; image from [59].

The better effectiveness of MWCNTs can be explained with the theoretical studies conducted by Gao et al [60], that have demonstrated that although SWCNTs possess higher thermal conductivity, they are characterised by higher interfacial resistance that lowers effective conductivity. As for the geometry of the nanotubes, it also plays an important role although results in literature are discordant. Indeed, while Fujii et al [61] observed that thermal conductivity increases when the nanotube diameter decreases, Yang et al [62] demonstrated that it is independent by the tube length. The work carried out by Che et al [63] identified in the anisotropic character of the graphite which forms the nanotube structure, the source for the observed change of the thermal conductivity along different crystal axis. Moreover, the observed values are comparable to the ones typical of diamond crystal or single graphite sheet.

4.2.2 Sensing and Actuation

Sensing feature represents one of the most desirable functions that a smart material can exhibit, enabling the capability of self-detecting deteriorations and potential

damages at early stage, preventing catastrophic failures. Usually, the behaviour of structural components is monitored through a wide variety of classical Non Destructive Evaluation (NDE) techniques. Some of these, including eddy currents, shearography, thermography, liquid penetrant and radiography require a detailed inspection of the system components and, most of the time, they need the structure to be disassembled during the inspections. To overcome these problems, multifunctional materials with Structural Health Monitoring (SHM) feature were developed in the last decade, in order to provide autonomous inspection of structures integrity, guaranteeing safety and reducing maintenance costs [64]. SHM systems have a common basis with NDE techniques; in fact, several NDE methods can be converted in SHM techniques by adapting or embedding sensors and actuators inside the monitored structure. These complex sensor-based systems can accommodate integrated capabilities such as signal analysis and transmission to obtain an *in situ* quantification of the structural damage and a strain sensing evaluation in real-time. In particular, these multifunctional composites can be based on the inclusion of piezoelectric sensors [65], sensitive nanocomposite sensors [66], fiber optic sensors [67], carbon nanotube sensors [68], comparative vacuum sensors [69] and Micro-Electro-Mechanical Systems (MEMS) [70]. Among all these systems, the inclusion of specific components characterized by sensing and actuation capabilities is one of the most important, as it is possible to observe from the large number of scientific researches published during the last 15 years.

4.2.2.1 Piezoelectric materials

Monolithic piezoelectrics are one of the most common materials that have been used to manufacture smart composites because of their unique behaviour when exposed to electric fields. Indeed, during the manufacturing process these materials (usually ferroelectric or ceramic) are subjected to a large electrical field that causes the alignment of the dipoles that form their structure. As a result, when the material is immersed in a smaller electrical field, those dipoles react with repulsive or attractive interactions, leading to mechanical shape modifications. These transformations are strictly dependent on the mutual direction of the external electrical field with respect to the direction of the dipoles within the material structure (called "poling"): if the

electric field is applied in the same direction of the dipoles, the material will react expanding (or contracting) itself along that direction, inducing an opposite deformation along the other axes.

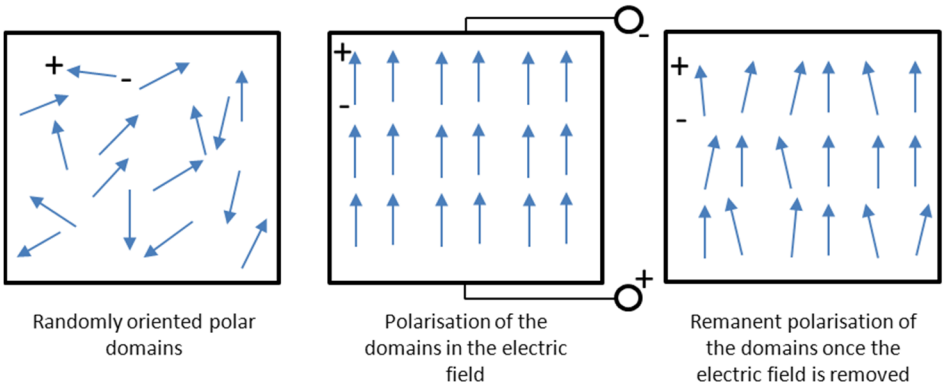

Figure 19 - Poling mechanisms in piezoelectric materials

This behaviour has been studied by several authors and exploited for various applications in the aeronautic sector [71, 72]. However, in terms of potential non-structural features to be included in multifunctional systems, the inverse mechanism is even more interesting. Indeed, as they respond to an external electric field with mechanical movements, piezoelectric materials are also able to generate an electrical current when subjected to external mechanical forces. Hence, by bonding them on the material surfaces or by direct embodiment within its structure, it is possible to monitor the loading distribution applied on a critical component by analysing the electric currents generated via piezoelectric effect. Based on these considerations, the behaviour of a piezoelectric material can be expressed by its *induced strain coefficient d*, which represents the strain per unit of applied electrical field in actuation mode or the electrical field generated per unit of applied stress in sensor mode. Because there is dependence in actuation mode between the direction of the applied electric field and the mechanical answer (or vice versa in sensor mode) this important coefficient is indicated in the form *dij*, where *i* and *j* stand for the direction of electric and mechanical fields respectively. In this kind of systems, the direction 3 is set as a reference and represents the poling direction of the piezoelectric material, while 1 and 2 are the two perpendicular directions. According to this nomenclature, one piezoelectric material will show its highest strain actuation (known also as "*primary*

piezo effect") when its properties are determined by the coefficient d33, or rather, when the strain developed in the direction of poling is due to the application of an electrical field along the same direction.

The manufacturing process used for embedding piezoelectric materials within a composite structure is an important issue for the production of this kind of smart materials. Indeed, even though monolithic piezoelectric materials are characterized by high frequency responses and linear responses when exposed to low fields, there are some processing problems strictly connected to the fact that they are made mostly of brittle ceramic materials characterised by high density and small strains. Because of these weak mechanical properties, monolithic piezoelectrics are not used in multifunctional systems per se and several alternative structures have been developed during the last decades to overcome this problem.

Hagood and Bent [73] manufactured Piezoelectric fibres composites (PFC) by embedding microscaled piezoelectric fibres within an epoxy matrix in order to obtain active laminae characterised by anisotropic actuation to be used for multi-ply composites. However, because of the manufacturing specifications, the electric field is applied normally to the desired actuation direction, therefore the piezoelectric effect will depend on the d31 coefficient, which is way smaller than d33, therefore leading to lower piezo effects.

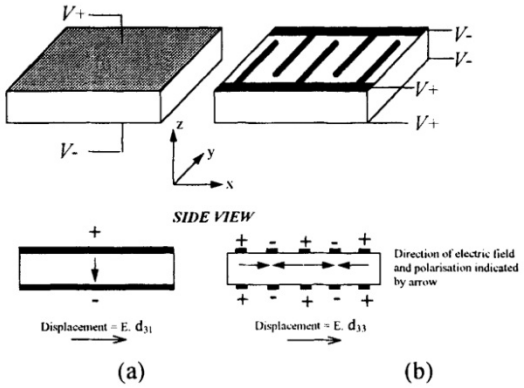

Figure 20 -Direction of the applied electrical field and displacement for: a) traditional piezoelectric materials with conventional electrodes; b) innovative piezoelectrics with interdigitatated electrodes; image from [74]

To overcome this problem, Interdigitated electrodes (IDE) have been developed and applied on traditional monolithic piezoelectric actuators in order to direct the

electrical field into the poling direction and exploit the primary piezo effect [75]. The limitations of such devices has been studied by Bowen et al [74], which observed an inhomogeneous electric field circulation generated by the IDE that can lead to the formation of cracks due to the irregular strain distribution.

Macro-fibres reinforced composite actuators (MFCs) are devices that exploit piezoelectric materials developed by NASA [76] and are based on piezoelectric fibres embedded within a polymeric film. The arrangement of the filaments imparts specific actuation direction and guarantees a good level of stiffness, while the resin gives structural integrity to the composite and provides a correct loads transfer between the different structural components.

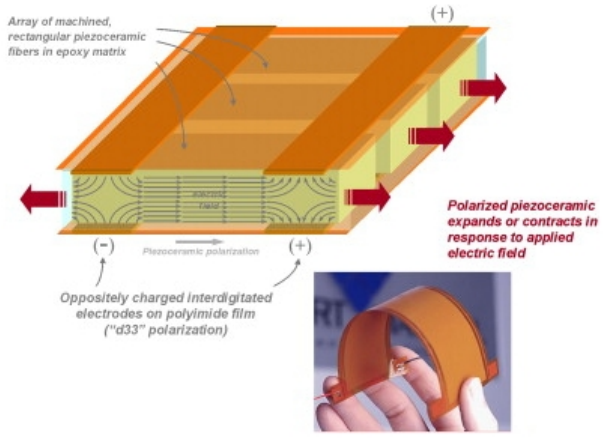

Figure 21 - Schematics of a Macro-fibre-Composite (MFC) piezoelectric actuator; image from Drossel et al. [77]

Moreover, these systems exploit the advantages of an interdigitated electrode pattern in order to apply the electrical field in the longitudinal direction to produce large displacements. Sodano et al [78] investigated experimentally the performances of MFCs and concluded that they are able to provide better performances in terms of electromechanical coupling, fatigue resistance and reliability in comparison with traditional monolithic piezoelectrics for both actuation and sensing applications.

Active Fibres Composites (AFCs) are another kind of devices that have been developed and patented by the Massachusetts Institute of Technology [79]. Although the basic design of these systems is not very different from the one of MFCs (piezoelectric fibres embedded in resin and covered by interdigitated electrodes), there is an important difference in the manufacturing process of the fibres. Indeed, while for

MFCs the fibres are chopped from monolithic piezoelectric blocks, the filaments used in AFCs are obtained via sol-gel technique.

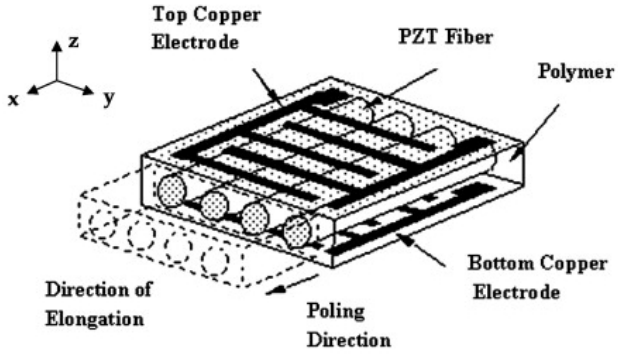

Figure 22 - Schematics of an Active Fibre Composite; image from Sarangi et al. [80]

The characterization of an AFCs system for active vibration control in helicopter components is the aim of the research conducted by Wickramasinghe et al [81] . In their system, the actuators are integrated within the blade as active plies in order to guarantee a good twist actuation of the structure. Results show a high robustness of the system under mechanical loading and a good recovery of actuation after unloading. Good results are also reported by Belloli et al [82], who characterise AFCs patches for vibration damping, matching FE analyses and numerical simulations with experimental data.

The use of AFCs as sensors is the main objective of the study made by Schoecker et al [83] who analysed the performance of GFRP with integrated AFCs subjected to impact loadings. The outcomes of the experimental campaign demonstrate the feasibility of this kind of devices for impact sensing, showing an easy measurable charge generated from the deformation of the piezoelectric filaments.

An example of piezoelectric hybridised composite is presented in the work of Melnykowycz et al [84] who studied the performances of multifunctional GFRP laminates. The results obtained from an experimental campaign show a stable performance of the AFCs up to a strain of 0.20%, while for larger values critical fragmentations in the piezoelectric layer were observed. This behaviour can be explained with the inhomogeneous polarization of the piezoelectric fibres.

Another multifunctional composite has been developed by Lin and Fu-kuo Chan [85] who designed and patented a smart sensing system based on a thin flexible layer of distributed sensors/actuators embedded within a carbon/epoxy composite structure. The so called "SMART" system (*Stanford Multi-Actuator-Receiver Transduction Layer*) is able to acquire information about the status of the composite through piezoceramic sensors, in order to monitor the health of the structure. An experimental campaign conducted on SMART reinforced composites has proved that the embodiment of the active sensing layer does not degrade the mechanical properties of the host structure.

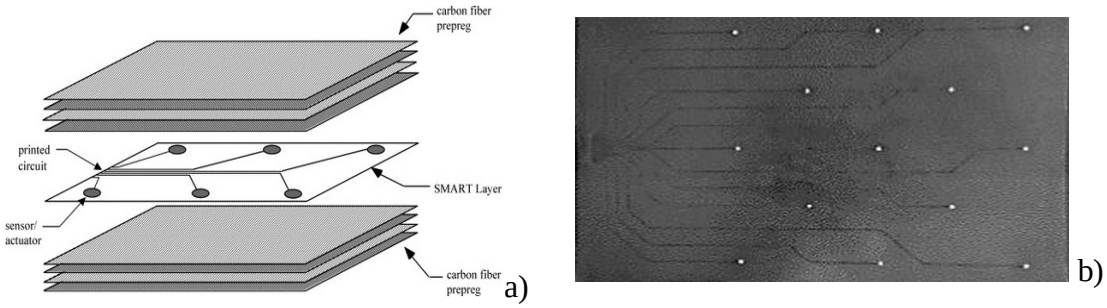

Figure 23 - "SMART layer" developed by Lin and Chang [85]: a) Schematics of the SMART layer integration within a composite laminate; b) an example of a SMART layer produced during the experimental campaign illustrated in the paper.

4.2.2.2 CNTs sensing

In addition to the influence on the electrical and thermal properties, the piezoresistive coupling between deformation and resistance observed in CNTs has broadened their use as sensing devices for *in situ* structural monitoring. Indeed, the small dimensions of nanotubes allow them to penetrate the polymeric matrix and create an intercalated network that covers all the matrix-rich regions within the structure. When the material is subjected to a certain strains distribution, the mechanical deformation of the electrically conductive network of CNTs induces a change in the electrical resistivity of the sample that can be easily measured and analysed [86]. Therefore, by integrating CNTs into a dry fabric reinforced composite it is possible to detect strains and damages in-plane and out-of-plane, according to the geometrical distribution of the nanotubes by monitoring the electrical resistance variations.

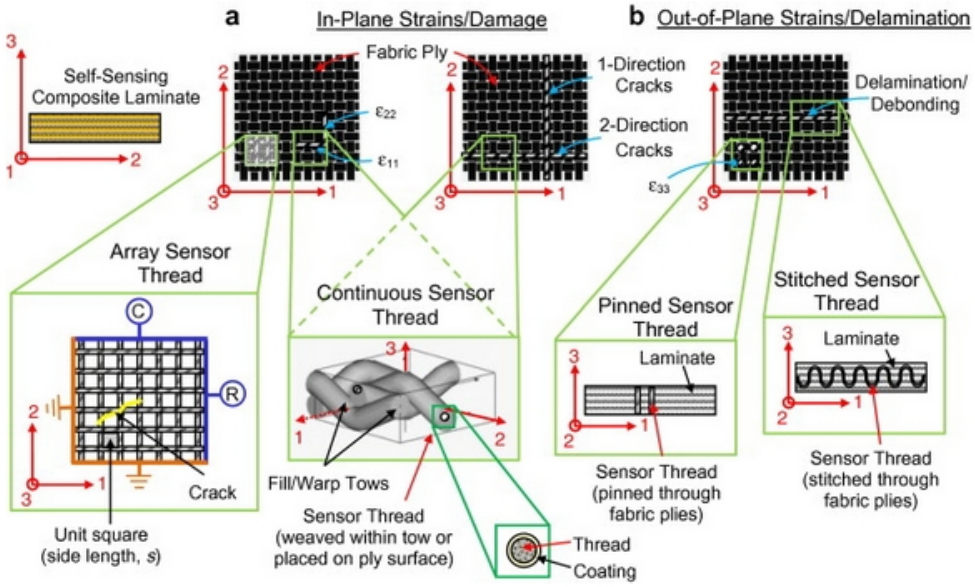

Figure 24 - Integration of CNT structures for strains and damages locations in layered composites: a) disposition of a squared array (CxR) of CNTs within the laminate stack in order to provide in-plane strains and damage monitoring; b) Perpendicular distribution of short CNTs used as a sensor for out-of-plane monitoring; image from [86].

By reinforcing polyelectrolyte films with SWCNTs and studying their electro mechanical properties Loh et al [87] observed a consistent trend between strain and electrical resistance variation. Moreover, the sensitivity of such strain sensor can be tuned adjusting the weight fraction of the nanoreinforcement within the polymer structure. PE/SWCNTs composites have been employed subsequently by the same authors [88] to manufacture a sensing skin for large metallic structures in order to monitor strains and potential impact damages over spatial areas via electric impedance tomographical (EIT) conductivity mapping.

The effectiveness of CNTs networks as sensing devices has been studied also by Myounggu et al [89] who manufactured polyethylene oxide (PZO) samples reinforced with different percentages of MWCNTs. Indeed, by recording continuously the strains and the electrical resistance changes during a tensile test, they observed that the measured electrical conductivity of the composite can be modeled as a combination of linear and non-linear regions which are function of the applied load. Other similar results have been obtained by other authors [90, 91].

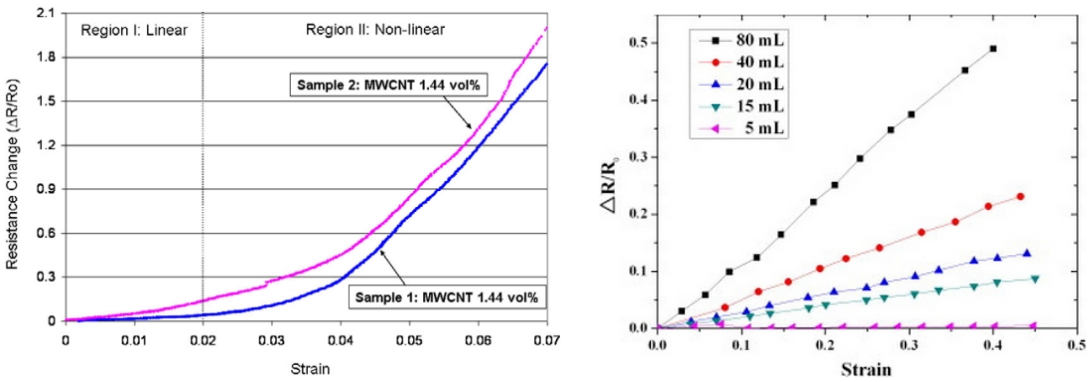

Figure 25 - Relationship between Strain and Electrical Resistance variation for CNTs reinforced composites: a) experimental results obtained by Myounggu [89] and b) Song[90].

Based on these studies, several works made by Thostenson et al [92, 93] are aimed towards the implementation of CNTs networks within traditional fibrous composites in order to exploit the nanoscaled phase not only to increase structural properties but also to enable additional non-structural features. Indeed, by analysing the behaviour of a multiphasic GFRP composite reinforced with a CNTs network during cyclic loadings, they observed that it is possible to monitor the evolution and accumulation of damages within the structure. Moreover, results showed the presence of hysteresis in the composite electrical response, arising from the crack opening/closing mechanism during the load cycles. Similar results were obtained by Monti et al [94], who investigated the response of a similar CNTs/GFRP multifunctional system to low velocity impacts. Their results demonstrated that the presence of non-catastrophic damages leads to significant increase in the electrical resistance; therefore by monitoring continuously the electrical properties, it is possible to develop a dynamic damages detection system for multifunctional structures able to avoid critical failures.

4.2.2.3 Optical Fibres Sensor

Sensing capability can be imparted to a composite material by embedding optical fibres within its structure to create an internal sensors network able to monitor strains distribution. Fibre Bragg Grating (FBG) sensors are cylindrical waveguides formed by an outer cladding made by pure fuse silica and an internal core of doped silica containing germanium and characterised by a spatially periodic modulation in the

refractive index due to the exposure to intense UV sources during the manufacturing process (grating).

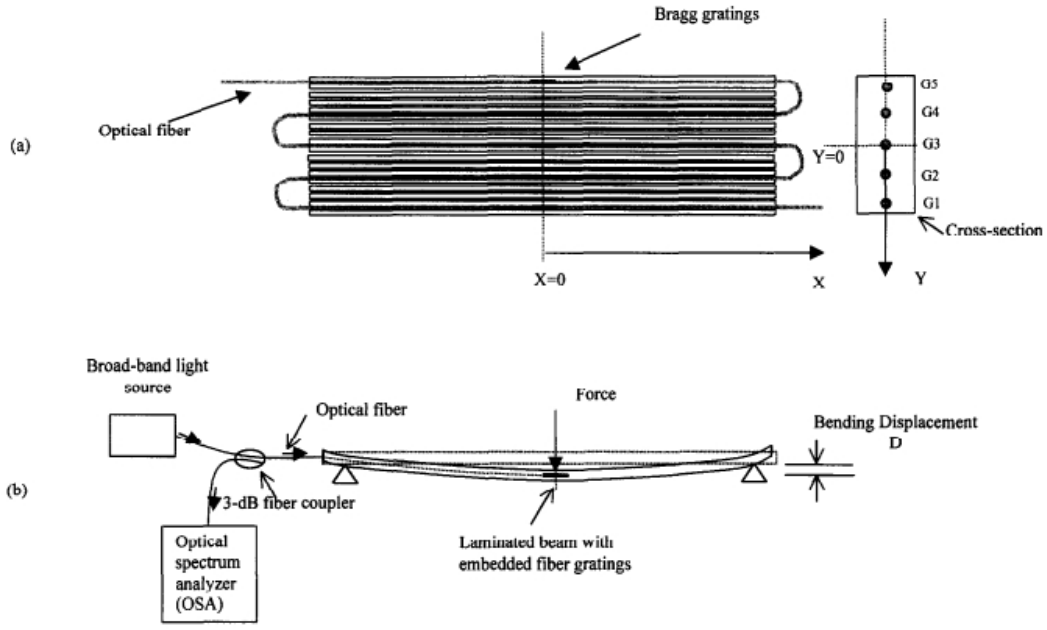

Figure 26 - FBG based composites: a) schematics of the laminated composite beam used by Du et al during their experimental campaign; b) three point bending test setup to measuring the internal strain distribution of the beam; image from [95].

The sensitivity feature of these fibres rises from the variation in the reflective index and the spatial pitch, due to changes in the reflective signal from the grating as a response to external solicitations [95].

Okabe et al. [96] manufactured a multifunctional system embedding FBG sensors within a composite structure for detection of transverse cracks by measuring their reflection spectra during a tensile test. Results indicate that the onset of transverse cracks can be detected from the broadening of the spectrum and the appearance of new peaks. Moreover, the evolution of the transverse cracks density can be monitored measuring the spectrum width at the half maximum.

These sensors were also employed by Takeda et al. [97] to detect delaminations in CFRP using an FBG array as active layer into the laminate structure.

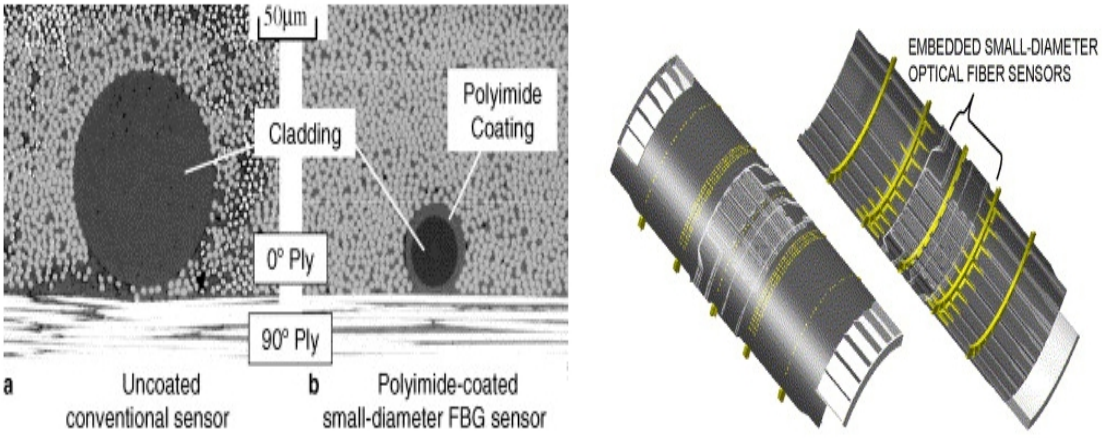

Figure 27 - FBG based smart composite structures manufactured by Takeda et al. : a) optical fibres embedded within the composite structure; b)integration of smart sensors within the upper panel of a composite fuselage; images taken from [97].

Analysing the spectra acquired during a four points bending, they observed a correlation between the form of the spectrum and the extent of the delamination. Indeed, the spectrum intensity ratio can be used as an indicator of the delamination length when it starts outside the FBG sensor. The effect of bonding characteristics between the FBG and the host structure on the accuracy of the strain measurement was investigated by Lau et al [98]. Theoretical models and numerical analyses indicated that part of the strain energy is converted into shear deformation due to the presence of the adhesive layer, therefore the strain measured by the optical sensor is lower than the true elongation of the composite material.

FBG is not the only optical sensor that is used for manufacturing multifunctional composites with sensing features. Extrinsic Fabry-Perot interferometers are sensors for acoustic emission (AE) transient events characterised by higher sensitivity but that require data demodulation. De Olivera et al [99] analysed the performances of composite structures reinforced with EFPI sensors and made a comparison with an FBG based system. Results show that FBG systems work better for dynamic strain measurements at low frequencies, while EFPI are the best option for AE waves sensing.

4.2.2.4 Shape Memory Alloys

Sensing feature can be enabled in a multifunctional system by including particular metallic alloys named Shape Memory Alloys within the laminate structure. Furthermore, because of their unique structural and not-structural features they can also be used to enhance mechanical properties in multistructural hybrid systems. Since a conspicuous part of the experimental work of this thesis is focused on the development of multifunctional SMA based composites, a more complete review on these materials can be found in Chapter 8 where the results present in literature are compared with the experimental data obtained during this work.

4.2.3 Self-Healing Materials

The possibility to include within a material the capability to heal from mechanical or thermal damages without human intervention holds the promise of broadening the lifetime of a composite structure, and it has been the main objective of a considerable amount of literature works during the last decade. White and Sottos [100] developed a self-healing structural polymeric material obtained embedding dicyclopentadiene (DCPD) filled microcapsules and a catalytic chemical trigger within an epoxy matrix.

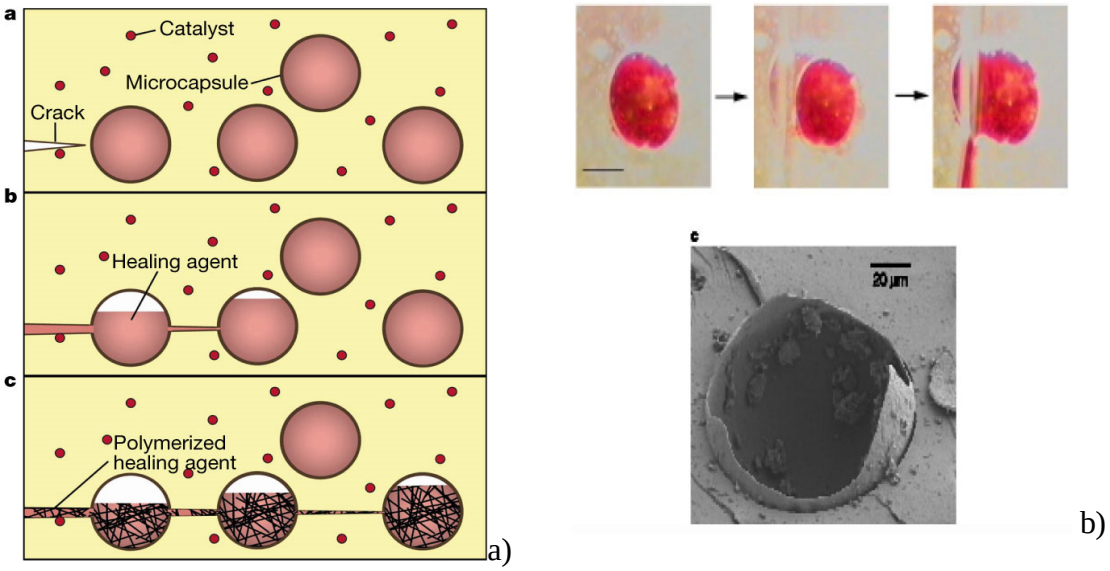

Figure 28 – Self-healing material developed by White and Sottos : a) schematics of the interaction between healing agent and catalyst during the propagation of a crack through an epoxy resin; b) time sequence and SEM image of a destroyed microcapsule during the healing process; images from [100].

When a crack generates, it propagates through one of the microcapsules, releasing the liquid healing agent. Subsequently, through capillary action, the DCPD fills the crack plane and reacts with the catalyst, bonding the crack faces together.

To assess the efficiency of the healed material, fracture tests were conducted using tapered double cantilever beam specimens, and revealed that the healing feature is able to recover almost 75% of the virgin fracture load. In a following study [101], the same authors, improved the microsphere system (which could not provide multiple repairing because of the complete deployment of the DCPD after the microsphere breakage), designing a complex three-dimensional microvascular network able to feed continuously damaged parts with the repair medium. The healing performance of these systems can be improved by embedding SMA wires within the laminate structure in order to bridge the fracture plane. Indeed during the self-healing process, the presence of SMA decreases the fracture extent, increasing the fill factor (the ratio between healing media and fracture volumes), thus lowering the amount of required DCPD. In addition, by exploiting the thermoelectric properties of the SMA wires it is possible to increase the temperature in the fracture area in order to improve the curing reaction [102, 103].
Kirk et al [104] have studied alternative systems based on the incorporation of nanoporous silica capsules filled with epoxy and hardener. The components are situated along the porous nanochannels of the silica capsules and come in contact only when a crack breaks them, activating the curing reaction and healing the structure. This system represents a very good example of multifunctionality because the silica nanoparticles enable not only self-healing of the composite structure, but also enhance mechanical properties increasing fracture toughness by almost 20% for 10% wt. loading. Similar results with silica based fibres were obtained by Privman et al. [105].

Another approach followed to manufacture self-healing materials is described in the work by Pang and Bond [106] who manufactured a smart “bleeding” composite, using hollow fibres to contain a healing agent and embedding them within a the traditional laminate stack.

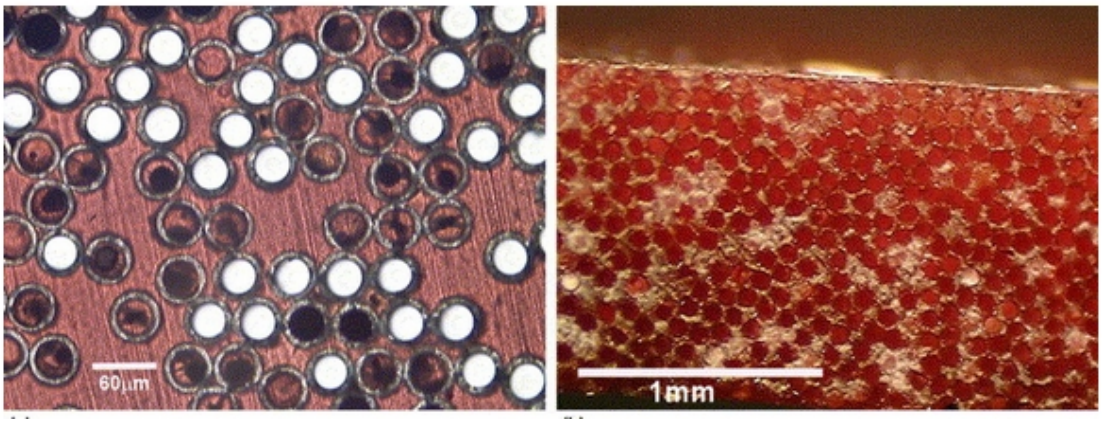

Figure 29 - Micrographs of the "bleeding composite" realised by Pang and Bond, based on the inclusion of hollow fibre containing an healing agent; images from [106].

Results collected from flexural tests demonstrate that a good fraction of the flexural strength lost because of damages can be restored from the repairing media contained into the fibres. Moreover, by including a UV fluorescent dye it is possible to easily detect damaged zones and have a quick assessment of their severity.

4.2.4 Power Harvesting and Storage

The manufacturing of self-powered structures that do not require any replaceable power supplies and are able to generate electrical currents, represents another important goal for the development of new generation smart materials. On these bases, the most promising researches of the last decade are aimed towards the production of multifunctional materials able to extract the energy from mechanical deformations or structural vibrations, and convert it into electrical current to be stored and used for other purposes. In other words, this particular feature can be implemented exploiting mechanical solicitations to deform a piezoelectric material or to displace an electromagnetic coil. Umeda et al. [107] studied the efficiency of a piezoelectric based power generator able to transform the mechanical energy generated from impacts into electric energy. Test were conducted by measuring electrical readings coming from a piezoelectric material subjected to impacts with a steel ball and the data collected were analysed in comparison with an electrical circuit model, showing good matching with the experimental results. The efficiency of the transformation from mechanical impact energy to electric energy was estimated around 35% (3 times more than a solar cell) [108], and it can be enhanced by tuning

the PZT resonant frequency to match the ambient vibrations, reaching an improvement of almost 25% [109]. A proper multifunctional composite structure was developed by Churchill et al. [110] by embedding unidirectional aligned PZT fibres in a polymeric matrix in order to exploit their electromechanical properties to feed an embedded wireless sensor without batteries. Tests were conducted loading the samples in three point cyclic bending using electrodynamic actuators with a range of frequencies from 60 to 180 Hz and stimulating strains of 70-300 με. During the loading cycles, the strain energy is converted in electrical current and subsequently driven in a capacitor bank. When the stored energy reaches a certain threshold it is transferred to the integrated wireless sensor. Results show that it was possible to store 0.75 mW of electrical energy by soliciting the samples with a frequency of 180Hz. Moreover, the time to fully charge the sensor depends on the amplitude of the deformation induced by the actuator.

As for energy storage systems, the possibility to embed such devices within composite structures was analysed by Pereira et al [111] by including a thin film of energy cells into a CFRP structure. The embedded cells are able to withstand temperature and pressure of the curing process, with no variations of the charge/discharge rate. Quasi-static tests indicate that mechanical properties of the multifunctional composite (Young's Modulus and tensile strength) are not affected by the presence of the active layer; however it was found that the maximum tensile load bearable from the power cells before the degradation of their performances was around 50% of the tensile strength CFRP.

Another example of a multifunctional composite structure with enabled power harvesting and storage functionalities is examined in the work by Kim et al [112]. Using a copper nano-ink to print inkjet electrodes on a polymeric film, they were able to interconnect a thin-film solar module and a thin-film battery to the structure of a prepreg based composite laminate. Results obtained from mechanical tests have demonstrated good reliability of the multifunctional system, showing good energy absorption rate, however the electrodes are maintained fully operational until a strain of 1% is developed.

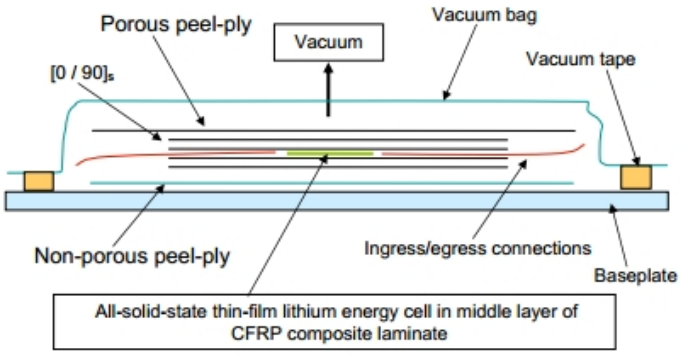

Figure 30 - Layout of the integration process required to embedd a thin-film lithium energy cell within the structure of a traditional composite laminate; image from [111]

4.3 Conclusive remarks

As it has been illustrated in this Section, the potentialities of multifunctional composites are technically infinite because of the vast range of properties that it is possible to include into traditional structures coupled with the multiplicity of the design configurations and manufacturing techniques available to realise these complex systems. As a consequence, in order investigate the feasibility and effectiveness of multifunctional materials, a certain level of schematisation is required. Based on these considerations, the next Sections will be focused on the analysis and the experimental validation of five different multifunctional systems, which will be realised following different design approaches (nanomodification or hybridisation) and characterised by different degrees of multifunctionality (enhancement of multi-structural properties or embodiment of additional non-structural properties).

PART II:

Smart Nanocomposite systems for mechanical properties improvement

As mentioned in the section 4.1, the embodiment of small scale stiff materials is a valid technique to increase the mechanical properties of composite systems and it is widely used in several industrial applications even though the price of fillers is generally higher than normal polymers [113]. However since these materials are usually based on the inclusion of microscaled particles, the minimum amounts of filler needed to obtain sensible improvements are quite high (around 30%), therefore other important matrix properties such as processability, density and, as a consequence, weight are affected.

To come through this inconvenience, Chilstom et al. [114] have studied the properties of polymeric systems reinforced with SiC particles with different dimensions. Their results showed that for a given loading fraction, the improvements given by nanometric particles is significantly superior than the one given by micro-sized ones in terms of mechanical and thermal properties of the resulting composites. Similar results were obtained by Sumita et al [115].

Based on these premises, there have been several studies aimed towards the development of new nanoscaled composite systems during the last twenty years. However, until the end of 90's, the majority of the investigations were focused on the study of biphasic systems, in which the nanofiller is dispersed within a polymeric matrix, usually a thermoplastic one. Thermoplastic resins were chosen because of their widespread usage in expendable goods and in automotive industry as well as the great performances enhancement that can be obtained by reinforcing them with nanoscaled fillers [29, 116-118]; however during the last decade, an increasing number of researches has been aimed also towards the nanomodification of thermoset resins [119].

The aim of this chapter is to analyse two different smart nanoscaled systems that have been designed and tested in order to evaluate the effect given by the presence of nanosized phases to traditional microscaled systems. The first part will be aimed to the production and testing of a graphene based nanocomposite, in which graphene nanoplatelets are used to reinforce Low-density Polyethylene films. The second part will be focused on the design, manufacturing and testing of a multiscaled composite based on the embodiment of silica nanoparticles within a traditional CFRP laminate. Both systems have been studied with an experimental campaign using different techniques and instrumentations and compared with traditional, unreinforced systems in order to clearly identify the effects given by the nanofiller.

5 Biphasic graphene-based nanocomposite for mechanical properties enhancement

As seen in Section 4.1.2 bi-dimensional nanocomposites are manufactured by doping traditional polymers with nanoplatelets usually obtained from layered silicates.
Graphite shows a similar planar structure, which consists of planes of covalent bonded honeycomb carbon hexagons stacked in a ABAB sequence [120] with a constant interlayer distance of ca. 0.34 nm [121]. Each layer can be considered as a sort of two-dimensional macromolecule, made of sp^2-hybridized carbon atoms involved in both σ and π C-C covalent bonds delocalized to the full molecular structure, while the different graphene layers are bonded together only by van der Waals forces [122].

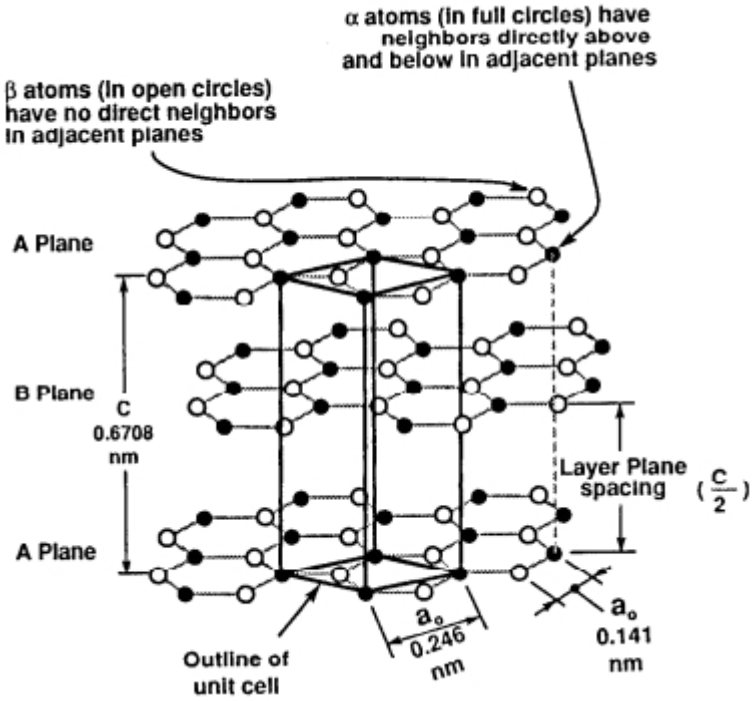

Figure 31 - Layered structures of graphite. Image taken from [122]

Even though Natural Graphite (NG) is characterised by low mechanical properties, it has been used to manufacture composites mostly for electronic applications such as batteries [123] or electrodes [124]. However, using high temperature processes it is possible to obtain Expanded Graphite (EG) which is a swollen material characterised

by low density and high temperature resistance. The low cohesion of this high-porous structure allows it to be partially disaggregated using an intensive sonication treatment, leading to the formation of graphene nanoplatelets, which are characterised by excellent mechanical and physical properties that can be exploited to reinforce traditional polymeric systems [125].

The thickness of graphene nanoplatelets can vary from several to dozens nanometres while the other two dimensions are in the micron scale, resulting in a unique aspect ratio and high specific surface area (2630-2965 m^2/g for completely exfoliated graphene sheets [126]).

Compared with nanoclays, graphene nanoplatelets exhibit lower mass density and show a high electrical and thermal conductivity due to the sp^2-hybridised carbon atoms bonds plus the absence of electron scattering phenomena. Moreover, each graphene layer has a number of unusual characteristics, for example its molecular structure is not permeable to very small molecules such as H_2 or noble gas [127], and it shields electromagnetic waves (ultraviolet, visible, infrared and microwaves).

Mechanical properties are also impressive, with a reported Young's Modulus of 1TPa [128] that makes graphene based composites a valid alternative to CNTs reinforced systems. Furthermore due to the higher surface-to-volume ratio of graphene nanolayers in comparison with CNTs (in which the internal surface is inaccessible to the polymer chains), they are able to better enhance mechanical and rheological proprieties of all the matrices in which they are embedded [129].

Another important advantage that makes graphene nanoplatelets particularly interesting for structural applications is the relatively simple process required for mass production. Indeed, unlike traditional carbon based nanoreinforcements (nanotubes and nanofibres) which require complex and expensive processes such as Chemical Vapor Deposition and laser vaporization [130, 131], nanoplatelets can be produced from natural graphite through simple techniques [121, 132].

The principal aim of this section is to characterize a polymer nanocomposite obtained embedding graphene nanoplatelets (GNP) within a Low-Density Polyethylene matrix.

LDPE is a cheap, easy-recyclable, engineered thermoplastic that is largely used for packaging applications and it was chosen because of the possibility to use the resulting composite also as a structural material once its mechanical properties are improved. To analyse the morphology of the composites, scanning electron microscopy (SEM), transmission electron microscopy (TEM) and X-ray diffraction (XRD) analysis were conducted in order to determine the dimensions of the nanofiller, and mechanical and thermal properties were evaluated with several tests on nanocomposite films. Samples were obtained using different manufacturing processes in order to analyse the orientation effect of the nanoreinforcements and the results were compared with traditional unreinforced films.

5.1 Experimental: Material preparation

Figure 32 illustrates the manufacturing process used to embed GNPs in the polymer structure. Nanofilms were produced by dispersing large aggregates of graphene into the molten LDPE using a micro-extruder. Graphene aggregates were obtained by breaking up small pieces of the fragile "graphene sponge" structure, resulted from the drying of a concentrated colloidal suspension (ca. 33 g/l) of graphene in octane. These colloidal graphene suspensions were prepared by exfoliation of expanded graphite using ultrasound. Either a powerful sonication bath or sonication tip can be used, but in order to achieve a complete exfoliation, the expanded graphite must be slowly added to the colloidal suspension during the sonication treatment. The expanded graphite was obtained through the fast heating of mildly oxidized graphite (expandable graphite).

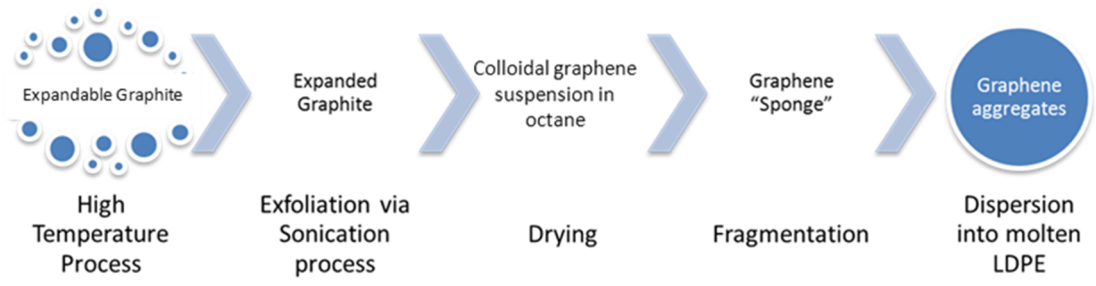

Figure 32 - Graphene Nanoplatelets manufacturing process

Specifically, expandable graphite flakes were placed into a steel crucible covered by a metallic mesh and allowed to expand in air by applying a strong thermal shock; a muffle furnace set at ca. 800°C was used for the expansion process using a heating time of 4 min. The obtained expanded graphite was dispersed in octane (Aldrich, 98%) by gradually adding it to the liquid phase; intensive sonication was applied to this liquid phase using a tip-sonicator (Hielscher, 1000W) in order to achieve a complete exfoliation of the expanded graphite, resulting in a silvery-grey colloidal suspension. This concentrated (paste) suspension was allowed to air dry at room temperature for 24h in order to obtain the fragile graphite sponge, which was subsequently broken into the small grains required for the nanocomposite preparation. GNP were dispersed within the LDPE by preparing an highly filled LDPE/GNP master batch solution (60 wt.% GNP) by intensive rolling process. Subsequently pure LDPE was added to dilute the master batch via melt mixing method until the final concentration of polymer/GNP was obtained.

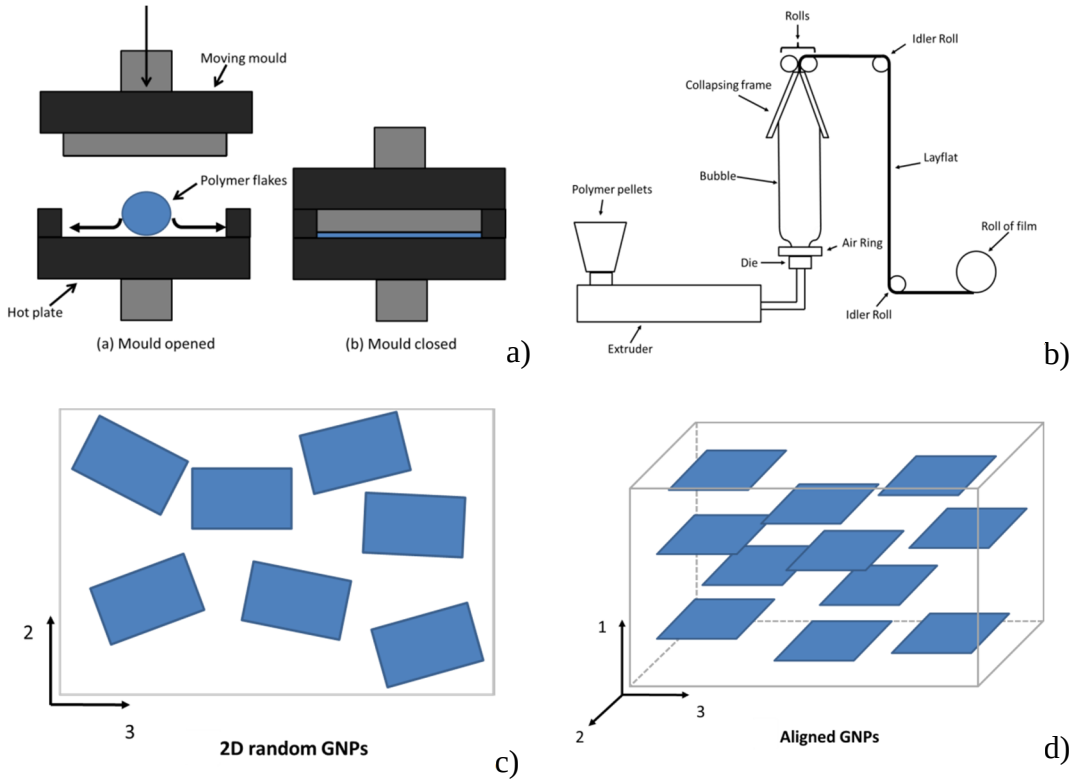

Figure 33 -a) Schematic of Compression Moulding process; b) Schematic of Blown Extrusion process; c) Schematics of randomly in plane oriented nanoparticles; d) Schematics of three-dimensional nanoparticles

Nanofilms were produced by following two different manufacturing processes: compression moulding (Figure 33*a*) and blown extrusion (Figure 33*b*), in order to investigate the effects of orientation of the GNPs within the polymeric matrix.

Indeed, because of the irregularity of the nanoplatelets, their orientation inside the LDPE is strongly influenced by the manufacturing process, resulting in a two-dimensional random distribution for the compression moulding (Figure 33*c*) and in a more aligned three-dimensional orientation for the blown extruded samples (Figure 33*d*). As a consequence, samples obtained with blown extrusion will present a higher level of anisotropy in comparison with the samples manufactured by compression moulding.

5.2 Composite characterisation

Figure 34*a* shows the microstructure of expandable graphite flakes (graphite intercalated by sulfuric acid molecules) before and after the thermal shock treatment.

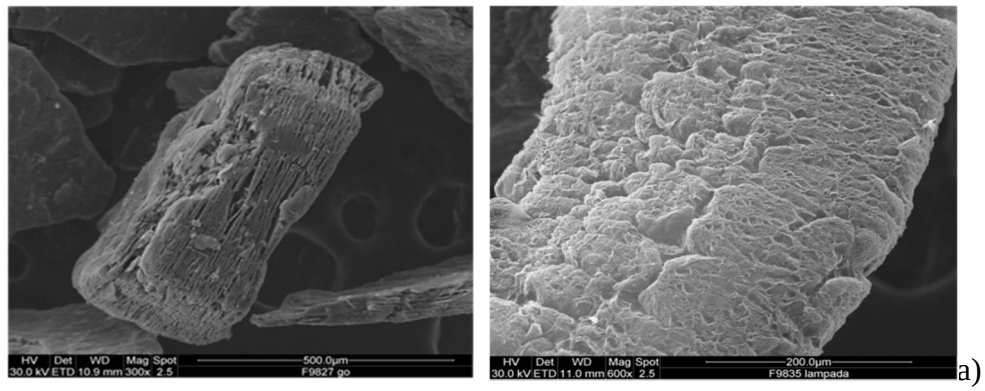

a)

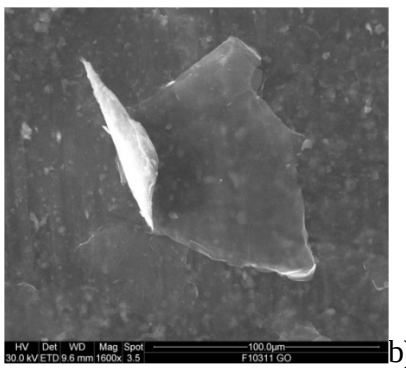

b)

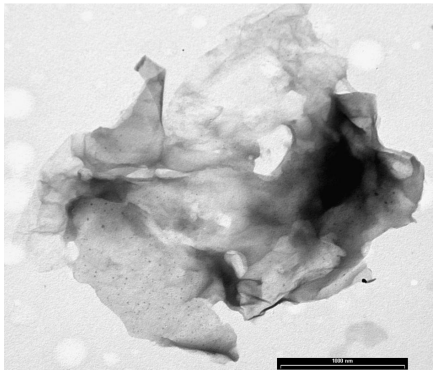

c)

Figure 34 - a) SEM micrograph of the expandable graphite flake (left side) and of expanded graphite filament (right side) ; b) and c) TEM micrographs of GNP after the drying process

As can be seen from the pictures, a worm-like structure is produced at the end of the expansion process because of the gas produced by the following reaction: $C + H_2SO_4 = CO_2 + H_2O + SO_2$. The solid phase produced at the end of the sonication and drying process consists of GNPs with a thickness of approximately 20 nm and a length of 1-2 microns (Figure 34*b and* Figure 34*c*). `

5.2.1 XRD Analysis:

In order to analyse the structure of the nanofilms, XRD was conducted using CuK_α radiation with a wavelength of 1.5406 Å.

The analysis clearly provides some evidences that a significant exfoliation has taken place during the material processing stage. In fact, the very intensive diffraction peak contained in the diffraction pattern of graphite and generated by the (002) planes (see Figure 35a) is almost completely disappeared in the final composite material (Figure 35b). Visibly, the diffractogram shown in Figure 35c contains, in addition to the two main peaks of the LDPE crystallites (which are placed over the diffuse-alone generated by the amorphous fraction of the polymer) at 21.26° and 23.61°, only a low intensity peak at 26.27° corresponding to the (002) planes of graphite nanoplatelets (GNP) present in the sample [121, 133-135]. The amplitude of this peak increases with the percentage of GNPs within the polymer matrix indicating the presence of unexfoliated aggregates due to the formation of platelets agglomerates.

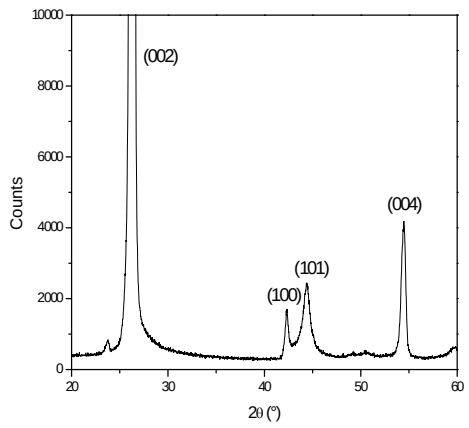

a)

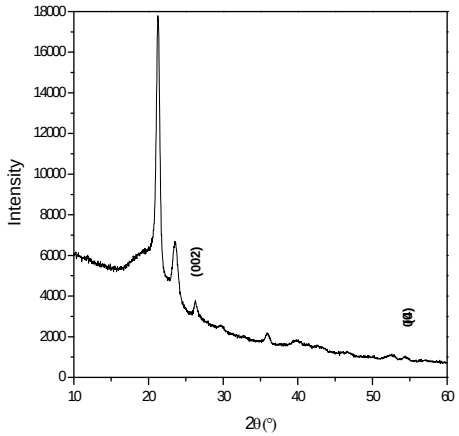

b)

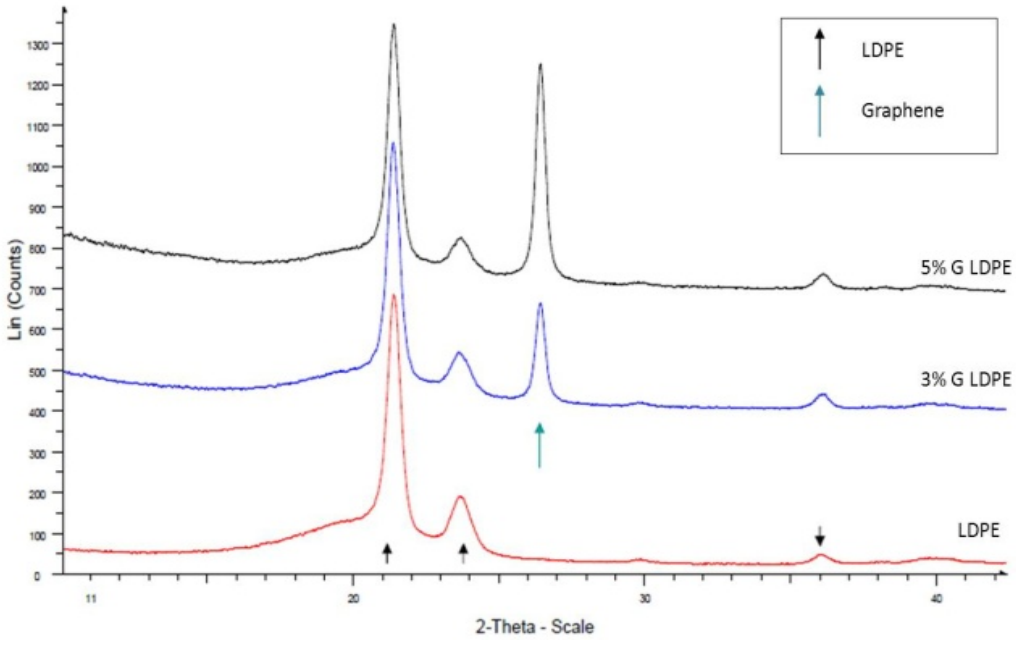

c)

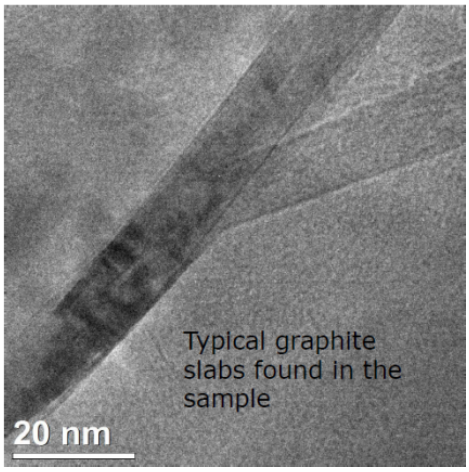

d)

Figure 35 - XRD of graphite (a), LDPE/GNP composites (b) and effect of GNP concentration (c). Figure (d) represents the typical microstructure of the LDPE/GNP composite

A TEM image of thin slices of film cross-section confirms the presence of these graphite nanoplatelets having a thickness of ca. 14nm (see Figure 35d).

5.2.2 Thermal Analysis

The mechanical properties of a composite are strongly dependent on the amount of crystalline phase of the matrix, therefore, since LDPE is a semi-crystalline material, it is important to establish whether the degree of crystallinity is affected by the presence of graphene nanoplatelets. For this reason, DSC analyses were conducted on pure LDPE, and a comparison was made with composites with increasing nanofiller content. Samples weighting 8 mg were heated up from room temperature to 120 °C at a rate of 10 °C/min under nitrogen atmosphere to eliminate any thermal history of the sample and tested using a TA Instruments Differential Scanning Calorimeter .

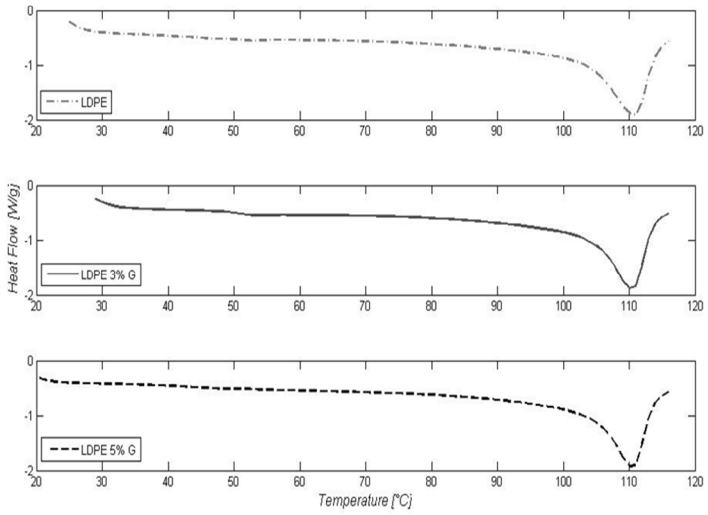

	T_m^P(°C)	ΔH_f(J·g^{-1})	W_c^{DSC}(%)*
Pure LDPE	109.5	86.43	29.4 ± 1
3% GNP LDPE	109.3	84.58	28.8 ± 1
5% GNP LDPE	109.8	85.68	29.2± 1

Figure 36 - DSC thermograms and results for LDPE and LDPE/GNP nanocomposites

Figure 36 illustrates the thermograms for LDPE and LDPE/GNP composites, showing the same patterns for all the curves, with melting peaks at a temperature of 109-110 °C. The degree of crystallinity for all the samples was calculated using the equation $W_c^{DSC}=\Delta H_f/\Delta H°$, where ΔH_f was estimated by integrating the melting peak for each sample and $\Delta H°$ is the reference heat of fusion (293 J·g^{-1}) for polyethylene with 100% crystallinity grade [136].

By analysing the results it is possible to conclude that the inclusion of GNPs within the LDPE matrix does not affect the mass percent of crystallinity of the polymer, therefore the variation of the mechanical properties of the composite cannot be

attributed to a microscopic modification of the polymer structure, but is related to the macroscopic reinforcement effect, due to the presence of the nanoscaled filler. Similar results are reported in literature for carbon nanotube/polymer and Graphene/PVA nanocomposites [137, 138].

5.2.3 Dynamic Mechanical Analysis, Frequency Sweep

The dynamic behaviour of the composite was studied with DMA tests conducted on LDPE film with an increasing amount of GNPs.

The test consists in applying an oscillating (sinusoidal) load on the sample and analysing the corresponding material displacement using a position transducer.

Measuring the amplitude of stress, strain and phase angle between the two curves, it is possible to obtain the complex modulus E*, that can be split in two different compontents: one on phase, which is called “Storage Modulus” (E’), and one out of phase, named “Loss Modulus” (E’’). Storage Modulus represents the elastic portion of the complex modulus and can be associated with the energy stored during each mechanical solicitations, while the Loss Modulus represents the viscous behaviour of the material and it is related to the energy converted to heat during the deformation due to “internal friction” [139]. The relationship between these components can be rapresented in the Argand-Gauss diagram represented in Figure 37.

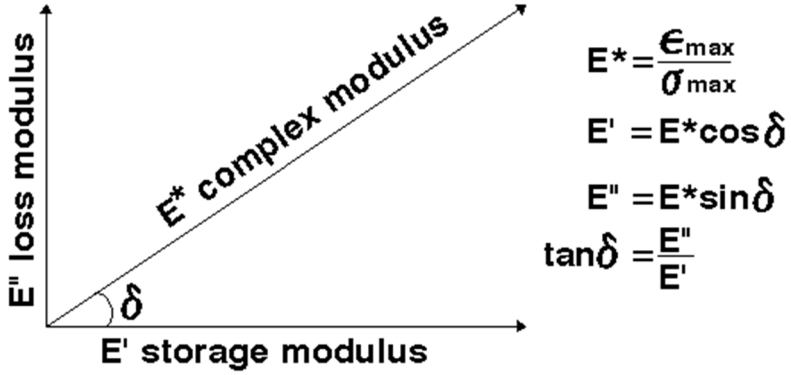

Figure 37 - Argand-Gauss diagram of the Complex Modulus

Storage Modulus can also be interpreted as a representation of the elastic behaviour of a material when it is subjected to an external load, therefore it is ideally related to Young's Modulus, showing a similar behaviour with temperature. However since these quantities are related to distinct material charateristics, their numerical values will be different. DMA is also able to analyse the temperature dependence of several mechanical properties, in order to study behaviour of phase transitions as the glass transition temperature (T_g) and analyse morphological transoformation of the material structure. Another important physical parameter that is possible to determine with a DMA test, is the damping factor (or tan δ), which can be defined as the ratio between E'' and E' and represents a measure of the amplitude reduction of an oscillatory system. This value is equal to zero for an ideal elastic material, whilst for an ideal viscoelastic material it is infinitive.

Samples were tested in tensile mode at room temperature (25 °C) with a frequency sweep between 10^{-2} and 10^{1} Hz. In order to test all the samples within the viscoelastic range, tests were conducted with a strain of 0.1%.

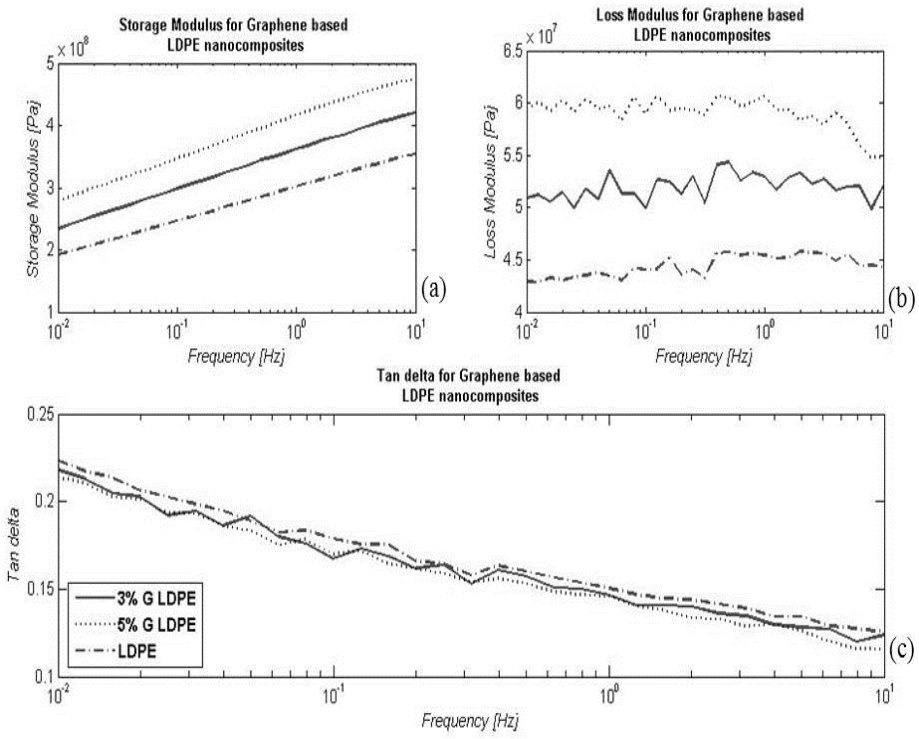

Figure 38 - DMA frequency sweep curves for LDPE/GNP composites: (a) storage modulus, (b) loss modulus, (c) Tan delta

Data obtained from the test are summarised in Figure 38 and Figure 39 and represent the behaviour of Storage Modulus, Loss Modulus and tan delta for pure LDPE and LDPE with 3 wt.% and 5 wt.% nanoplatelets concentrations. The results show an increase in the general trend of the Storage Modulus as the frequency increases and an enhancement of its absolute value with increasing nanoplatelets content (Figure 38*a*).

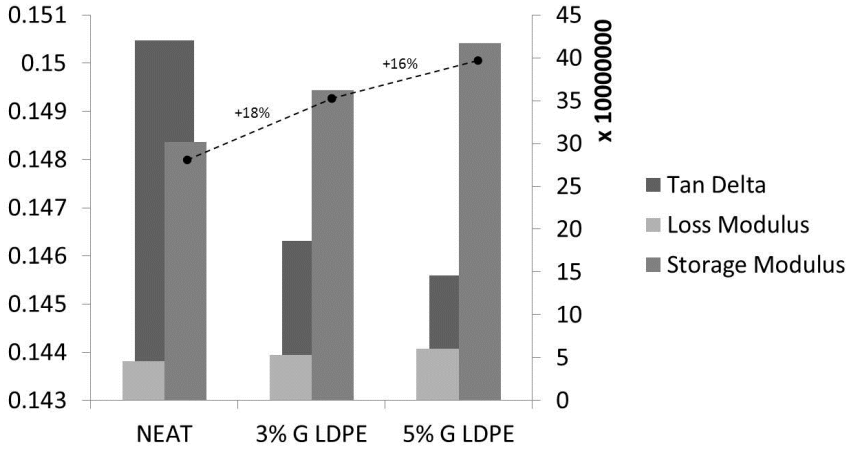

Figure 39 - Storage Modulus, Loss Modulus and Tan delta results at 1Hz for LDPE and LDPE/GNP composites

The shift between the curves of LDPE and LDPE3%G is approximately 15%. A similar increment was observed when increasing the nanofiller content from 3 to 5 wt.%. The behaviour of the Storage Modulus can be explained by two different mechanisms. First, the mobility of the polymer chains is restricted by the interaction between the polymer matrix and the GNPs due to their large surface area, resulting in a stiffened interphase between the two components. Secondly, increasing the percentage of nanofiller within the polymer, GNPs are able to form a mechanically stable network inside the matrix that contributes to increase the modulus of the composite [140].

The behaviour of loss modulus versus frequency is shown in Figure 38*b*, and the general trend seems to be unaffected by the increase in frequency. However, as the amount of nanoreinforcement within the polymer grows, it leads to higher absolute values of Loss Modulus, which is increased by 16% for a 3wt.% GNPs concentration

and 14% for a 5 wt.% concentration. Another important parameter in characterising the mechanical properties of a composite is the mechanical damping (*tan delta*), shown in Figure 38*c*. Results show an overall reduction in damping as frequency is increased (which has been reported for LDPE in previous works [141]), and a slight decrease in tan delta passing from pure LDPE (0.150) to LDPE5%G (0.145) is recorded. Because tan delta is obtained by the ratio of loss modulus (proportional to the energy dissipated during each cycle) to storage modulus (proportional to the total amount of energy that is stored during each cycle), such behaviour is consistent with the other results obtained and it confirms the increase in brittleness of the GNP based LDPE nanocomposites.

5.2.4 Mechanical Analysis, Tensile Test:

To investigate the mechanical performance of the LDPE/GNP composites, samples were tested using an Instron 3369 Tensile test Machine. The crosshead speed was set at 100 mm/min in accordance with EN ISO 527-1:1996.

5.2.4.1 Compression moulding samples

Figure 40*a* shows some representative stress-strain curves for LDPE and LDPE/GNP composites manufactured using the compression moulding technique with an increasing percentage of nanoreinforcement (3 wt.% and 5 wt.%). The inlets in the stress-strain figures show the modifications of the linear elastic region for different samples.

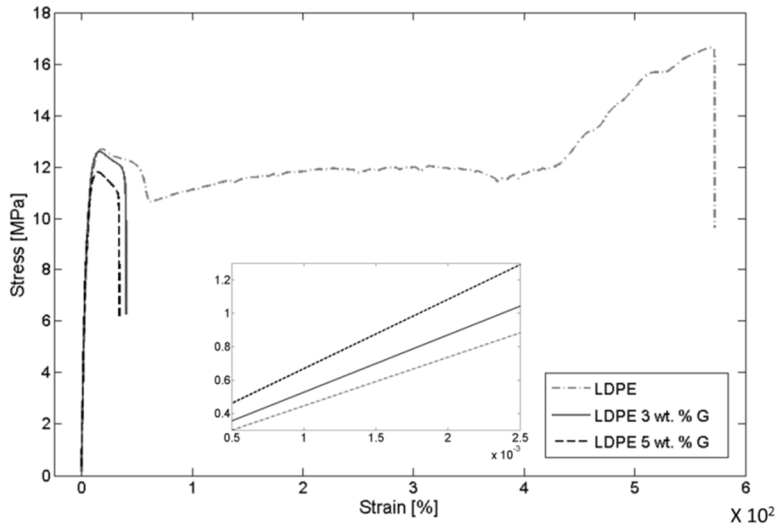

(a)

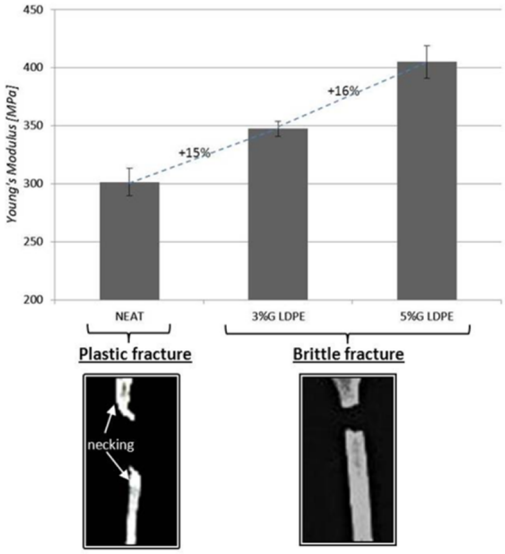

(b)

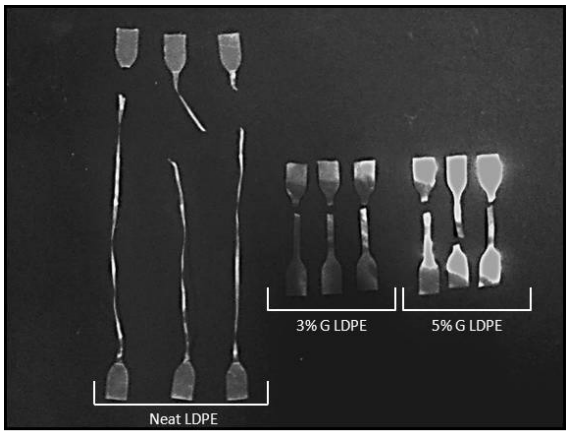

(c)

Figure 40 - a) Stress-Strain curves for neat LDPE and composites with increasing content of GNP. The inlet shows the slopes of the curves; b) Relation between Young's modulus increasing and change in fracture mode for LDPE and LDPE/GNP composites; c) LDPE and LD

As a consequence of the pressure applied, GNPs are orientated randomly in plane, leading to an in-plane isotropy. It can be seen that LDPE with a GNP loading of 3 wt.% shows a 15% increase in Young's Modulus going from 301 MPa of the pure LDPE to 347 MPa. Increasing the GNP content to 5 wt.%, the elastic modulus is increased by an additional 16%, reaching 407 MPa. However, as the nanofiller

content is increased, maximum strain dramatically decreases from 580 to 33%, while a slight decrease in maximum stress (from 16 MPa to 12 MPa) was also observed. The presence of the GNPs within the LDPE matrix appears to strongly affect the ductility of the polymer, shifting the stress strain curves to a more brittle behaviour. As shown in Figure 40*b*, while after yielding LDPE is capable of withstands much greater extension (up to 600%) by activating necking and cold-drawing mechanisms, GNP based composites exhibit a very small plastic region (covering strains of 20-30%) resulting in an almost brittle fracture immediately after the yield point (Figure 40*c*). The reason for this modification may be attributed to the reduced polymer mobility due to the presence of graphene sheets. Indeed, the large aspect ratio of the filler and the interaction with the LDPE matrix can obstruct the reciprocal chains' movements, resulting in a more brittle material [142]. Moreover, the reduction in tensile strength could be explained by the presence of relatively large inhomogeneities (graphite agglomerates) within the LDPE matrix that lead to structural imperfections and generate premature cracks [143, 144].

5.2.4.2 Blown extrusion samples

As explained in section 5.1, blown extrusion process leads to composites films characterised by a higher grade of anisotropy. Because the material is stretched after the insufflations of air, polymer chains and GNPs will be orientated in the direction of the flow, resulting in a material which is characterised by different mechanical properties in the machine direction (MD) and in transverse direction (TD). The first series of tests were carried out on unreinforced LDPE, and are shown in Figure 41*a*. As it is possible to observe from the differences in the stress-strain curves, LDPE shows in transverse direction (TD) a behaviour which is very similar to the one observed in the previous section, although the maximum strain reached is only 300%, while it was almost twice this value for compression moulded samples. The orientation effect of the polymeric chains is clearly shown in the curve relative to the machine direction (MD) samples where LDPE acts more like a brittle material, reaching higher values of tensile strength but a lower maximum strain. Similar results were reported by Guichon et al [145].

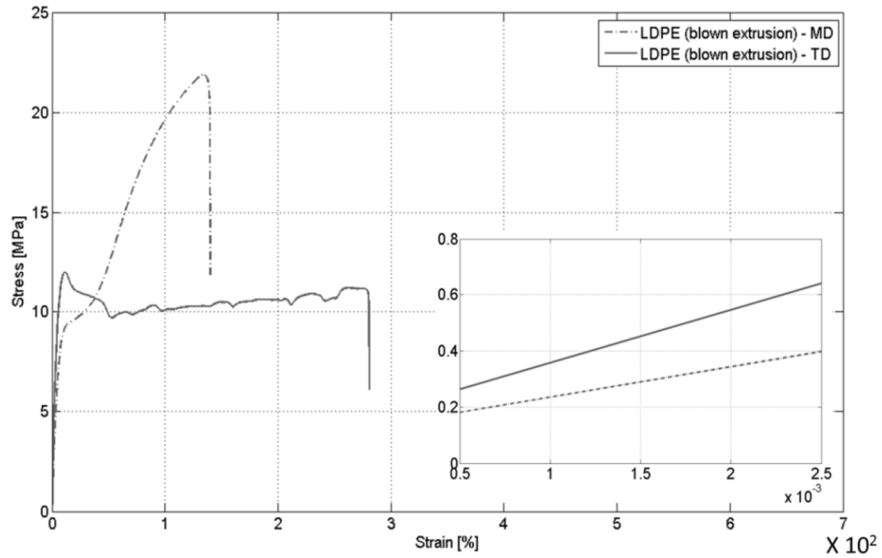

a)

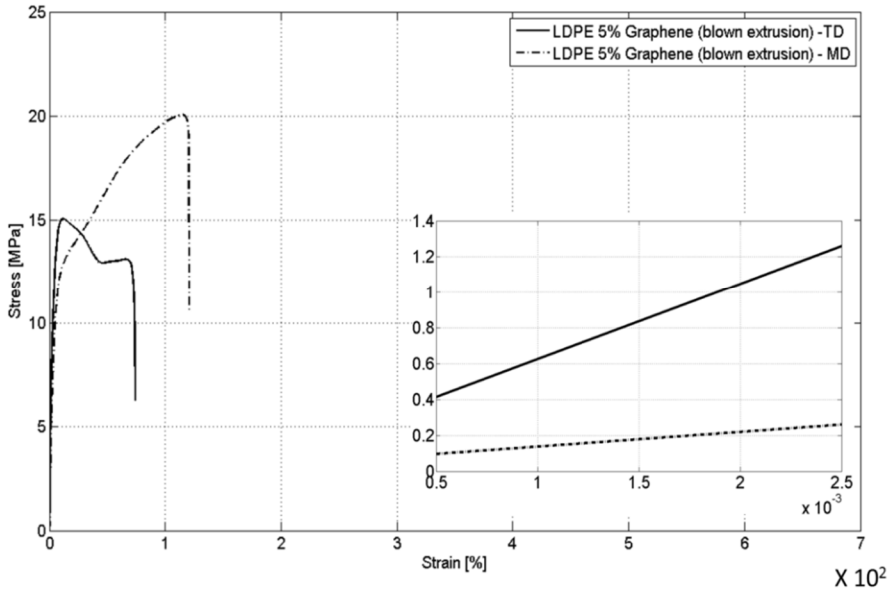

b)

Figure 41 - a) Stress-Strain curves for neat LDPE in blown extrusion process; b) Stress-Strain curves for LDPE/GNP composites in blown extrusion process. The inlets show the slopes of the curves.

Another important consideration regards the Young's Modulus of LDPE which is only slightly affected by the passage from transverse to machine direction (180 MPa for TD and 185 MPa for MD), meaning that the orientation of the chains affects

principally the necking and re-crystallisation phases and not the elasticity of the polymer.

In Figure 41*b* the stress-strain curves for nanoreinforced LDPE with 5 wt.% of GNPs in both machine and transverse direction is shown. Like for pure LDPE, it is possible to observe the effect produced by the alignment of the polymer chains coupled in this case with the higher orientation of graphene nanoplatelets. Indeed, along the transverse direction a brittleness similar to that of the compression moulded nanocomposite is observed, while in the machine direction the orientation of both LDPE and GNPs leads to higher tensile strength (increasing from 15 to 23 MPa) and also higher strain (increasing from 70% to 110%).

Young's Modulus dependence on the orientation is more pronounced in the case of the composite than for the neat polymer, increasing from 430 to 477MPa (+10%). Since the pure LDPE samples did not show any modification in the elastic behaviour due to the polymer chains orientation, this behaviour can be explained with the presence of oriented GNPs that are able to affects the elastic behaviour of the composite, increasing its stiffness.

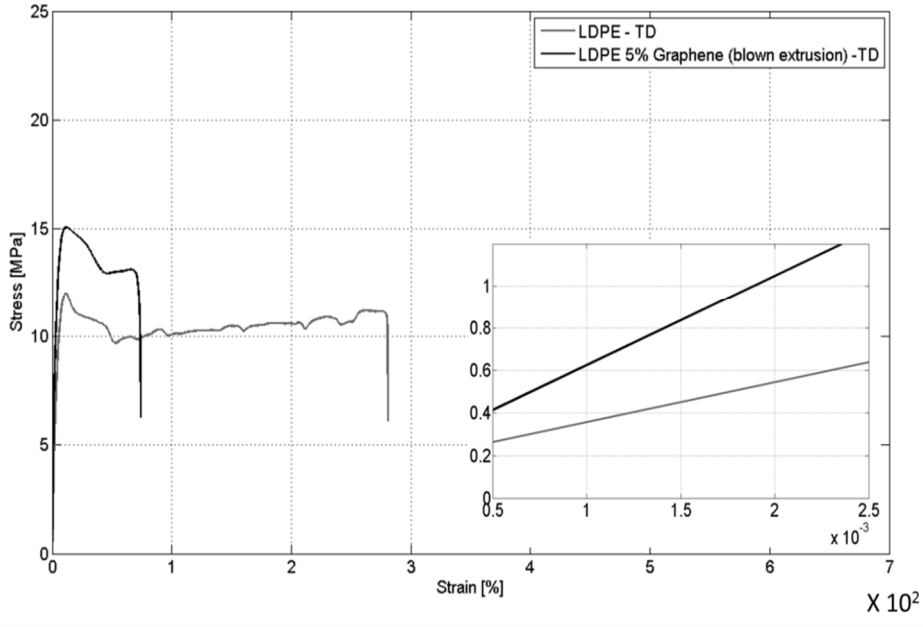

a)

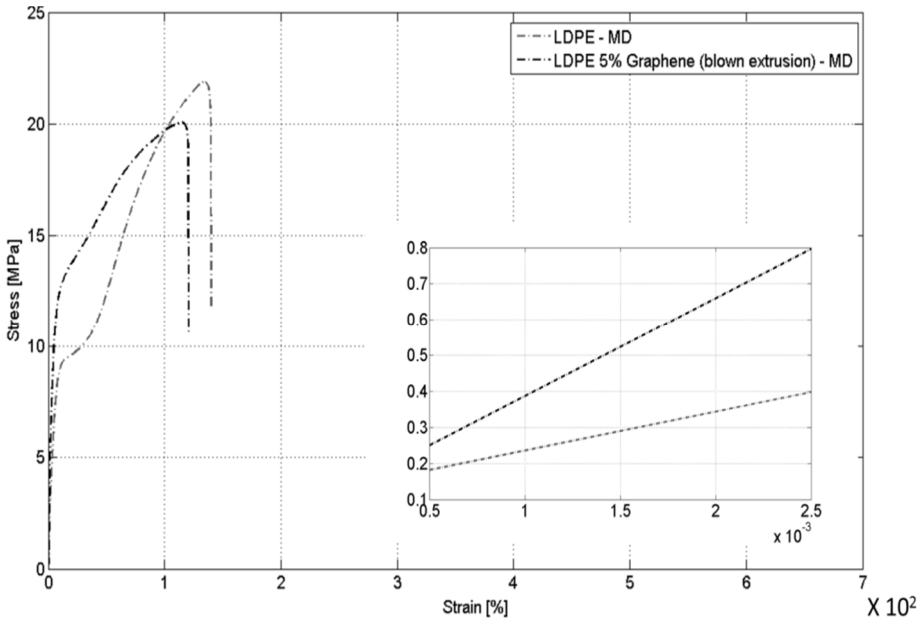

b)

Figure 42 - Comparison between Stress-Strain curves for LDPE/GNP composites and pure LDPE in transverse direction (a) and machined direction (b); The inlets show the slopes of the curves.

Figure 42*a* and Figure 42*b* illustrates the stress-strain curves comparison for neat LDPE and GNP composites for blown extruded film in transverse and machine directions. Young's Modulus is increased for both TD (from 180 to 425 MPa, +135%) and MD (from 187 to 477 MPa, +155%) (see Figure 43), while the maximum strain is reduced by 75% for TD and by 10% for MD. However, analysing the behaviour of the tensile strength for TD samples, the doping of GNPs within the LDPE matrix leads to an increase of 30%, while it is almost constant for MD samples, although a small reduction is recorded (~8%), which falls within the bounds of intrinsic experimental error.

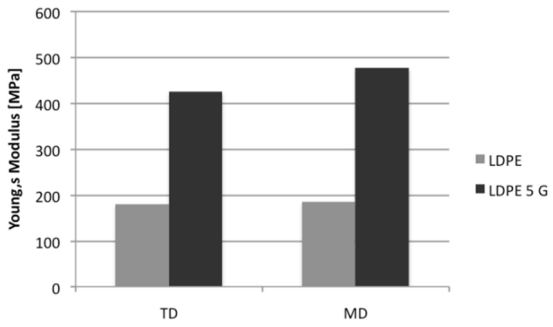

Figure 43 - Young's modulus increase for LDPE/GNP in both transverseal and machine direction.

5.2.4.3 Halpin-Tsai Young's Modulus evaluation model

The Halpin-Tsai model is widely used to predict the elastic modulus of both unidirectional and randomly distributed nanofiller-reinforced polymers [138, 146, 147]. Considering the compression moulded LDPE/GNP samples, the Halpin-Tsai equation is written as:

$$E_{random} = E_p \left[\frac{3}{8} \frac{1+\left(\frac{2l_G}{3t_G}\right)\eta_L V_G}{1-(\eta_L V_G)} + \frac{5}{8} \frac{1+(2\eta_T V_G)}{1-(\eta_T V_G)} \right] \quad (1)$$

$$\eta_L = \frac{\left(\frac{E_G}{E_P}\right)-1}{\left(\frac{E_G}{E_P}\right)+\left(\frac{2l_G}{3t_G}\right)} \quad (2)$$

$$\eta_T = \frac{\left(\frac{E_G}{E_P}\right)-1}{\left(\frac{E_G}{E_P}\right)+2} \quad (3)$$

Where E is the Young's Modulus of the composite with randomly oriented nanofillers, E_p and E_g are the tensile moduli of LDPE (obtained from the tensile test) and graphene (~1 TPa), l_G, t_G and V_G are respectively the length of one GNP (~1 μm), its thickness (~20 nm) and the volume fraction of the nanoreinforcement, which is calculated from the weight fraction.

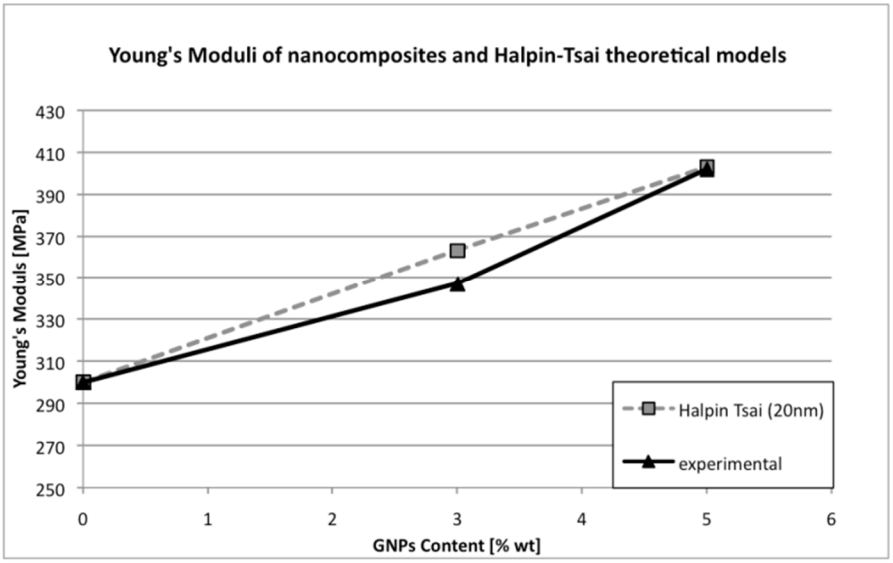

a)

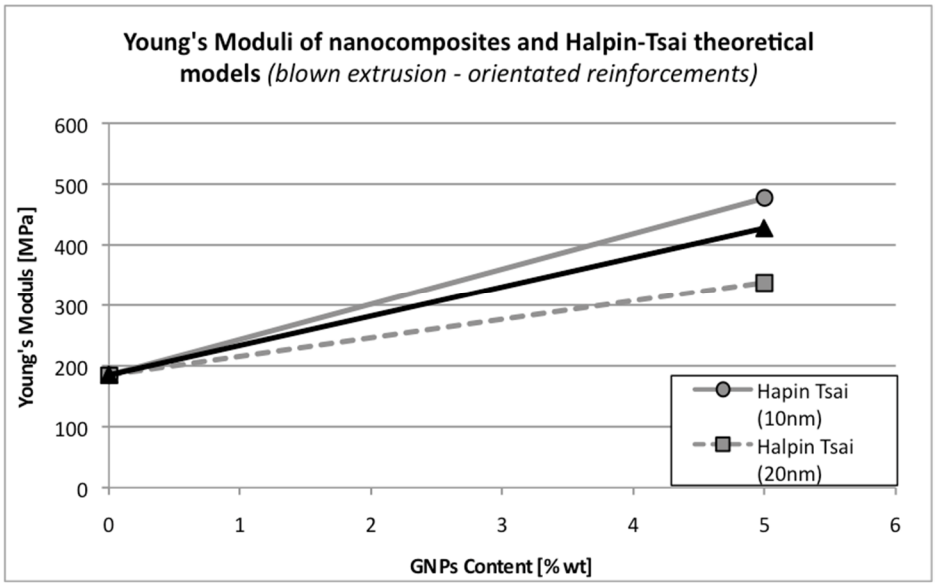

b)

Figure 44 - a) Comparison between Halpin-Tsai modulus evaluation model and experimental data for compression moulded LDPE/GNP composites; b) Comparison between Halpin-Tsai modulus evaluation model and experimental data for blown extruded LDPE/GNP composites

The results in Figure 44*a* illustrate how the experimental data match the theoretical model. For blown extruded samples, GNPs are oriented in the flow direction, therefore the previous model cannot be used and the Halpin-Tsai equation becomes:

$$E_{oriented} = E_p \left[\frac{1+\left(\frac{2l_G}{3t_G}\right)\eta_L V_G}{1-(\eta_L V_G)} \right] \quad (4)$$

Figure 44*b* shows the comparison between the theoretical model and the experimental data for the blown extruded LDPE/GNP composites. As it can be seen from the curves, the experimental value of Young's Modulus for the composites is higher than that predicted by the Halpin-Tsai equation by almost 50%. One possible explanation for this difference could be due to the dimensions of the nanoplatelets after the manufacturing process. During the extrusion process, GNP are strongly stretched in the machine direction, therefore, because the different graphene layers are bonded together only by weak van der Waals forces, this "stretching effect" could lead to a thinning of the graphene nanoplatelets. This thickness reduction is confirmed by the positioning of the experimental data between the 20nm and 10nm thickness theoretical curves, suggesting an intermediate out of plane dimension (~15nm) for the GNPs.

5.3 Discussion

Graphene nanoplatelets reinforced LDPE composites were prepared by incorporating dried nanoplatelets obtained by exfoliation of expanded graphite within a low-density polyethylene matrix. The thickness of the GNPs was evaluated by SEM and TEM analyses, and an average value of 20 nm and length of ~ 1-2 μm was found. XRD analysis was carried out to evaluate the presence of GNPs within the composites and the results confirmed the semi-crystalline structure of LDPE with the detected peak at ~26.5° related to the distance between the different layers of graphene nanoplatelets. The amplitude of this peak increases with the percentage of GNPs within the polymeric matrix indicating the presence of unexfoliated platelets aggregation. Thermograms obtained by DSC analysis were analysed in order to fully understand the effect of GNPs on the microscopic structure of the LDPE and the results show that the inclusion of the nanofillers does not affect the mass percent crystallinity of the polymer. As a consequence, the variation of the mechanical properties of the nanocomposite cannot be attributed to a microscopic modification of the polymer structure, but only to the macroscopic reinforcement effect caused by the presence of the nanoscaled fillers. DMA data show an increase in both storage and loss modulus.

For compression moulded samples, an increase of the tensile modulus of ~30% for a 3 wt. % GNP and of 36% for a 5 wt.% of GNP is reported. Moreover, the stress-strain curve of the composites exhibits a very small plastic region resulting in an almost brittle fracture in comparison with the pure LDPE, due to the presence of the nanosheets that hinder polymer's chains movements. Blown extruded samples showed a higher level of anisotropy due to the stretching of LDPE and GNPs during the manufacturing process. For both machine and transverse direction samples the presence of GNPs leads to a larger increase in the tensile modulus (~135% in transverse direction and ~160% in machine direction) resulting in more brittle behaviour for the TD samples. Tensile strength is increased by almost 30% in transverse direction, while it slightly decreases (~8%) for the machine direction samples. Results obtained by tensile tests were compared with the Halpin-Tsai model showing good matches for samples obtained with compression moulding (in-plane randomly oriented nanofillers), while the experimental data curve for blown extruded samples (highly oriented nanoplatelets) presented slightly higher values than the theoretical model. This result can be explained by a reduction in the thickness of GNPs within the polymeric matrix due to the strong orientation acquired during the extrusion process.

6 Threephasic SiO_2-based nanocomposite for mechanical properties enhancement

As seen in the previous Section, nanoscaled filler can be used as reinforcement to improve mechanical properties of thermoplastic and thermoset polymers [119]. A further evolution of these smart systems is based on the employment of the same nanomodified resins as matrices to manufacture multiscaled threephasic systems, in which the nanoscaled reinforce acts together with the traditional micrometric fibres to improve physical and mechanical properties of the final composite [148-151].

On these basis, nanometric silica particles (SiO_2) exhibit a great range of specific properties that have contributed to their large diffusion in several sectors: structural materials, biomaterials, sensors, surface treatments and especially nanoreinforced composites [152, 153]. Indeed, there are several works in literature that have reported how the embodiment of silica nanoparticles in epoxy matrices enhances stiffness of epoxy matrices. This is basically due to the great difference in terms of elastic modulus between epoxy resins [~3 GPa] and silica [~70 GPa].
Unfortunately, one of the most serious silica disadvantages relies in the resin modification process, which is the procedure required to obtain a good dispersion of nanoparticles within the polymeric matrix. To this end, there are several studies in literature that have demonstrated that the addition of pure nanosilica does not involve necessarily an increase of the mechanical properties, and in some cases, it might weakens the resulting composite [21, 154]. This behaviour can be explained considering the low surface energy and high hydrophilicity of silica nanoparticles. Hence, it is necessary to modify their surface in order to avoid the formation of agglomerates and to enhance interface bonding with the hydrophobic polymeric matrix [155-157]. However, even though by following these techniques it is possible to improve the mechanical properties of the materials, those surface modification processes also increase the degree of complexity of the whole manufacturing procedure, leading to higher costs for raw materials and instrumentation required.

A typical example can be found in the work made by Lai et al. [158], in which SiO_2 nanoparticles are first modified with stearic acid and then dispersed within a Polyether ether ketone (PEEK) matrix. Results from an experimental campaign showed that the presence of the modified silica is able to increase the Young's Modulus by 13-18%, while decreases the tensile elongation of the composite. Another indicative work is the study carried out by Kornman and Rees, in which organosilicates obtained by cation-exchange are used to realize a nanoreinforced resin to be used as a matrix for the manufacturing of a triphasic composites [159].

The aim of this Section starts from these considerations, and it is focused on the design, manufacturing and characterisation of a triphasic composite, in which silica nanoparticles are embedded within the structure of a traditional epoxy resin/carbon fabric composite. The mutual interactions between the nanometric particles and the micrometric long fibres lead to the formation of a multiscaled nano-system, which is characterised by enhanced mechanical properties.

The original contribution of this chapter is mainly based on the threephasic material manufacturing technique, especially for what concerns the nanoscaled particles reinforcement process. Indeed, unlike the classic procedures in which, as mentioned before, the polymeric resin is doped with nanoparticles and then used as a matrix, a novel direct impregnation approach was employed to obtain multiscaled reinforcements. In this method, dry carbon fabric layers are directly impregnated with an aqueous solution that contains the nanoscaled silica particles and then kept under airflow to help the solvent evaporation. At the end of the process, the solvent is volatised while the particles stay on the fibre surface without agglomeration, thus avoiding all the problems related with their dispersion within the polymeric matrix and, consequently, reducing the whole cost of the process and its complexity. In addition, because of the direct impregnation of the carbon fabric, with our technique it is possible to exploit the presence of nanosilica for selective growth of carbon nanotubes to create complex three-dimensional nanostructures.

6.1 Experimental: Thripasic Nanocomposite Manufacturing

This paragraph summarises the manufacturing procedure for the production of the triphasic composite by first analysing the characteristics of the carbon fabric, the nanoparticles and the resin, and then focusing on the impregnation techniques and the analyses carried out on the single fabric layer to evaluate the effectiveness of the impregnation process.

6.1.1 Raw materials

6.1.1.1 Fibres

The fibrous reinforcement used for composite manufacturing is a TeXtreme® carbon fabric produced by Oxeon.

Figure 45 - TeXtreme fabric

Its properties can be summarized as follows:

- Weight: 100g/m^2
- Texture style: plain weave
- Fibres: TR50S
- Stabilizer: Web, one side
- Woof length: 20mm (80g/m^2)
- Warp length: 20mm (80g/m^2)
- Melting point: 3500 °C
- Degradation temperature: >650 °C (in air)

This fabric is characterised by a particular geometry based on fibres tapes weaving instead of yarns that allows the formation of a more compact structure, giving the possibility to increase the fibres content within the composite structure. As a consequence, the properties of the fabric are enhanced in terms of:

- mechanical properties: The tapes reduce the number of weaving in the structure that usually weaken the final composite
- weight: considering the same final weight of the composite, the possibility of higher fibres contents leads to higher properties of the final product

Furthermore, the fabric is characterised by the presence of a bisphenol-A based binder on one of the fabric surfaces, used for keeping the fibres in position and to permit the processability of the dry fabric during the layup process.

6.1.1.2 Resin

The technique chosen for the manufacturing of the multiscaled composite was the *Vacuum Assisted Resin Film Infusion* (VA-RFI). This process is similar to the classic Resin Transfer Moulding technique, however, for this procedure the resin is not in a liquid state, but in form of sheets made of pre-catalysed resin. The use of films adds handling and simplicity to the layup procedure, reducing the time of the entire manufacturing process.

Figure 46 - VTM264 resin film

The resin used was a VTM264 epoxy resin produced by ACG (Advanced Composites Group) and its characteristics can be summarised as follows:

- medium viscosity
- intermediate tack
- curing temperature: 100 °C
- suitable for films preparation and, consequently, for RFI process

6.1.1.3 Nanoreinforcement

According to the analysis made at the beginning of this chapter, nanosilica particles appear to be a very promising candidate for being employed as nanoscaled reinforcement in the development of triphasic nanocomposites, therefore they were chosen as nanoreinforcement in this project.

Nanoparticles used are manufactured by Sigma Aldrich and they have a nominal diameter of 200 nm.

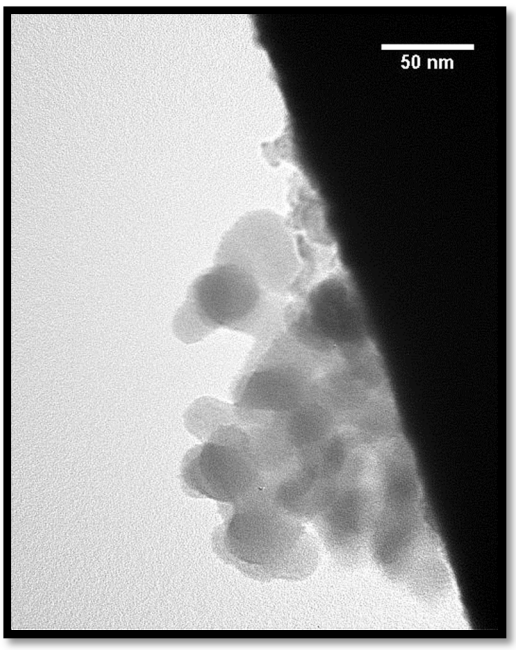

Figure 47 – TEM image of the silica nanoparticles

6.1.2 Impregnation process

In order to obtain an adequate distribution of nanoparticles on the fabric surface, several solutions were prepared with an increasing content of nanosilica particles. Water was used as a carrier for solution preparation and aqueous solutions with a silica content of 5, 10 and 20% wt. were produced following the procedure illustrated in Figure 48. During the preparation, the solutions were subject to mechanical stirring process for two hours in order to avoid the formation of agglomerates and to obtain a good nanoparticles distribution.

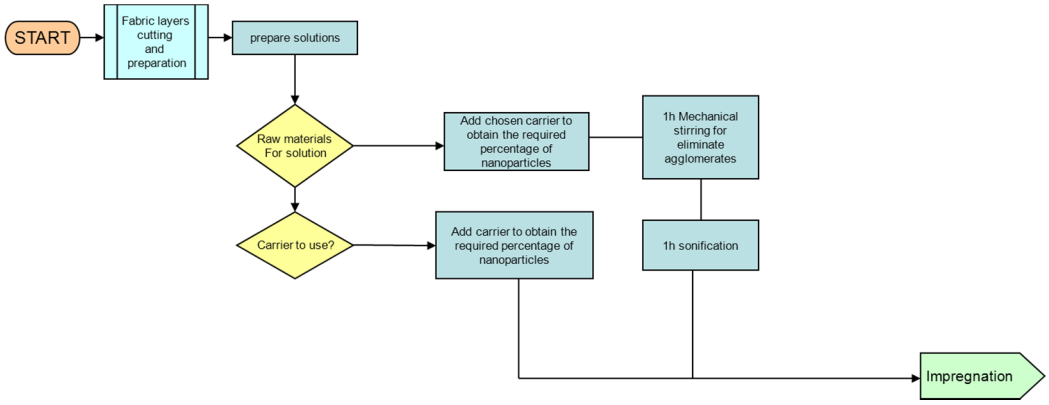

Figure 48 - Solution preparing flow chart

Note: Ethylene Glycol was also used as a carrier due to its higher wetability in comparison with water [35]. Unfortunately, the solutions obtained had to be discarded because the application of ethylene glycol resulted in the dissolution of unreacted epoxy binder, unravelling the different fibre tows thus making the fabrics too difficult to handle for the manufacturing process.

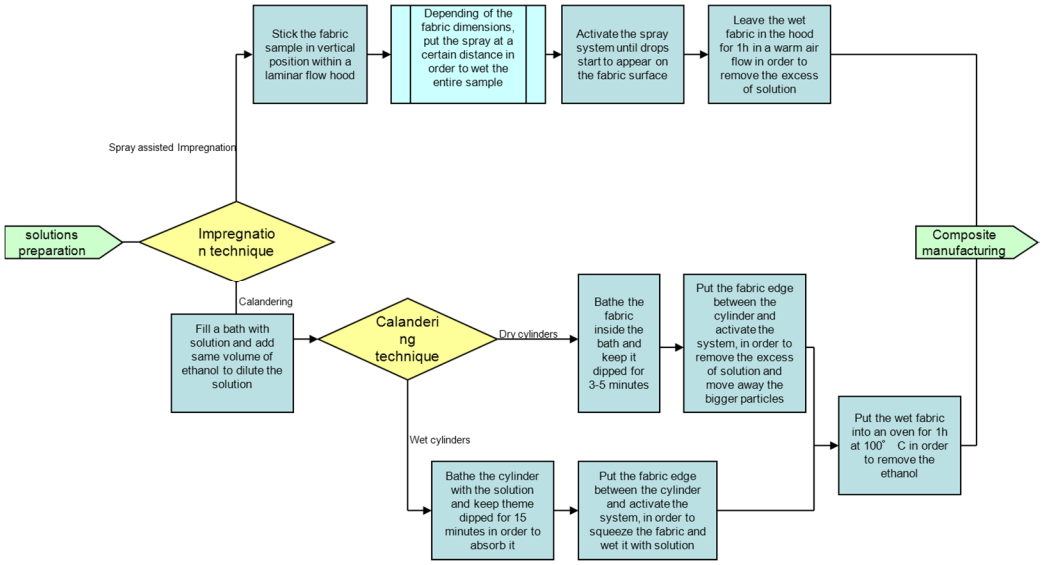

Figure 49 - fabric impregnation flow chart

Once the solutions were prepared, the attention was focused on the development of an efficient impregnation method able to transfer the nanoparticles based solutions on the fabric surface avoiding the formation of agglomerates during the process.

This part of the project would not be explained in details as the procedure is currently under examination with Bath Ventures for a patent.

Figure 49 illustrates the flow chart for the fabric impregnation process tested during the experimental campaign, while Figure 50 shows some of the techniques used to dope the fabric with nanoparticles.

Briefly we can outline the processes tested as:

- *direct sinking*
- *roll-up procedure*
- *aerosol impregnation*
- *calendering*
- *spray*
- *pressured impregnation*


a)

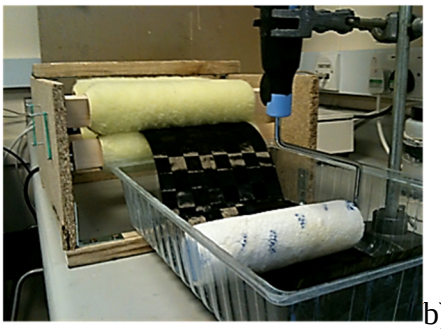
b)


c)

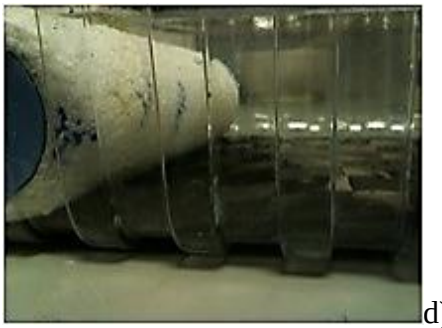
d)

Figure 50 - Some of the impregnation techniques tested: (a) aerosol, (b) calendering, (c) spray, (d) roll-up

The efficiency of the different processes was evaluated by weighing the fabric before the impregnation and again at the end of the process. Results show that the best results were given by the Spray Pressured Impregnation (SPI) technique, as it is possible to observe from Table 1 and Figure 51.

Table 1 - fabric weight increase percentage after impregnation with Spray Pressured Impregnation technique (SPI)

	Neat Weight [g]	*Impregnated Weight [g]*	*Increase [%]*	*Average [%]*
	21.8	23	5.5	
	21.9	23.1	5.5	
	21.8	23	5.5	
	21.8	23.1	6	5.5
	21.8	23	5.5	
	21.9	23.1	5.5	

	21.7	22.9	5.5	
	21.8	22.9	5	
Average	21.8125	23.0125	5.5	
Standard Deviation	0.0599479	0.078062475	0.25	
	22	24.4	10.9	
	21.8	23.9	9.6	
	21.8	24.1	10.6	
	21.8	24.1	10.6	10.1
	21.5	23.5	9.3	
	21.8	24	10.1	
	21.7	23.8	9.7	
	21.9	24.1	10	
Average	21.7875	23.9875	10.1	
Standard Deviation	0.1363589	0.247171499	0.524404	
	21.8	27	23.9	
	21.6	26	20.4	
	21.8	27.2	24.8	
	21.8	26.5	21.6	23.1
	21.9	26.7	21.9	
	21.8	26.6	22	
	21.8	26.9	23.4	
	22	27.9	26.8	
Average	21.8125	26.85	23.1	
Standard Deviation	0.1053269	0.522015325	1.920286	

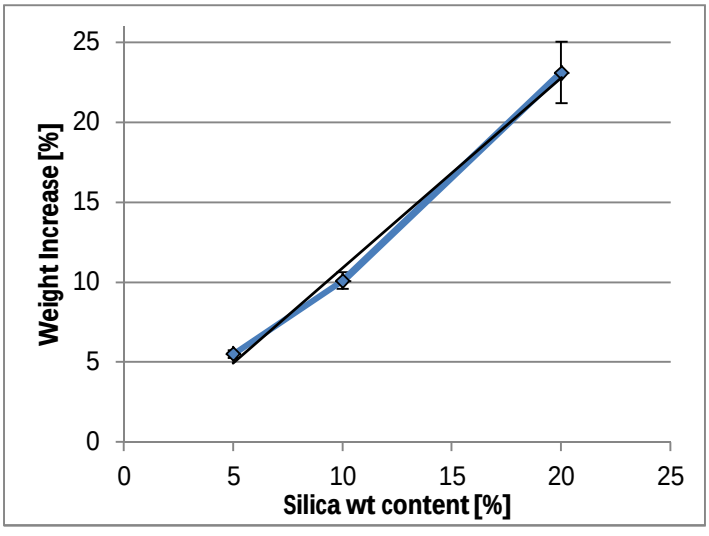

Figure 51 - silica percentage versus weight increase

Figure 51 represents the relationship between weight variation and silica loading percentages (5%, 10% and 20% wt.) for the dry fabric treated with the SPI technique. The linear trend suggests a good consistency of the method which is characterised by low losses even with increasing nanosilica concentration.

6.1.3 Analysis of single impregnated fabrics

In order to evaluate the effectiveness of the impregnation process and to investigate the geometrical dispersion of silica nanoparticles on the fabric surface, SEM and X-RAY analyses were performed on fabrics reinforced with SPI technique and a comparison was made with a neat dry fabric sample and a sample reinforced using the Roll-up technique.

Samples were cut by 1x1 cm and a rigid support was used for the analysis. Because non-conductive materials charge up when subject to the electron beam of the instrument causing errors in the visualization, samples were coated with a thin gold layer using a low vacuum sputter. The coating prevents the accumulation of charges during the electron irradiation and increases backscattering and secondary electrons emission in the proximity of the surface, resulting in a better resolution of the acquired images.

Images were taken at x100, x370 and x2200 magnifications for neat and roll-up samples, while for the SPI ones a further magnification of x7500 was used in order to better analyse the interphase between silica nanoparticles and the surface of the microscaled carbon fibres (Figure 52,Figure 53 and Figure 54).

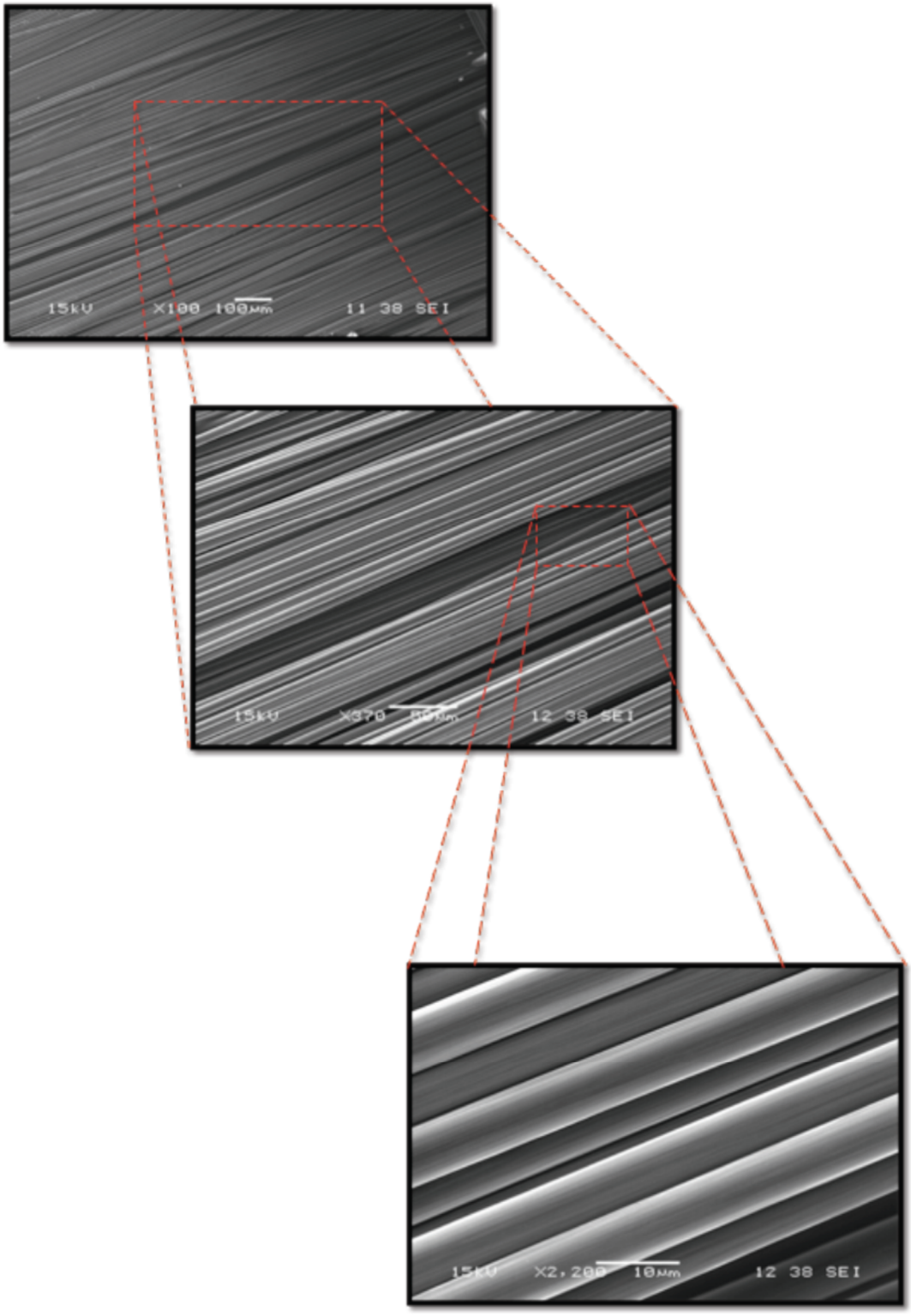

Figure 52 - SEM images of neat carbon fabric sample

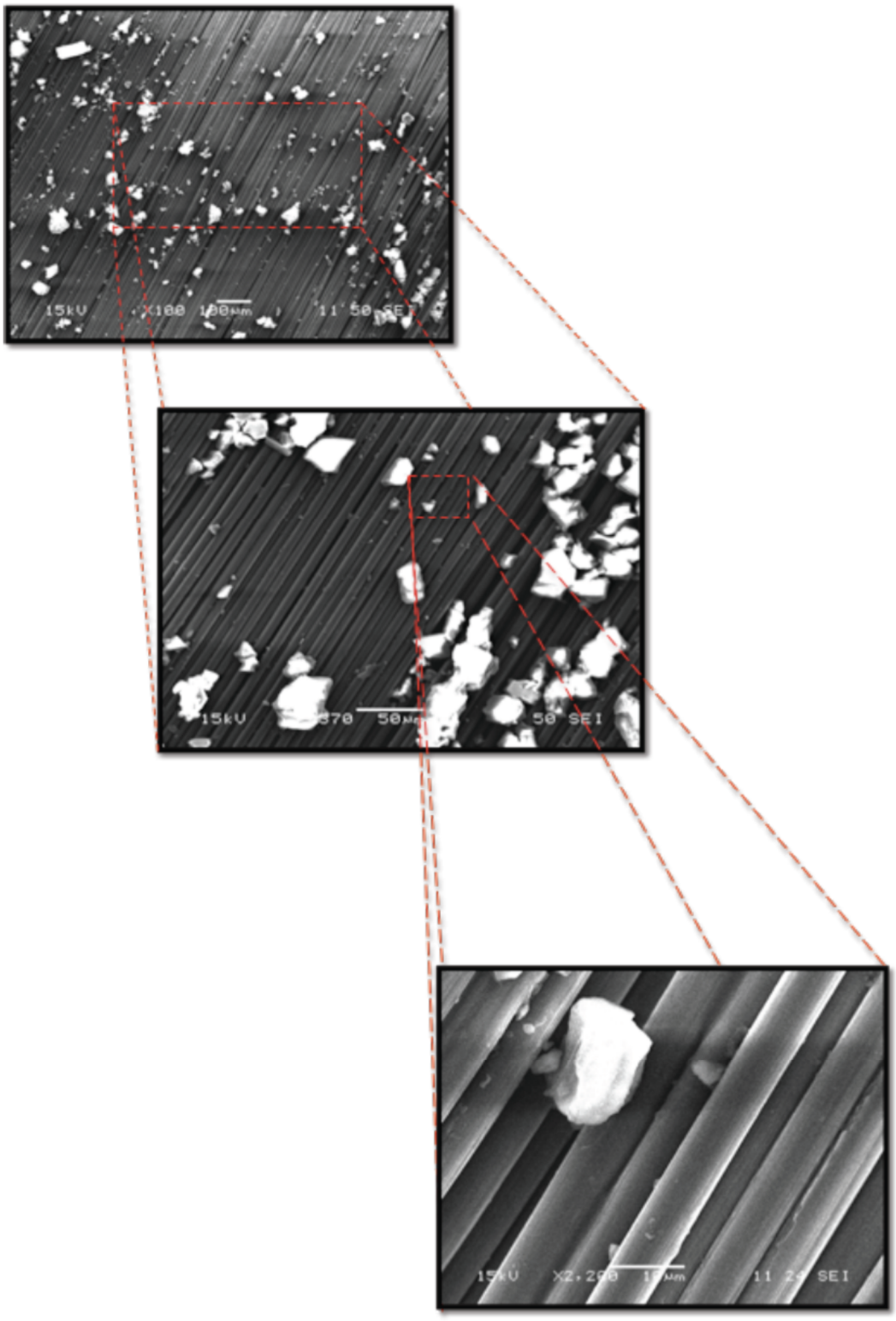

Figure 53 - SEM images of rolled-up sample

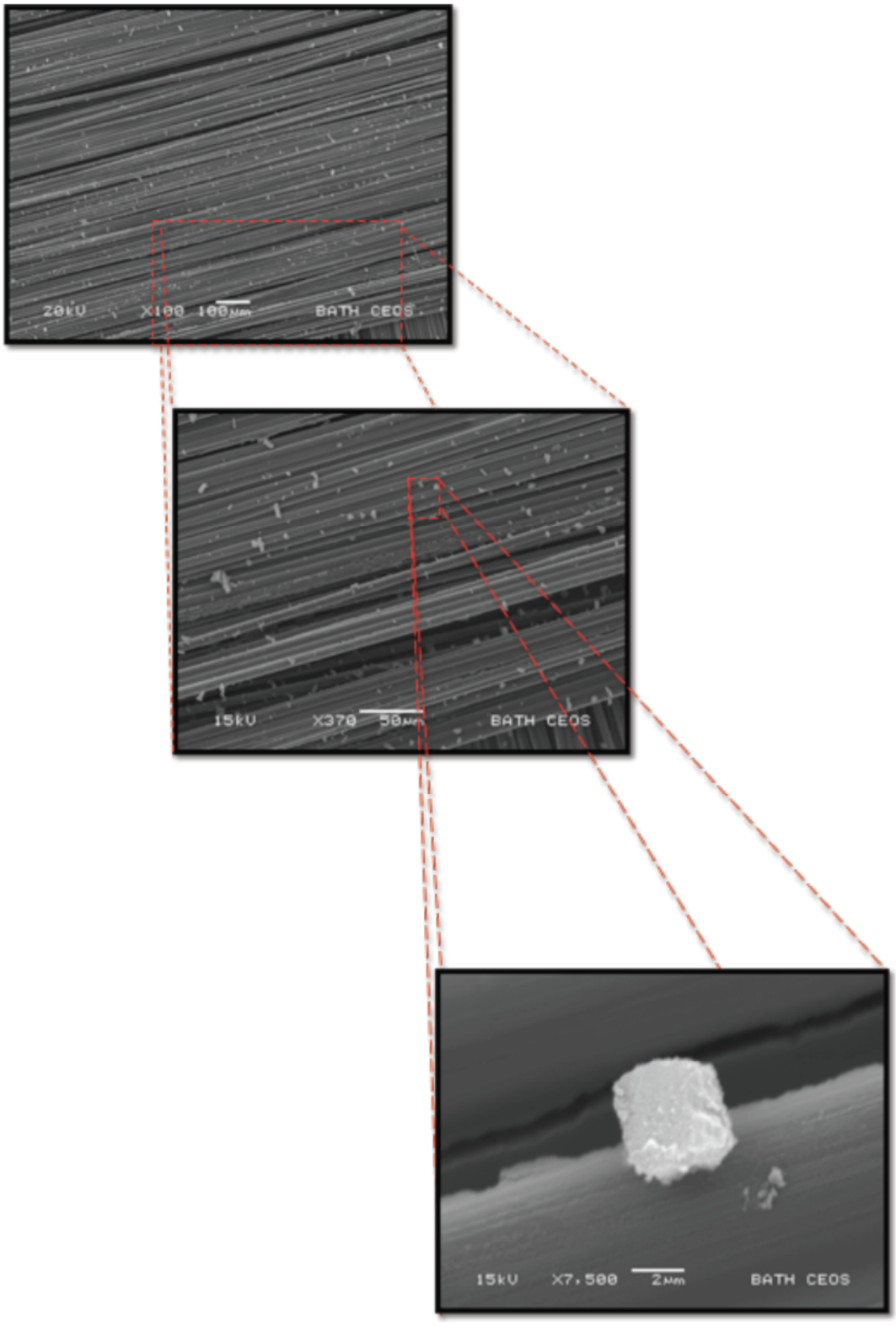

Figure 54 - SEM images of fabric treated with SPI technique

As it is possible to observe from the images, the samples impregnated using the SPI technique present better results than the sample subjected to Roll-up process, providing a more uniform nanoparticles distribution with a smaller presence of agglomerates. Therefore, more images of SPI samples were taken at higher magnitudes (see Figure 55), in order to analyse more in depth the geometry, distribution and shape of the silica nanoparticles.

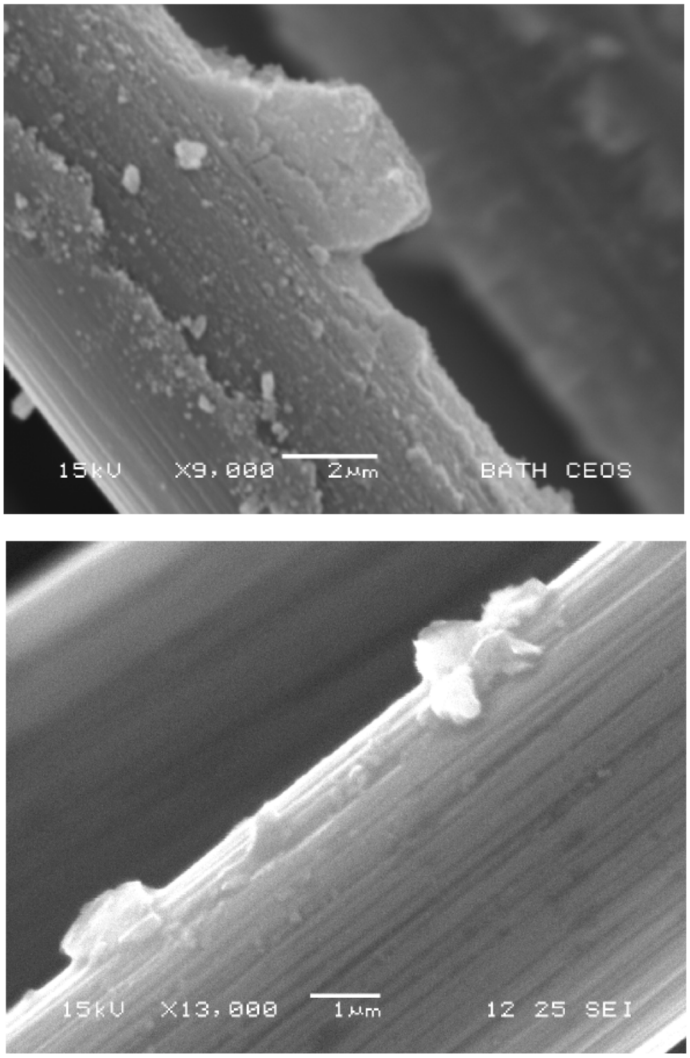

Figure 55 - agglomerates and nanometric particles on the fibres after impregnation

Examining the images it is possible to observe a quite uniform distribution of the SiO_2 nanoparticles all over the sample, showing a good disposition along the entire length of the carbon fibres (although there is a certain adhesion preference on the fabric side

that was directly in front of the spray head). Small presence of micrometric agglomerate has been detected also on SPI samples, although in modest quantity.

To investigate more in depth the spatial distribution and the granulometry of the nanoscaled silica particles, further analyses were conducted on the impregnated layers. In particular, samples impregnated with SPI and Roll techniques were scanned with a SEM elemental analysis (Oxford INCA X-Act SDD x-ray detector) in order to map all the elements on their surfaces and have a better understanding of the impregnation phenomena.

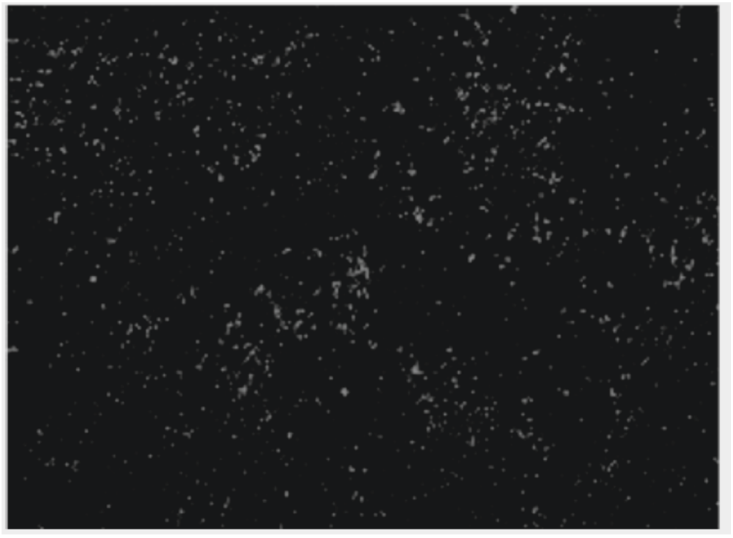

a)

b)

Figure 56 – Silica XRAY mapping for (a) rolled-up sample and (b) pressured sample

Results from the X-Ray analysis are shown in Figure 56 and give a further prove of the findings obtained with the SEM analysis. Indeed, observing the images the difference between the two samples in terms of granulometry is pretty clear. In particular, on the samples subjected to Roll-up process (Figure 56) it is possible to observe several areas of the fabric which are completely clean and the presence of big agglomerates all over the surface. On the other side, on the SPI sample (Figure 56b) SiO_2 nanoparticles are distributed evenly on the entire area and agglomerates are just few and characterised by smaller dimensions.

6.1.4 Composite manufacturing

Based on the results obtained by the single fabric analyses the SPI technique was chosen as production method to dope the carbon fabric with the nanofiller, hence several composite plates were manufactured in order to proceed with mechanical characterisation. Laminates were prepared with a stacking sequence of 8 plies, reinforced with silica percentages from 5 to 20 wt. % and the content of fibres of the finite parts was around 60%.

Note: In a second phase of the project, others plates were manufactured, using fabrics impregnated with both calendering and SPI techniques for further testing.

Figure 57 - Laminates produced for mechanical characterisation

LAMINATE LABEL	*IMPREGNATION TECNIQUE*	*SILICA AMOUNT*
A - 8NEAT	-	none
B - 8NEAT	-	none
5S	spray pressured	5% wt
10S	spray pressured	10% wt
20S	spray pressured	20% wt
5B	calendering	5% wt
10B	calendering	10% wt

Table 2 - Laminates produced during the experimental campaign

Table 2 summarizes the laminates produced during the project, while the Figure 57 represents one of the finite laminates obtained after the curing process in autoclave.

6.1.4.1 Layup and Vacuum Bagging

As we mentioned before, RFI method was chosen for samples manufacturing, in order to force the resin to flow principally through the thickness of the laminate and to simplify the entire infusion procedure.

The manufacturing procedure can be outlined as follows:

1) Measurement, cut and preparation of both dry carbon fabric and resin film layers


(a)
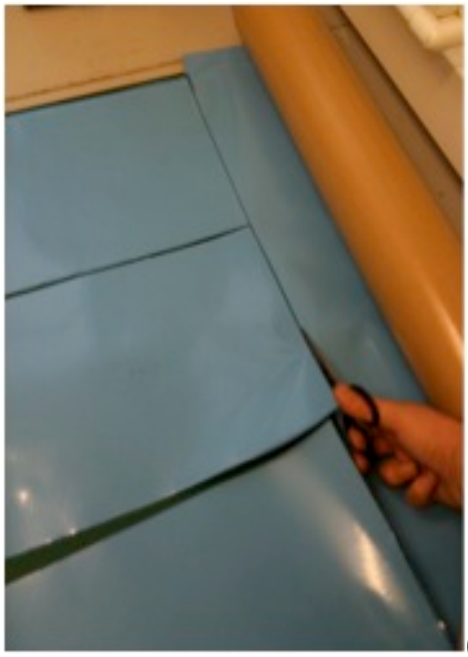
(b)

Figure 58 – Samples manufacturing procedure**:** (a) fabric used for laminates manufacturing, (b) resin film cutting

2) Impregnation process of the carbon fabrics

3) Application of release film layer (PTFE) on the top surface of the autoclave table in order to avoid undesired adhesion between the laminate and the top surface of the autoclave tool.

4) Positioning of the first resin film sheet and lay-up of a fabric ply on its top. Afterwards the procedure is repeated, alternating resin and fabric layers, until the required final thickness is reached.

5) Preparation of the different layers required for the vacuum bag (perforated PTFE, peel-ply film, breather – see Figure 59 for a complete scheme).

6) Connect the valves on the top of the bag and compact the laminate applying vacuum.

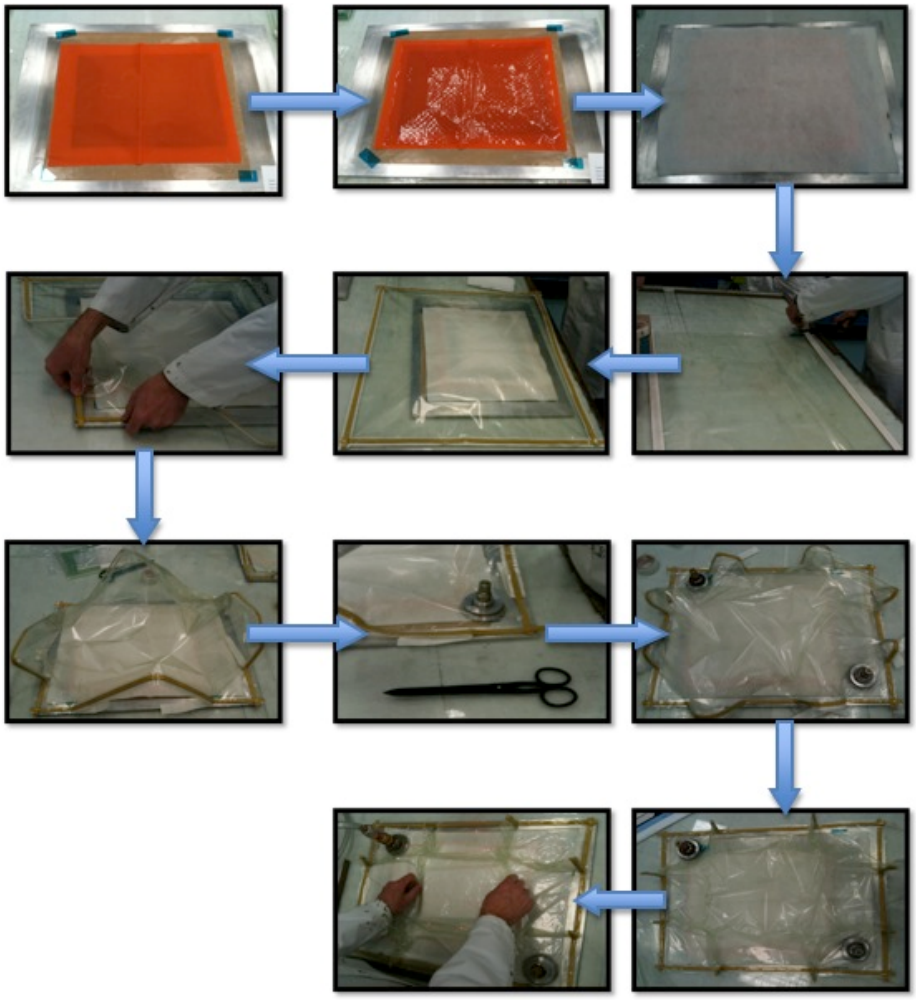

Figure 59 - vacuum bagging procedure: peel-ply positioning, perforated release film, breather, bag preparation, bag positioning on the tool, crinkles formation, valves positioning

7) Once the laminate is under vacuum and all the leaks have been removed compacting the tacky tape on the edges of the bag, the pump is removed and the bag is tested for 3 minutes to check sealing efficiency.

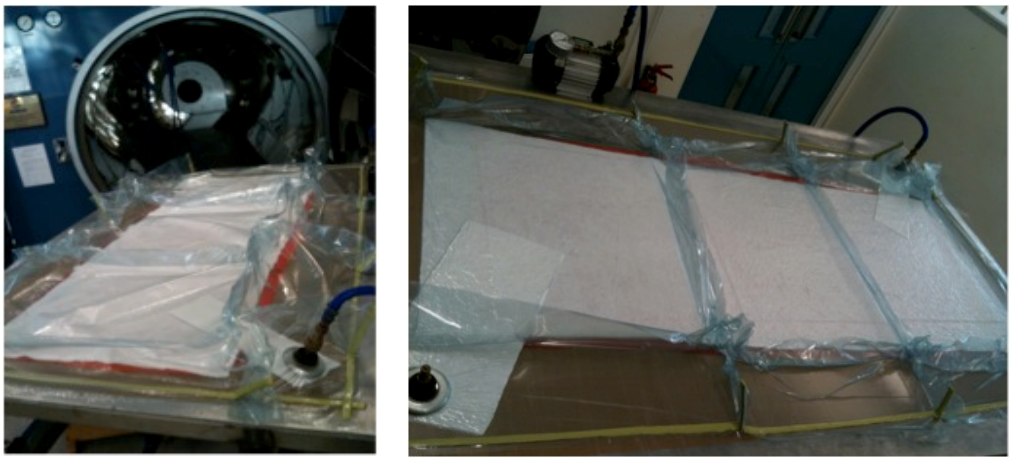

Figure 60 - Samples under vacuum and ready for autoclave curing

In order to activate the resin curing reaction of the thermoset resin, the autoclave was heated up to 100 ºC with a rate of 2 ºC/min. Once the curing temperature was reached, samples were kept at 5 bars for 2 hours to complete the polymerisation and then cooled down to room temperature with a rate of 3 ºC/min.

The relative position of the nanoscaled reinforcement was analysed again with SEM and X-Ray analyses after the curing process to determine the modification induced by the resin flow during the autoclave process. Results show that silica nanoparticles are not removed by the resin flow but, on the contrary, they are complitely intercalated among the yarns, coating all the fibres in a threedimensional disposition (see Figure 61).

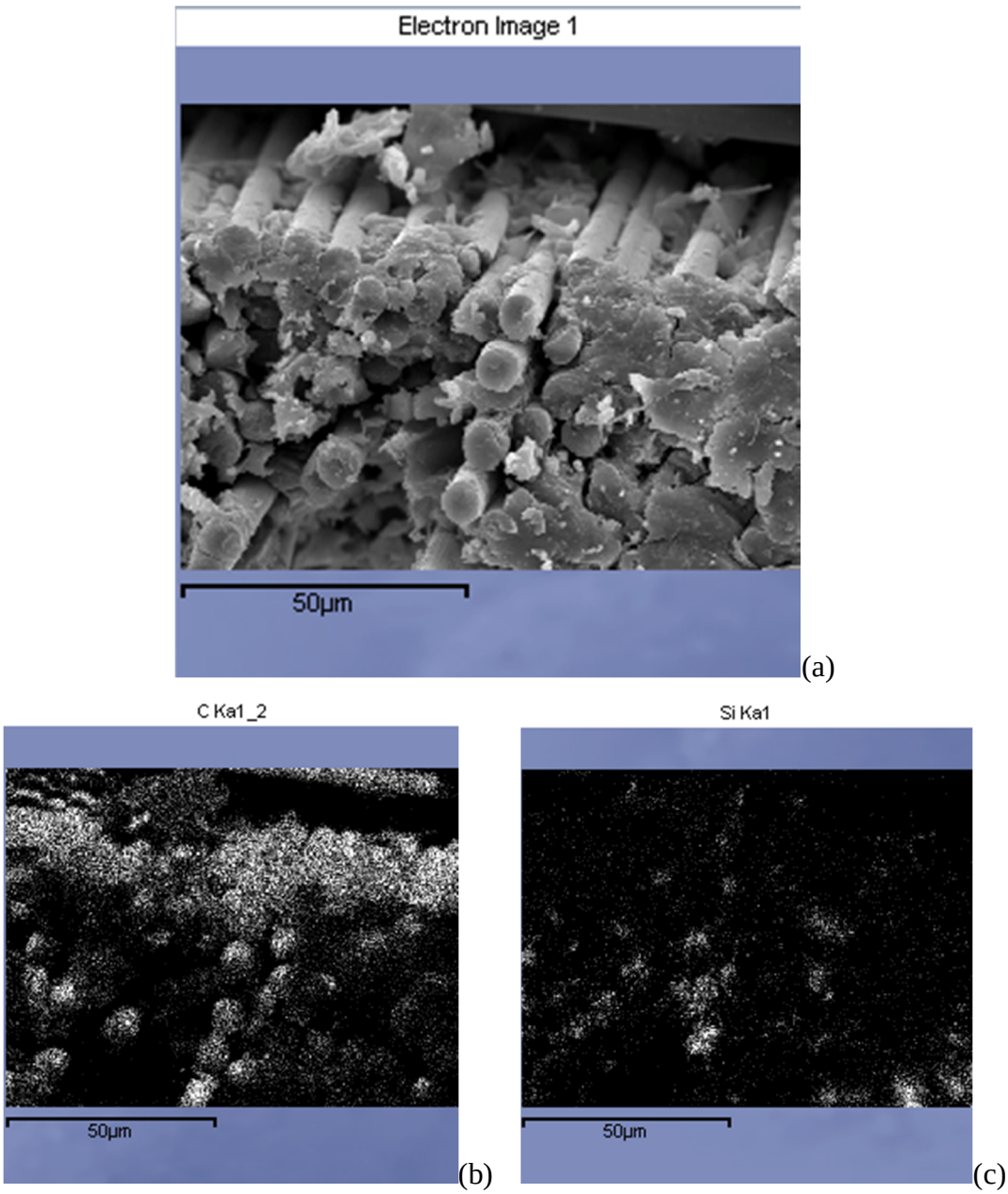

Figure 61 – Post-cure inspection: (a) SEM analysis of the triphasic system, (b) and (c) XRAY mapping of silicium and carbon elements

6.2 Composite Mechanical Characterisation

The effects of the nanoparticles inclusion have been analysed by carrying out a complete experimental campaign aimed to investigate several aspects of mechanical behaviour of the threephasic multiscaled composite. In particular multiscaled samples were subjected to the following tests:

- **Three-point bending** (*flexural behaviour*)
- **Tensile test** (*elastic behaviour*)
- **DMA** (*thermo-mechanic behaviour*)

6.2.1 Three Point Bending Test

Three-point bending tests were conducted on an Instron Universal Tester 3369 on several hybridised samples to analyse the effect of the nanoscaled inclusion on the flexural behaviour of the multiscaled composite. The applied load is measured by a load cell mounted between the specimen and the crosshead by converting forces into electrical signals that can be subsequently processed by the control system.

Samples were dimensioned according to ASTM D790 (Figure 62) from 8 plies plates with 60% of fibres content and with layers impregnated with a percentage of silica from 5 wt. % to 20 wt. % (labelled laminate 5S, 10S and 20S respectively). Results obtained from the tests were compared with a traditional CFRP, characterised by an equal content of fibres and obtained with the same lay-up sequence (labelled C8N).

Figure 62 - Samples prepared for three point bending test

Table 3 below shows samples dimensions and the span length, calculated by imposing a ratio of 1:60 with the thickness, while the results of the tests are illustrated in Figure

63, which represents *load* versus *flexural extension* curves for the multiscaled samples and the un-reinforced ones.

SAMPLE ID	*length [mm]*	*width [mm]*	*thickness [mm]*	*span [mm]*
C8N-1	80.53	13.75	0.86	52
C8N-2	80.31	12.7	0.99	59
C8N-3	79.92	13.14	1.12	67
M5S-1	79.63	12.93	0.78	47
M5S-2	79.41	13.02	0.75	45
M5S-1	80.74	13.05	0.77	46
M10S-1	76.89	13.55	0.79	47
M10S-2	80.59	13.56	0.82	49
M10S-3	79.7	13.25	0.8	48
M10S-4	79.49	13.38	0.81	49
M20S-1	79.96	13.55	0.86	52
M20S-2	80.08	13.62	0.87	52
M20S-3	80.63	13.52	0.85	51

Table 3 - Samples dimensions

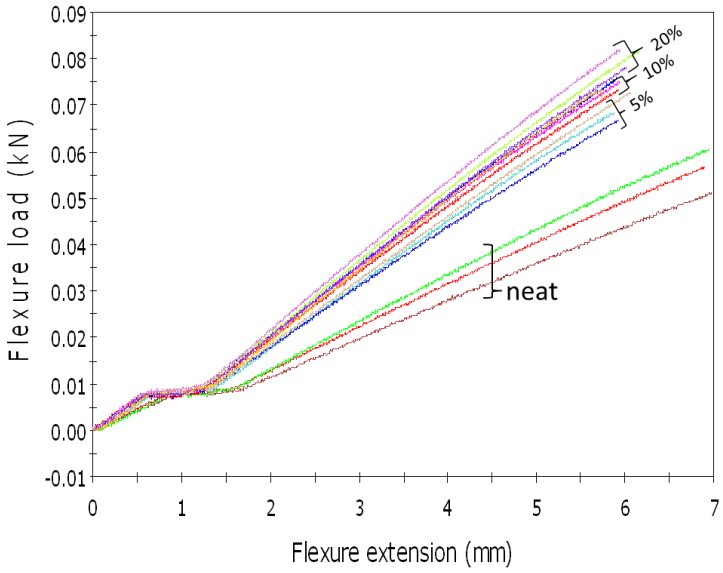

Figure 63 - Load/displacement curves for NEAT and silica-doped samples

Once the curves were obtained by the instrumentation, Bending Modulus was calculated according to the equation below:

$$E_b = \frac{S^3 m}{4bh^3}$$

Where *S* represents the span lenght, *m* is the slope of the load/extension cruve, whilst *b* and *h* are the width and thickness of the specimen, respectively.

6.2.1.1 Results And Discussion

Data obtained from three point bending tests are reported in Table 4 below, while the results are shown in Figure 64.

SAMPLE ID	*Silica Content in fabric [wt. %]*	*Eb [MpA]*	*Average*	*Standard Deviation*	*Bending Modulus Enhancement [%]*
C8N-1	0	40787.57			
C8N-2	0	41098.72	38721.78	3144.052	0
C8N-3	0	34279.05			
M5S-1	5	56484.75			
M5S-2	5	59400	58083.42333	1206.746	50.00195
M5S-1	5	58365.52			
M10S-1	10	60087.34			
M10S-2	10	57463.8	58704.875	943.1983	51.60686
M10S-3	10	58854.43			
M10S-4	10	58413.93			
M20S-1	20	62569.59			
M20S-2	20	60387.19	62348.8	1519.552	61.01739
M20S-3	20	64089.62			

Table 4 - Results obtained from three point bending test

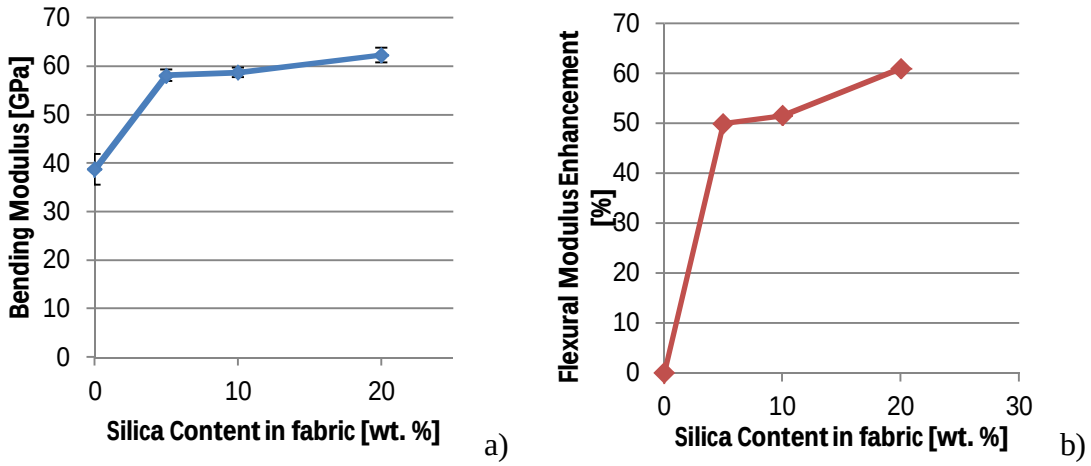

Figure 64 - Three Point Bending results: a) Bending modulus for multiscaled composite with increasing nanosilica content; b) modulus enhancement

Analysing the results it is possible to conclude that:

- Multiscaled composite samples made with fabrics impregnated with silica nanoparticles exhibit higher Bending module in comparison with traditional laminates (see Figure 64a).

- samples prepared with fabrics impregnated with 5% wt. silica nanoparticles show an increase of almost 50% of bending modulus (see Figure 64b).

- increasing the percentage of nanoparticles within the composite from 5 to 20 wt. % leads to just small enhancement of bending modulus (see Figure 64b).

This reinforcing effect of the nanomodified composite could be explained with crack pinning and crack deflection mechanisms [48]. Moreover, the reciprocal sliding of the different layers is impeded by the presence of the nanoscaled phase, leading to an increase of the flexural modulus. However, for samples with higher nanosilica contents, the presence of agglomerates characterised by larger dimensions all over the fabrics surfaces results in the formation of larger discontinuities within the structure, weakening the composite and hindering further enhancements of the mechanical properties.

6.2.2 Tensile Test

Samples for tensile test were prepared according to ASTM D638 (Figure 65), using laminates obtained with fabrics impregnated with 5 wt.% and 10 wt. % of silica nanoparticles and a comparison was made with a traditional unreinforced laminate obtained with the same layup procedure and manufacturing technique.

Figure 65 – Samples prepared for tensile test

By following the regulation mentioned above, aluminium tabs were cut in order to increase samples grip between the clamps and they were attached to the specimens using a bi-component resin (50 gr Araldite + 7,5% wt. hardener). Both multiscaled and traditional laminate samples were hold under pression for 24 hours in order to have a complete solidification of the resin (see Figure 66).

Figure 66 - Tabs attached on samples

Test were conducted on the same Instron Universal Tester 3369 used for Three-point bending test.

6.2.2.1 Results And Discussion

Force/displacement curves obtained from the instrumentation were stored and the values of stress and strain were calculated by dividing the load by the samples section and the displacement by the initial free length of each sample. Figure 67 illustrates the resulting stress/strain curves for the multiscaled composites and the traditional laminate, while Figure 68 a and b show the effect of the nanoscaled inclusion on the Young's Modulus of the composite (see Table 5).

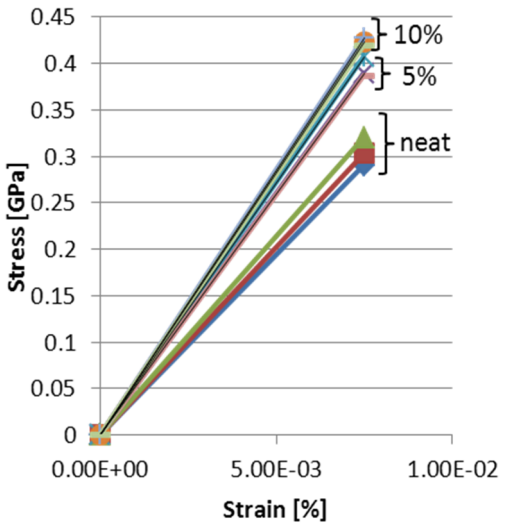

Figure 67 - stress/strain curves for nanosilica reinforced multiscaled samples and traditional laminates

Sample ID	*Young's Modulus*	*Average*	*Standard Deviation*
8N-1	37.77		
8N-2	39.49	39.57	1.50342
8N-3	41.45		
M5S-1	56.808		
M5S-2	51.49	52.734	2.95262
M5S-1	49.904		
M10S-1	55.73		
M10S-2	51.413	53.568	1.76241
M10S-3	53.561		

Table 5 - Young's modulus evaluation

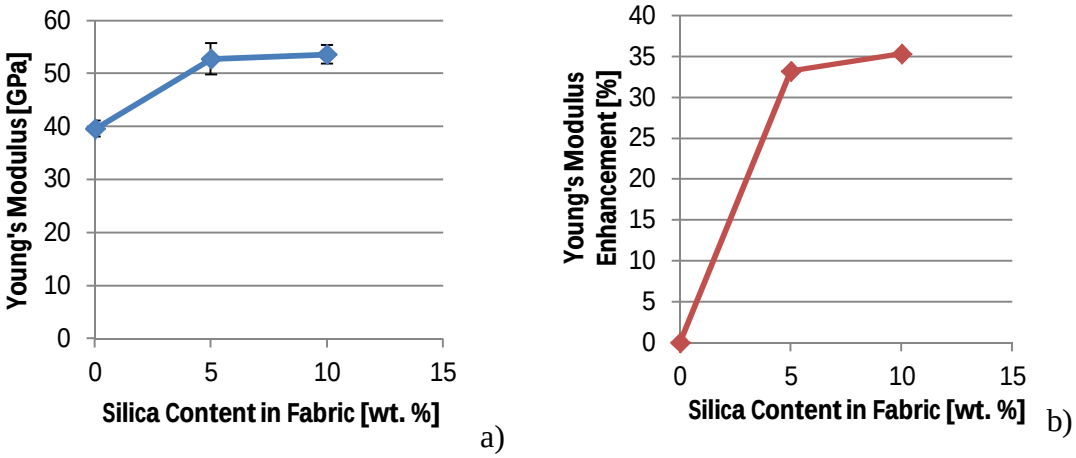

Figure 68 –Tensile Test results: a) Young's modulus for multiscaled composite with increasing nanosilica content; b) effect of nanosized filler on the Young's Modulus

The results can be sumarized as follows:

- The presence of the embedded nanosilica particles within the composite structure enhances mechanical properties of CFRP, increasing the stiffness of the composite as it was recorded for the three-point bending test. Indeed, the same trend observed for the Bending Modulus can be seen again analysing the behaviour of the Young's Modulus for samples with an increased content of nanoparticles.

- Young's Modulus is enhanced from neat samples to 5% impregnated ones, increasing its value by 32% (see Figure 68b).

- For samples with higher concentration of nanosilica, the improvement in elastic Modulus is much lower, passing from 32, to only 5% (see Figure 68b).

Young's Modulus trend can be explained with the interactions between the two species of reinforcements included in the material structure, which activates what have been previously called nanoeffects (see Section 4.1.4). Indeed, considering the same composite weight, reducing the dimensions of the particles involves an higher contact area between them and the other phases, which prevents fibres pull-out and, consequently, leads to a toughened material characterised by higer values of stiffness.

6.2.3 Dynamic Mechanical Analysis

In order to investigate the effects of the nanofillers on the thermomechanical properties of the composite, Dynamic Mechanical Analysis (DMA) was undertaken on sample laminates with an increasing presence of SiO_2 nanoparticles, comparing the results with a traditional unreinforced laminate.

Samples were dimensioned from 8 plies plates with 60% of fibres content and with layers impregnated with a percentage of silica of 5 wt. % and 10 wt. % (5S and 10S laminates). Further analyses were conducted with samples made with calendering-impregnated fabrics (labelled 5C and 10C).


a)
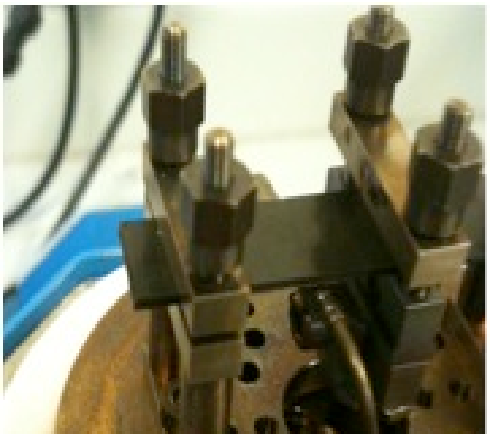
b)

Figure 69 - *DMA test equipment: a) the instrumentation used for the test campaign; b) detail of the experimental setup*

Tests were conducted in three-point-bending mode with a frequency of 1 Hz, with a temperature sweep from room temperature to to 140 °C using a 2°C/min ramp.

6.2.3.1 Results And Discussion

Data results are illustrated in the graphs below:

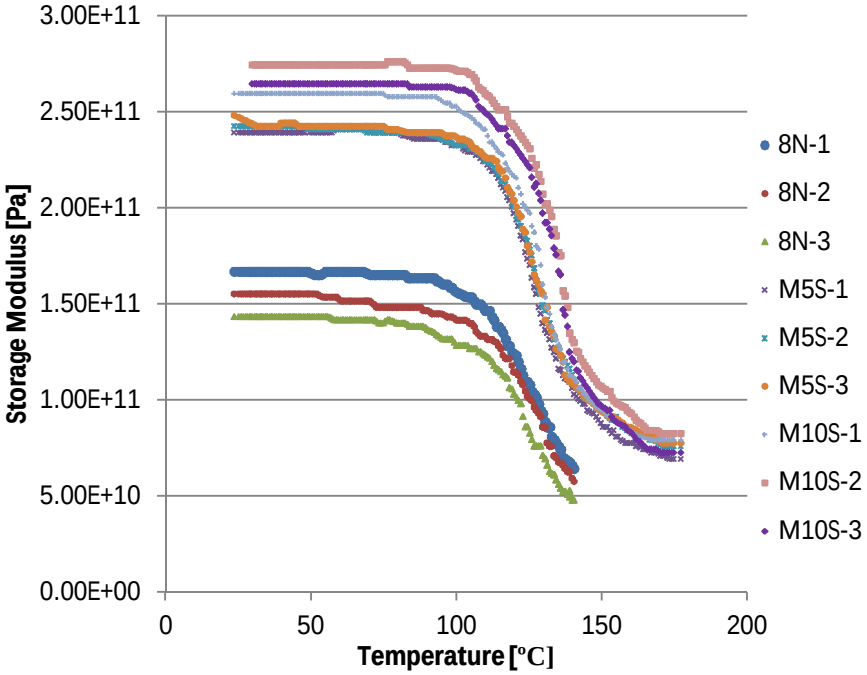

Figure 70 - *DMA analysis: Storage Modulus Behaviour for silica based multiscaled nanocomposites and traditional microscaled laminates*

Figure 70 shows the temperature dependence of Storage Modulus for samples doped with different percentage of nanosilica in comparison with traditional laminates. Storage Modulus appears to be affected by the presence of the silica nanofiller in the glassy and rubbery regions and all the curves show the characteristic drop in modulus that corresponds to the glass transition temperature of the material. Analysing the results, it is possible to observe a 60% increase of the Storage Modulus in the passage between neat sample and 5 wt. % one, while increasing the nanoparticles content within the fabrics, this increment becomes smaller (~15%) (see Figure 72a). Similar results have been found in literature for silica based nanocomposites [160].

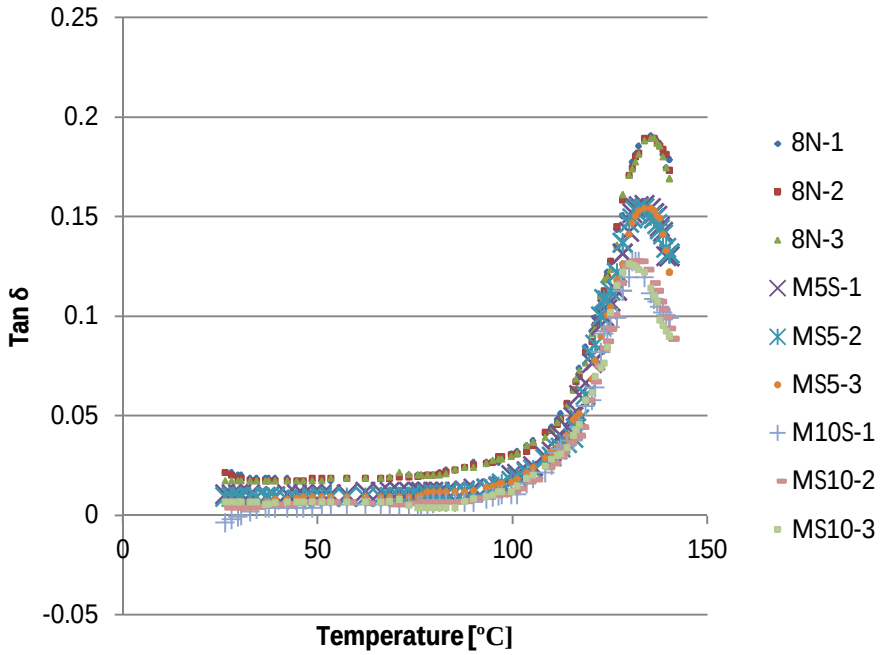

Figure 71 - *DMA analysis: Tan δ behaviour for silica based multiscaled nanocomposites and traditional microscaled laminates*

The second image (see Figure 71) illustrates tan δ values for the samples tested and depicts clearly that embedding the nanoparticles within the dry carbon fabrics affects the damping properties of the material, decreasing it from 0,2 to 0,15 (-30%), thus reducing the energy dissipation rate for the multiscaled composites (Figure 72b).

SAMPLE ID	*STORAGE MODULUS [Pa]*	*AVERAGE*	*STANDARD DEVIATION*	*tan delta*	*AVERAGE*	*STANDARD DEVIATION*
8N-1	1.67E+11			0.1909		
8N-2	1.55E+11	1.551E+11	1.18E+10	0.1895	0.19	8E-04
8N-3	1.43E+11			0.1895		
M5S-1	2.39E+11			0.1559		
M5S-2	2.43E+11	2.416E+11	1.946E+09	0.1546	0.1551	7E-04
M5S-1	2.43E+11			0.1549		
M10S-1	2.6E+11			0.1277		
M10S-2	2.75E+11	2.663E+11	7.711E+09	0.1287	0.1276	0.001
M10S-3	2.65E+11			0.1263		

Table 6 - Results obtained from DMA test

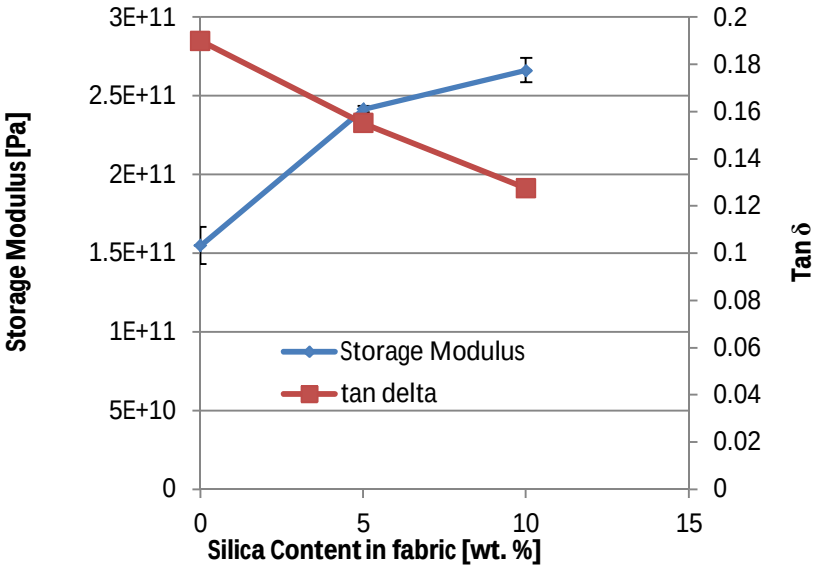

a)

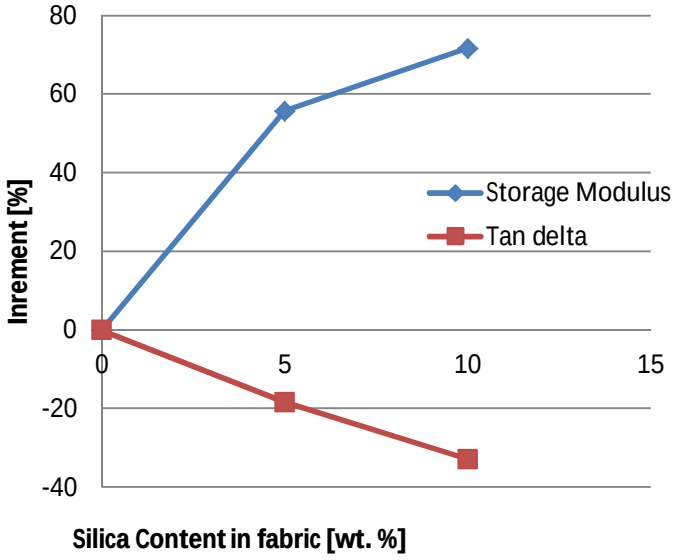

b)

Figure 72 - Tensile Test results: a) Storage Modulus and Tan delta for multiscaled composite with increasing nanosilica content; b) effect of nanosized filler on Storage Modulus and Tan delta

According to theoretical model [161], the damping behaviour of filled polymers is affected by the presence of the filler, as shown in the following equation:

$$\tan \delta_m = \tan \delta_s \cdot (1 - \varphi_{SIO_2})$$

where φ_{SIO2} represents the volume fraction of silica nanoparticles within the composite, while tan δ_m and tan δ_s are the damping factor of the multiscaled composite and the traditional laminate, respectively. This behaviour can be interpreted as a result of interfacial interaction between the silica nanoparticles and the thermoset resin which can hinder the energy dissipation of the polymeric chains [162]. The small differences between the experimental results and the theoretical model shown in Figure 73 are related to the experimental uncertainties associated to the resin amount in composites obtained with RFI technique (±5%).

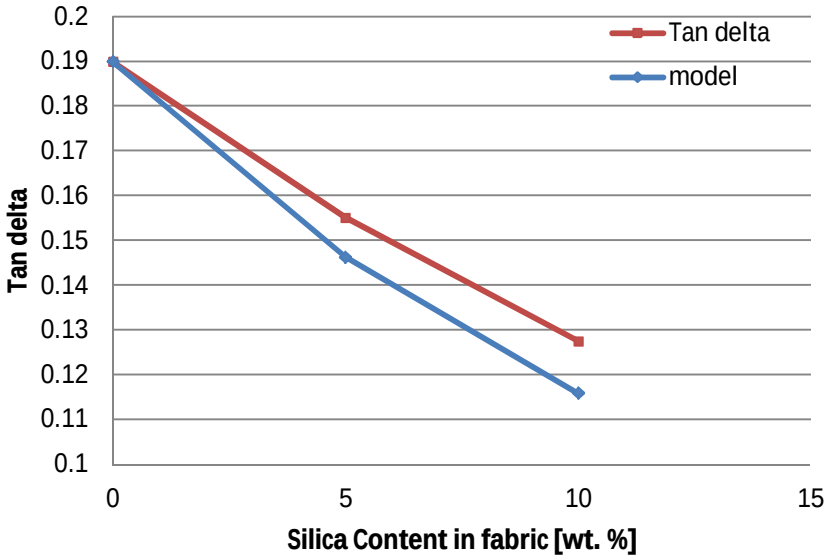

Figure 73 - Comparison between experimental results and theoretical model for tan delta depression due to increasing nanofiller content

Storage Modulus and tan δ curves are also able to provide some information regarding the behaviour of the glass transition temperature of the multiscaled composite. Indeed, it seems to be a slight increase in Tg (~5 ºC) for the nanoscaled composites that could result from the presence of silica nanoparticles within the cross-linked network of the thermoset resin. Indeed, due to their small dimensions, nanofillers could be able to decrease the segmental motion and hinder large scale movements of the polymer chains resulting in a slight increase of the glass transition temperature of the composite [160].

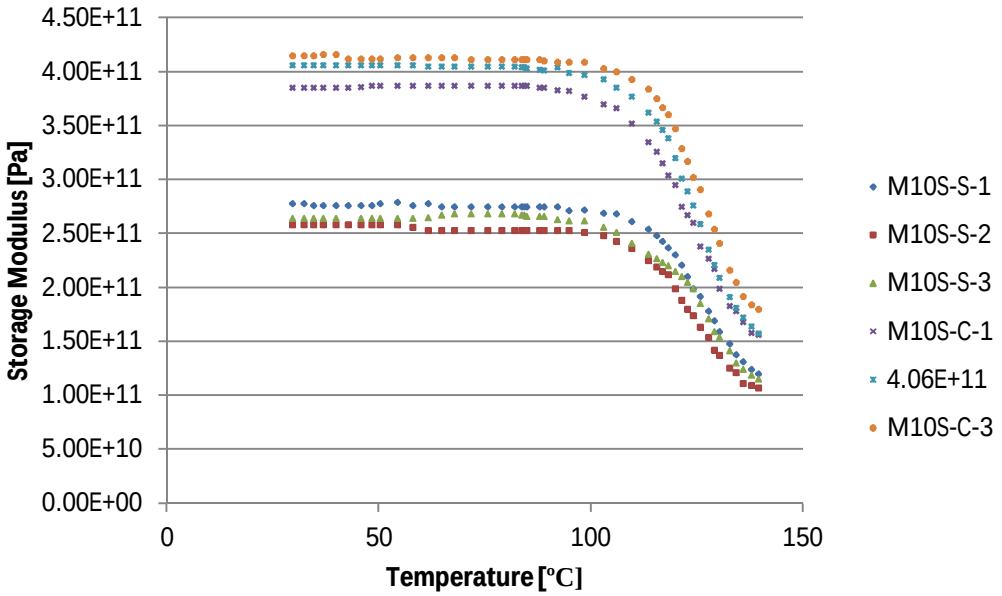

Figure 74 – Storage Modulus behaviour: Comparison between SPI technique and calendering

The last result was giving when two different impregnation techniques were compared in terms of reinforcing effecs. Indeed, the curves illustrated in Figure 74 represent the storage modulus for samples obtained SPI and calendering processes. Looking more in the depth the different curves, it is possible to state that the calendering sample is the most efficient technique in terms of thougening effect for nanoscaled composites.

6.2.4 Indentation and Hardness Test

Hardness tests were carried out under a load of 300g using a calibrated Leco M-400 hardness indentation machine. In order to analyse how the presence of the SiO_2 nanoparticles affects the hardness properties of the resulting composite, test were conducted on resin-embedded samples in both parallel and perpendicular direction.

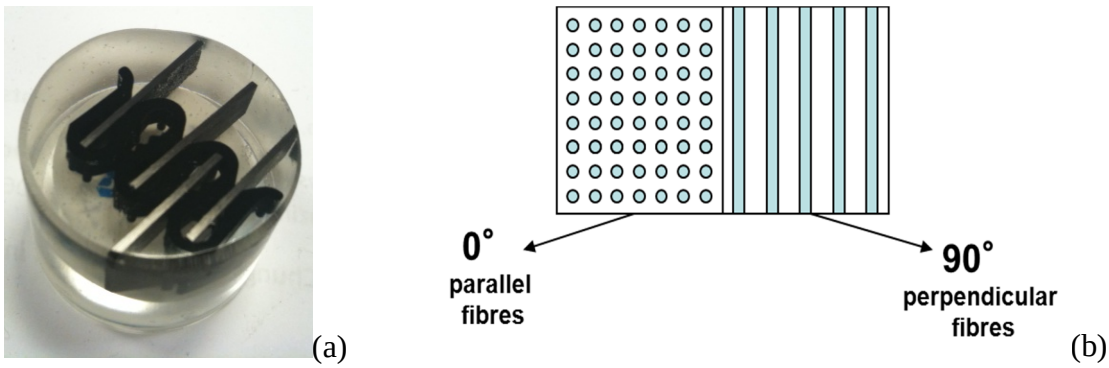

(a) (b)

Figure 75 - a) hardness test sample; b) sample's geometry

As it is possible to observe from Figure 76a, the presence of SiO_2 has an overall strengthening effect on the carbon fibres. However, analysing the difference between the indents produced on areas characterised by the presence of 0 or 90 degrees fibres, it is clear that the perpendicular fibres are more affected by the nanoparticles, with a decrease of more than 20 wt. % in the indent dimensions. As for the parallel fibres, the silica still produces a decrease of the indent but only by ~5%. The same trend is observed in figure, which represents the variation of Vickers Hardness for both perpendicular and parallel fibres characterised with an increased percentage of SiO2 nanoparticles (see Figure 76b).

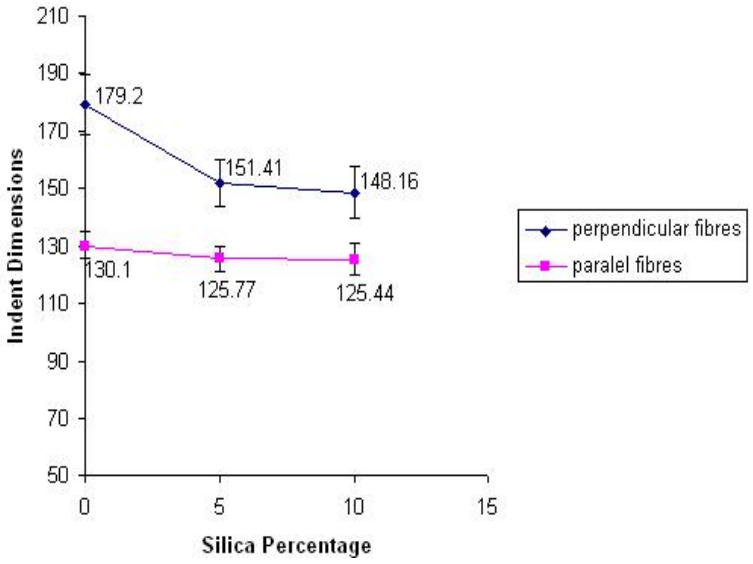

a)

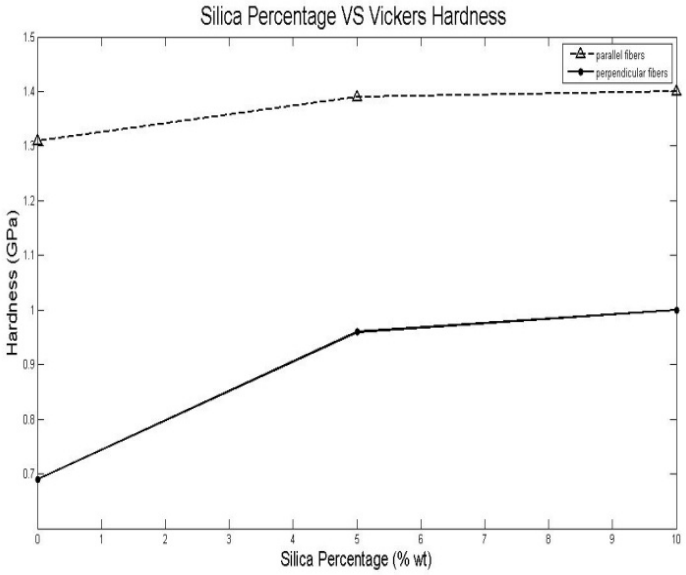

b)

Figure 76 - Hardness Test Results: a) Indent dimensions variations, b) Vickers number behaviour with increasing concentration of SiO2 nanoparticles

This result confirms what observed during the other tests, showing a strengthening effect for nanoreinforced samples due to the presence of the silica nanoparticles. Because of the reciprocal orientation of the fibres, this effect is more evident on the perpendicular fibres.

6.3 CNT hybridisation of nanoreinforced carbon fabric

As seen in Section 4.2, several non-structural properties can be included into multifunctional systems by growing carbon nanotubes on the surface of traditional microscaled composites. Another important property of the nanoreinforced fabrics developed for this work is that silica nanoparticles can be used as support in a chemical vapour deposition (CVD) process for growing CNTs directly on the surface of the fabric instead of using rigid silicon substrates. The CVD process is based on the decomposition of carbon-containing organometallic compounds, which produces the carbon atoms required to grow graphitic structures such as carbon nanotubes. It is reported in literature that silicon dioxide (SiO_2) can be used as a substrate for substrate-dependent site-selective growth of CNTs, eliminating the need for the traditional deposition of metal catalysts patterns used to activate selective nanotubes growth [163-165]. Following the same procedure, in our case it is possible to obtain

multiscaled reinforced dry fabrics in which the microscaled carbon fibres are first reinforced with silica nanoparticles and then subjected to a CVD process which induces the formation of carbon nanotubes on the nanofillers, generating a complex multiscaled structure that can be used subsequently as a preform in a traditional Resin Infusion process, or to create CNT/SiO_2 hybridised prepregs (see Figure 77).

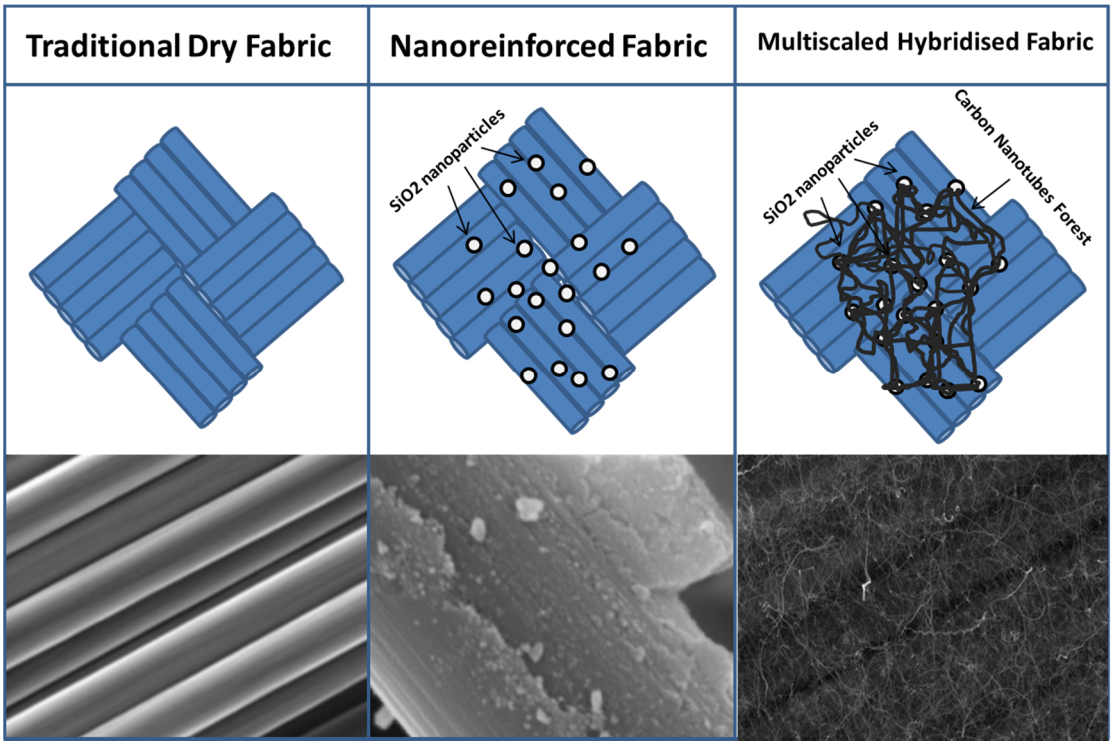

Figure 77 - schematics of the reinforcement procedure of a multiscaled hybridised fabric

In order to analyse the feasability of the nanofiller included within the impregnated carbon fabric to act as a substrate, CNTs were grown via CVD using ferrocene as carbon source. The samples were heated up to 900 ºC and the gas flow was directed on the surface of several fabrics characterised by an increasing content of SiO2. The results were analysed through SEM to investigate the dimension and distribution of CNTs. It is important to underline that the temperatures used during the CVS are high enough to completely remove the binder from the surface of the fabric making it difficult to handle similarly to what reported previously for the ethylene glycol impregnation. However, because of the small dimensions of the samples and due to

presence of the entangled CNTs sponge between the fibres, the fabrics kept their integrity after the CVD process and were rigid enough to be tested and handled.

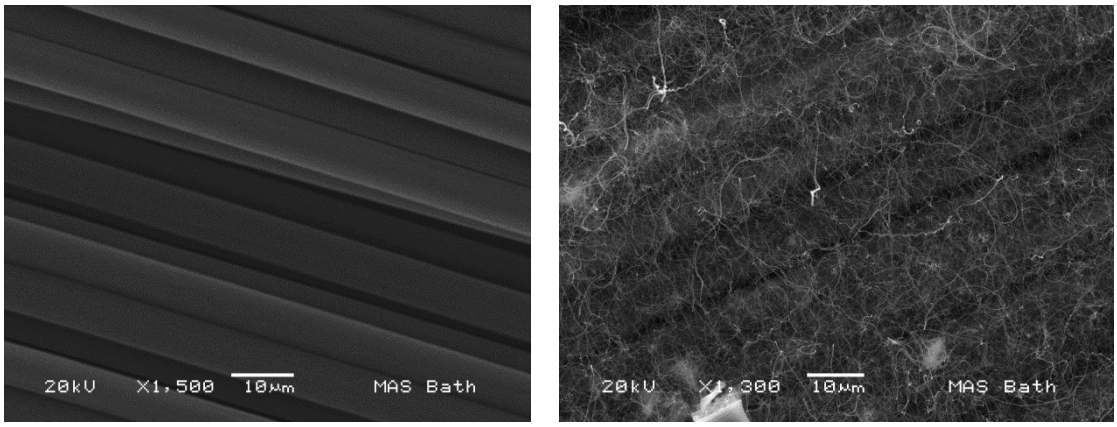

Figure 78 - CVD results on carbon fabric: a) dry unreinforced fabric; b) CNT growing on nanosilica substrate

Figure 78 shows a comparison between the unreinforced carbon fabric and the nanomodified one. As it is possible to see from Figure 78a, neat fibres does not provide any growing point for nanotubes as the metal catalyst particles cannot find an adequate substrate to support them. On the contrary, when the dry carbon fabric is impregnated with silica nanoparticles, nanotubes grow all over the fabric because of the strong interaction between the catalyst and the SiO_2 support [166], as it is possible to observe from Figure 78b. Indeed, in this case the entire fabric is completely covered by a high density Velcro-like structure made with very long carbon nanotubes (20 μm and more) characterised by a large number of entanglements.

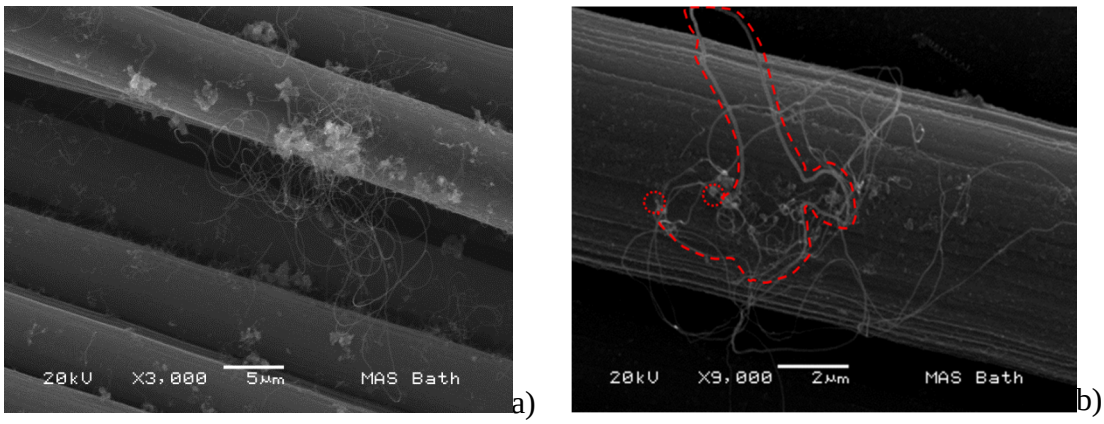

a) b)

Figure 79 - CNTs growing on SiO2 substrate: 1) closeup on a large agglomerate of silica and on the entangled CNTs forest grown from it. b) Bridging of a CNT from two different silica nanoparticles

The strict correlation between silica impregnated areas and CNTs growth can be seen on Figure 79a, which represents a close-up on a large agglomerate of silica deposited on the surface of a fibre that belongs to a discarded impregnated fabric. Indeed, while the rest of the fibre looks completely neat after the CVD, the area covered by the SiO_2 agglomerate positively influences the catalytic activity of the metal catalyst, activating the CNTs growing process. Another important finding can be observed in Figure 79b, which shows a nanotube with a length of more than 40μm that bridges two different silica nanoparticles deposited on the same microscaled carbon fibre. This mechanism can be used to create complex three-dimensional structures in which several layers of carbon fabrics are overlapped and joined together by CNTs to form a complex entangled structure that can be used as hybridised multiscaled reinforcement for composite manufacturing.

6.4 Discussion

A multiscaled composite has been manufactured, based on carbon fabric as microosized fibrous reinforcement (Oxeon TeXtreme), epoxy resin as polymeric matrix (VTM265 resin film by ACG) and nanosilica particles as nanosized filler (Sigma Aldrich).

In order to evaluate the effect given by the presence of the nanoscaled filler, an experimental campaign has been carried out, analysing the mechanical properties of the triphasic system (fibres, matrix and nanoreinforcement) in comparison with a traditional bifasic one (fibres and matrix).

The approach followed for the design of the triphasic system is different from the traditional approach used to manufacture nanocomposites. Indeed, in our novel process, the nanoscaled phase is added directly to the fibrous reinforcement via impregnation of dry carbon fabrics, while in classical methods it is added to the polymeric matrix, leading to particles agglomeration and the formation of weaker interphases.

Resulting modified fabrics were analysed via scanning electron microsope in order to examine nanoparticles granulometry, while X-RAY mapping was performed to investigate the spatial distribution of the nanoreinforcement. SPI impregnated fabrics provided the best results in terms of nanosilica spatial distribution and agglomerate formation, therefore the technique was chosen as doping method for composites manufacturing.

Eight plies laminates were obtained via vacuum-assisted resin film infusion technique, with an increasing content of nanoreinforcement and a campaign test was undertaken to investigate how the presence of a nanoscaled additional phase affects mechanical properties.

Results of mechanical tests can be summarised as follows:

- Flexural properties analysis (tested in three-point-bending mode) showed more than 50% increase in bending modulus (Eb) for 5 wt. % nanosilica composites

compared with traditional laminates. These results can be explained with crack pinning and crack defletion thoughening mechanisms which are activated due to the small dimensions of the nanoparticles.

Increasing silica content poorly affects flexural behaviour, giving a 4,5% *Eb* variation going from 5 wt. % to 20 wt. % samples, due to the presence of larger silica aglomerates.

- Tensile properties variation exhibited similar behaviour of flexural ones. Analysing the stress-strain curves of unreinforced samples in comparison with 5 wt. % samples, it is possible to observe a 31% increase of Young's Modulus, that drops to just 2% in the passage form 5 wt. % to 10 wt. % nanocomposites. This behaviour can be explained with the same toughening mechanisms previously described for flexural properties. In addition the presence of nanoparticles between the fibres, increases material pull-out resistance in the fiber direction.

- Thermomechanical analysis results showed a behaviour that is coherent with the other tests. Indeed, Storage Modulus is highly affected by the doping process, showing a 50% increase in the passage from the traditional unreiforced laminates to 5 wr. % samples, while increasing silica content, this enhacement come down to 10%. Doping process seems to modify also damping properties, decreasing tan δ from 0,2 to 0,15. Glass transition temperature seem to be slightly affected by the presence of silica nanoparticles, showing a slight increase due to the hindering od large scale movements of the polymeric chains.

- Data obtained from Hardness Test showed that the presence of the nanoscaled phase affects more the perpendicular fibres than the parallel ones. Indeed, analysing the results it is possible to observe an reduction of 20% in the dimension of the indent in the passage from the traditional unreinforced laminate to the 5wt. % nanocomposite. Same trend is observed for the calculated Vickers Hardness. Increasing the nanofiller content leads only to small enahcement of the

hardness. On the other side, results have shown that parallel fibres are not affected by the presence of the nanoparticles..

The addition of nanoparticles within the composite materials acts with two distinct mechanisms. The first effect is an increasing of the compatibility between the thermoset matrix and the carbon fibres by a modification of the roughness of the carbon surface (proved by SEM analysis and X-RAY mapping) that leads to higher mechanical properties [167]. In addition the second mechanism includes those effects (so called “nanoeffects”) that are due to the presence of nanoparticles characterised by dimensions that are on the same order of magnitude of the polymer chains gyration radius, including in-plane strengthen mechanisms such as crack pinning or bowing and crack deflection.

In conclusion, the experimental campaign, proved that by adding a nanoscaled phase in a traditional carbon fabric based laminate it is possible to toughen the material, increasing mechanical properties by almost 50% in comparison with unreinforced samples. Results from the different tests suggest the exixstence of a threshold for the content of nanofiller that it is possible to embedd within the composite structure without affecting negatively the composite behaviour. Indeed, increasing silica content leads to the formation of large agglomerates that act as critical stress points that weaken the material. As for the silica doping process, fabric direct nanomodification seems to be a valid method for the creation of multiscaled nanocomposites, that simplifies the process and reduces production costs.

PART III:

Smart Multifunctional systems for impact properties enhancement

As seen in Section 4.1 by mixing a nanoscaled phase within a traditional polymer or by inclusion in a traditional laminate structure, it is possible to improve some aspects of the mechanical behaviour of a material. In particular we have seen that small percentages of both graphene nanoplatelets and nanosilica particles are able to simultaneously strengthen and toughen the host material, enhancing Young's Modulus, Storage Modulus and Hardness, hence resulting in materials able to withstand higher loads with small weight increase.

However, another important issue that concerns all the structural materials and, more in particular composite structures, is constituted by the behavioural uncertainties associated with impacts with foreign objects. Indeed, because of their weak resistance to through-the-thickness solicitations, these materials are susceptible to delamination damages under impact loads that can compromise their integrity and lead to catastrophic failures (see Section 2.1).

Over the past years, a considerable amount of research has been devoted to evaluate an effective solution to this issue, in order to improve impact resistance of composite structures. According to these researches, this can be achieved following two different approaches, depending on the kind of intervention on the material structure.

A first approach is the modification of one of the components of the material in order to increase its specific properties, reducing its weaknesses, thus improving the compatibility between the different phases that form the composite structure. Strengthen mechanisms such as matrix toughening [168], interface toughening [169] and fibres surface modification [170] belong to this category as they operate by increasing the properties of the existing phases within the material structure. On the other hand, a different approach consists of hybridise the composite by embedding an additional engineered component characterised by particular properties within a traditional laminate in order to exploit its particular behaviour to improve impact resistance without affecting the other (desirable and needed) mechanical properties.

The great advantage of these systems is the possibility to employ hybrid materials able to respond dynamically to external solicitations, guaranteeing that "environmental awareness" described in Section 3.1 via activating specific dissipation mechanisms only when the material is subjected to an impact with a foreign body.
Hybrid materials reinforced with several engineered phases (such as hollow fibres [171], single and multi-walled carbon nanotubes [172, 173], graphene nanolayers and through-the-thickness reinforcements [174]) have been studied extensively during the last decade in order to evaluate how they affect the impact resistance of traditional laminates showing good results in terms of energy absorption rate and damping of structural vibrations.

The aim of this Section is to investigate two different composite systems that have been hybridised with an additional smart component in order to dynamically increase the impact properties of the material. In the first system, a non-Newtonian fluid has been studied and tested in order to exploit its nonlinear damping properties in a hybridised prepreg based CFRP. The characteristics of the fluid have been analysed with rheological tests and an experimental campaign has been carried out in order to analyse the variation of the energy absorption rate and the internal delamination extent for hybridised composites in comparison with traditional laminates.
The second part is focused on the embodiment of Shape Memory Alloy (SMA) wires in order to exploit their unique superelasticity and the hysteretic loop that characterises their stress-strain curves. Composite laminates where hybridised by embedding a network of SMA within the laminate structure and subjected to low velocity impacts in order to analyse their responses in comparison with a traditional composite. Ultrasonic C-Scan analysis was undertaken on the samples after the impact, in order to estimate the extent of the internal delamination.

7 Multifunctional composites based on the inclusion of non-Newtonian Fluids for improved impact properties

The results obtained for the threephasic SiO_2 composite have demonstrated that the inclusion of raw silica nanoparticles is able to enhance the stiffness of the host material, however it negatively affects the damping properties of the composite, lowering the amount of energy that the system is able to dissipate when it is subjected to an external load.

As said in Section 3, one of the greatest advantages of these new-generation multifunctional systems is the possibility to modify specific properties of the material by adding or modifying specific phases within the composite structure. Indeed, by following this approach, it is possible to enhance the impact properties of a traditional laminate by modifying the silica-based solutions used in Section 6.1.2 in order to manufacture a Shear Thickening Fluid that can subsequently be included within the composite. The original contribution of this chapter is the development of a new hybrid material in which the presence of this highly non-linear phase is able to modify the energy absorption behaviour increasing the impact resistance of complex structures.

Shear Thickening Fluids (STF) are non-Newtonian fluids with remarkable properties that behave like a liquid when there are no forces applied and turn in a very stiff solid-like structure in presence of high shear rates [175]. Because this liquid-solid transition is the result of a rapid increase of viscosity, these highly nonlinear fluids can be exploited for the design of damping systems and shock absorbers.

Figure 80 – STF based Liquid Body Armour produced by the University of Delaware and the US Army Research Laboratory

Liquid body armour based on the inclusion of STF have been studied intensively during the last decade [176-179], and several commercial products (mostly reinforced soft protections based generally on aramid fibres - see Figure 80) are available on the market. However, very few works have been done on the design of stiff composite materials with embedded STF (without the use of aramid woven fabric). In the work carried out by Fisher et al, an STF was sandwiched between polyvinyl chloride beams, showing good results in damping the vibrations of the entire structure [180], while Soutrenon et al. have realised a structural damper by embedding the STF within an open-cell foam encapsulated in silicone [181]. Another multifunctional system patented by Picken [182] is based on the realisation of an STF using a supramolecular polymer (polymers made of monomers held together by noncovalent interactions [183]) that is then used to impregnate the fibres and produce a composite material. In the procedure illustrated in this Section, an engineered STF is directly embedded as an active layer within the fibrous reinforcement of a composite laminate to obtain stiff CFRP parts characterised by higher levels of energy absorption due to the thickening of the solution during impacts with foreign objects. The technique does not imply any modification of the thermoset resin used for the composite manufacturing, therefore the procedure can be carried out using commercial thermoset/carbon fibres prepregs.

7.1 Theoretical Aspects

Generally, a non-Newtonian fluid can be defined as a material whose viscosity is dependent on the shear rate or shear rate history. However, included in the group there are some fluids in which it is possible to observe normal stress-differences or other non-Newtonian behaviour even if they are characterised by shear-independent viscosity. Table 7 summarises the different kind of non-Newtonian fluids and classifies their particular behaviour under different subcategories.

Time-independent viscosity	*Shear Thickening (dilatant)*	Apparent viscosity increases with increasing shear stress
	Shear Thinning (pseudoplastic)	Apparent viscosity decreases with increasing shear stress
	Generalised Newtonian fluid	Constant viscosity. Stress depends on normal and shear strain rates and also the pressure applied on it
Viscoelastic	*Kelvin material*	Combination of elastic and viscous effect
	Thixotropic	Apparent viscosity decreases with the duration of stress

Table 7 - Non-Newtonian fluid characterisation

Figure 81 shows the rheology of different kinds of Non Newtonian fluids, according to the different relationships between shear stress and shear rate.

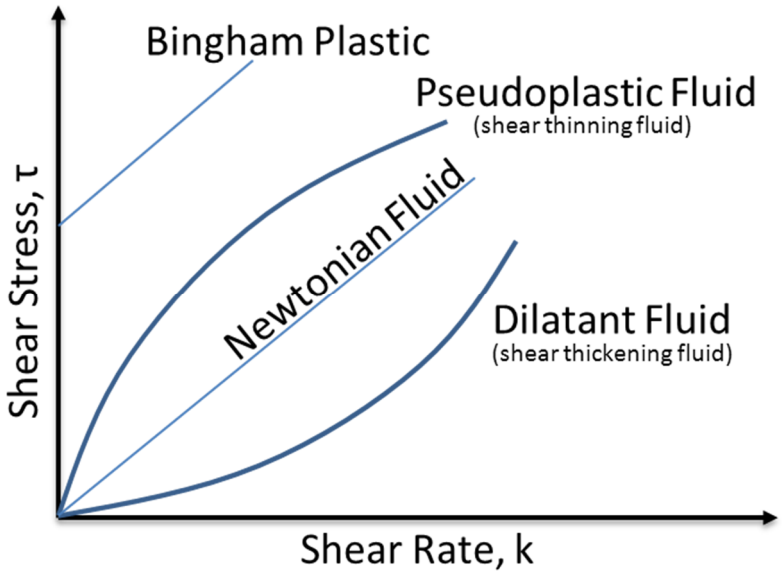

Figure 81 - Rheology of non-Newtonian fluids

A Shear Thickening Fluid (see red curve in the figure above) is a non-Newtonian fluid obtained by dispersing spherical nanoscaled particles (dispersed phase) within a liquid phase (continuous phase). By increasing the particles concentration beyond dilute

limit leads to the activation of particle-particle interactions and to the creation of long range order, resulting in non-Newtonian effects such as shear thinning or shear thickening. These effects can be explained with transitions from an ordered to a disordered state that occur when a high stress is applied. Indeed, when this fluid is subjected to a relatively low shear rate, the repulsive interactions between particles are able to create an ordered and layered structure that consents a more effective particles flow through the liquid phase, thus reducing the viscosity of the solution. Increasing the shear rate above a critical point (γ_c), the particle-particle interactions are overcome by shear forces and the particles are squeezed together, moving the fluid out from its equilibrium state and resulting in a disordered and more complex structure. In particular, shear thickening occurs when the repulsive Brownian forces are overcome by attractive hydrodynamic shear forces, leading to the formation and perculation of shear induced transient aggregates called "hydroclusters" that thickens the fluid. Those hydroclusters are made of particles momentarily compressed together to form agglomerates and as a result of their formation, the ability of the particles to flow around each other is hindered and requires more energy, leading to an abrupt increase in viscosity [184, 185]. When the shear stress is removed, the hydroclusters spread apart and the nanoparticles are separated, forming again a stable suspension.

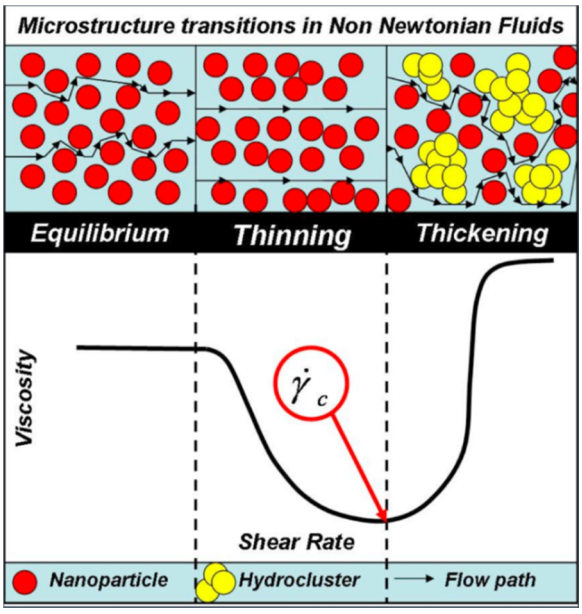

Figure 82 - Schematics of Shear Thinning and Shear Thickening Effect

In order to observe shear-thickening behaviour in a suspension, there are three important factors to consider:

- Increasing the concentration of particles within the fluid will lead to an enhancement of the thickening effect, therefore the weight fraction has to be evaluated according to the system viscosity requirement. For our purposes the concentration required is around 20-25 % wt. as it gives good results in terms of impact resistance and workability for composite applications. Further increase of the nanoparticles concentration leads to a very high level of initial viscosity of the solution (which is also dependent on the molecular weight of the continuous phase), decreasing its workability during the embedding process within the laminate. This problem can be partially solved by increasing the temperature during the manufacturing process. Moreover, volume fraction is strictly connected with particles dimensions as it can change the electrostatic interactions, leading to different forces interaction in the liquid/particles system.

- Suspension must not flocculate (destabilisation of the suspension): particles have to be neutral or repel one another by electrostatic, steric or entropic interactions. To achieve this, the continuous phase must induce steric or electrosteric stabilisation in order to enhance the colloid stability. Several carriers can be used for the preparation of the STF, such as ethylene glycol [186, 187], water [188] and other organic solvents, however the most used one for structural application is polyethylene glycol due to its tendency to form very stable suspension [178, 189] coupled with its biocompatibility.

- Particle volume fraction at which shear thickening behaviour is first observed ($\dot{\gamma}_c$) decreases as particle ratio increases. Studies present in literature report thickening behaviour observed for particles with a dimension range from 1nm to 5000nm [190]. Another important effect is given from the shape of the dispersed phase, however in case of irregular particles it is more difficult to

understand the energy dispersion mechanism due to the superimposition of the thickening effect and the reciprocal friction between the inclusions [191].

Based on these considerations, the STF realised for this study forms a complex system which is characterised by a double change in its microstructure with the increase of the shear rate. Indeed, at low shear rate, the particles are rearranged from the equilibrium and become more organised in the flow, decreasing the fluid viscosity (shear thinning). A further increase of the shear rate leads to the formation of the hydroclusters and, consequently, to the thickening effect.

As for the particles used, there are several examples in literature of the different materials that can be employed, such as $CaCO_3$ [191], PMMA[192, 193], PVC[194], PS and SiO_2[180, 185, 191]. For our purposes, different solutions were produced using two types of commercially available SiO_2 nanoparticles with average diameters of 7 and 14 nanometers (Sigma Aldrich). Good thickening effects have been obtained for particles with a nominal diameter of 200nm.

7.2 Experimental: Solution Preparing

As said in the previous paragraph, the components needed for manufacturing an STF are nanosized particles and a liquid carrier. For this work, several solution were produced by mixing an increasing percentage of silica (SiO_2) nanoparticles (from 10 to 25% wt.) with PolyEthylene Glycol ($HO\text{-}CH_2\text{-}(CH_2\text{-}O\text{-}CH_2\text{-})n\text{-}CH_2\text{-}OH$).

To ensure a good distribution of nanoparticles within the carrier and to avoid the formation of agglomerates, an ultrasonic cavitation mixing method was used. Small quantities of silica nanopowder were gradually added to the PEG and stirred in manually. Once a viscous gel was formed, the ultrasonic probe was immersed in gel and activated for 10 minutes (see Figure 83). High amplitude compressive waves generate localised low-pressure zones in the carrier, ensuring homogenous mixing of nanosilica and PEG. At the end of the process the solution were stored under vacuum for 12h in order to remove air bubbles and further improve the dispersibility.

Figure 83 - STF preparation

7.2.1 Rheological Analysis

As said in Section 7.1, the volume fraction of nanoparticles within the continuous phase represents a key point for the final properties of the STF. Hence, several solutions were prepared with an increasing percentage of silica and the flow properties were measured using a Bohlin C-VOR Rheometer in parallel plate geometry (PP40).

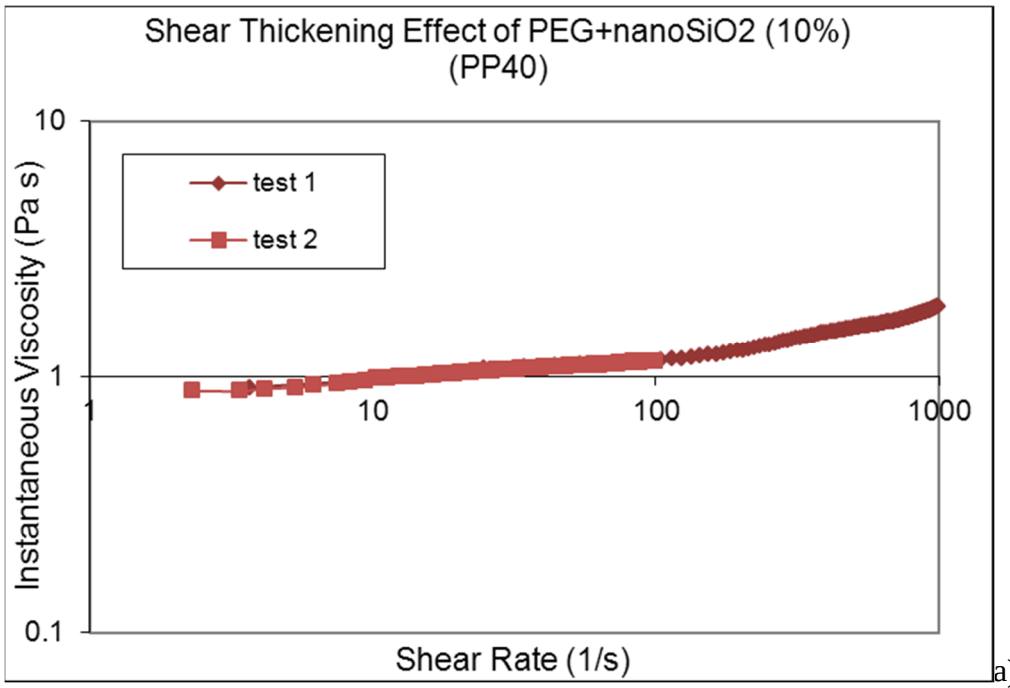

a)

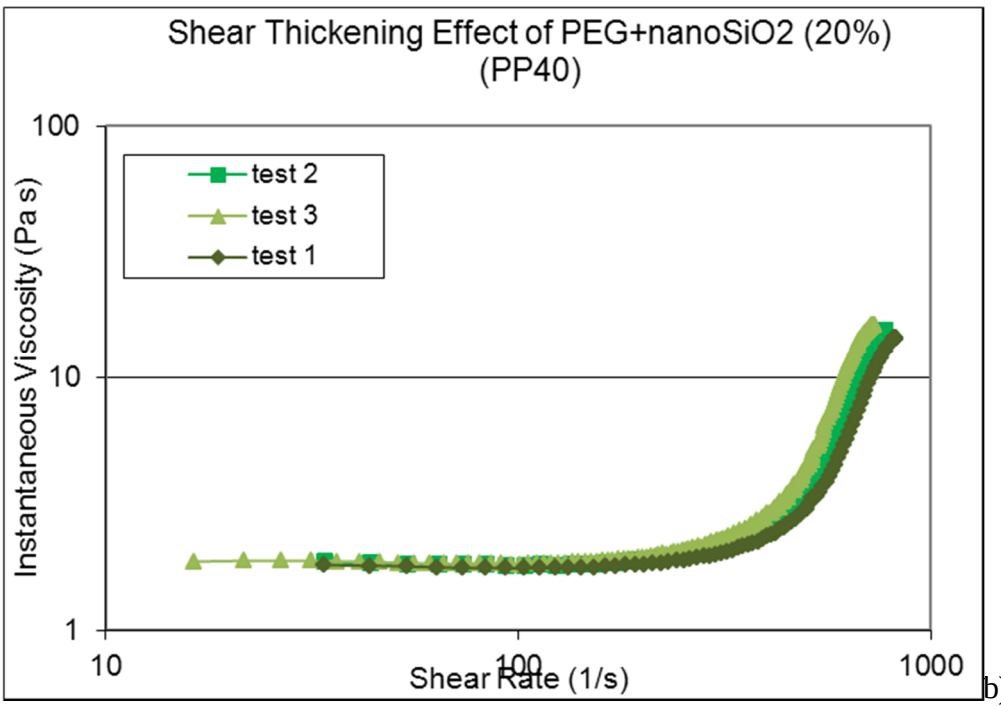
Shear Thickening Effect of PEG+nanoSiO2 (20%)
(PP40)
Instantaneous Viscosity (Pa s)
100
10
1
test 2
test 3
test 1
10
100
1000
Shear Rate (1/s)

b)

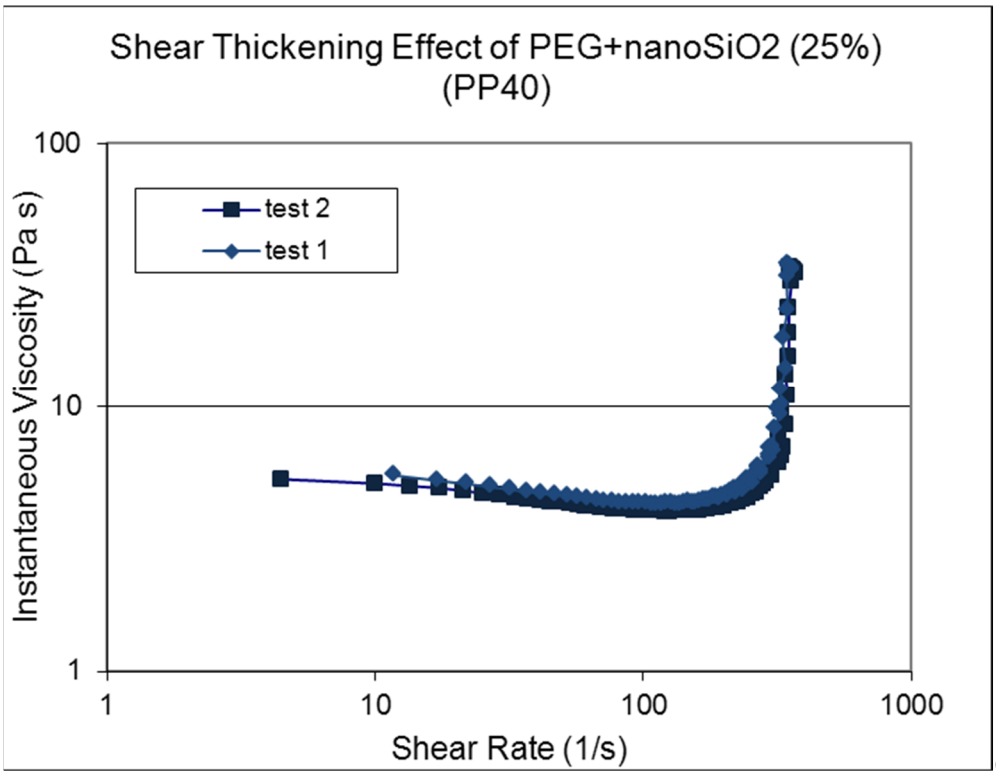
Shear Thickening Effect of PEG+nanoSiO2 (25%)
(PP40)
Instantaneous Viscosity (Pa s)
100
10
1
test 2
test 1
1
10
100
1000
Shear Rate (1/s)

c)

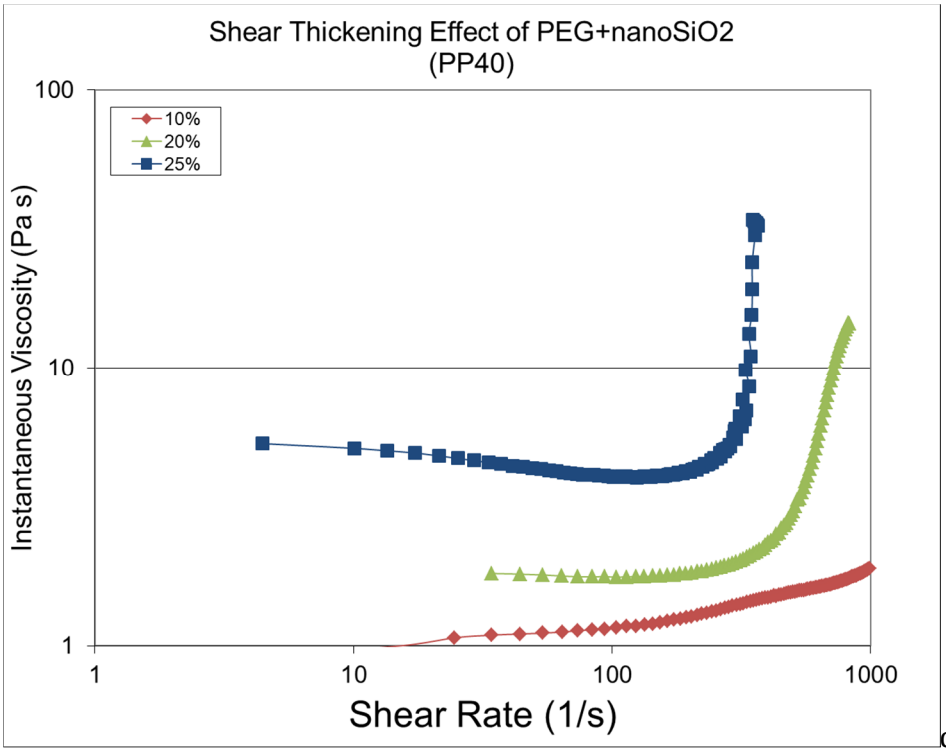

d)

Figure 84 - Rheological analysis for STF at different nanoparticles concentrations: a) STF/15; b) STF/20; c) STF/25; d) comparison between the different curves

The results obtained from the rheometric analyses are shown in Figure 84 and are quite revealing in several ways for all the tested solutions. First, it is clearly shown from the curves that both thinning and thickening effects are present for highly concentrated solutions, while for lower concentration the presence of secondary flows prevents accurate measurements of the weak thickening effect. Indeed, after an initial equilibrium state in which the fluid behaves almost like a Newtonian fluid, it is possible to observe a slight trend of decreasing viscosity for relatively low shear rates, while, when higher rates of shear are applied, the viscosity reaches a critical point in which the magnitudes of repulsive interparticle forces are balanced by shear forces. When the shear stress exceed this critical level the shear forces that push the particles together become larger than the repulsive interactions so that the particles are moved from their equilibrium state, distrupting the ordered structure and leading to an abrupt increase of viscosity that thickens the fluid. Since the concentration of hydroclusters within the continuous phase is strictly related on the nanoparticles concentration [195], increasing the volume fraction of silica nanoparticles within the STF makes the

nonlinear effects more evident, enhancing thinning/thickening behaviours (see Figure 85).

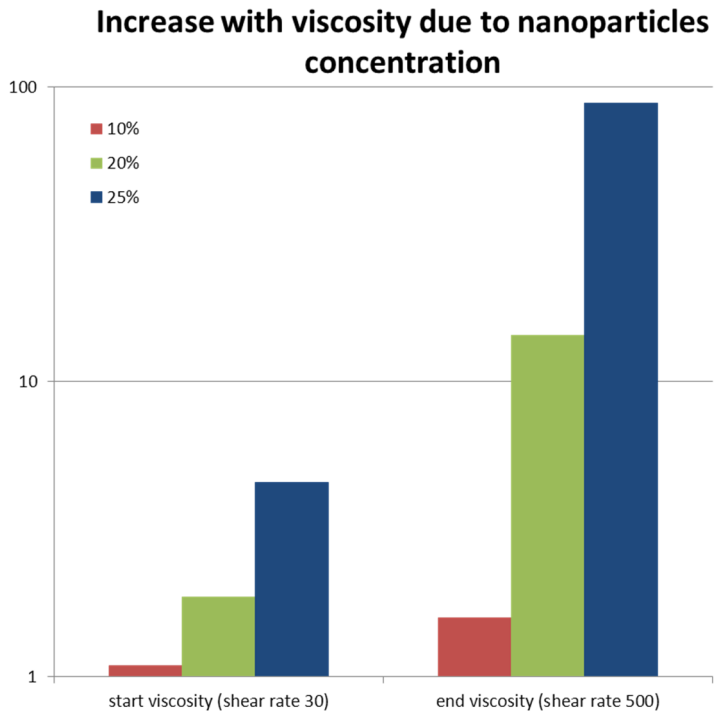

Figure 85 - viscosity increase with increasing nanoparticles concentration

Initial viscosity of the solution depends strongly also on the molecular weight of the carrier. In this case the carrier used was a PEG 200g mol^{-1}. Results in terms of viscosity change due to thickening effects (two orders of magnitude increase) are not dissimilar to the ones found in literature [196].

Another important result can be observed in Figure 86, which illustrates the existence of a strong relationship between volume fraction and the critical shear rate. Indeed, for higher nanoparticles concentrations, γ_c moves to lower values because of the reduced intra-particles distance, anticipating the transition between thinning and thickening effects, as reported by Maranzano et al [197].

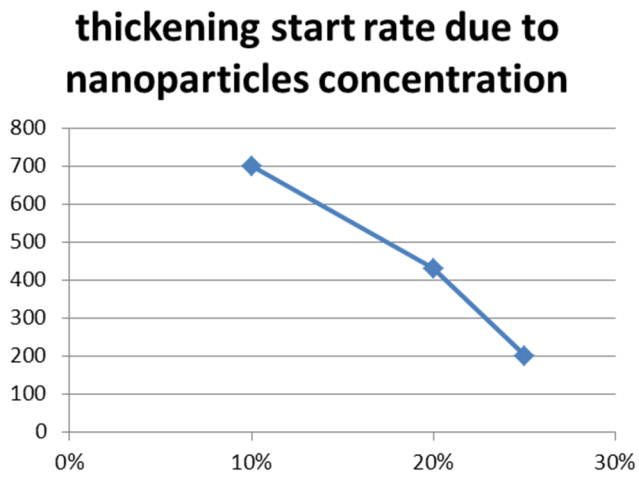

Figure 86 - Behaviour of critical shear rate with increasing nanoparticles concentration

7.3 Composite Mechanical Characterisation

The structural composite material was manufactured sandwiching a thin layer of STF between several layers of Carbon Fabric prepregs (see Figure 87). The amount of fluid used in every sample has been kept constant for all the tests undertaken (10 grams for 300x150mm plates), therefore we will refer to "STF percentage" as for the amount of silica nanoparticles within the fluid. Moreover, because of the small amount of STF involved in the hybridisation process, the total weight of the final laminate is not affected. Samples were prepared via Vacuum Assisted stratification followed by Autoclave consolidation in order to activate the curing reaction of the epoxy resin, and cut in 10x15cm plates for impact testing.

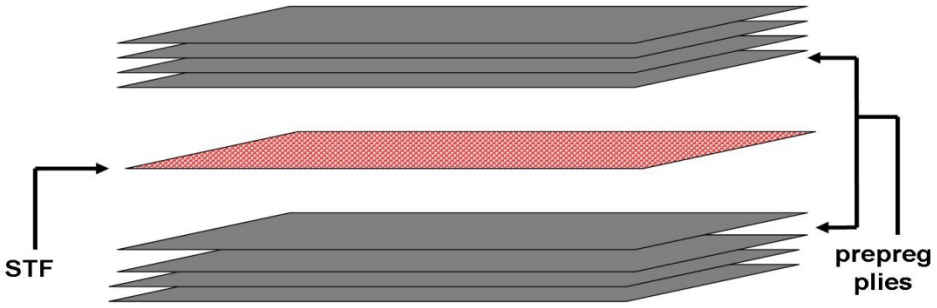

Figure 87 - Schematics of STF/CFRP composite preparation

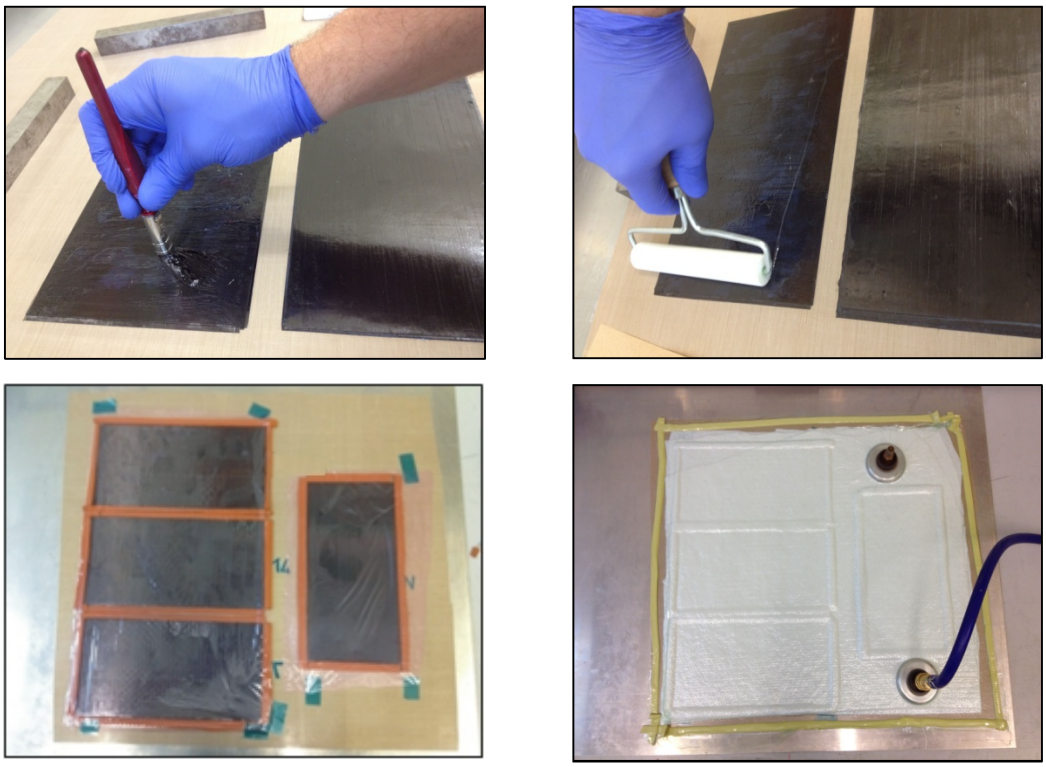

Figure 88 - manufacturing procedure of STF/CFRP composite samples

In a second stage of the work, in order to test the sensitivity of the STF reinforcement for more complex geometries, a CFRP leading edge has been manufactured using a different manufacturing technique. In this procedure a calendering method similar to the one used in Section 6.1.2, was used to impregnate a dry carbon fabric layer with the STF. In this procedure, the dry fabric is first immersed in a bath containing a solution made diluting STF with ethanol and then it is forced to pass through a series of polymeric cylinders. The turning action of the cylinders helps to achieve a better distribution of the solution within the fabric and to absorb the solution in excess resulted from the immersion process (see Figure 89a). After the impregnation the STF-fabric was sandwiched in a stack of traditional prepreg plies and then cured in autoclave.

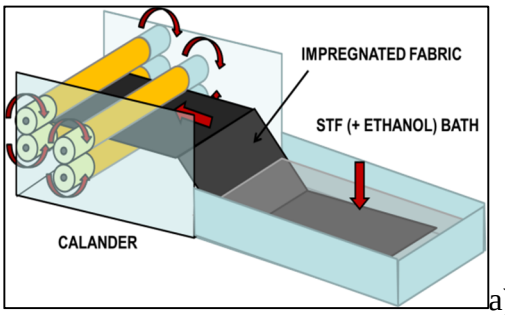

a)

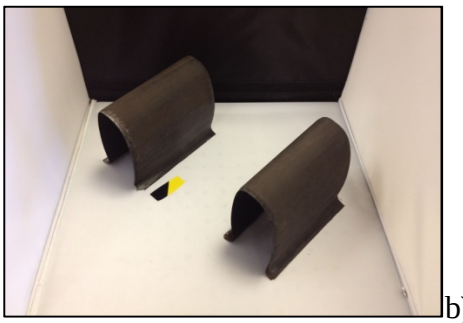
b)

Figure 89 – a) schematics of the calendering technique used for complex geometry samples; b) leading edge samples

7.3.1.1 Damping analysis

In order to fully understand how the material would behave when subjected to an impact, experiments were conducted to evaluate the energy absorption of the STF/CFRP composite and a comparison was made with a traditional laminate, obtained with the same prepreg and the same lay-up sequence. A first series of test was undertaken to analyse the behaviour of the samples when subjected to a forced vibration using a PZT actuator to input a chirp signal over a 0-10kHz range of frequencies. Fast Fourier Transform (FFT) was performed in order to obtain the frequency content of the acquired vibration signals and evaluate the resonance frequencies of the samples.

The resonance frequencies of a structure are proportional to its stiffness, according to the relation $f_i \propto \sqrt{k/m}$, therefore it is possible to evaluate this mechanical characteristic by comparing the relative shift of frequencies peaks patterns of hybridised samples and traditional unreinforced laminates. Moreover, since the relative amplitude of the resonance peaks is a measurement of the ability of the material to store energy when subjected to an external load, it is possible to have an estimation of the damping ability of the structure by analysing its variation between the hybridised samples and the control ones,.

Results from the tests are illustrated in Figure 90 which clearly shows a visible shift to higher frequencies between the control sample and the hybridised one, indicating an

increase in stiffness for the STF sample. Similar results have been observed for CNT reinforced composite structures [198]. In addition, the shifting of the amplitude of the entire frequency spectrum to lower levels suggests an enhancement of the damping behaviour of the structure due to the dynamic change in viscosity of the embedded STF.

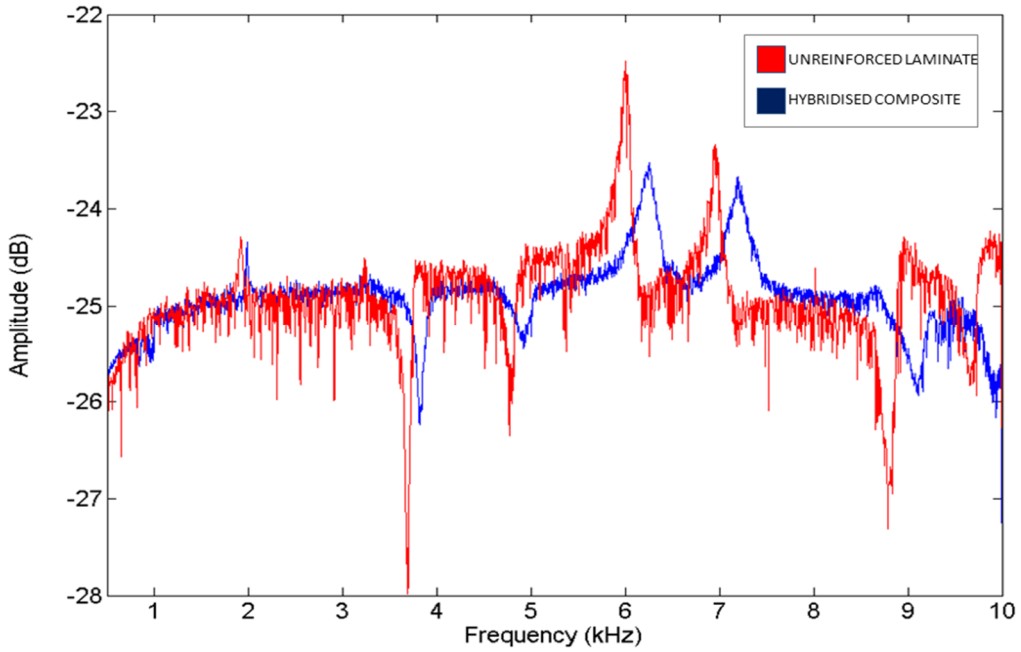

Figure 90 – Forced vibration signals for STF and Neat samples

A more in depth analysis on the damping behaviour of the STF based composites was carried out with free vibration tests in order to quantify the dissipation effect of the hybrid phase. Samples were tested in single cantilever beam geometry, clamping them to an optical bench and vibrations signals were collected using piezoelectric sensors. Logarithmic decrement δ was evaluated from the acquired signals, following the equation:

$$\delta = \frac{1}{n} ln \frac{x(t)}{x(t + nT)}$$

Where *x(t)* is the amplitude at time *t*, and *x(t+nT)* is the amplitude calculated for a peak *n* periods away.

Subsequently, results obtained can be used to evaluate the damping ratio, by using the following equation:

$$\zeta = \frac{1}{\sqrt{1 + \left(\frac{2\pi}{\delta}\right)^2}}$$

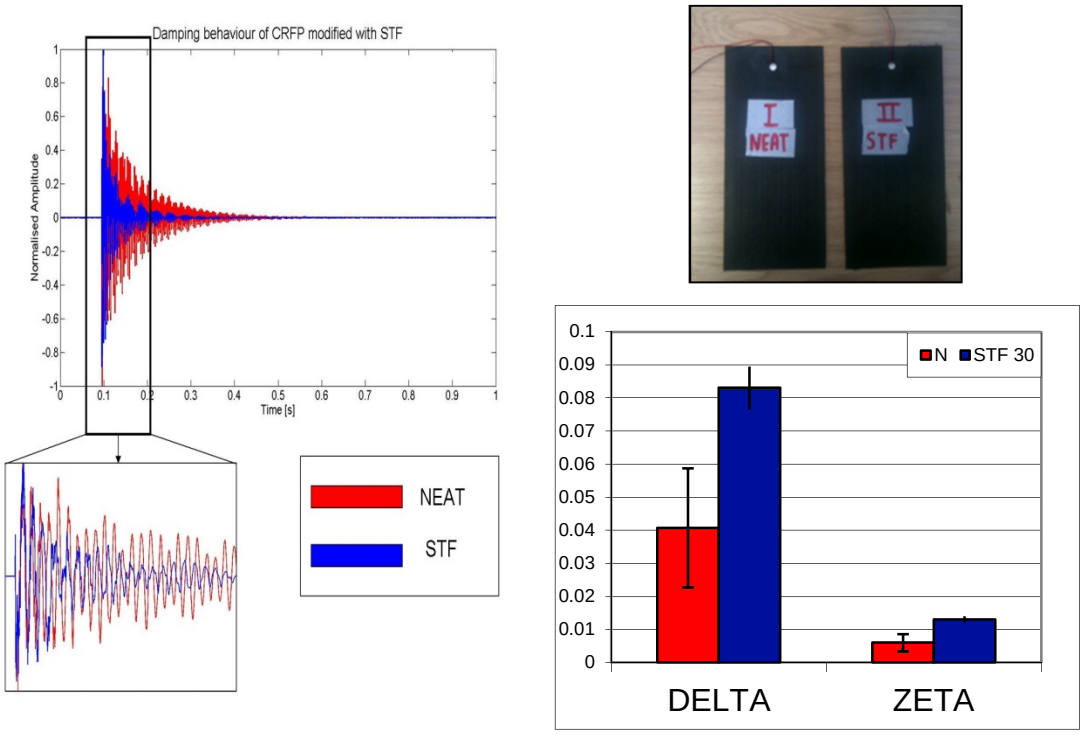

Figure 91 - Free vibration signals and results for STF and unreinforced samples

Results from this series of tests demonstrate the effectiveness of the STF embodiment within the CFRP structure as structural damper (see Figure 91). The trends of both logarithmic decrement and damping ratio (+50% for both δ and ζ), clearly indicate how the inclusion of STF changes the damping properties of the material. This difference can be explained by the dynamic microstructure modification of the non-Newtonian fluid in the composite structure. Indeed, when the composite is subjected to an impact, part of the stress is transferred to the embedded STF and it activates the transient formation of hydroclusters. The abrupt increase in viscosity enhances the energy dissipation rate for the entire structure.

7.3.1.2 Impact testing

In order to fully characterise the impact properties of the hybridised composite, several test were conducted on the STF reinforced samples and a comparison was made with traditional laminates obtained with the same prepreg and the same layup procedure. Two different variables have been taken in account during these tests: nanosilica particles dimensions (7 and 14nm) and particles concentration within the STF (from 10 to 25%).

Tests were conducted using a drop tower rig with an impactor mass of 12,8 kg and a semi-spherical head geometry (20mm diameter). Impacts were undertaken at 6, 20 and 40J with velocities of 0.8, 1.7 and 2.5 m/s.

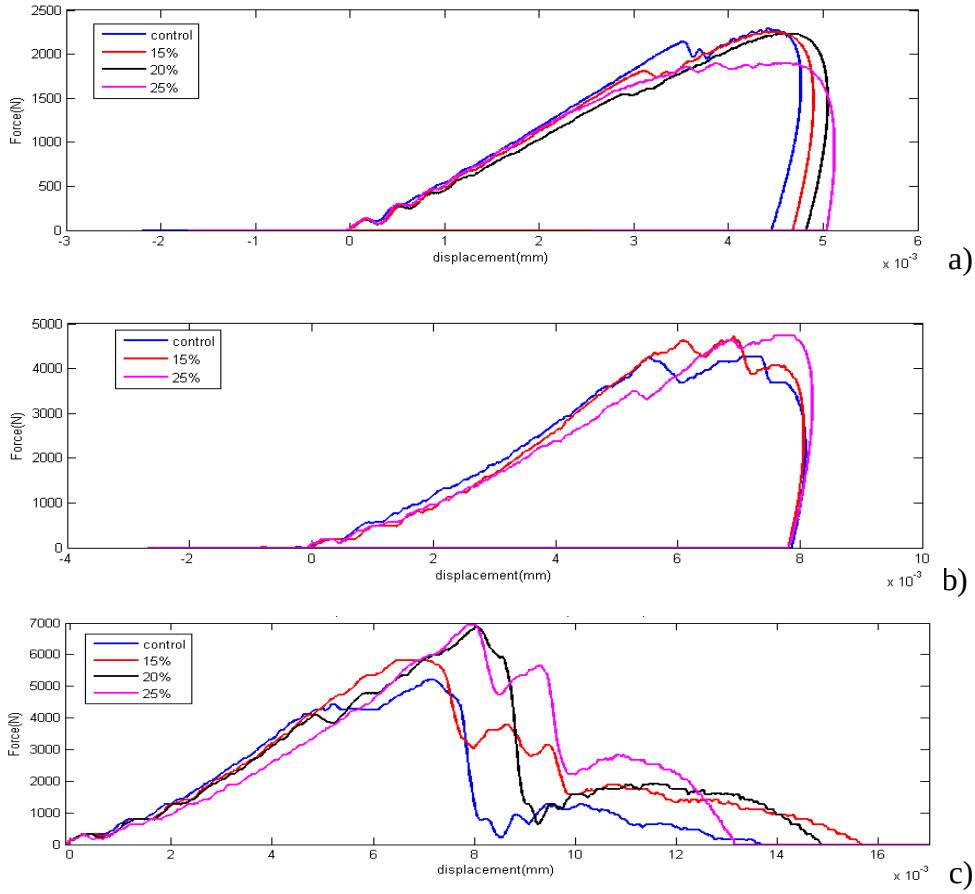

Figure 92 - Force Displacement curves from the impact test on 7nm Silica STF reinforced CFRP: a) 6J; b) 20J: c) 40J:

Figure 92 shows the curves obtained with the same impact energy for samples with increasing 7nm nanoparticles concentration within the STF (herein referred as STF7/XX where XX stands for the silica concentration), while Figure 93 represents the curves acquired for each energy level at the same STF concentration.

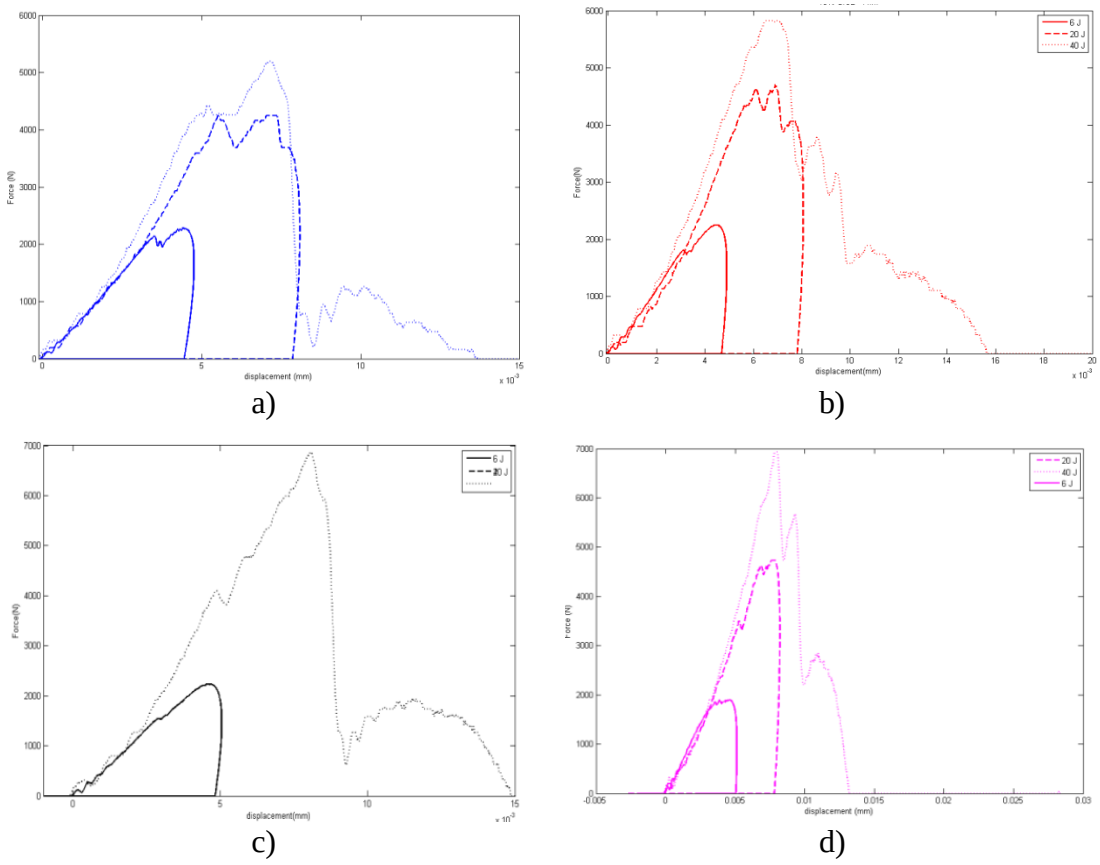

Figure 93 - Force Displacement curves for 7nm Silica STF reinforced CFRP: a) control sample; b) STF7/10; c)STF7/20; d)STF7/25

Results are summarised in Figure 94 in which it is possible to observe that for low velocity impacts (6J) the peak force stays linear (or within the experimental error) showing no large variations between control and reinforced samples.

For higher velocity impacts the effects of the hybridisation process becomes more consistent and affects the value of both force peak and the energy absorption rate.

Indeed, for the 20J impacts, the presence of the STF leads to a slight increase (~12%) in the value of the force peaks, going from 4252 N (unreinforced samples) to 4724 N (STF25 samples), while there is no variation in the energy absorption rate.

The effects of the hybridisation are more evident for the 40J impacts, where the curves show a dramatic increase in the force peaks, going from 5197 N for the unreinforced samples to a maximum of 6929 N for the STF based ones (~30%). It is possible to observe a relationship between this increment and the concentration of silica nanoparticles within the solution, as the force peaks values are enhanced by 12% for the STF15 and by an additional 20% for STF25.

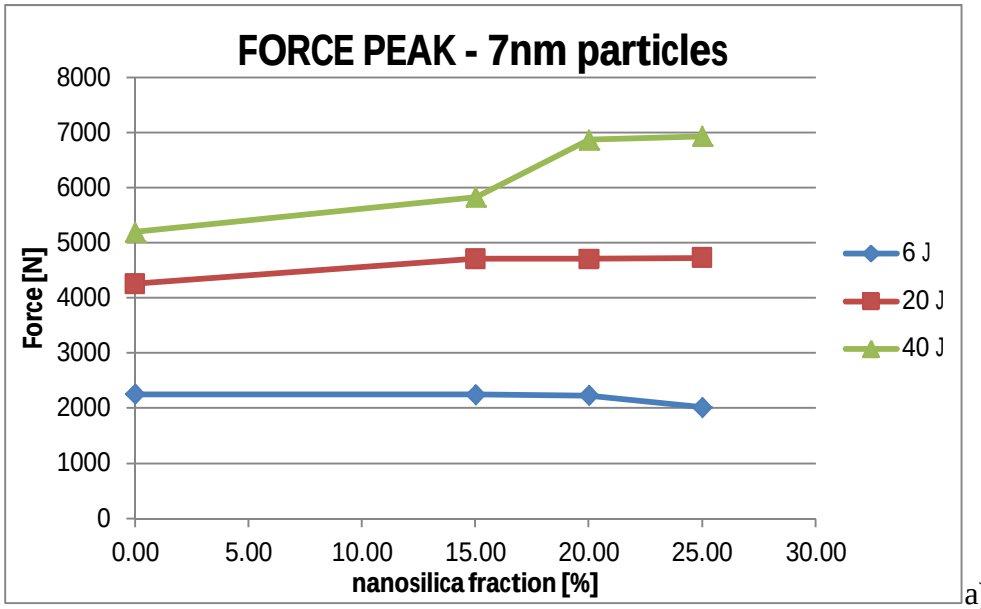

a)

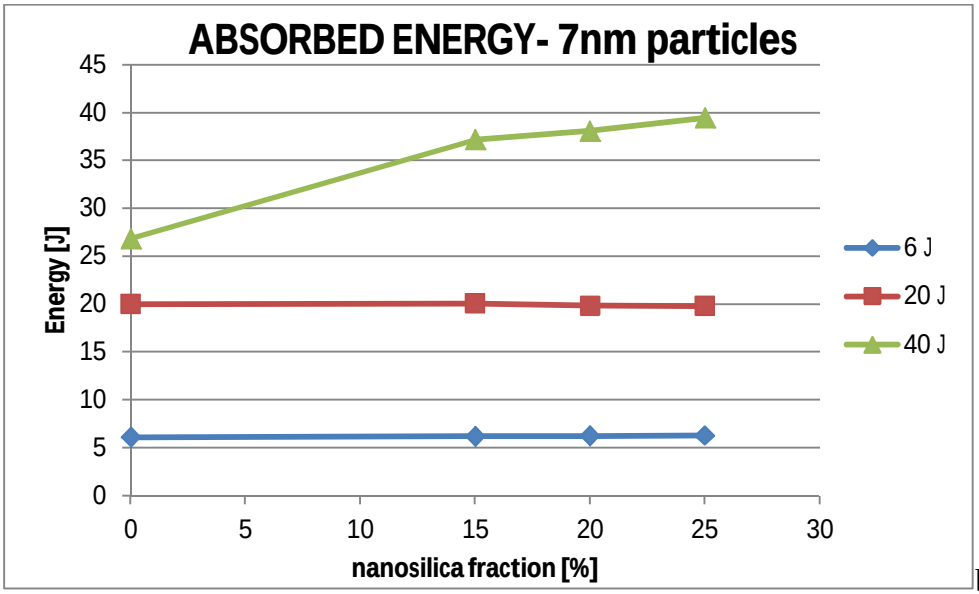

b)

Figure 94 - Summary of the results for impact on STF7 reinforce samples: a) Force Peak variation at different energies and different silica concentration in STF; b) Energy absorption variation at different energies and different silica concentration in STF

Same trend can be observed for the energy absorption rate during the impact. In this case the effect of the percentage of SiO_2 nanoparticles within the STF is even more evident. Indeed as it is possible to observe from Figure 94b, while for 6 and 20J impacts the trend is basically linear, when the impact velocity is raised up to 2.5 m/s the presence of the STF increases the energy absorption rate by 38% for STF7/15 and almost 50% for STF7/25. These results confirm what observed in the previous paragraph and they can be explained because of the dynamic behaviour of the STF, which activates the formation of the hydroclusters only when it is subjected to high shear stresses, thickening the fluid and enabling improved energy absorption mechanisms.

In order to understand the role of nanoparticles dimensions within the STF, a second series of test has been undertaken using 14nm silica nanoparticles for the STF reinforcement.

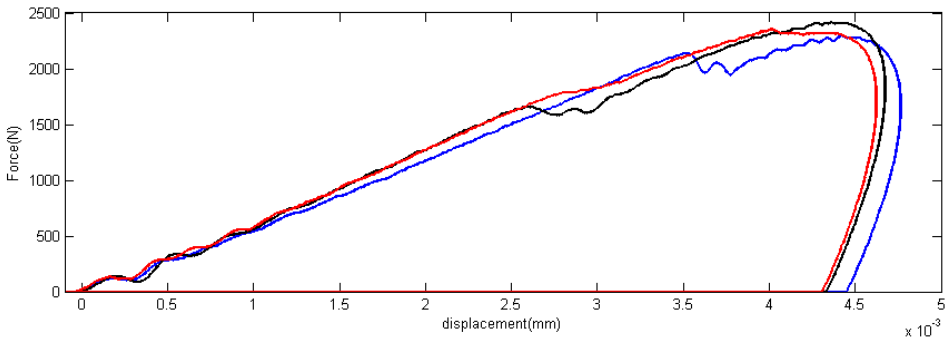

a)

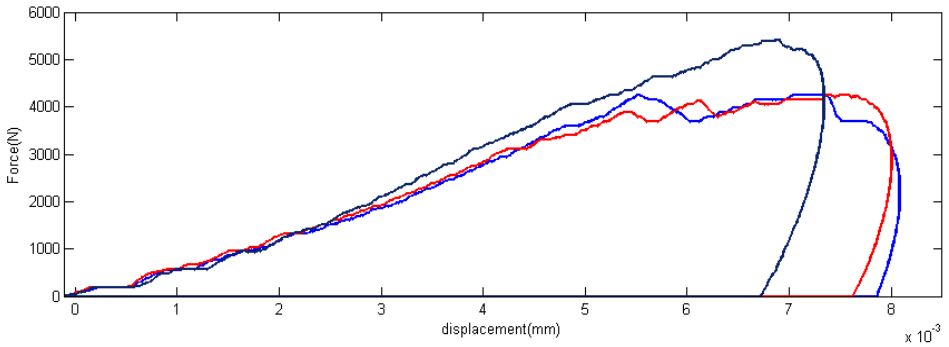

b)

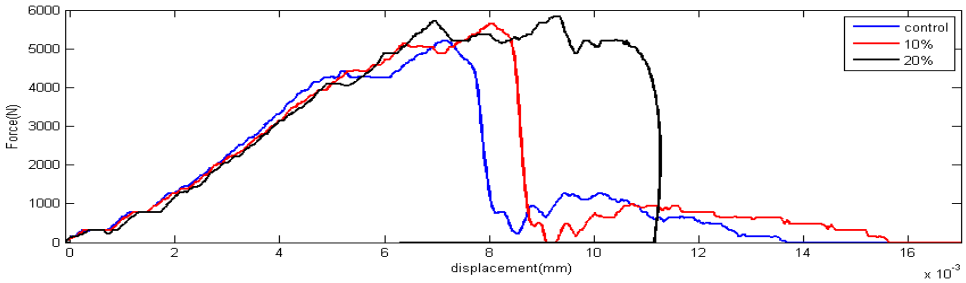

c)

Figure 95 - Force Displacement curves from the impact test on 14nm Silica STF reinforced CFRP: a) 6J; b) 20J: c) 40J:

Figure 95 and Figure 96 represent the Force-Displacement curves grouped in terms of energies and in terms of percentage of SiO_2 nanoparticles (14nm) within the STF.

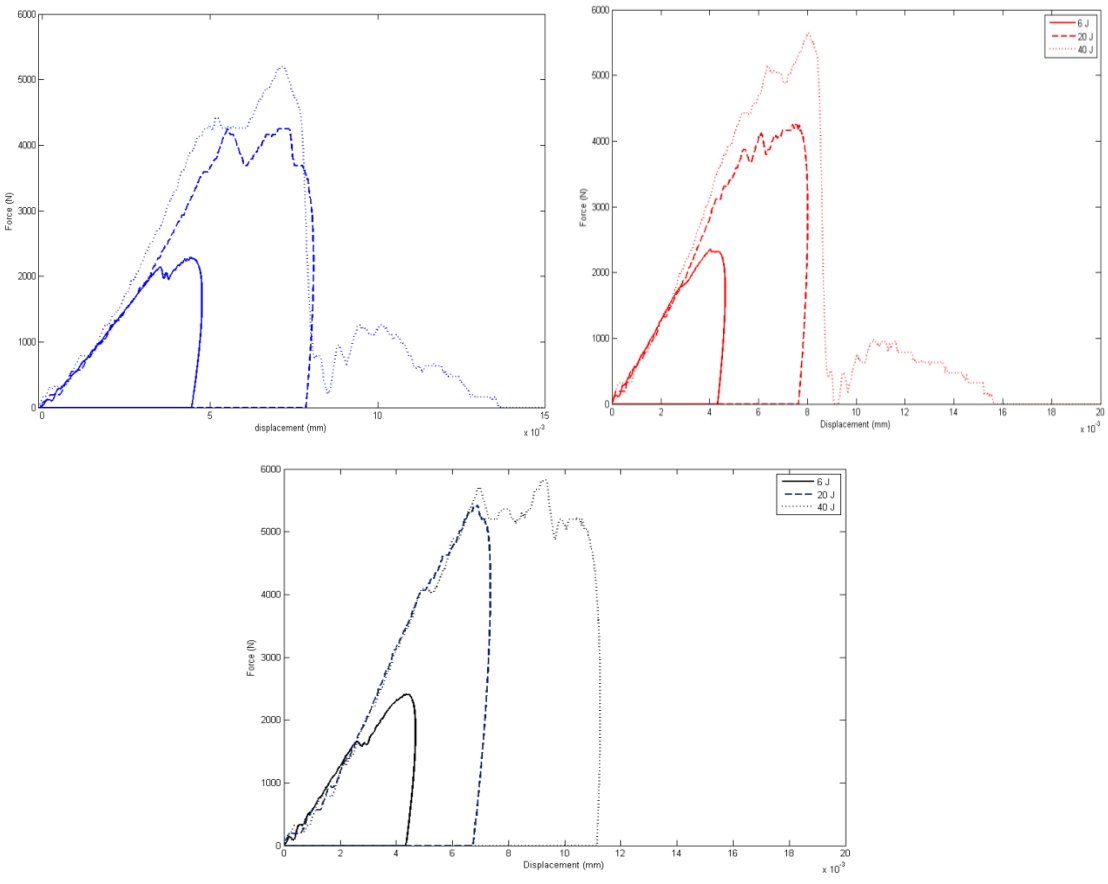

Figure 96 - Force Displacement curves for 14nm Silica STF reinforced CFRP: a) control sample; b) STF7/15; c)STF7/25;

As it is possible to observe from the results (Figure 97), in this case the presence of bigger particles leads to an additional enhancement of the hybridisation effects which

is particularly visible especially from the energy absorption curves. Indeed, by analysing the energy absorbed during the different impacts it is possible to observe an increase of more than 50% for the STF14/20, while for the 7nm nanoparticles the percentage required in order to reach this value was 25% (STF7/20). For lower impact velocities the energy absorption levels stay basically linear as for the previous samples.

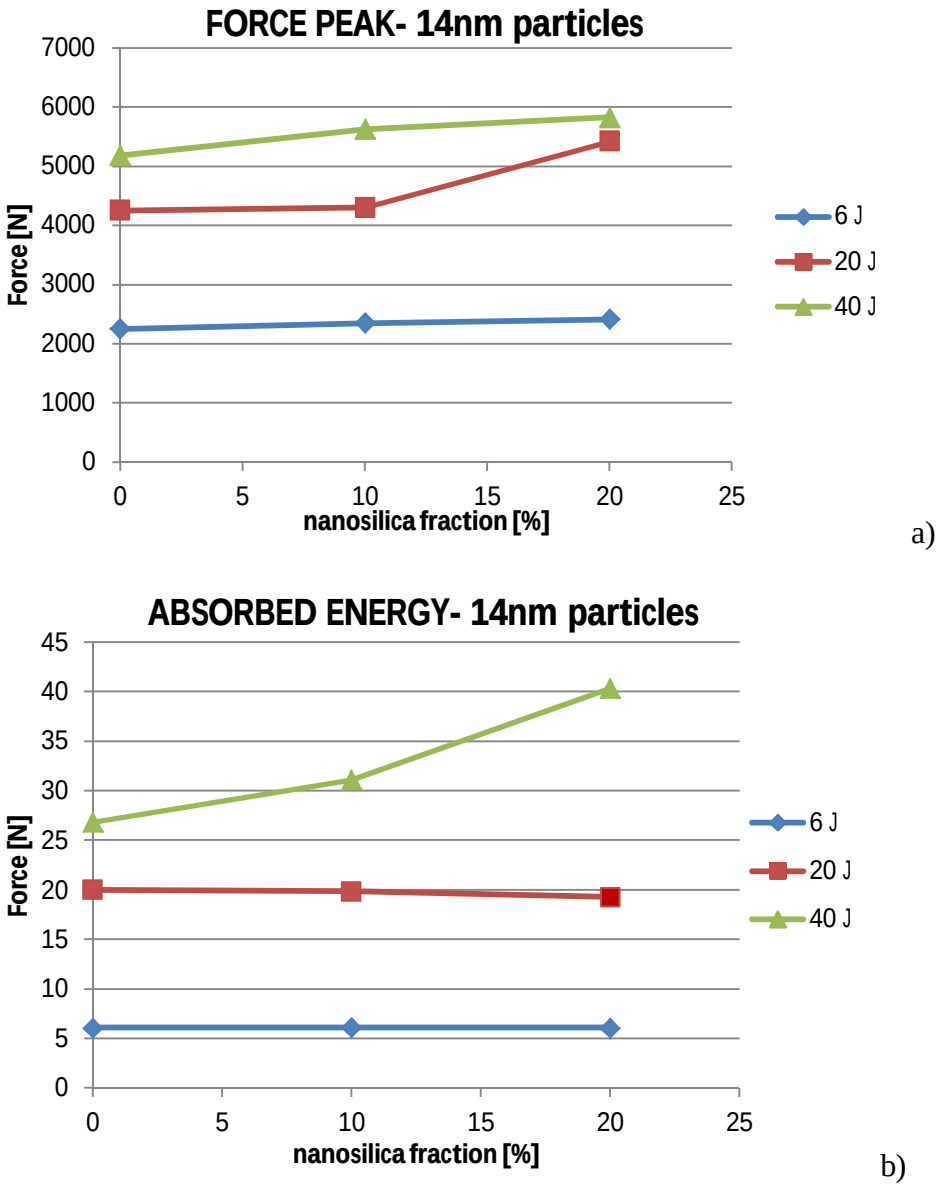

Figure 97 - Summary of the results for impact on STF14 reinforce samples: a) Force Peak variation at different energies and different silica concentration in STF; b) Energy absorption variation at different energies and different silica concentrations in STF

It is possible to have a clear idea of the hybridisation effects given by the presence of the STF within the CFRP by analysing Figure 98, in which the nanoreinforced sample is compared with an unreinforced one after the impact tests. As it is possible to see from Figure Figure 98a and b, the solicitations generated by a 40J impact were high enough to reach critical values on the traditional laminate, resulting in a total failure of the fibres on the top surface and a complete delamination on the bottom face. On the contrary, the STF based composite keeps its structural integrity after the impact showing no superficial failure on the top surface and only a small internal delamination on the bottom one (see Figure 98a and d).

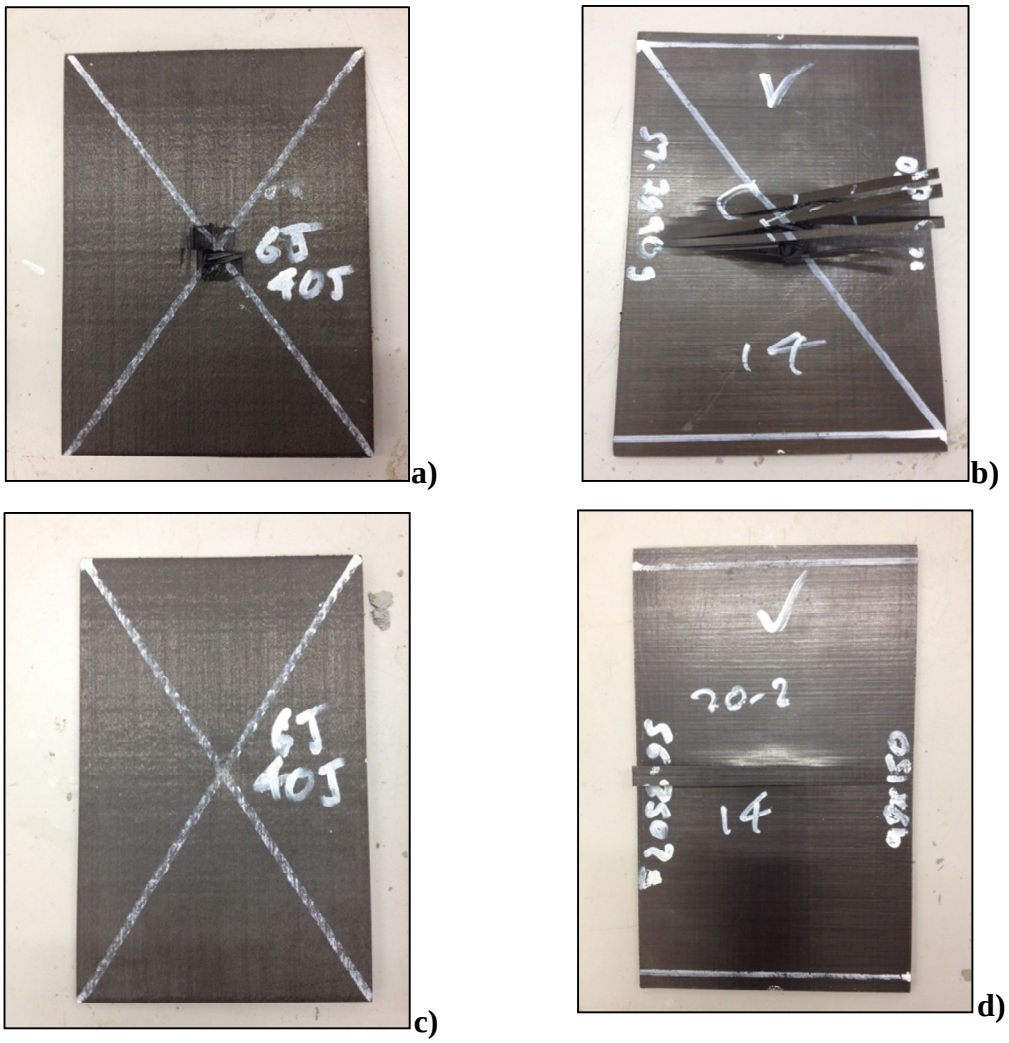

Figure 98 - post impact image of STF reinforced sample in comparison with a traditional CFRP subjected to the same impact; a) Control sample, top surface; b) Control sample, bottom surface; c) STF reinforced CFRP top surface; d) STF reinforced CFRP bottom surface;

Further impact tests were conducted on the leading edge samples, to investigate the feasibility of the STF reinforcement process for complex geometries. A STF impregnated carbon fabric was embedded in a stack of prepreg plies and a control sample was realised embedding the same fabric without the reinforcement within the CFRP. As it is possible to see from Figure 99a, the control sample (on the left) did not survive the test resulting in a complete failure with cracks propagating all over its width in three different points. On the contrary, the hybrid composite responded elastically to the impact showing no visible damage on the surface (Figure 99b).

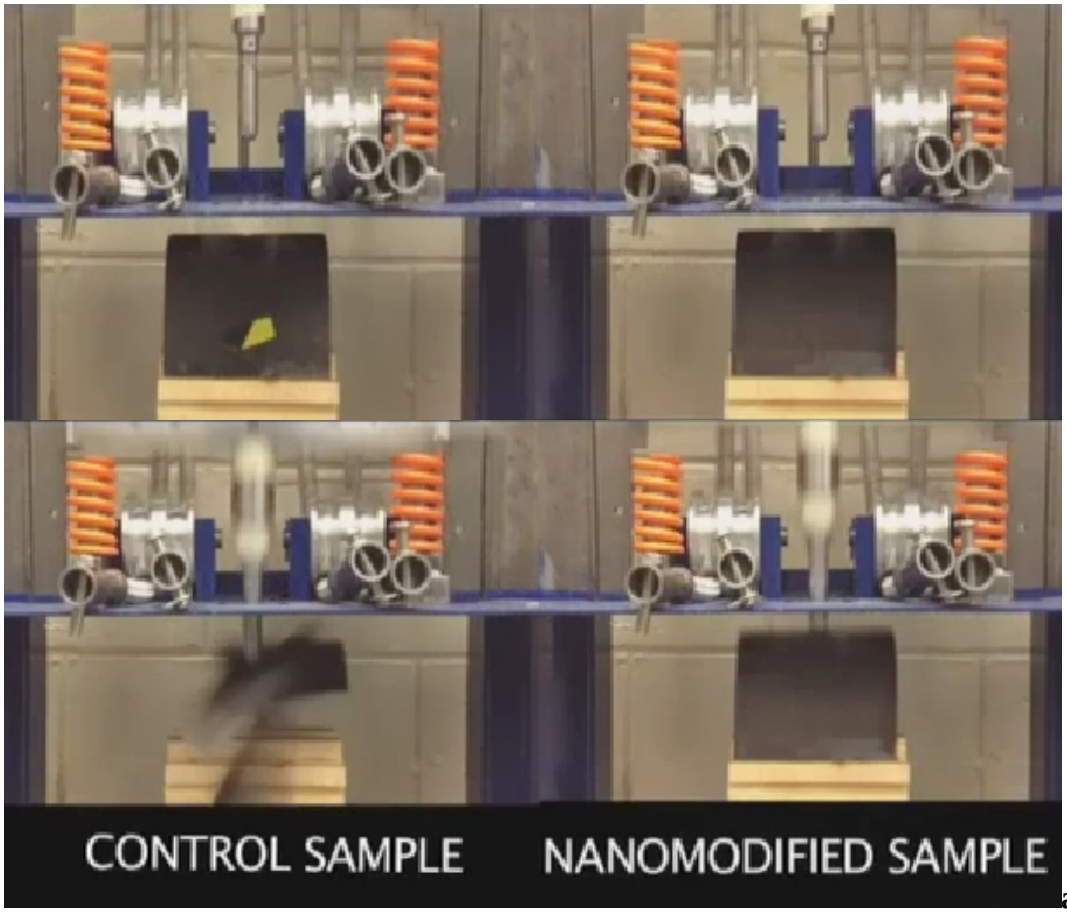

a)

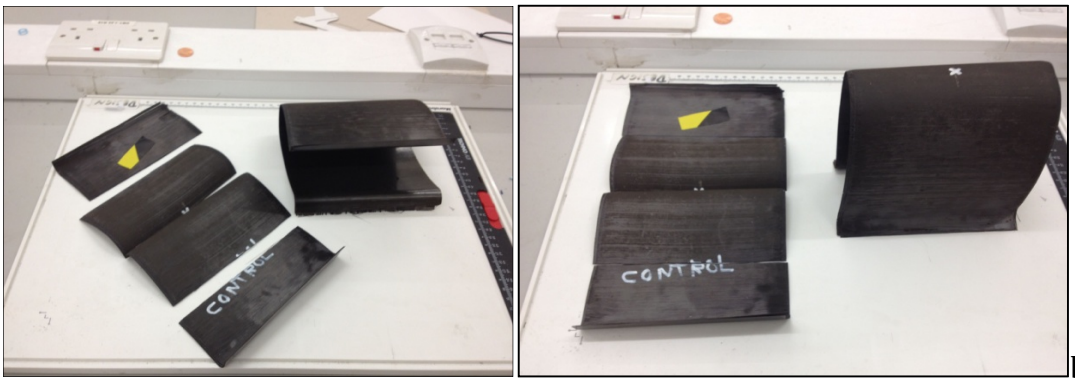

b)

Figure 99 - Impact test on leading edge sample: a) failure of the control sample in comparison with the nanoreinforced one; b) samples after the impact

7.3.2 C-Scan Analysis

The internal delamination extents of the impacted samples were evaluated analysing some of the CFRP/STF samples using a C-Scan system.

C-Scan is a non-destructive technique that uses a piezoelectric probe to send ultrasonic waves through a sample and measures the reflected signal obtained when a barrier (like a defect or the back of the sample) is reached. Analysing the difference between the signal sent and the one collected by the detector it is possible to assess the delamination region within a laminate. Figure 100 represents several ultrasonic images of the control sample in comparison with hybridised laminates. As it is possible to observe, the presence of the nanofluid reduces the extent of the delamination by more than 30%. Increasing the concentration of nanoparticles within the STF leads to an additional 10% reduction of the extension of the internal damage, confirming the results obtained with the impact tests.

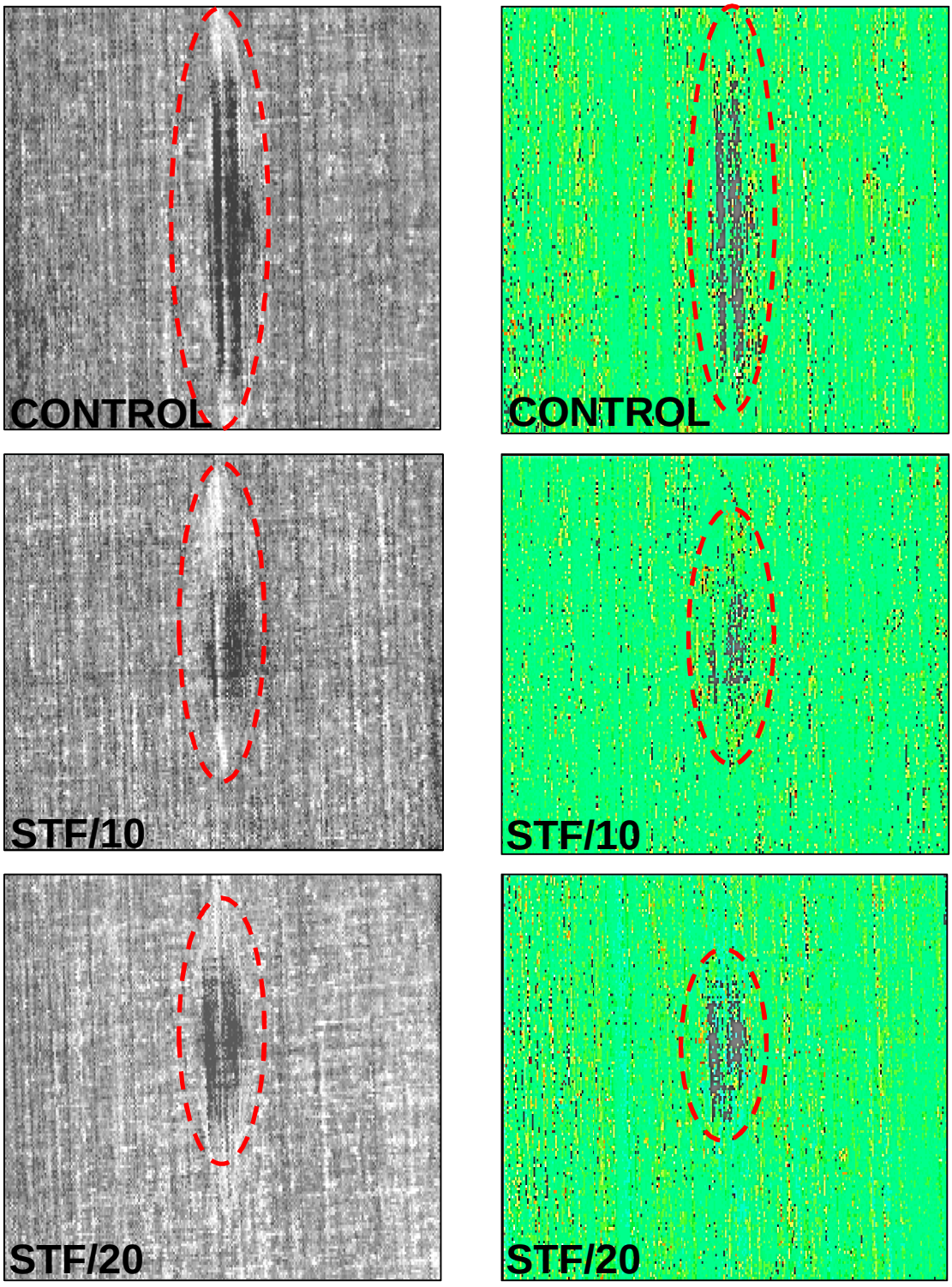

Figure 100 - C-Scan analysis of Impacted STF samples and traditional CFRP

7.3.3 Soundwaves Absorption test

Because of its excellent damping properties, the possibility to use the STF as a soundwaves absorber has been investigated with a specific test.

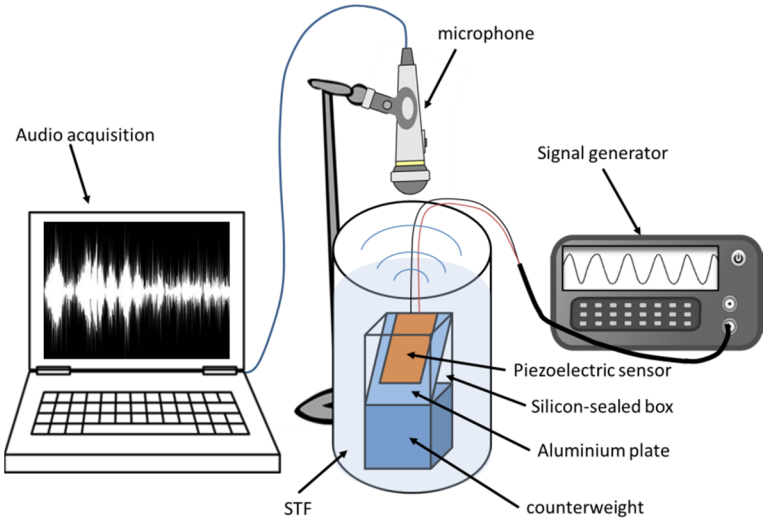

Figure 101 - Schematic of soundwaves absorption test

The procedure, illustrated in Figure 101, consists in sending a chirp signal with a piezoelectric sensor embedded in the STF and capturing the external audio emission with an audio recording device. The sensor is first attached on an aluminium plate and then sealed in counterweighed box which is completely immersed within the STF (Figure 102). The signal used was a frequency sweep between 3000 and 15000 kHz and a comparison has been made between air, water and the STF fluid.

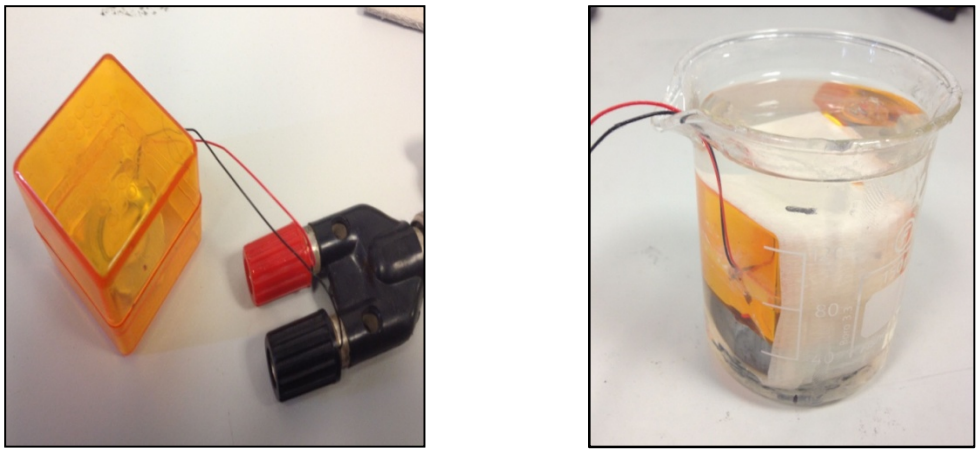

Figure 102 - Sample preparation for sound absorption test

Figure 103a shows the signal collected when air is used as a damping media, and represents the baseline for the experiment. In the second image (Figure 103b), the sensor box has been immersed in water (a traditional insulating media used in several applications [199]) and, as a consequence, the external audio emission shows a general decreasing of the recorded signal. However it is still possible to see several peaks at different frequencies and even a peak higher than the one observed for air at 13kHz.

The results from the STF embedded sensor are illustrated in Figure 103c. In this case it is clear that the sound absorption is almost total, showing no peaks all over the range of frequencies. This result is even more evident from Figure 103d, which shows a comparison between the three damping media tested.

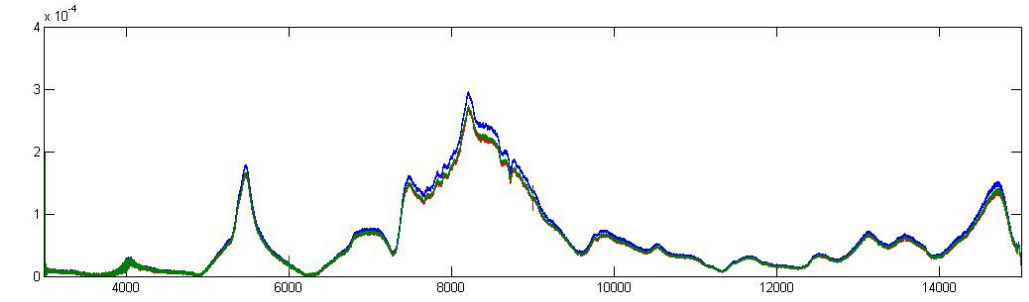

a)

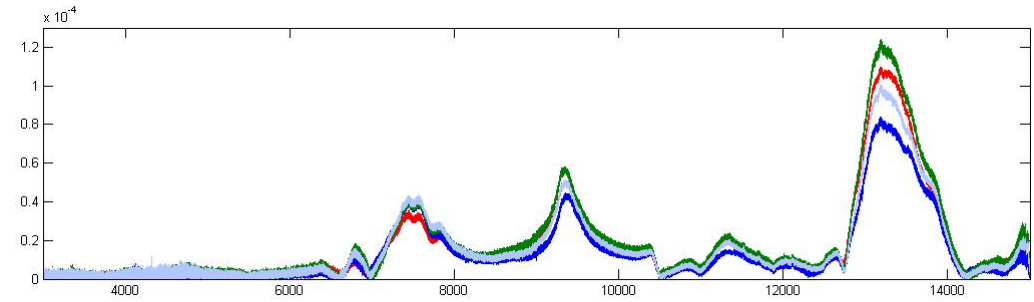

b)

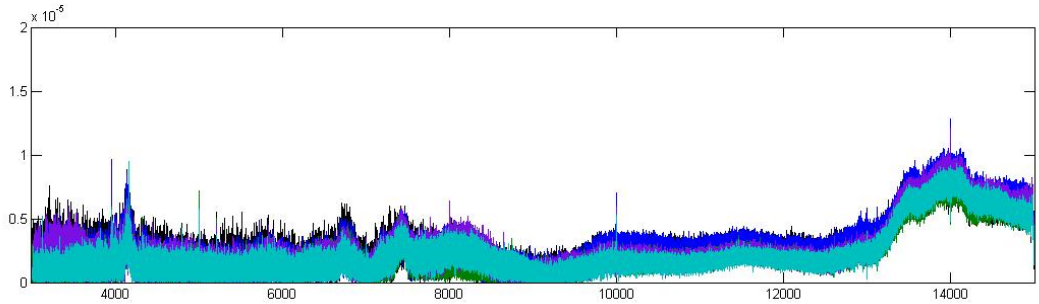

c)

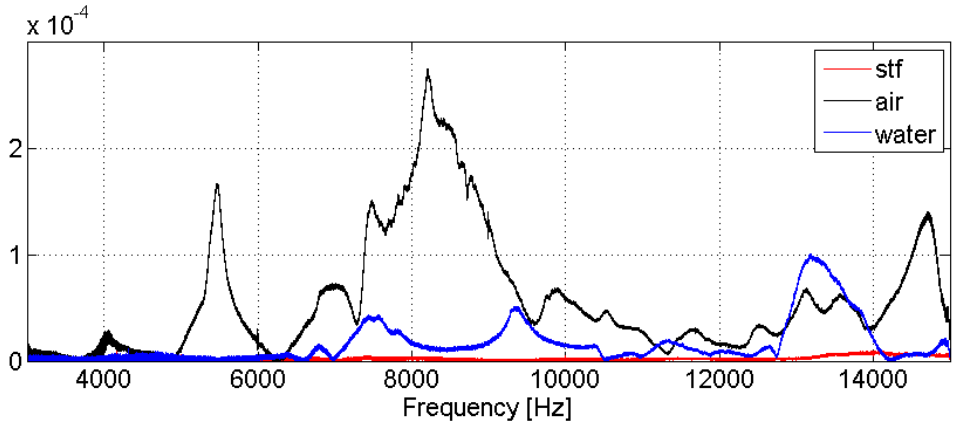

d)

Figure 103 - Recorded audio signal for different damping media: a) air; b) water; c) STF; d) comparison of the media

7.4 Discussion

The aim of this Section was to investigate the possibility to embed nanosilica based Shear Thickening Fluids as shock absorber media within structural CFRP parts, in order to increase mechanical and impact properties. Several solutions have been prepared using nanoscaled silica particles with different dimensions and mixed with Polyethylene Glycol at different concentrations. The viscosities of the solutions have been analysed with rheological measurements and the results showed an evident increase of the viscosity once a critical shear rate $\dot{\gamma}_c$ is reached. Further tests have also find out that increasing the concentration of nanoparticles within the solutions enhances the thickening effect, leading to higher level of final viscosity. Critical shear rate is also inversely proportional to the nanoparticles concentration within the STF.

Composite samples were manufactured sandwiching an STF layer between traditional prepregs and were tested in free and forced vibration in order to estimate the damping properties. Forced vibration analyses showed that the amplitudes of the natural frequencies of the hybridised samples are decreased and shifted to higher frequencies in comparison with a traditional CFRP, suggesting an increase of stiffness and damping ratio for the nanomodified material. Free vibration tests confirmed the previous results showing an increase in both damping ratio and logarithmic decrement of more than 50% for the STF reinforced samples in comparison with the unreinforced laminates.

Impact test were conducted on samples with STF characterised by an increasing concentration of silica nanoparticles and with different dimensions. The results showed that for high velocity impacts (40J) the presence of the embedded fluid within the CFRP structure is able to enhance the energy absorption rate by more than 50%. This effect cannot be seen for lower velocity impacts (6 and 20J) because the hydroclusters activation mechanism requires relatively higher shear solicitations; moreover, the elastic answer given by the material when subjected to lower velocity impacts does not activate any deformation of the embedded fluid, therefore the STF is not involved in the energy dissipation mechanism. Raising the concentration of nanoparticles or increasing the dimension of the nanoparticles within the STF leads to an increase of the energy absorption.

These results have been confirmed by C-Scan analysis, which showed how the inclusion of the STF is able to reduce by more than 30% the extension of the internal delamination for samples subjected to high velocity impacts. Increasing the concentration of nanoparticles within the STF enhances this effect.

In addition, the silica based STF has been proved to be an excellent soundwaves insulator, showing an almost complete absorption of signals in the audible range in comparison with air and water.

8 Multifunctional hybrid composites based on the inclusion of Shape Memory Alloys for improved impact properties

As said in the beginning of Part III, one possible solution to enhance damping and impact resistance of a structure is to include an additional engineered phase within the laminate and the experimental results illustrated in the previous Section represent a good example of the advantages gained through such hybridisation process.

By following a similar approach, impact properties can be improved by embedding SMA wires within a traditional laminate in order exploit their superelastic behaviour to reduce the extent of the internal delamination caused by low velocity impacts. This particular property of SMA rises from the transition between two different crystalline structures which is activated when the material is subjected to an external load. Indeed, the phase transformation generates a plateau region in the stress-strain curve, resulting in an hysteretic behaviour of the material. This unique property makes SMAs able to absorb more energy during an impact event and can increase the damage impact resistance of a composite part when they are embedded within its structure.

8.1 SMA-Composites

The idea of using SMA as reinforcement for composite panels was first proposed by Rogers and Robertshaw in 1988 [200]. A comprehensive review of the state of the art of SMA hybridised composites for the purpose of damage suppression has been undertaken by Angioni et al [201]. Paine and Rogers [202] investigated experimentally the possibility to exploit the superelasticity of SMA for improving the impact resistance of composite parts subjected to low velocity impacts (LVI). High-energy impact tests (18 and 23 J) were conducted on samples manufactured with a cross-ply layup of graphite/bismaleide hybridised with Nickel Titanium (NiTi) wires in the lower 0º/90º interface. Their results showed that the presence of the SMA

within the composite structure prevented the samples to be completely perforated and reduced the internal delamination area in comparison with a traditional graphite laminate. Moreover they determined that the peak impact forces of the hybrid samples were much higher than the ones recorded for the un-reinforced material.

The study conducted by Birman et al [203] analysed the design optimisation of hybrid cross-ply composite laminates, concluding that the embodiment of SMA fibres enhances impact resistance and that a further improvement can be given optimising their distribution throughout the structure.

Khalili et al [204] developed a complete model for studying the effect of an impact on smart hybrid composites with or without prestrain in the SMA wires. Results have demonstrated that the hybrid composites are able to dissipate energy more uniformly and rapidly than the unreinforced laminates for thin-walled structures, while no positive effects were seen for thick-walled structures. Moreover, they observed that the volume of SMA wires within the composite plays a key role as it can affect maximum contact force and contact time during the impact event.

SMA prestrain effect was also studied by Tsoi et al [205] together with other specific aspects that need to be taken in account when looking at the impact damage behaviour of hybrid composites. They find out that increasing the prestrain of the SMA wires, the internal delamination area decreases; moreover, in order to improve impact resistance to fibre breakage damages it is preferable to embed the SMA wires in the lower half of the sample.

8.1.1 Theoretical Aspects

SMA are characterised by two different crystalline phases [206]: the martensitic phase (M), which is stable at low temperature (hence $T < Mf$, martensite finish transformation temperature) and the austenitic phase (A), stable at high temperature (hence $T > Af$, austenite finish transformation with $Af > Mf$) (Figure 104).

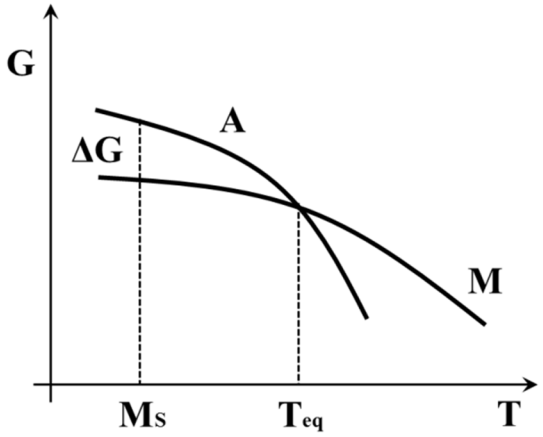

Figure 104 - Gibbs free energy variation for austenite (A) and martensite (M) phases.

Each of these structures is characterised by its own crystalline organisation (Figure 105): martensite presents tetragonal body centred crystalline configuration, while austenite is arranged in face centred cubic structure.

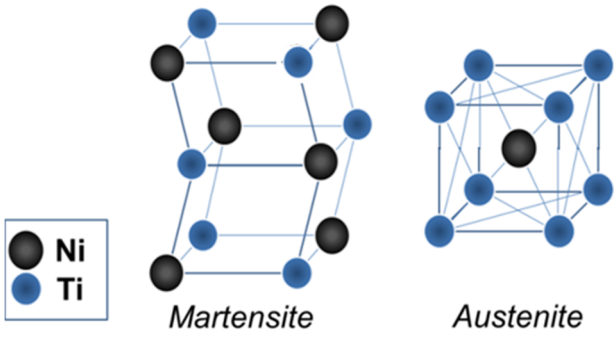

Figure 105 - Lattice configuration for Martensite and Austenite in NiTi SMA

Since the lattice of austenite has higher symmetry than the lattice of martensite [207], when the single crystal of austenite is cooled down below Mf, the martensite phase can assume multiple configurations, called variants. As a consequence, the martensitic phase can assume two different configurations: stress-free martensite, characterised by a multi-variant twinned configuration (TM) which can minimise the effects only of small local deformations, and stress-induced martensite (SIM), characterised by a detwinned configuration (DTM) in which the variants are aligned in a single direction, leading to a material capable of higher macroscopic deformation [208].

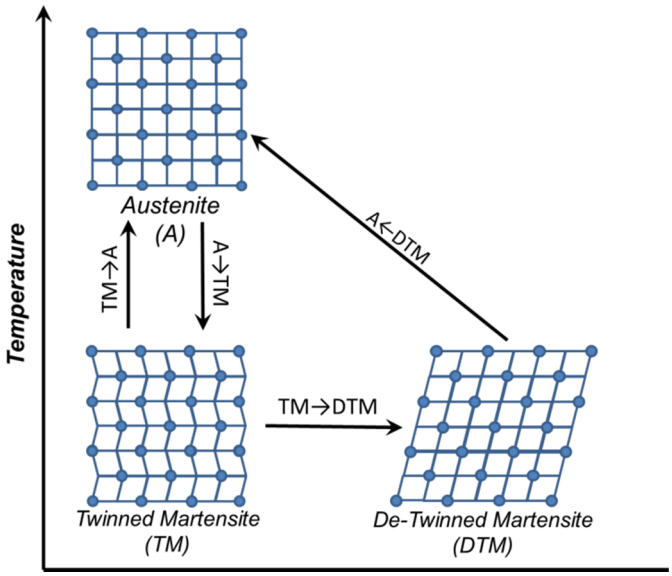

Figure 106 - Trasformation mechanisms between Austenite and both de-twinned and twinned Martensite

The particular properties of SMA rise from the diffusionless thermoelastic phase transition between austenite and martensite that can be thermally or stress/pressure induced. This thermoelastic transformation is a result of the need of the crystalline structure to accommodate itself at the lower energy state for a given temperature.

For temperatures below *Mf* the material is completely in its martensitic phase, therefore, when it is subjected to a stress, it first deforms elastically and then, once a critical value $\sigma_{(TM\text{-}DTM)}$ is reached, it changes its structure, activating a transformation from multivariant to single-variant martensite (TM→DTM) (Figure 106). Once the stress is removed a residual transformation takes place. At this point, if the material is heated up above *Af*, it is able to fully recover the residual strain, showing what it has been called "shape memory effect". This phenomena occurs because for T > Af the detwinned martensite is not stable, therefore the inverse transformation (DTM→A) is immediately activated and the material recovers its original shape. Finally, when the material is cooled down again at T < Mf, it moves back to the ductile multivariant martensite structure without any macroscopic deformation, recovering its original shape.

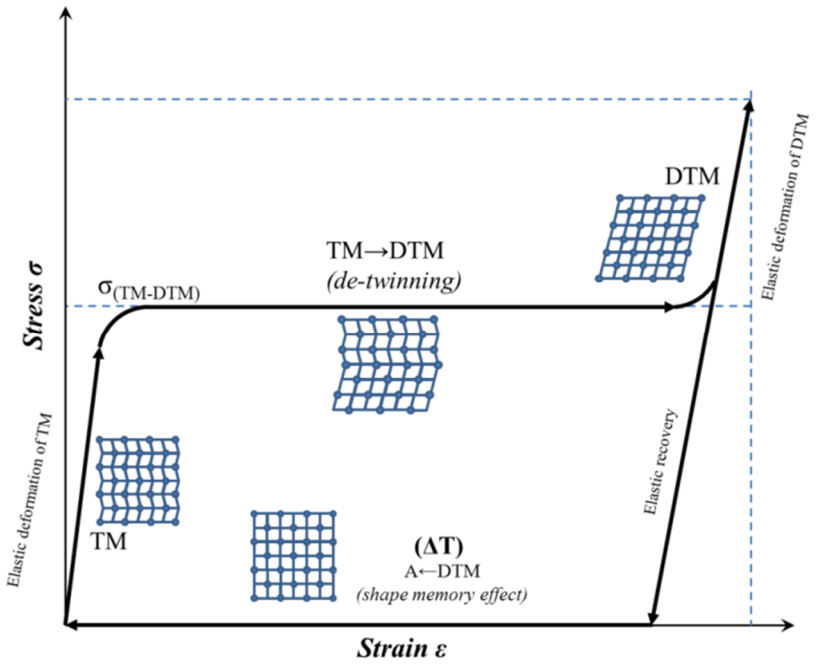

Figure 107 - Shape memory effect (T<Mf): a) elastic deformation of twinned martensite; b) de-twinning transformation from multi-variant (twinned) martensite to single-variant (de-twinned) martensite; c) elastic transformation of de-twinned martensite ; d) elastic recovery obtained with the removal of the load; e) shape memory effect obtained applying a thermal loading ΔT, heating up the material to a T>Af

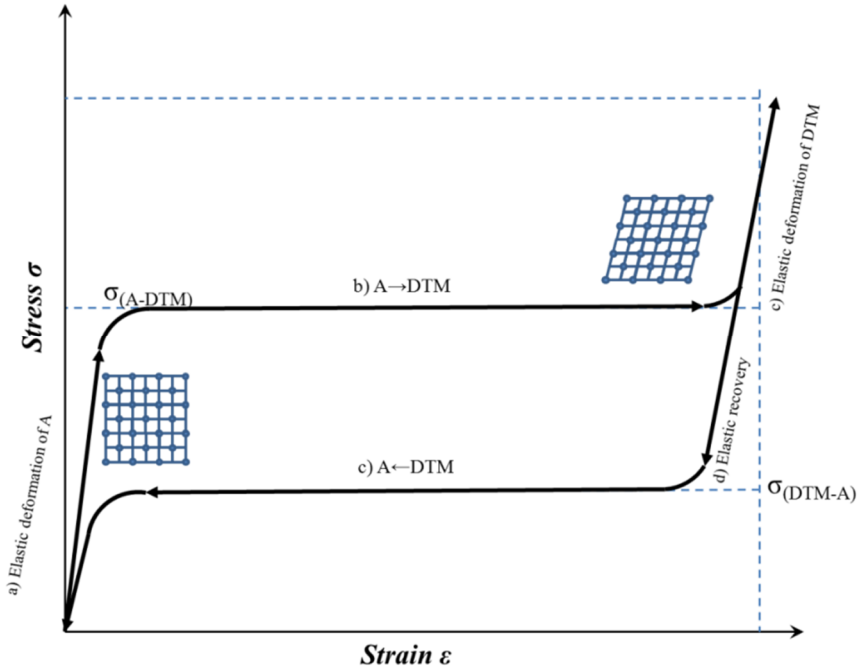

Figure 108 - Super-elasticity (T>Af): a) elastic deformation of Austenite; b) transformation from austenite to single-variant (de-twinned) martensite (Stress Induced Martensite); 3) elastic deformation of DTM; 4) elastic recovery after load removal; 5) super-elasticity effect due to the instability of DTM for T>Af

Another important effect of SMA is shown when the material is stressed at T > Af. In this case, once the stress reaches a critical value $\sigma_{(A\text{-}DTM)}$, the transformation from austenite to detwinned martensite (A→DTM) is activated (Figure 107). When the load is removed, the material reaches $\sigma_{(DTM\text{-}A)}$ therefore, because DTM is not stable at T>Af, the transformation (DTM→A) takes place and the response of the material is purely elastic. This effect of SMA for T>Af is called "super-elasticity" or "pseudo-elasticity".

8.2 Experimental: Sample Manufacturing

In order to test the mechanical properties of SMA composites, hybrid laminates panels were manufactured by Alenia Aeronautica S.p.A. embedding an aramid warp knitted biaxial tape reinforced with SMA wires within a thermoplastic Polyphenylene Sulfide/Carbon fibres (PPS/CF) laminate. The samples were produced via compression moulding technique. As it is possible to observe from Figure 109, which represents the lay-up schematics for the hybrid composite, the SMA/aramid plies are sandwiched between two extra layers of PPS in order to ensure a good impregnation of the SMA wires with the thermoplastic matrix.

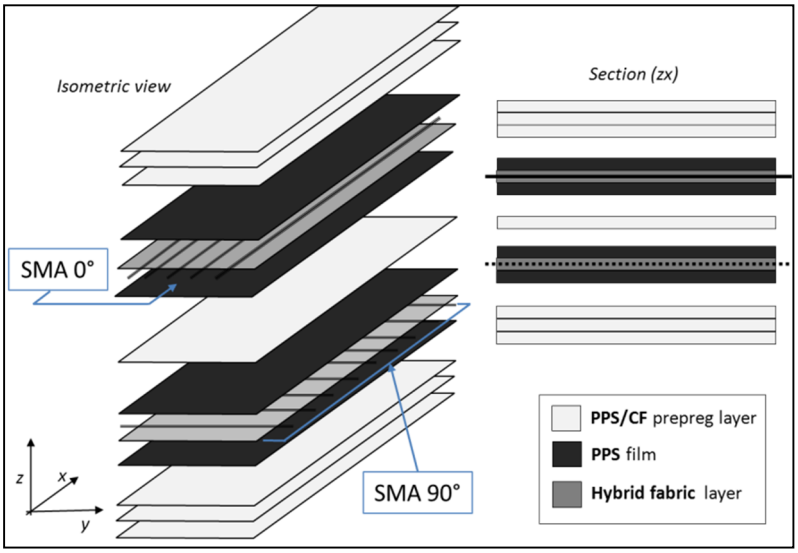

Figure 109 - Manufacturing schematic of PPS/CF SMA hybrid composite

In order to analyse the impact properties enhancements of the hybrid composite, a traditional PPS/CF laminate has been also manufactured and used as a baseline. After the forming process, composite plates were cut to 100mm squares with a thickness of 2.6mm using a diamond cutter.

8.3 Composite Mechanical Characterisation

8.3.1 Low-velocity impact test

Low velocity impact tests were conducted using a drop tower and Force-time histories were acquired using a load cell. The values for the impact Energy (E_{imp}), height of the falling mass (h_{imp}) and impact velocity (v_0) are summarised in Table 8 together with the specifications of the impactor.

The impact height h_{imp} was calculated from the equation: $h_{imp} = E_{imp}/mg$, where g is the acceleration due to gravity (~9.8ms^{-2}). The final velocity of the impactor (v_0) is independent from the mass and can be calculated from the conservation of energy (neglecting the drag force caused by air resistance), obtaining: $v_0 = \sqrt{2gh_{imp}}$

E_{imp}	h_{imp}	v_0
(J)	*(m)*	*(m/s)*
20	0.16	1.7
30	0.24	2.1
40	0.32	2.5
Impactor mass	head geometry	head diameter
(*kg*)		(*mm*)
12.6	hemispherical	20

Table 8 - Specification for LVI tests

Samples were clamped in order to reduce the chance of any movements or vibrations of the sample during the impact. It is important to underline that the type of clamp

used strongly affects the final results [209], therefore tests obtained using different clamping conditions may be different.
In order to evaluate acceleration, velocity and displacement history during the impact, a numerical method has been applied.

The velocity of the impactor v(t) can be obtained by integrating the force history (F_{imp}) following the equation:

$$v(t) = v_0 - \frac{1}{m}\int_{t0}^{t} F_{imp}\,dt$$

In the same way, the displacement can be calculated by integrating the velocity history. Moreover, based on the values of velocity, it is possible to evaluate the time-history of the energy transferred from the impactor to the composite sample by solving the equation:

$$KE(t) = \frac{1}{2}mv_0^2 - \frac{1}{2}m[v(t)]^2$$

As for the internal damage evaluation, according to several authors [210-212], ultrasonic technique can be used to evaluate the size of the projected damage area, in order to identify the principal fracture mechanism that occurs when a composite panel is subjected to a LVI. In this work, a C-Scan probe with a frequency of 5MHz was set to scan the entire surface of the sample, using x-y increments of 500μm.

Results obtained from the impact tests are shown in Figure 110 and Figure 111, which represent data collected for the PPS/CF samples and for the PPS/CF+SMA hybrid composites respectively.

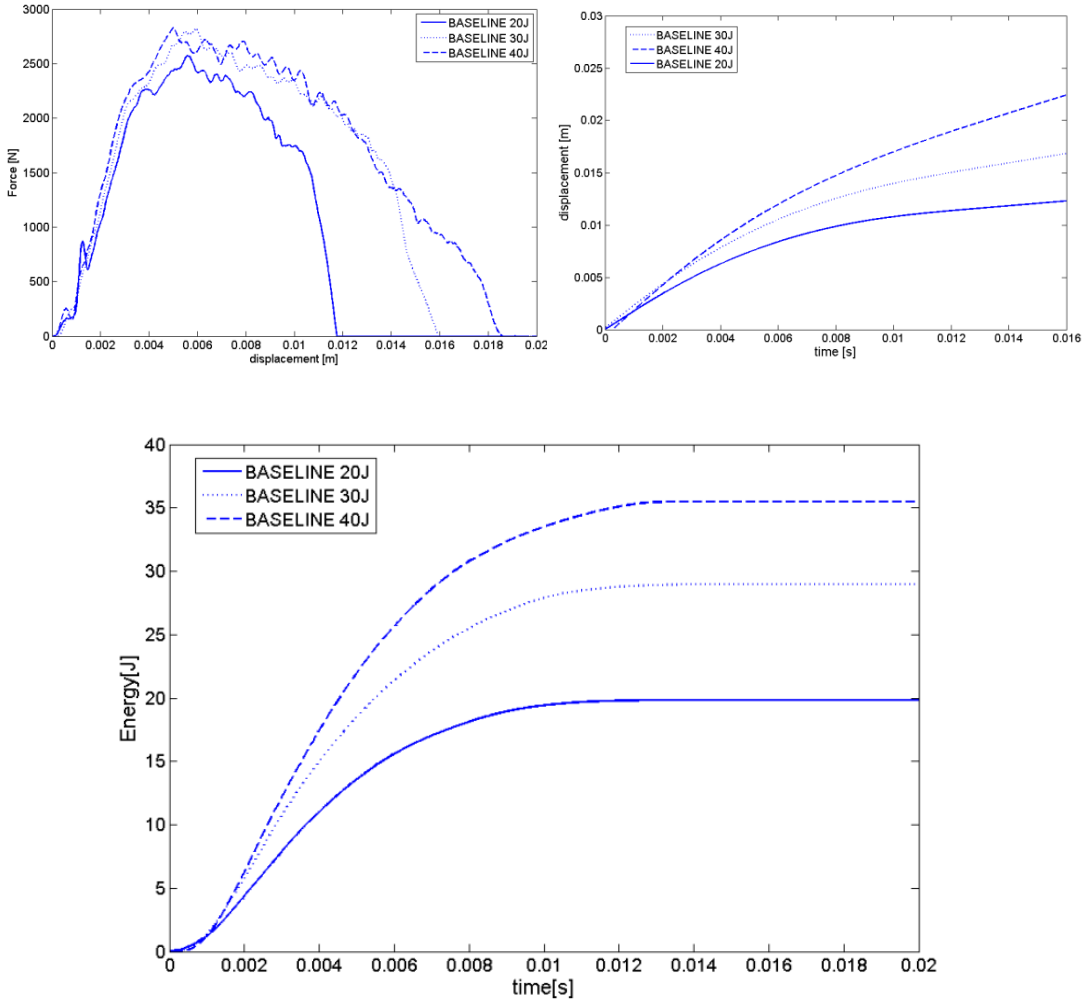

Figure 110 - data results for baseline (PPS/CF) samples: a) force displacement behaviour; b) time displacement; c) Energy absorption history

Figure 110a represents the typical force/displacement curves for impacts on the baseline samples (control) with three different impact energies (20, 30 and 40J). As it is possible to observe from the curves, the force peak reaches higher values when the energy of the impact increases due to the higher velocity of the impactor [213]. Indeed, moving from 20J impact to 30J, the maximum force recorded during the impact event shows an increase of ~9%, while for the higher energy impact (40J) there is almost no improvement (~0.7%).

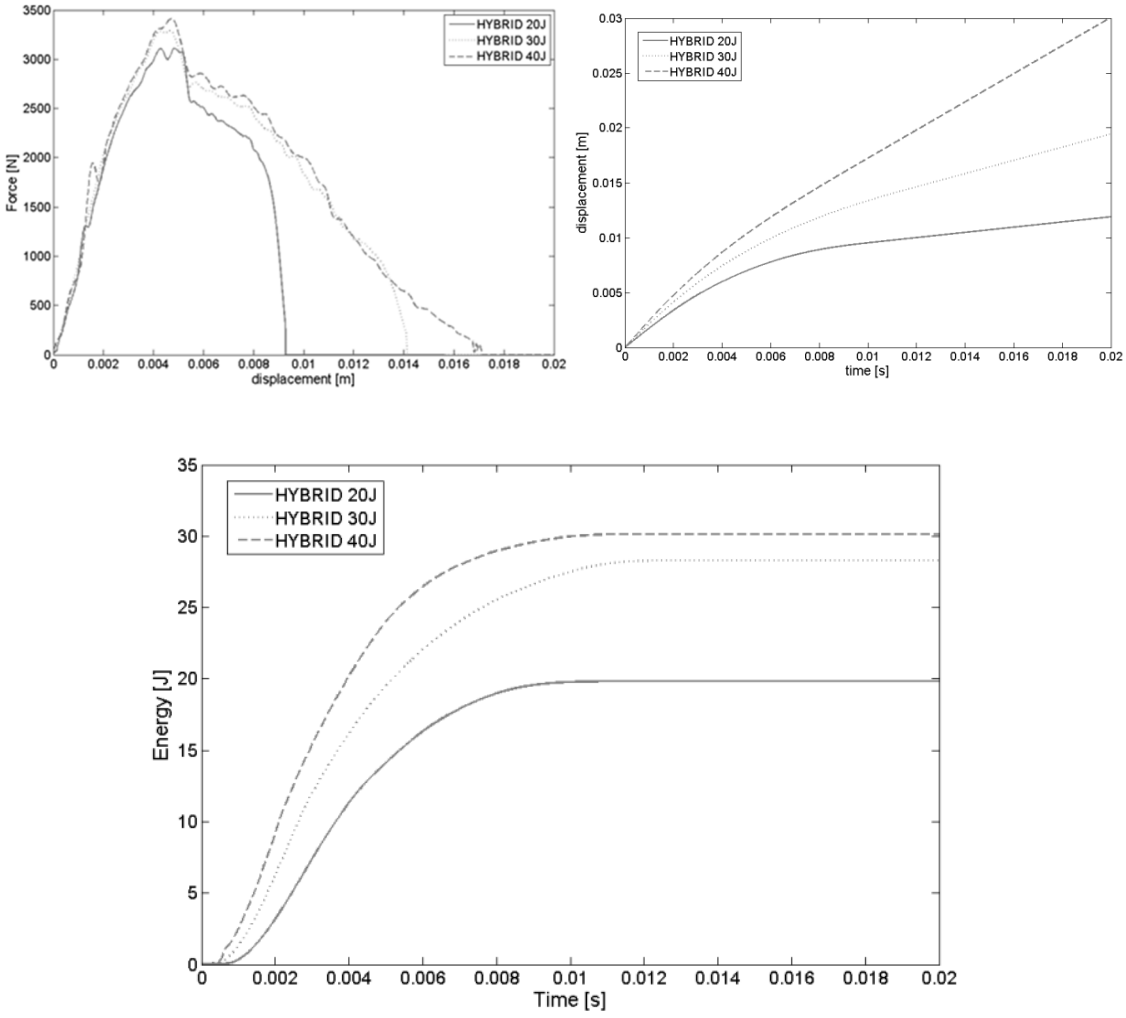

Figure 111 - data results for hybrid (PPS/CF+SMA) samples: a) force displacement behaviour; b) time displacement; c) Energy absorption history

Same trend can be observed in Figure 111a for the impacts on the hybrid samples, in which it is possible to observe that the maximum force is increased by 6% in the passage between 20 and 30J and by an additional 4% for the 40J impact.

Analysing Figure 110b and Figure 111b, which represent the behaviour of the displacement recorded from the instrumentation during the impact time for both the unreinforced and hybrid composites, it is possible to notice that for all the tests the impactor penetrated within the sample thickness without any elastic rebound. The penetration depth however, reaches higher values for higher energy levels as the

number of fibres that are actually broken by the impactor head increases taking the more the shape of a 'volcano' (see Fig Figure 112).

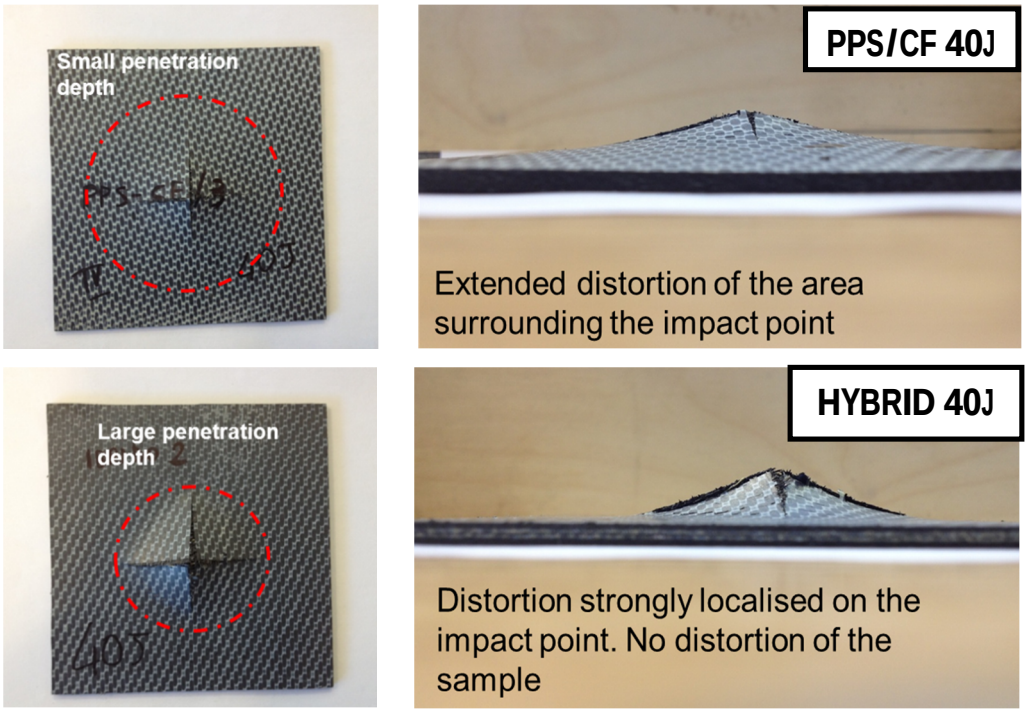

Figure 112 - Visual inspection of impacted samples: a) PPS/CF unreinforced sample; b) PPS/CF+SMA hybrid sample

The behaviour of the kinematic energy transferred from the impactor to the sample is represented in Figure 110c and Figure 111c for both PPS/CF and hybrid samples. As it is possible to observe, increasing the incidental energy, the quantity of energy absorbed during the impact event increases almost linearly for the unreinforced composite showing an increase by 44% from 20 to 30J and by 25% from 30 to 40J. Hybrid samples present a different behaviour, showing an increase of 43% between 20 and 30J and just a slightly improvement for the 40J impact (~6%).

It is important to underline that all the data recorded during the impacts are taken on singular point on the sample surface, therefore in order to analyse more in depth the behaviour of the hybrid composite, it is necessary to take in account the whole area that surrounds the impact point. Based on this consideration, Figure 113 represents C-Scan images taken for both PPS/CF unreinforced and SMA hybrid samples after the

impact tests. The extent of the internal delamination has been evaluated for sample subjected to impact with increasing incidental energy.

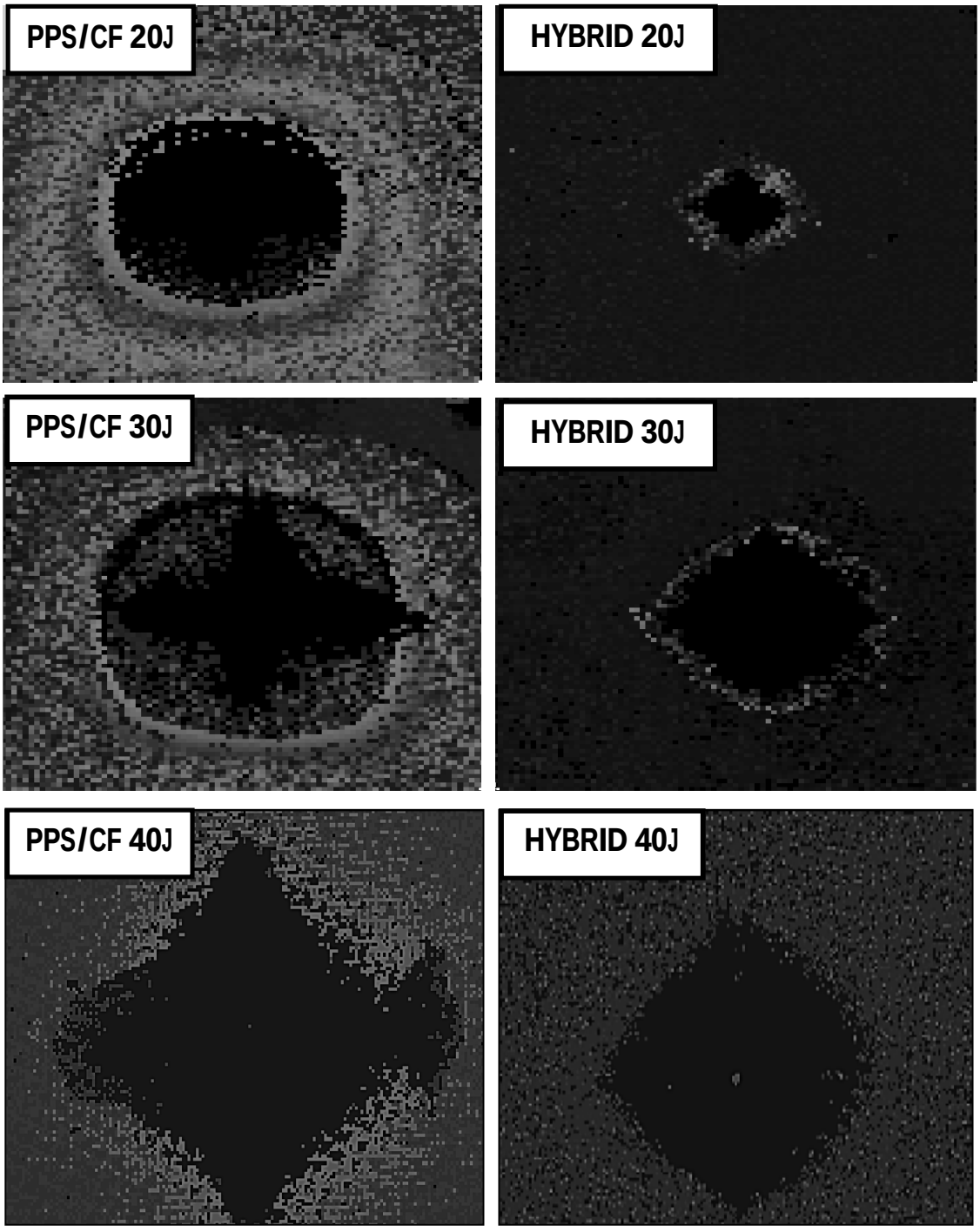

Figure 113 - C-Scan images for hybrid and unreinforced PPS/CF

The comparison between the hybrid composite and the PPS/CF baseline is summarised in Figure 114. As it is possible to see from Figure 114a the curve for maximum force is shifted to higher values for the SMA based hybrid composite, showing an increase of ~20% for all the incidental energies. This result suggests that the presence of the SMA within the laminate structure improves the stiffness of the composite resulting in a material which is able to withstand higher-energy impacts (see Force-Displacement curves on Figure 115) [214].

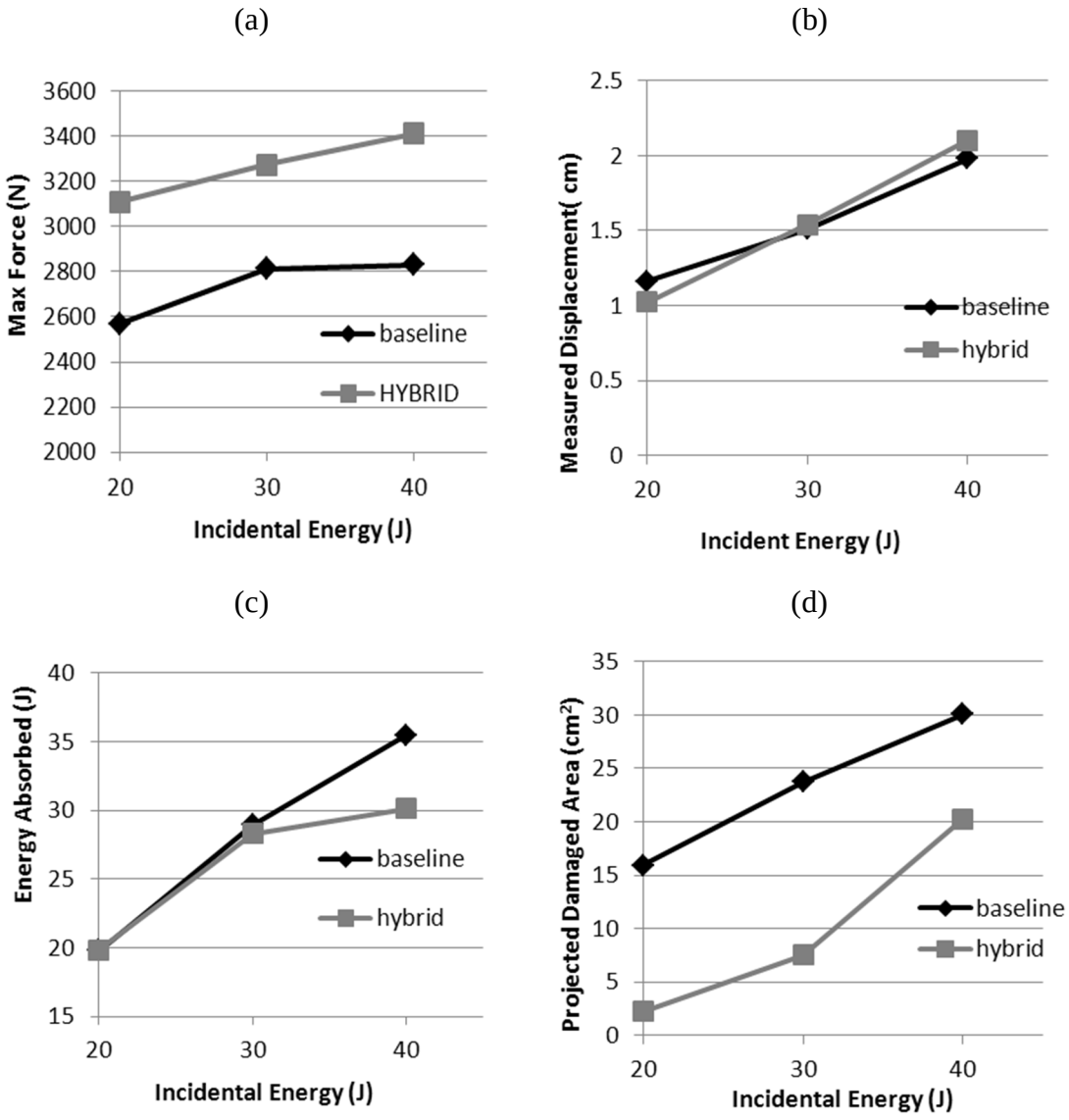

Figure 114 - Comparison between PPS/CF and hybrid composite: a) Maximum Force; b) Penetration Depth; c) Energy Absorption; d) Projected damaged Area

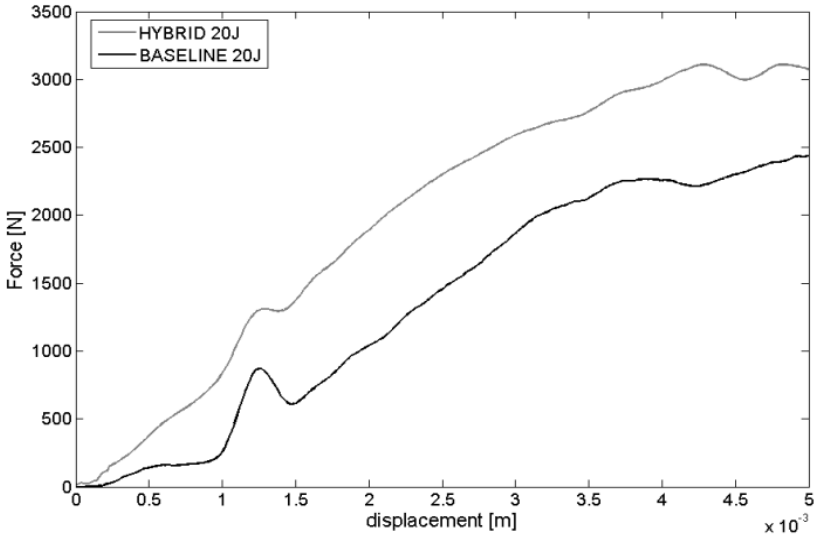

Figure 115 - variation of the elastic behaviour between PPS/CF unreinforced samples and SMA based hybrid ones

Another important result is given by the analysis of the measured displacement at different values of incident energy. Indeed, as it is possible to see in Figure 114b, the behaviour of the two materials is quite similar, however at the lower impact energy (20J) the displacement measured for the hybrid samples is slightly lower than the one of PPS/CF composites (-15%). Increasing the incident energy, this trend starts to revert, showing the same value of displacement for 30J impacts and a higher displacement for the hybrid samples in the 40J impacts data (+6%). Even if those differences fall within the experimental error, this slight change in behaviour could be explained with the increased velocity of the impact when the incident energy reaches higher values. Indeed, while for the 20J impact the predominant effect is the increased stiffness of the SMA which reduces the bending movement of the entire sample, when the velocity is raised the impact event is more localised, therefore the probability that the sample will be able to dissipate energy through bending decreases and shear driven phenomena become more important, enhancing the local SMA hysteretic behaviour which allows larger localised deformations.

Figure 114c represents the energy absorption values for increasing levels of incidental energy. For the lower impact energy (20J), hybrid composites show a very slight increase of energy absorption (~0.5%), while for 30J impact this trend is inverted, showing a decrease of (~1%) in the passage between the unreinforced composites to the hybrid ones. This effect is more evident in the data collected for the 40J impacts in which the hybrid composite shows a decrease of the absorbed energy of more than 15%.

As said earlier in this section, when a laminate is subjected to an impact, the energy is transferred and absorbed with a complex mechanism, which comprehends the combination of different sub-mechanisms (fibres breakage, matrix and interphase cracking, structural vibration, material damping, etc.), therefore the values of the absorbed energy have to be analysed in relation with the corresponding delamination areas measured from the C-Scan images. Figure 114d represents the extension of the internal delamination for the samples tested at 20, 30 and 40J. As it is possible to see from the curves and from the ultrasonic images (see Figure 113), the presence of the SMA within the laminate thickness decreases the tendency of the material to dissipate energy through internal delamination, reducing by 7 times the projected damaged area for the lower impact energy (see Figure 113a). This effect tends to decrease when the energy of the impact reaches higher values. However, the hybrid samples still record smaller extent of the internal delamination in comparison with the unreinforced ones (less than 300% for the 30J impacts and less than 50% for the 40J ones). Similar results on PPS/CF hybrid composite have been obtained by Meo et al [215] for the lower velocity impact (20J).

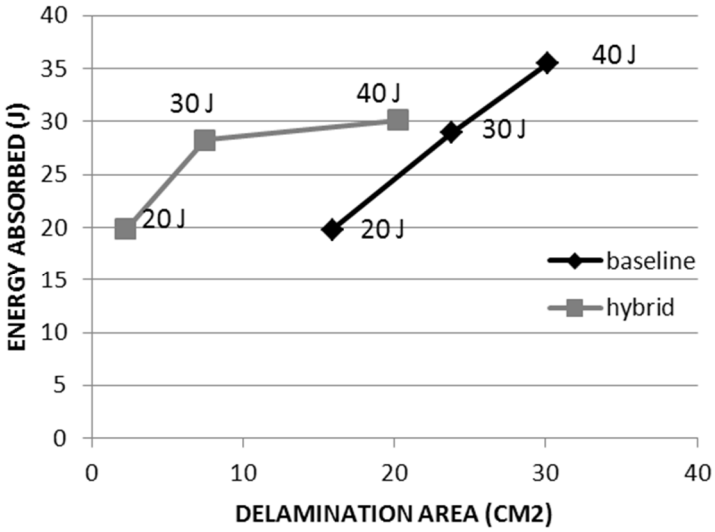

Figure 116 - Relationship between extent of the delamination and energy absorptio for PPS/CF and hybrid composites

Figure 116, clearly summarizes the change in LVI response between traditional PPS/CF composite and hybrid SMA based laminates. Indeed, when subjected to medium velocity impacts (20 and 30J), both the materials absorb the same amount of energy, however, comparing the dimension of the internal delamination, the damaged area for the unreinforced sample is much more extended than the hybrid ones. This indicates that the hybridisation process changes the response to low velocity impacts for the reinforced material, modifying the energy absorption mechanisms of the structure. The behaviour of the hybrid composites can be explained with the superelastic and hysteretic properties of the SMA wires embedded within the structure, which are able to absorb a large amount of energy during the impact, therefore reducing the amount of energy dissipated through intra-laminar damages formation. The change in the trend for the energy absorption and the decreasing of the delamination extent difference between the baseline and the hybrid composite with increased incidental energy can be explained with the progressive fracture of the SMA wires within the laminates which hinders the SMA superelastic dissipation, lowering the energy absorption.

8.4 Discussion

This Section investigates experimentally the response of PPS/CF composites reinforced with superelastic SMA wires and subjected to low velocity impacts. Impacts at different incident energies (20, 30 and 40J) were carried out and a comparison has been made with a traditional unreinforced composite laminate. Furthermore, the extension of the internal delamination has been evaluated through ultrasonic C-Scan analysis. Results showed that the presence of the SMA wires within the laminate structure increases the stiffness of the composite, shifting the maximum force values to higher levels. Analysing the energy absorption in relationship with the extension of the internal delamination it is possible to observe that for medium incidental energies the amount of energy transferred from the impactor to the samples is almost the same for both unreinforced and hybrid composites. However the hybridisation process changes the energy dissipation mechanism showing a reduction of more than 500% in the extent of the intra-laminar damage for the SMA reinforced samples. This behaviour is less evident when the incidental energy is increased to higher levels because of the progressive failure of the SMA wires.

In conclusion, the results given by the experimental campaign have demonstrated that the SMA hybridisation process is a valid design technique to increase low velocity impact resistance of composite laminates.

PART IV:

Multifunctional composites for non-structural applications

The previous Sections of this study have proved experimentally that it is possible to improve some particular aspects of the mechanical behaviour of a material by including additional phases within the structure of a traditional laminate. These modifications can be based on the inclusion of different species of reinforcements such as nanolayers (Section 5), nanoparticles (Section 6), nanofluids (Section 7) or metal alloys (Section 8). However, as seen in Section 4.2, the feasibility of a composite part can be further improved by activating additional features which are not strictly structural and can overcome some technical problems such as maintenance and costs, broadening the range of applications in which it could be employed.
Among all the additional abilities that it is possible to include within a multifunctional system, the possibility to enable an autonomous assessment of the health status of the structure is one of the most appealing ones, as demonstrated by the large amount of studies present in literature already illustrated in Section 4.2.2. In line with this concept, SMA based composites represent a good candidate for a new class of multifunctional composites in which the mechanical improvements given by the presence of SMA wires (as seen in Section 8.3.1) are coupled with additional non-structural features, such as strain sensing, structural health monitoring and de-icing.

This Section investigates the sensitivity of SHM/NDE features in SMA based composites. The original contribution of this chapter relies on the possibility to exploit the electro-thermal properties of the embedded SMA network to simultaneously enable a real time assessment of the stress distribution over the entire structure by monitoring the electrical resistance variation and localise potential internal damages using the SMA network as an embedded heat source and measuring the variation in the apparent temperature on the composite surface via active thermography.

9 Multifunctional hybrid composite based on the inclusion of Shape Memory Alloys for SHM and NDT features

In order to enable SHM/NDT features within a multifunctional composite system, there are two different approaches that can be followed, which are both important and, in a way, mutually connected.

The first approach is based on the real time monitoring of the stress distribution on the material during its lifespan using a strain sensing material. Indeed, knowing the critical points of the structure, a sensing device can be effectively used to know when a critical point is undergone to tensile or compressive strain above a certain threshold. In this way, the strain (or stress) state near the tip of a crack caused by a remote load (as in case of an impact event) or residual stress can be more accurately predicted. As illustrated in Section 4.2.2, this particular ability can be enabled by embedding a large number of materials, however, during the last decade, SMA based composites have attracted the attentions of a large number of researchers due to the good matching between their structural properties and their non-structural features.
In the study conducted by Seguin et al [216], crystallised Nickel-Titanium (NiTi) SMA films deposited on polyimide substrate have been tested as potential micro-actuator to be used as strain sensors. Their results showed that NiTi films can be employed in the development of new MEMS devices that do not require high temperature annealing. Cui et al [217] investigated the relationship between strain and electrical resistance variation in a SMA to exploit the sensing ability of such material, concluding that this relationship is linear and independent from the temperature only when the material is in the martensite phase (while for austenitic phase it becomes more complex). Similar results were obtained by Hideki et al [218], who demonstrated that the amount of damage in a hybridised GFRP can be evaluated via monitoring the electrical resistance variations of the embedded SMA.

The second approach relies on the possibility to analyse the structural integrity of the material once a critical load has occurred, using different NDE techniques such as X-Ray tomography [219], shearography [220], ultrasonic imaging [211] and many others. Among those, active Infrared Thermography (IT) plays an important role in the area of non-destructive evaluation of subsurface defects for a wide variety of structural materials, including metallic and composite media [221]. In this technique, the temperature gradient generated at the medium surface due to heat stimulation are recorded and analysed by an infrared camera (IR), providing information about the integrity of the structural components. Indeed, as thermal waves propagate through the sample thickness, the heat diffusion rate over a structural defect (cracks or delamination) will differ with reference to the surrounding area [222]. As a consequence, analysing the thermal response on the sample surface it is possible to quantify the internal integrity state of a material.

Depending on the type of external heat source used to generate the thermal wave, the most common methods used in active IT can be distinguished in lock-in (or modulated) thermography [223], pulsed thermography [224] and step-heating thermography [225]. Lock-in thermography (LT) employs a periodic heat excitation to collect information on the structural damage, by using the reflected and incident thermal waves magnitude or phase. However, as the probing depth is determined by the excitation frequency, LT is time consuming for defects located at various depths in the test specimen, and requires sophisticated data acquisition systems to input the heat source. In pulsed thermography (PT), a short duration energy pulse is applied and the specimen subsurface structure is detected through the surface temperature evolution. Nevertheless, this approach is not suitable for thick structures and low conductive materials, as the intensity of the pulse is limited in order to avoid any damage of the structure. Unlike PT, in step-heating thermography (SHT) a low intensity pulse (heat source) is applied for a long period, thus enabling a longer heating time to locate deeper defects.

Although all the above-mentioned techniques are quite effective in monitoring the structural integrity of a composite part, one of their bigger disadvantages is that they

all need external heat sources as high-power photographic flashes [225] or infrared radiators [226], which may limit their use for *in situ* aerospace or civil applications.
Based on these considerations, it appears clear that the possibility to directly embed an internal heating source within the material structure could be able to overcome this problem, guaranteeing a good and rapid damage assessment without the need to use large external heaters or complex signal processing techniques.

9.1 Experimental: SMA samples manufacturing

Several samples have been manufactured during the experimental campaign, in order to test the multifunctionality of SMA based composites for strain sensing, damage detection and de-ice feature. The composite plates were obtained with a T800 carbon fibre using a M21 prepreg provided by Airtech, while the SMA used were NiTi SMA wires with a diameter of 350 μm (see Figure 117). Thermoset resin was used in this experimental work because the thermal solicitations given by the flowing current could affect the properties of thermoplastic matrices in the area surrounding the NiTi wires.

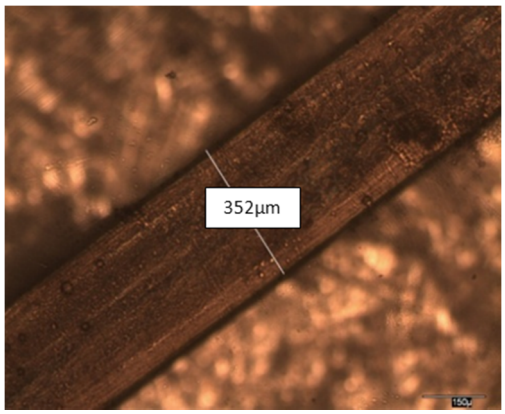

Figure 117 - Optical microscope image of a single NiTi wire

In order to carry out the entire test campaign, several hybrid laminates were manufactured via manual layup. The curing reaction was assured by holding the laminate under a hydraulic hot press at 180ºC for 2 hours.

A first samples (labelled *Sample 1*) was obtained by embedding a single NiTi wire between 4 layers of carbon prepreg in order to test its sensitivity as a strain sensor (see Figure 118).

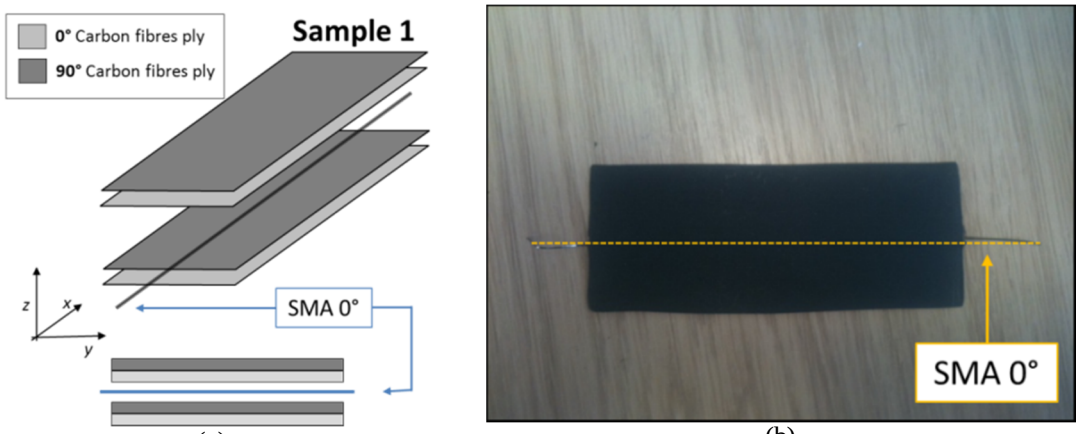

(a) (b)

Figure 118 - Stratification layout of Sample 1 (4 plies, 1 SMA wire) (a), and finished specimen (b)

A second, more complex sample (named *Sample 2, see* Figure 119) was manufactured for the damage assessment test. In this case, two series of NiTi wires were embedded within the cross section of a four plies laminate. Each ply was cut 110 mm in length (*l*) and 60 mm in width (*w*).

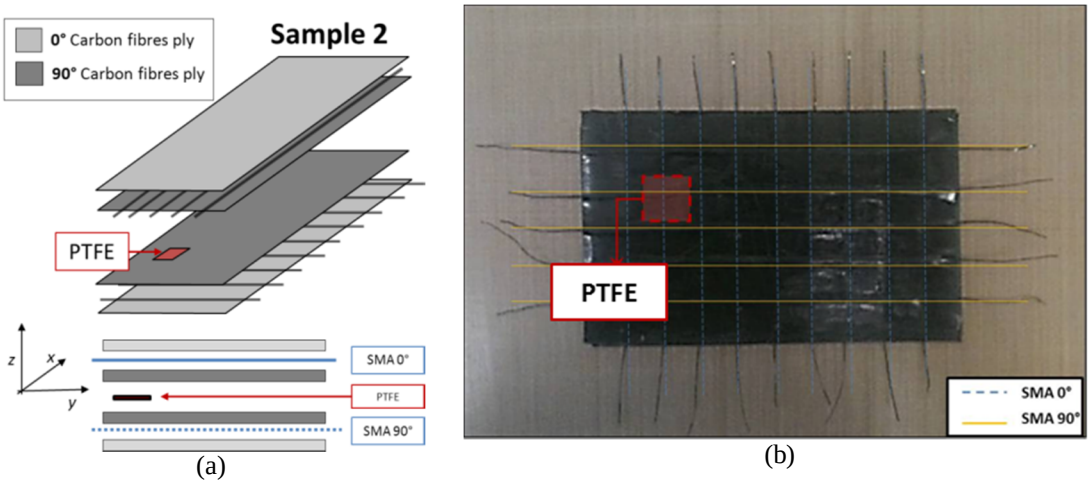

(a) (b)

Figure 119 - Stratification layout of Sample 2 (4 plies, SMA network, 1 defect) (a), and finished specimen (b)

The wires were positioned in order to create a 0º-90º sensors network with an inter-wire distance (*d*) of 10 mm in both horizontal and vertical direction, covering the entire surface of the sample. In order to simulate the presence of a delamination, a

small patch of PTFE (10x10 mm) was inserted in the middle of the sample (at 0.250 mm from the top surface) [227]. Simulation of internal delaminations with embedded PTFE patches is a common procedure that has been reported previously in several experimental works on composite laminates [228-230].

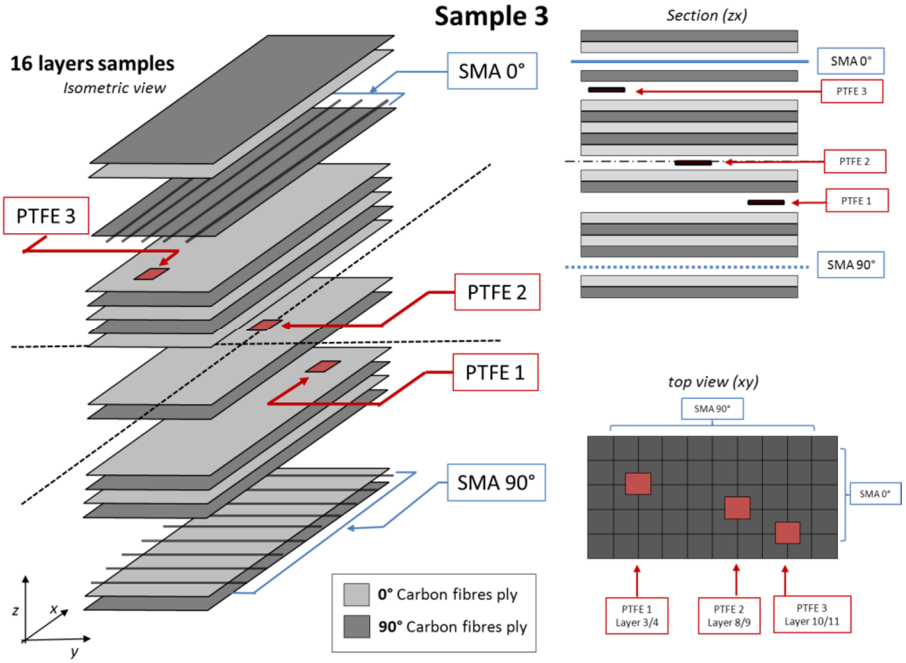

Figure 120 - Stratification layout of Sample 3 (16 plies, 2 SMA networks, 3 defects)

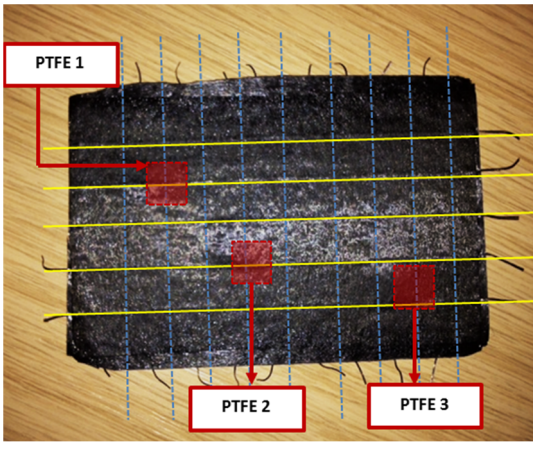

Figure 121 - Sample 3

	x *(mm)*	y *(mm)*	z *(mm) (from top surface)*
PTFE 1	20	30	1.25
PTFE 2	60	20	1
PTFE 3	80	10	0.575

Table 9 - Position of the three PTFE patches embedded in Sample 3

Furthermore, in order to test the sensitivity of the SMA network in monitoring the structural integrity of a panel with multiple damages, a third sample (labelled *Sample*

3) was prepared. The laminate was obtained with 16 plies of prepreg $[90,0]_8$ and three PTFE patches were embedded at different depths (1.25, 1 and 0.575 mm from the top surface). The 0º-90º SMA sensors grid was layered within the sample thickness with the same inter-wires distance of *Sample 2* (Figure 121).

9.2 Strain Sensing Ability of SMA based hybrid composites

Results obtained from Cui et al [231] have shown that there is a relationship between the strain and the electrical resistance variation of SMA wires. However, such a relationship is linear and temperature independent only when the material is in its fully martensite phase, whilst for the austenitic phase some non-linear effects must be taken in account, resulting to a more complex formulation. Therefore, temperature during all the tests was set in order to be always below Mf. The parts of the machine in contact with the pins connected to the samples were covered with PTFE in order to avoid any electrical interference that could affect the readings. The sensing feature of the SMA wires was first tested by loading a single NiTi wire (characterised by a resistance of 2.5 Ω.) in a tensile machine and measuring the resistance variation with a 6-digit precision multimeter (Figure 122*a*).

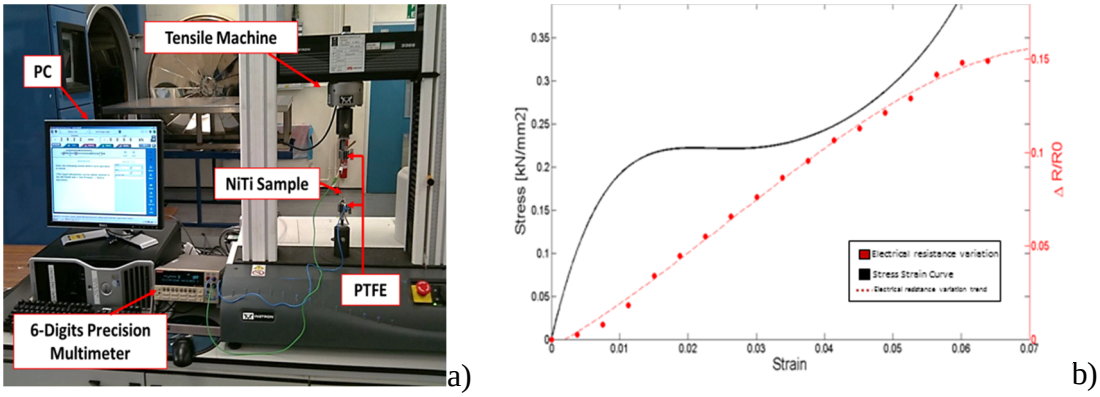

Figure 122 - Single NiTi tensile behaviour: a) experimental setup; b) Stress-Strain behaviour and electrical resistance variation of NiTi wire in tensile mode

As it is possible to observe from Figure 122b, the NiTi wire shows the typical behaviour of a SMA. Indeed, when a load is applied on the wire, it reacts with an elastic deformation while the electrical resistance increases linearly with the increase

in strain. Afterwards, once the stress reaches a critical value, the detwinning of martensite is activated and the curve changes its slope showing a plateau during the entire transformation. However, during the phase changing, the variation of electrical resistance still increases almost linearly with the strain. Hence, this first series of tests confirmed the sensing ability of the hybrid composite, showing that it is possible to measure the strain percentage by measuring the in-situ variation of the electrical resistance of the NiTi wires. Similar results were obtained by other authors in literature [232].

Nevertheless, it is important to underline that the nature of an impact event is very different from a tensile loading in terms of stress distribution. Indeed, while during a tensile test the NiTi wires are loaded in the perpendicular and transversal directions, when an impact occurs, the material is also stressed in the out of plane direction. Therefore, in order to investigate the sensitivity of the hybrid composite in case of a load distribution through the cross section, a three point bending test was carried out using the *Sample 1*. Results of the test are illustrated in Figure 123, and they clearly show that the variation of the electrical resistance with the increasing of the flexural extension remains linear. Thereby, it is possible to analyse the strain distribution within the structure by simply measuring the behaviour of electrical resistance with time of the embedded SMA network.

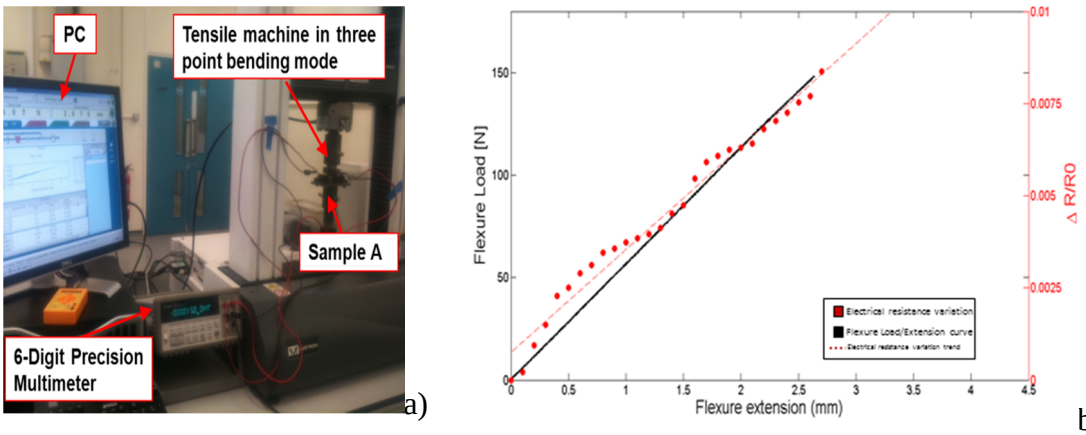

Figure 123 - SMA based composites Three Point Bending test: a) experimental setup; b) Flexural Load versus Flexural Extension and electrical resistance variation for hybrid composites

9.3 Thermographic inspection of SMA based Hybrid Composites

This paragraph is focused on the thermal properties of SMA wires embedded in CFRP composite laminates. In particular, by generating an *in situ* low power resistive heating (Joule effect), a novel technique for the detection and assessment of structural damages was developed. Such a methodology here introduced, combines the multi-physics properties of SMA based composites, with the advantages of thermography inspection, in order to obtain a built-in accurate NDT/SHM technique for anisotropic structures. Moreover, as the heat source is embedded into the material, this methodology is able to overcome the drawbacks of standard infrared thermography for the detection of damages in thick structures and deep-lying defects [233].

Figure 124a represents the experimental setup used for the thermographic inspection of the SMA based composite. Samples were heated up by applying a long pulse of electric current with a period *T* of 2 sec and a constant amplitude of 1 A to each SMA wire. The electric current was provided using a power supply equipment, and the thermal images were taken using an electrically cooled IR camera (CEDIP) with resolution of 320 x 240 (width x height), temperature sensitivity of 30 mK and maximum frame rate up to 150 Hz. All measurements were taken at ambient conditions (20°C).

The selected active thermography method was the SHT method for the evaluation of the magnitude of the apparent temperature at the test piece surface. Unlike other methods, step-heating thermography allows monitoring the temperature evolution during and after the heating process [234]. The thermal images were acquired at an interval of 0.01 sec for an observation time of 5 sec (Figure 124b).
Thermal gradients are caused not only by hidden defects, but are also affected by uniformities due to imperfect heating and local variations of apparent temperature (heat noise) as well as optical and electromagnetic noise, which can further degrade the signal acquired. Hence, to overcome this issue, a background subtraction was

carried out by selecting a number of frames before the long pulse excitation and then computing the average for every pixel across the pre-excitation frames. In our case, the first 100 frames (duration of 1 sec) were used for the background subtraction.

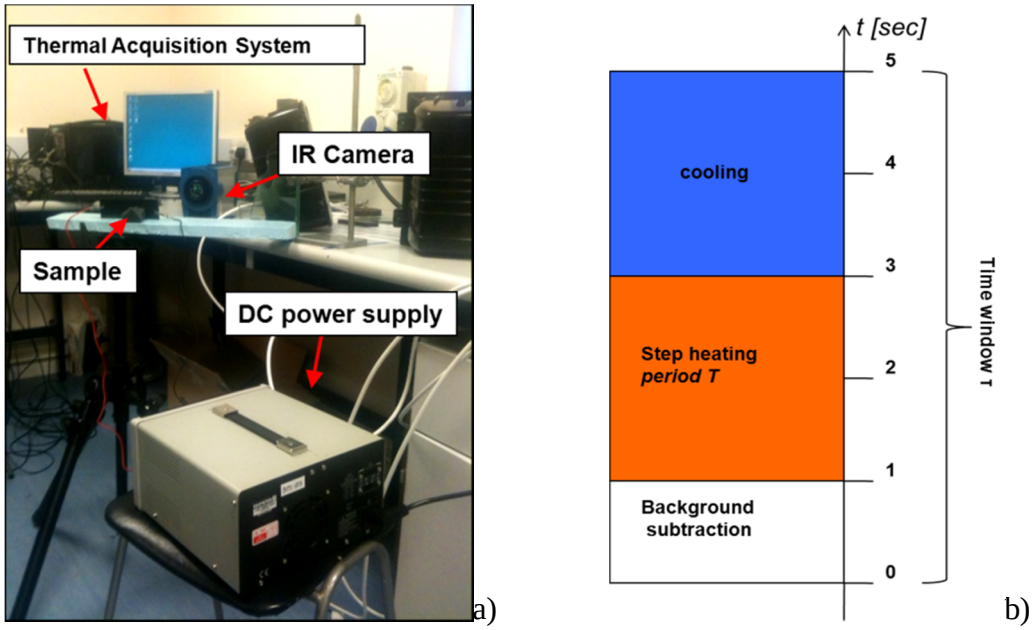

Figure 124 - Themographic inspection of SMA based composites: a) experimental setup; b) opservation time of the IR camera in the step-heating process

Tests conducted on *Sample B* are shown below and they represent the thermograms measured at the end of the step-heat excitation (t=3 sec). Since the epoxy resin within the CFRP is characterised by a low thermal diffusivity, the heat generated via Joule effect in the NiTi wires does not spread immediately through the sample but it is initially confined only in the area surrounding the SMA. This is clearly shown in Figure 125a and Figure 125*b*, which represent the thermal response of the composite when the current flows on a vertically and horizontally aligned NiTi wire through undamaged areas. As it is possible to notice from the images, the variation in apparent temperature changes uniformly all over the area in which the current is flowing, while the surrounding areas are not affected.

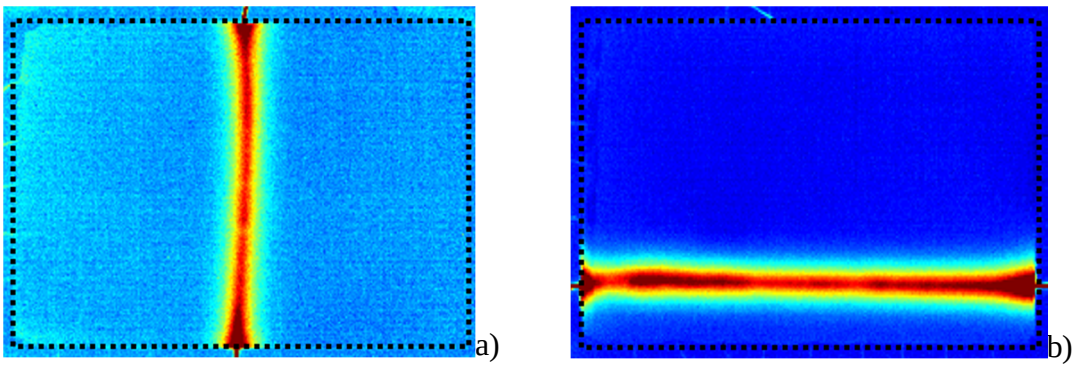
a) b)

Figure 125 - Thermography images for undefective areas of sample 2 (sample dimensions - 100x60 mm – are represented with the dashed line) at t=3s

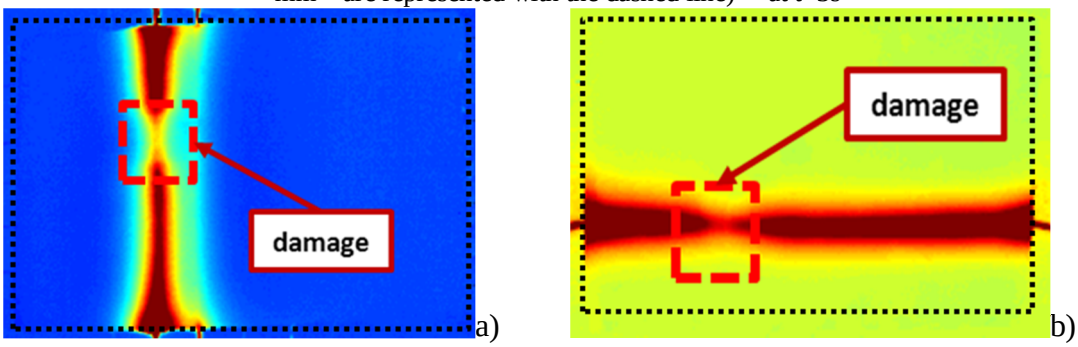

a) b)

Figure 126 - Thermography images for defective areas of sample 2 (sample dimensions - 100x60 mm – are represented with the dashed line) at t=3s

The thermal response of the hybrid composite when damaged parts are analysed is shown in Figure 126a and Figure 126b. Indeed, the presence of the damage within the thickness is immediately identified by a large variation in the apparent temperature of the sample. This effect is generated because the heat flow, due to Joule heating, is impeded by the increase of thermal resistance (due to the different heat conductivity of the PTFE patch) around the damaged area.

In other words, the diffusion rate at that specific point is reduced by the presence of a subsurface discontinuity, resulting in a recorded apparent temperature variation on the surface (see Figure 127).

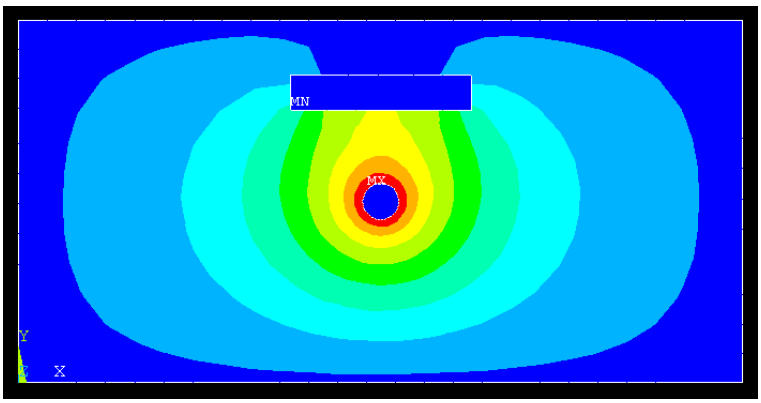

Figure 127 - Schematics of the heat flow diffusion impeded by the PTFE patch

Information regarding the structural integrity of the sample can be also collected analysing the time history of the apparent temperature for the pixels associated to a non-defective area in comparison with those from a defective area. Figure 128 represents the behaviour of the observed temperature during the entire test for a damaged (continuous curve) and an un-damaged point (dashed curve).

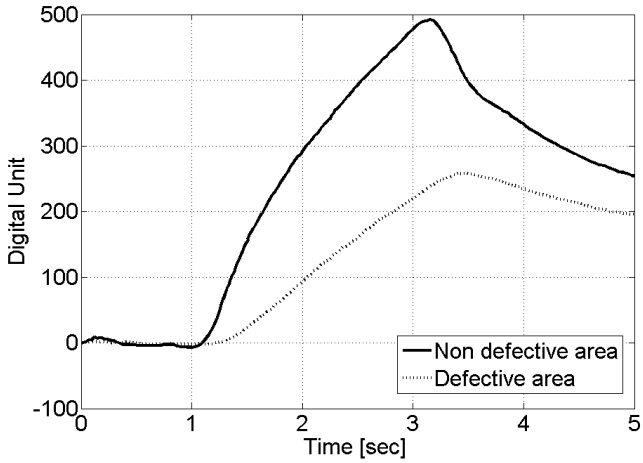

Figure 128 - Apparent temperature variation over time for damaged and undamaged areas

Analysing the curves it is possible to observe that the presence of the damage has several effects on apparent temperature over time. Indeed, not only the peak of apparent temperature is lower for a damaged part in comparison with an un-damaged one (which is the effect seen in the thermograms), but also both heating and cooling rates are affected by the PFTE discontinuity.

Another important results obtained with this technique is the possibility to assess the severity of a detected damage with high spatial resolution (even below the inter-wire distance). Indeed, by simply recording the thermal waves after heating two NiTi wires surrounding the damage and then looking at the high apparent temperature variation around the PTFE patch, it is possible to obtain a qualitative imaging of the defect size (Figure 129). By means of a simple calibration obtained with *a priori* knowledge of the inter-wire distance and the length of the SMA wires, a rough estimation of the size of the internal damage can be provided (in this case, approximately 10 mm length and 10 mm width).

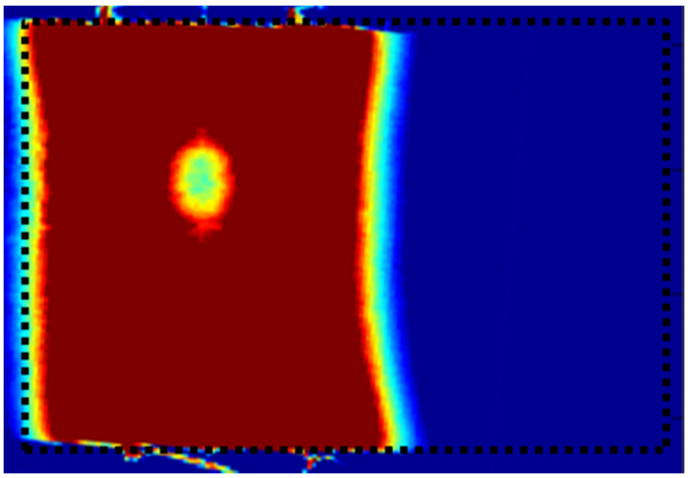

Figure 129 - Thermal image of the apparent temperature for sample 2 (sample dimensions - 100x60 mm – are represented with the dashed line) obtained at t=3 sec with double vertically aligned NiTi wires surrounding the PFTE patch

Further tests were conducted on *Sample C*, in order to analyse the behaviour of the hybrid composite when multiple damages are located within the thickness. 130 represents the results for the experiments carried out on the multi-damaged sample. A current of 1A was driven in two different NiTi wires using a two-channel power supply, in order to analyse the sensitivity of the technique with damages far from the top surface. As illustrated in Figure 129a, the technique provides good results also for damages that are located deeper within the sample. Indeed, the positions of *PTFE3* (positioned at 1.25 mm from the surface) and *PTFE1* (positioned at 0.575 mm from the surface) are immediately detected by the IR-camera as the apparent temperature

shows large variations for both discontinuities. Signals acquired from the camera were analysed separately and a contrast observed temperature analysis was carried out in order to evaluate only the effect given by the damages, according to the following equation:

$$C_{A_i} = \|A_{und_i} - A_{dam_i}\|$$

where C_{Ai} is the contrast signal, A_{undi} is the signal recorded for a undamaged part on the *i*th wire and A_{dami} is the signal recorder for a damaged point on the same *i*th wire. Results in Figure 130 show a slight decrease of the apparent temperature peak for PFTE3 in comparison with PFTE1.

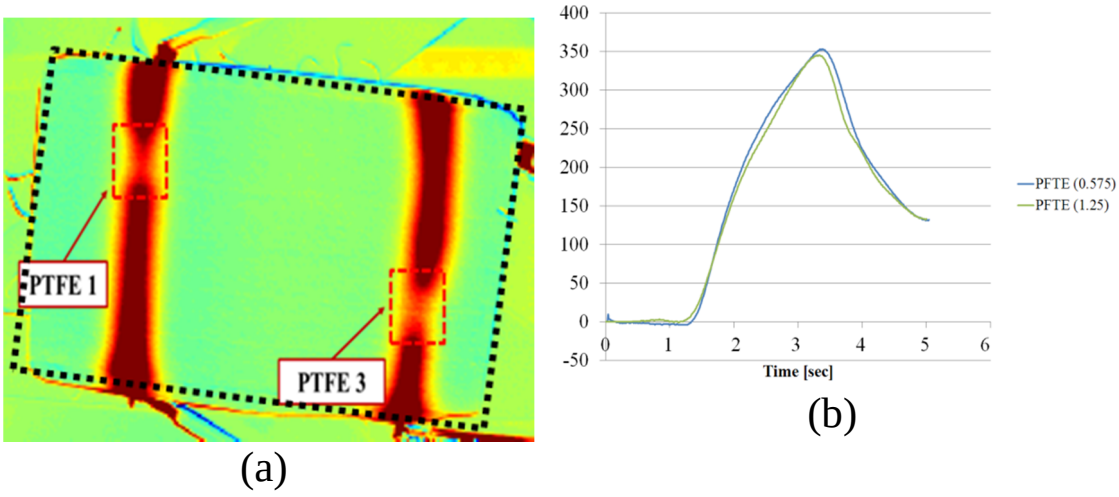

Figure 130 – a) Thermography images for multiple defective parts of *Sample 3* (sample dimensions - 100x60 mm – are represented with the dashed line) at t=3s; b) Amplitude contrast of apparent temperature variation for PFTE1 (0.575mm) and PFTE3 (1.25)

9.4 De-Ice feature for SMA-based hybrid Composites

The problem of ice formation on airplanes surfaces has always been a major concern in the aircraft industry since the very early years of flight for both commercial and military aircrafts [235, 236] . Since ice is able to change the shape and the roughness of control surfaces, the aerodynamics of crucial parts can be altered resulting in a

reduced ability of the wings to generate lift. This unfortunate situation can result in severe stability problems that can lead to catastrophic failures. Moreover, large ice agglomerates can be suddenly torn away from the wing surface and sucked within the engine, thus causing damages. Ice can form during the passage inside clouds by the presence of super-cooled water droplet. Super cooled water is liquid water below its freezing point that is not able to turn in ice due to the absence of ice nucleus on which the drops can freeze. However, when the aircraft flies trough these droplets, the plane itself can act as ice nucleus allowing the droplets to freeze on its external surface.

Among the several types of ice protection systems developed, the most used ones are mechanical systems like pneumatic de-icing boots and electro-mechanical tools. A de-icing boot is a rubber made membrane that it is usually installed on the leading edges of wings and it is inflated when ice is detected. Its expansion generates cracks on the ice layer that is subsequently taken away by the airflow. On the other side, electro mechanical systems are generally actuators positioned underneath the skin of the structures that can generate a shock force in order to knock off the ice layers from aircraft structures. The major drawback of the de-icing boots and the electro mechanical tools are the stresses that they induce on the structure every time they are activated which can damage the part leading to the formation of cracks and BVIDs.
Another important typology of de-icing/anti-icing systems are the thermal systems, which are engineered materials specially designed for de-ice applications. An example is made by the *Thermawing* (patented and manufactured by Kelly Aerospace Thermal Systems [237]) which uses a conductive graphite layer attached to the wings leading edges in order to melt the ice in formation. The problem with this kind of material is mainly in the large power consumption that is usually connected with their usage because of the vast surface to heat.

Based on these considerations, SMA-based hybrid composites showed interesting properties that can be exploited for both de-ice and anti-ice applications. Indeed, the Shape Memory Alloys embedded within the composite structure can be used to locally increase the temperature of specific parts of the structure with a small

consumption of power. This is due to the extraordinary heating capability of the SMA coupled with the presence of the carbon fibres which help the control of the heat propagation throughout the material structure, resulting in a heat flow that can be directed only in the critical parts of the aircraft or where the ice has been detected.

Figure 131a shows the thermal image of an hybridised laminate recorded with the IR camera. The upper part of the sample was connected with crocodile pins to a power supply, while the lower part was intentionally left "cold" in order to make a comparison between the temperatures of the two parts. The test was conducted with a current of 0.5 A for 20 seconds with an applied voltage of 0.1 V. The curves in Figure 131b represent the evolution in time of the apparent temperature recorded by the IR camera for two points on the hybrid composite surface. Background noise was subtracted from the signal following the same procedure descripted in Section 9.3.

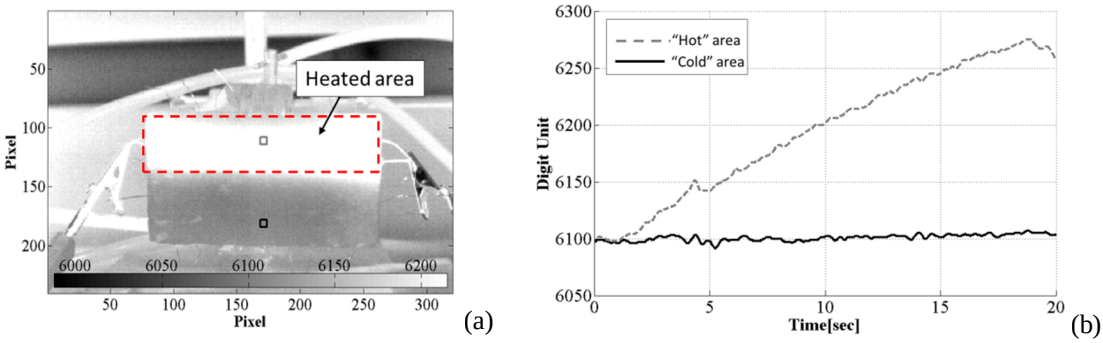

Figure 131 - Thermography image with a current of 0.5 A (a) and time histories for the "hot" and the "cold" area of the sample (b); SMArt Thermography image with a current of 1 A

The grey curve is related to a point taken in the "hot" part of the sample (grey marker in Figure b), while the black one is in the "cold" part (black marker in Figure b). From the images above, it is clearly possible to observe the difference between the thermal emissions in the two points. After 20 seconds, the hot part records an increase in apparent temperature of approximately 180 digital units. Since the temperature sensitivity of the IR camera is 30mK, it is possible to estimate the variation in temperature around 5.5 °C.

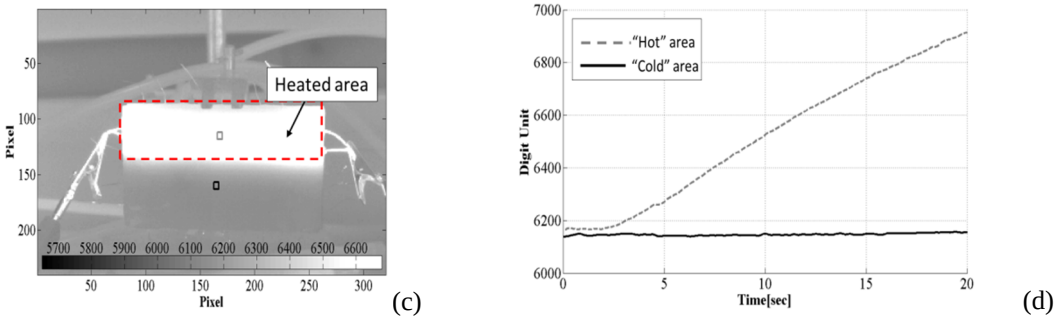

Figure 132 - SMArt Thermography image with a current of 1 A (c) and time histories for the "hot" and the "cold" area of the sample (d)

Figure 132 shows the behaviour of the SMA hybrid composite when a current of 1 A is applied to the edges of the embedded SMA wires for 20 sec. When the current flows within the samples with an applied voltage of 1.1 V, the change in apparent temperature is much more evident than in the previous case, with an increase of almost 800 digital units after 20 seconds (from 6100 to nearly 6900). From this value, it is possible to estimate the increase in temperature that is almost 24 ºC.

Ice formation usually occurs when the static air temperature (SAT) is between +2ºC and -20ºC therefore an increase of temperature around ~25 ºC is enough to melt the ice on the top surface of a structural component. Moreover, it is important to underline that the ΔT can be enhanced by increasing the voltage applied on the SMA wires or adjusting the time window of the current excitation. In this manner, high flexibility can be provided to the system as it can be optimised according to the external environmental conditions.

In conclusion, results from the test clearly demonstrated that SMA based hybrid composites are very promising for both anti-ice and de-ice applications. Indeed, for anti-ice purposes, a low current (between 0.1 and 0.5 A) can be induced within the samples to avoid the ice accretion phenomena, while using higher values of current (1 A or more) the same system can be used for de-ice application, being capable of melting ice eventually formed on the aircraft surfaces.

9.5 Discussion

The aim of this Section was to investigate the particular properties of an SMA-based hybrid composite in which the embedded SMA enables additional non-structural features in the system. These new properties coupled with the enhanced mechanical properties discussed in Section 8 represent the multifunctionality of this new class of hybrid composites.

In particular, the electrical resistance variations and the internal Joule heating source provided by the SMA network, allowed a quick detection of the material strain distribution, and an *in situ* damage imaging using a step heating thermography technique. The efficiency of these methodologies was experimentally validated on a number of hybrid laminates with single and multiple damages. The results showed that the strain sensing and defect detection were achieved with high accuracy and depth resolution, without the need to use large external heaters or complex signal processing techniques. Moreover, as the heat source is embedded into the material, this methodology is able to overcome the drawbacks of standard Infrared Thermography for the detection of damages in thick structures and deep-lying defects.

The current can be supplied by a power supply (ideally an electronic wireless system) and since the currents used for both sensing and thermography are not above 0.1A the power requirements are very low (5W for a 10x10cm tile). As the temperature increase generated by Joule effect for de-ice features has to reach higher values, the current needed is between 1 and 2A and subsequent power needed is between 10 and 15W for the same 10x10cm tile. However, an important advantage of SMA based composites is that the NiTi network can be adapted to every kind of complex structure in order to minimise the power requirements.

10 Conclusions

The aim of this thesis was to analyse the feasibility of multifunctional composite systems for structural and non-structural applications. The idea itself of multifunctionality in the context of material science is very complex and can be approached from different point of views. This complexity arises from the potentially infinite possibilities available to the researcher during the design of the internal structure of a composite material. Indeed, in order to impart new multiple features or enhance its existing properties, it is possible to intervene with different approaches like the inclusion of nano-scaled phases, the development of multiscaled structures, the hybridisation with additional phases or three-dimensional reinforcement and many others.

In order to investigate these multiple aspects of the same topic, a comprehensive conspectus has been presented focusing on the state of the art in multifunctional and smart materials. From this analysis, five different systems based on different structural and manufacturing approaches were developed and experimentally validated.

The first tested system was aimed to investigate how the presence of small percentages of nanostructured fillers would affect the mechanical behaviour of a traditional polymer. Hence, a bi-phasic system obtained by embedding low percentages of Graphene Nanoplatelets (GNP) within the structure of a thermoplastic film of Low Density Polyethylene was developed, and an experimental campaign was carried out to analyse the effect of the nanomodification. XRD and SEM analyses confirmed the exfoliation process of the Expanded Graphite used to obtain the GNPs, while DSC analysis demonstrates that the inclusion of the nanoscaled phase does not modify the microscopic structure of the polymer. Based on these considerations, the results given by DMA (improvement of both storage and loss moduli) and tensile tests (~150% enhancement in Young's Modulus) can be interpreted as strengthening effects given by the presence of GNPs. Another important aspect of the experimental campaign was the evaluation of the effects given by different manufacturing methods to the mechanical properties of the nanoreinforced film. Results showed that the

GNPs nano-effects are enhanced when the nanoplatelets are oriented during an extrusion process.

Having demonstrated that a nanoscaled phase can be used as an effective reinforcement within traditional materials, the further step was the development of a more complex multifunctional system, in which nanoscaled fillers are used in combination with a microscaled carbon fabric and a conventional thermoset resin. Such three-phasic system was obtained by doping the dry carbon fabric with SiO_2 nanoparticles and then using the resulting nanomodified reinforcement to manufacture a multiscaled laminate in order to exploit the nanoeffects arising from the nanosized phase to enhance the mechanical behaviour of the composite. X-RAY mapping and SEM analyses have been used to determine the spatial geometry and the distribution of the nanoscaled phase on the carbon fabric and a complete experimental campaign have been conducted on the multiscaled samples, comparing the results with a traditional laminate. Results from the experiments showed that the nanoscaled phase is able to strengthen the composites, increasing both bending and Young's Modulus, moreover an enhancement of hardness and Storage Modulus was also observed. In addition, the nanoreinforced fabric can be used as a substrate for selective growth of Carbon Nanotubes, creating an entangled three-dimensional structure that can be used as a preform in traditional composite manufacturing process.

Another approach to manufacture multifunctional smart materials consists in the addition of particular engineered components, characterised by unique properties that can be exploited to dynamically enhance some particular material properties. In order to investigate the possible advantages of such hybridation process, two different systems were manufactured and tested, both aimed to improve material damping and energy absorption rate when the laminate is subjected to an impact event. The first system tested was obtained by embedding a silica-based Nanofluid within the laminate structure, using the load-dependent variation of its viscosity as strengthen mechanism for enhancing impact properties. The Non-newtonian fluid was prepared and its nonlinear properties were investigated with rheometric tests. Low-velocity impact tests and C-Scan analysis were carried out on hybridised samples and the results showed that the presence of the embedded fluid within the CFRP increases the

damping and energy absorption rate by more than 50% for high velocity impacts and decrease the extent of the internal delamination by more than 30%.
Following the same hybridisation approach, a different smart system was obtained by including Shape Memory Alloys in the composite laminate. Experimental results pointed out that superelastic behaviour and hysteresis of SMA wires are able to modify the energy absorption mechanisms of the composite part, reducing the extent of internal delamination by more than 300%. These results were confirmed by C-Scan analyses conducted on impacted test.

Based on the findings of the previous Section, the presence of the embedded SMA network within the composite structure was exploited to enable additional non-structural features in the material. Indeed, the thermo-electrical properties of NiTi were used to enable strain sensing feature, obtained measuring the variation of the electrical resistance of the wires, thus monitoring the strain distribution in the entire part. In addition, the enhanced electrical conductivity of the SMA was exploited to ohmically heat the network by transmitting a low amperage current via simple electrical contacts. Emitted thermal waves were recorded with an IR-Camera and by analysing the apparent temperature variations on the sample surface the presence of internal impact damage was successfully monitored in real time. By following the same approach the embedded SMA network can be employed as an integrated heat source for selective de-ice applications.

10.1 Future Works

Multifunctional composite systems have shown considerable promises in terms of structural properties improvement and activation of additional non-structural features. In particular, both nanomodification and hybridisation processes developed during this PhD programme have proved to be valid procedures to improve specific aspects of the mechanical behaviour of traditional composite materials and enable SHM/NDT features. However, additional research is necessary to investigate more in depth some structural and non-structural aspects of each system and, moreover, to transfer what observed on laboratory scale into full-scale operational processes.

In particular, the procedure to manufacture three-dimensional multiscaled preforms based on the mutual entanglement of CNTs, SiO_2 nanoparticles and micron-sized carbon fibres should be investigated more in depth to analyse the effects given by the CNTs on the mechanical properties of such a complex structure. Moreover, particular attention should be given to the optimisation of the system, by scaling up the reactor for CNTs growth in order to create more complex structures. In addition, the development of an automatic process able to obtain tetra-phasical prepregs could be a step further for a future industrial production, followed by a complete mechanical characterisation of the resulting composites.

As for the STF embedded composites, the results obtained by sandwiching a layer of nanofluid within the laminate structure have demonstrated the feasibility of the embedded nanofluid as structural damper. However, these effects could be enhanced by achieving a better control on the final distribution of the fluid within the composite, especially during the curing reaction of the laminate. Indeed, a possible alternative could be to embed the STF in a hollow glass fibres fabric and then using it as an active layer during a traditional lay-up procedure. This technique could guarantee a better distribution of the nanofluid after the curing reaction and a more efficient manufacturing process, reducing costs and waste of material.

Hybridisation process based on SMAs has also proved to be valid technique to increase impact resistance of composite laminates without dramatic weight increase, however the high cost of the NiTi wires could hinder a possible industrial exploitation. Therefore an in-depth analysis of possible alternative materials characterised by similar hysteresis behaviour should be provided to reduce manufacturing costs. As for the SHM features of SMA based composites, the accuracy of the damage localisation should be further investigated by analysing damaged and cracked samples in comparison with traditional NDT techniques such as C-SCAN or X-RAY tomography. Moreover the spatial resolution through the cross-section could be improved by studying the behaviour of the heat flow during the thermo-electrical excitation, and analysing the phase of the thermal wave, which is related to the propagation time delay.

10.2 PHD Activities

During the PhD a number of scientific papers has been published in international peer-reviewed journals and presented at international conferences. Moreover, a patent is currently under examination:

Pinto F, White A, Meo M. - *Characterisation of Ductile Prepregs.* Applied Composite Materials. 2012:1-17.

Pinto F, Ciampa F, Polimeno U, Meo M. - *In-situ damage detection in SMA reinforced CFRP*. Proc of SPIE Vol. 2012;8345:83452V-1.

Pinto F, Ciampa F, Meo M, Polimeno U. - *Multifunctional SMArt composite material for in situ NDT/SHM and de-icing.* Smart Materials and Structures. 2012;21(10):105010.

Pinto F, Carotenuto G, Meo M - *Preparation and thermo-mechanical characterisation of graphene nanoplatelets/low density polyethylene composites* Journal of Thermoplastic Composite Materials – *manuscript accepted for publication*

Meo M, **Pinto F**. - *Method for manufacturing a nanocomposite material*. WO Patent 2,013,011,256 2013.

References:

[1] Yaroshevsky A. Abundances of chemical elements in the Earth's crust. Geochemistry International. 2006;44(1):48-55.
[2] Seitz F, Einspruch NG. Electronic Genie: The Tangled History of Silicon: University of Illinois Press; 1998.
[3] Mason WP. Piezoelectricity, its history and applications. The Journal of the Acoustical Society of America. 1981;70(6):1561-6.
[4] Takagi T. A concept of intelligent materials. Journal of Intelligent Material Systems and Structures. 1990;1:149-56.
[5] Thompson BS, Gandhi MV, Kasiviswanathan S. An introduction to smart materials and structures. Materials & Design. 1992;13(1):3-9.
[6] Cannon WB. Physiological regulation of normal states: some tentative postulates concerning biological homeostatics. Jubilee volume for Charles Richet. 1926:91-3.
[7] Keller T, de Castro J. System ductility and redundancy of FRP beam structures with ductile adhesive joints. Composites Part B: Engineering. 2005;36(8):586-96.
[8] Törmälä P. Biodegradable self-reinforced composite materials; manufacturing structure and mechanical properties. Clinical materials. 1992;10(1):29-34.
[9] Rezwan K, Chen QZ, Blaker JJ, Boccaccini AR. Biodegradable and bioactive porous polymer/inorganic composite scaffolds for bone tissue engineering. Biomaterials. 2006;27(18):3413-31.
[10] Hosseinkhani H, Hosseinkhani M, Subramani K. Bone Regeneration Using Self-Assembled Nanoparticle-Based Scaffolds. 2012.
[11] Onuma Y, Serruys PW. Bioresorbable Scaffold. Circulation. 2011;123(7):779-97.
[12] Jonkers H. Self Healing Concrete: A Biological Approach
Self Healing Materials. In: Zwaag S, ed.: Springer Netherlands 2008, p. 195-204.
[13] Jones AS, Rule JD, Moore JS, Sottos NR, White SR. Life extension of self-healing polymers with rapidly growing fatigue cracks. Journal of The Royal Society Interface. 2007;4(13):395-403.
[14] Wool RP. Self-healing materials: a review. Soft Matter. 2008;4(3):400-18.
[15] Raghavan A, Cesnik CES. Review of guided-wave structural health monitoring. Shock and Vibration Digest. 2007;39(2):91-116.
[16] Lynch JP, Loh KJ. A summary review of wireless sensors and sensor networks for structural health monitoring. Shock and Vibration Digest. 2006;38(2):91-130.
[17] Montalvao D, Maia N, Ribeiro A. A review of vibration-based structural health monitoring with special emphasis on composite materials. Shock and Vibration Digest. 2006;38(4):295-326.
[18] Gibson RF, Chen Y, Zhao H. Improvement of vibration damping capacity and fracture toughness in composite laminates by the use of polymeric interleaves. Journal of engineering materials and technology. 2001;123(3):309-14.
[19] Manjunatha C, Taylor A, Kinloch A, Sprenger S. The tensile fatigue behavior of a GFRP composite with rubber particle modified epoxy matrix. Journal of Reinforced Plastics and Composites. 2010;29(14):2170-83.
[20] Cho J, Joshi M, Sun C. Effect of inclusion size on mechanical properties of polymeric composites with micro and nano particles. Composites Science and Technology. 2006;66(13):1941-52.

[21] Singh R, Zhang M, Chan D. Toughening of a brittle thermosetting polymer: Effects of reinforcement particle size and volume fraction. Journal of Materials Science. 2002;37(4):781-8.
[22] Lopez L, Song B, Hahn H. The effect of particle size in alumina nanocomposites. Proceedings of the 14th international conference on composite materials (ICCM-14), San Diego.
[23] Zhang H, Tang L-C, Zhang Z, Friedrich K, Sprenger S. Fracture behaviours of in situ silica nanoparticle-filled epoxy at different temperatures. Polymer. 2008;49(17):3816-25.
[24] Cho J, Sun C. A molecular dynamics simulation study of inclusion size effect on polymeric nanocomposites. Computational Materials Science. 2007;41(1):54-62.
[25] Adnan A, Sun C, Mahfuz H. A molecular dynamics simulation study to investigate the effect of filler size on elastic properties of polymer nanocomposites. Composites Science and Technology. 2007;67(3):348-56.
[26] Vlasveld DPN, Bersee HEN, Picken SJ. Nanocomposite matrix for increased fibre composite strength. Polymer. 2005;46(23):10269-78.
[27] Uddin MF, Sun C. Strength of unidirectional glass/epoxy composite with silica nanoparticle-enhanced matrix. Composites Science and Technology. 2008;68(7):1637-43.
[28] Naganuma T, Kagawa Y. Effect of particle size on the optically transparent nano meter-order glass particle-dispersed epoxy matrix composites. Composites Science and Technology. 2002;62(9):1187-9.
[29] Sinha Ray S, Okamoto M. Polymer/layered silicate nanocomposites: a review from preparation to processing. Progress in Polymer Science. 2003;28(11):1539-641.
[30] Gao F. Clay/polymer composites: the story. Materials Today. 2004;7(11):50-5.
[31] Alexandre M, Dubois P. Polymer-layered silicate nanocomposites: preparation, properties and uses of a new class of materials. Materials Science and Engineering: R: Reports. 2000;28(1):1-63.
[32] Okada A, Usuki A. The chemistry of polymer-clay hybrids. Materials Science and Engineering: C. 1995;3(2):109-15.
[33] Tsai JL, Wu MD. Organoclay effect on mechanical responses of glass/epoxy nanocomposites. Journal of Composite Materials. 2008;42(6):553-68.
[34] Gong D, Grimes C, Varghese OK, Hu W, Singh R, Chen Z, et al. Titanium oxide nanotube arrays prepared by anodic oxidation. Journal of Materials Research. 2001;16(12):3331-4.
[35] Wang Z, Gao RP, Gole J, Stout J. Silica nanotubes and nanofiber arrays. Advanced Materials. 2001;12(24):1938-40.
[36] Taguchi T, Igawa N, Yamamoto H, Jitsukawa S. Synthesis of silicon carbide nanotubes. Journal of the American Ceramic Society. 2005;88(2):459-61.
[37] Iijima S. Helical microtubules of graphitic carbon. Nature. 1991;354(6348):56-8.
[38] Rajoria H, Jalili N. Passive vibration damping enhancement using carbon nanotube-epoxy reinforced composites. Composites Science and Technology. 2005;65(14):2079-93.
[39] Tai N, Yeh M, Liu J. Enhancement of the Mechanical Properties of Carbon Nanotube/Phenolic Composites using a Carbon Nanotube Network as the Reiforcement. Carbon. 2004;42:2735-77.
[40] Gojny FH, Wichmann MHG, Fiedler B, Schulte K. Influence of different carbon nanotubes on the mechanical properties of epoxy matrix composites–A comparative study. Composites Science and Technology. 2005;65(15):2300-13.

[41] Thostenson E, Li W, Wang D, Ren Z, Chou T. Carbon nanotube/carbon fiber hybrid multiscale composites. Journal of Applied Physics. 2002;91(9):6034-7.
[42] Sager R, Klein P, Lagoudas D, Zhang Q, Liu J, Dai L, et al. Effect of carbon nanotubes on the interfacial shear strength of T650 carbon fiber in an epoxy matrix. Composites Science and Technology. 2009;69(7):898-904.
[43] Hung KH, Kuo WS, Ko TH, Tzeng SS, Yan CF. Processing and tensile characterization of composites composed of carbon nanotube-grown carbon fibers. Composites Part A: Applied Science and Manufacturing. 2009;40(8):1299-304.
[44] Veedu VP, Cao A, Li X, Ma K, Soldano C, Kar S, et al. Multifunctional composites using reinforced laminae with carbon-nanotube forests. Nature materials. 2006;5(6):457-62.
[45] Garcia EJ, Wardle BL, John Hart A. Joining prepreg composite interfaces with aligned carbon nanotubes. Composites Part A: Applied Science and Manufacturing. 2008;39(6):1065-70.
[46] Lange F. The interaction of a crack front with a second-phase dispersion. Philosophical Magazine. 1970;22(179):983-92.
[47] Kinloch A, Johnsen B, Mohammed R, Taylor A, Sprenger S. Toughening mechanisms in novel nano-silica epoxy polymers. Proceedings of the 5th Australasian Congress on Applied Mechanics: Engineers Australia; p. 441.
[48] Lange FF, Radford KC. Fracture energy of an epoxy composite system. Journal of Materials Science. 1971;6(9):1197-203.
[49] Faber KT, Evans AG. Crack deflection processes—I. Theory. Acta Metallurgica. 1983;31(4):565-76.
[50] Zhang H, Zhang Z, Friedrich K, Eger C. Property improvements of in situ epoxy nanocomposites with reduced interparticle distance at high nanosilica content. Acta Materialia. 2006;54(7):1833-42.
[51] Johnsen B, Kinloch A, Mohammed R, Taylor A, Sprenger S. Toughening mechanisms of nanoparticle-modified epoxy polymers. Polymer. 2007;48(2):530-41.
[52] Toon JJ. Metal fibers and fabrics as shielding materials for composites, missiles and airframes. Electromagnetic Compatibility, 1990 Symposium Record, 1990 IEEE International Symposium on; p. 5-7.
[53] Li C, Thostenson ET, Chou TW. Effect of nanotube waviness on the electrical conductivity of carbon nanotube-based composites. Composites Science and Technology. 2008;68(6):1445-52.
[54] Sandler JKW, Kirk JE, Kinloch IA, Shaffer MSP, Windle AH. Ultra-low electrical percolation threshold in carbon-nanotube-epoxy composites. Polymer. 2003;44(19):5893-9.
[55] Grimes C, Dickey E, Mungle C, Ong K, Qian D. Effect of purification of the electrical conductivity and complex permittivity of multiwall carbon nanotubes. Journal of Applied Physics. 2001;90(8):4134-7.
[56] Hu G, Zhao C, Zhang S, Yang M, Wang Z. Low percolation thresholds of electrical conductivity and rheology in poly (ethylene terephthalate) through the networks of multi-walled carbon nanotubes. Polymer. 2006;47(1):480-8.
[57] Shenogina N, Shenogin S, Xue L, Keblinski P. On the lack of thermal percolation in carbon nanotube composites. Applied Physics Letters. 2005;87(13):133106--3.
[58] Biercuk M, Llaguno MC, Radosavljevic M, Hyun J, Johnson AT, Fischer JE. Carbon nanotube composites for thermal management. Applied Physics Letters. 2002;80(15):2767-9.

[59] Moisala A, Li Q, Kinloch I, Windle A. Thermal and electrical conductivity of single-and multi-walled carbon nanotube-epoxy composites. Composites Science and Technology. 2006;66(10):1285-8.
[60] Gao L, Zhou X, Ding Y. Effective thermal and electrical conductivity of carbon nanotube composites. Chemical Physics Letters. 2007;434(4–6):297-300.
[61] Fujii M, Zhang X, Xie H, Ago H, Takahashi K, Ikuta T, et al. Measuring the Thermal Conductivity of a Single Carbon Nanotube. Physical Review Letters. 2005;95(6):065502.
[62] Yang DJ, Zhang Q, Chen G, Yoon SF, Ahn J, Wang SG, et al. Thermal conductivity of multiwalled carbon nanotubes. Physical Review B. 2002;66(16):165440.
[63] Jianwei C, Tahir Ç, William AG, III. Thermal conductivity of carbon nanotubes. Nanotechnology. 2000;11(2):65.
[64] Balageas D, Fritzen CP, Güemes A. Structural Health Monitoring: John Wiley & Sons; 2010.
[65] Crawley EF, Anderson EH. Detailed Models of Piezoceramic Actuation of Beams. Journal of Intelligent Material Systems and Structures. 1990;1(1):4-25.
[66] Capezzuto F, Ciampa F, Carotenuto G, Meo M, Milella E, Nicolais F. A smart multifunctional polymer nanocomposites layer for the estimation of low-velocity impact damage in composite structures. Composite Structures. 2010;92(8):1913-9.
[67] Udd E. Fiber optic smart structures: Wiley; 1995.
[68] Inpil K, Mark JS, Jay HK, Vesselin S, Donglu S. A carbon nanotube strain sensor for structural health monitoring. Smart Materials and Structures. 2006;15(3):737.
[69] Barton DP. Comparative Vacuum Monitoring (CVM™). Encyclopedia of Structural Health Monitoring: John Wiley & Sons, Ltd 2009.
[70] Khuri-Yakub BT, Degertekin FL, Jin XC, Calmes S, Ladabaum I, Hansen S, et al. Silicon micromachined ultrasonic transducers. Ultrasonics Symposium, 1998 Proceedings, 1998 IEEE; p. 985-91 vol.2.
[71] Fink DA, Hawkey TJ, Gaudreau MPJ, Wellman B, Ormiston RA. An electromagnetic actuator for individual blade control. AHS International, Annual Forum, 56 th, Virginia Beach, VA; p. 786-97.
[72] Louis RC, Edward CS, Brian M. Induced-shear piezoelectric actuators for rotor blade trailing edge flaps. Smart Materials and Structures. 2002;11(1):24.
[73] Hagood N, Bent A. Development of piezoelectric fiber composites for structural actuation. AIAA/ASME/ASCE/AHS/ASC 34th Structures, Structural Dynamics, and Materials Conference; p. 3625-38.
[74] Bowen CR, Bowles A, Drake S, Johnson N, Mahon S. Fabrication and finite element modelling of interdigitated electrodes. Ferroelectrics. 1999;228(1):257-69.
[75] Hagood NW, Kindel R, Ghandi K, Gaudenzi P. Improving transverse actuation of piezoceramics using interdigitated surface electrodes. 1993:341-52.
[76] Wilkie WK, Bryant RG, High JW, Fox RL, Hellbaum RF, Jalink Jr A, et al. Low-cost piezocomposite actuator for structural control applications. SPIE's 7th Annual International Symposium on Smart Structures and Materials: International Society for Optics and Photonics; p. 323-34.
[77] Drossel W-G, Hensel S, Kranz B, Nestler M, Goeschel A. Sheet metal forming of piezoceramic–metal-laminar structures—Simulation and experimental analysis. CIRP Annals - Manufacturing Technology. 2009;58(1):279-82.

[78] Sodano HA, Park G, Inman DJ. An investigation into the performance of macro-fiber composites for sensing and structural vibration applications. Mechanical Systems and Signal Processing. 2004;18(3):683-97.
[79] Hagood IV NW, Bent AA. Composites for structural control. Google Patents 2000.
[80] Sarangi SK, Ray MC. Active damping of geometrically nonlinear vibrations of doubly curved laminated composite shells. Composite Structures. 2011;93(12):3216-28.
[81] Wickramasinghe VK, Hagood NW. Performance characterization of active fiber-composite actuators for helicopter rotor blade applications. SPIE's 9th Annual International Symposium on Smart Structures and Materials: International Society for Optics and Photonics; p. 273-84.
[82] Belloli A, Niederberger D, Pietrzko S, Morari M, Ermanni P. Structural Vibration Control via R-L Shunted Active Fiber Composites. Journal of Intelligent Material Systems and Structures. 2007;18(3):275-87.
[83] Schönecker A, Keitel U, Kreher W, Sporn D, Watzka W, Pannkoke K. Smart structures by integrated piezoelectric thin fibres (II): properties of composites and their physical description. Ferroelectrics. 1999;224(1):7-12.
[84] Melnykowycz M, Kornmann X, Huber C, Barbezat M, Brunner A. Performance of integrated active fiber composites in fiber reinforced epoxy laminates. Smart Materials and Structures. 2006;15(1):204.
[85] Lin M, Chang FK. The manufacture of composite structures with a built-in network of piezoceramics. Composites Science and Technology. 2002;62(7):919-39.
[86] Abot JL, Song Y, Vatsavaya MS, Medikonda S, Kier Z, Jayasinghe C, et al. Delamination detection with carbon nanotube thread in self-sensing composite materials. Composites Science and Technology. 2010;70(7):1113-9.
[87] Loh KJ, Lynch JP, Shim BS, Kotov NA. Tailoring Piezoresistive Sensitivity of Multilayer Carbon Nanotube Composite Strain Sensors. Journal of Intelligent Material Systems and Structures. 2008;19(7):747-64.
[88] Loh K, Hou T-C, Lynch J, Kotov N. Carbon Nanotube Sensing Skins for Spatial Strain and Impact Damage Identification. J Nondestruct Eval. 2009;28(1):9-25.
[89] Myounggu P, Hyonny K, Jeffrey PY. Strain-dependent electrical resistance of multi-walled carbon nanotube/polymer composite films. Nanotechnology. 2008;19(5):055705.
[90] Song X, Liu S, Gan Z, Lv Q, Cao H, Yan H. Controllable fabrication of carbon nanotube-polymer hybrid thin film for strain sensing. Microelectronic Engineering. 2009;86(11):2330-3.
[91] Li X, Levy C, Elaadil L. Multiwalled carbon nanotube film for strain sensing. Nanotechnology. 2008;19(4):045501.
[92] Thostenson ET, Tsu-Wei C. Real-time in situ sensing of damage evolution in advanced fiber composites using carbon nanotube networks. Nanotechnology. 2008;19(21):215713.
[93] Thostenson ET, Chou TW. Carbon nanotube networks: sensing of distributed strain and damage for life prediction and self healing. Advanced Materials. 2006;18(21):2837-41.
[94] Monti M, Natali M, Petrucci R, Kenny JM, Torre L. Impact damage sensing in glass fiber reinforced composites based on carbon nanotubes by electrical resistance measurements. Journal of Applied Polymer Science. 2011;122(4):2829-36.

[95] Du W, Tao X, Tam H, Choy C. Fundamentals and applications of optical fiber Bragg grating sensors to textile structural composites. Composite Structures. 1998;42(3):217-29.
[96] Okabe Y, Yashiro S, Kosaka T, Takeda N. Detection of transverse cracks in CFRP composites using embedded fiber Bragg grating sensors. Smart Materials and Structures. 2000;9(6):832.
[97] Takeda N, Okabe Y, Kuwahara J, Kojima S, Ogisu T. Development of smart composite structures with small-diameter fiber Bragg grating sensors for damage detection: Quantitative evaluation of delamination length in CFRP laminates using Lamb wave sensing. Composites Science and Technology. 2005;65(15):2575-87.
[98] Lau K, Yuan L, Zhou L, Wu J, Woo C. Strain monitoring in FRP laminates and concrete beams using FBG sensors. Composite Structures. 2001;51(1):9-20.
[99] De Oliveira R, Ramos C, Marques A. Health monitoring of composite structures by embedded FBG and interferometric Fabry–Pérot sensors. Computers & structures. 2008;86(3):340-6.
[100] White SR, Sottos NR, Geubelle PH, Moore JS, Kessler MR, Sriram SR, et al. Autonomic healing of polymer composites. Nature. 2001;409(6822):794-7.
[101] Toohey KS, Sottos NR, Lewis JA, Moore JS, White SR. Self-healing materials with microvascular networks. Nat Mater. 2007;6(8):581-5.
[102] Kirkby EL, Rule JD, Michaud VJ, Sottos NR, White SR, Månson JAE. Embedded Shape-Memory Alloy Wires for Improved Performance of Self-Healing Polymers. Advanced Functional Materials. 2008;18(15):2253-60.
[103] Kirkby E, Michaud V, Månson JAE, Sottos N, White S. Performance of self-healing epoxy with microencapsulated healing agent and shape memory alloy wires. Polymer. 2009;50(23):5533-8.
[104] Kirk J, Naik S, Moosbrugger J, Morrison D, Volkov D, Sokolov I. Self-Healing Epoxy Composites Based on the Use of Nanoporous Silica Capsules. Int J Fract. 2009;159(1):101-2.
[105] Privman V, Dementsov A, Sokolov I. Modeling of self-healing polymer composites reinforced with nanoporous glass fibers. Journal of Computational and Theoretical Nanoscience. 2007;4(1):190-3.
[106] Pang JWC, Bond IP. A hollow fibre reinforced polymer composite encompassing self-healing and enhanced damage visibility. Composites Science and Technology. 2005;65(11–12):1791-9.
[107] Umeda M, Nakamura K, Ueha S. Analysis of the transformation of mechanical impact energy to electric energy using piezoelectric vibrator. Japanese Journal of Applied Physics. 1996;35(5):3267-73.
[108] Umeda M, Nakamura K, Ueha S. Energy storage characteristics of a piezo-generator using impact induced vibration. Japanese Journal of Applied Physics. 1997;36(part 1):3146-51.
[109] Wu W, Chen Y, Lee B, He J, Peng Y. Tunable resonant frequency power harvesting devices. Proceedings of SPIE, the International Society for Optical Engineering: Society of Photo-Optical Instrumentation Engineers; p. 61690A.
[110] Churchill DL, Hamel MJ, Townsend CP, Arms SW. Strain energy harvesting for wireless sensor networks. Smart Structures and Materials 2003. 2003;5055:319-27.
[111] Pereira T, Guo Z, Nieh S, Arias J, Hahn HT. Embedding thin-film lithium energy cells in structural composites. Composites Science and Technology. 2008;68(7):1935-41.

[112] Kim HS, Kang JS, Park JS, Hahn HT, Jung HC, Joung JW. Inkjet printed electronics for multifunctional composite structure. Composites Science and Technology. 2009;69(7):1256-64.
[113] Rothon RN. Particulate-Filled Polymer Composites (2nd Edition). Smithers Rapra Technology.
[114] Chisholm N, Mahfuz H, Rangari VK, Ashfaq A, Jeelani S. Fabrication and mechanical characterization of carbon/SiC-epoxy nanocomposites. Composite Structures. 2005;67(1):115-24.
[115] Sumita M, Shizuma T, Miyasaka K, Ishikawa K. Reducible properties of draw temperature, rate of strain and filler content in tensile yield stress of polymethylmethacrylate filled with ultrafine particles. Rheologica acta. 1984;23(4):396-400.
[116] Kuo MC, Tsai CM, Huang JC, Chen M. PEEK composites reinforced by nano-sized SiO2 and Al2O3 particulates. Materials Chemistry and Physics. 2005;90(1):185-95.
[117] Chan CM, Wu J, Li JX, Cheung YK. Polypropylene/calcium carbonate nanocomposites. Polymer. 2002;43(10):2981-92.
[118] Ding C, Jia D, He H, Guo B, Hong H. How organo-montmorillonite truly affects the structure and properties of polypropylene. Polymer testing. 2005;24(1):94-100.
[119] ADEBAHR T, Roscher C, Adam J. Reinforcing nanoparticles in reactive resins. European coatings journal. 2001(4):144-9.
[120] von Sturm F. Graphite fibers and filaments. Springer series in materials science, Vol. 5. By M. S. Dresselhaus, G. Dresselhaus, K. Sugihara, I. L. Spain and H. A. Goldberg. Springer, Berlin/Heidelberg 1988. x, 382 pp., hard cover, DM 122.00.— ISBN 3-540-18938-6. Advanced Materials. 1989;1(4):130-1.
[121] Fim FdC, Guterres JM, Basso NRS, Galland GB. Polyethylene/graphite nanocomposites obtained by in situ polymerization. Journal of Polymer Science Part A: Polymer Chemistry. 2010;48(3):692-8.
[122] Pierson HO. Handbook of Carbon, Graphite, Diamond, and Fullerenes: Properties, Processing, and Applications: Noyes Publications; 1993.
[123] Wang H, Yoshio M, Abe T, Ogumi Z. Characterization of Carbon-Coated Natural Graphite as a Lithium-Ion Battery Anode Material. Journal of the Electrochemical Society. 2002;149(4):A499-A503.
[124] Hochgatterer NS, Schweiger MR, Koller S, Raimann PR, Wöhrle T, Wurm C, et al. Silicon/Graphite Composite Electrodes for High-Capacity Anodes: Influence of Binder Chemistry on Cycling Stability. Electrochemical and Solid-State Letters. 2008;11(5):A76-A80.
[125] Stankovich S, Dikin DA, Dommett GHB, Kohlhaas KM, Zimney EJ, Stach EA, et al. Graphene-based composite materials. Nature. 2006;442(7100):282-6.
[126] Stankovich S, Dikin DA, Piner RD, Kohlhaas KA, Kleinhammes A, Jia Y, et al. Synthesis of graphene-based nanosheets via chemical reduction of exfoliated graphite oxide. Carbon. 2007;45(7):1558-65.
[127] Bunch JS, Verbridge SS, Alden JS, van der Zande AM, Parpia JM, Craighead HG, et al. Impermeable Atomic Membranes from Graphene Sheets. Nano Letters. 2008;8(8):2458-62.
[128] Jiang J-W, Wang J-S, Li B. Young's modulus of graphene: A molecular dynamics study. Physical Review B. 2009;80(11):113405.

[129] Rafiee MA, Rafiee J, Wang Z, Song H, Yu Z-Z, Koratkar N. Enhanced Mechanical Properties of Nanocomposites at Low Graphene Content. ACS Nano. 2009;3(12):3884-90.
[130] Guo T, Nikolaev P, Thess A, Colbert DT, Smalley RE. Catalytic growth of single-walled manotubes by laser vaporization. Chemical Physics Letters. 1995;243(1-2):49-54.
[131] Breuer O, Sundararaj U. Big returns from small fibers: A review of polymer/carbon nanotube composites. Polymer Composites. 2004;25(6):630-45.
[132] Kumar S, Sun LL, Caceres S, Li B, Wood W, Perugini A, et al. Dynamic synergy of graphitic nanoplatelets and multi-walled carbon nanotubes in polyetherimide nanocomposites. Nanotechnology. 2010;21(10):105702.
[133] Lian P, Zhu X, Liang S, Li Z, Yang W, Wang H. Large reversible capacity of high quality graphene sheets as an anode material for lithium-ion batteries. Electrochimica Acta. 2010;55(12):3909-14.
[134] Yang J, Zhang L-Q, Shi J-H, Quan Y-N, Wang L-L, Tian M. Mechanical and functional properties of composites based on graphite and carboxylated acrylonitrile butadiene rubber. Journal of Applied Polymer Science. 2010;116(5):2706-13.
[135] Jacob George J, Bandyopadhyay A, Bhowmick AK. New generation layered nanocomposites derived from ethylene-co-vinyl acetate and naturally occurring graphite. Journal of Applied Polymer Science. 2008;108(3):1603-16.
[136] Morawiec J, Pawlak A, Slouf M, Galeski A, Piorkowska E, Krasnikowa N. Preparation and properties of compatibilized LDPE/organo-modified montmorillonite nanocomposites. European Polymer Journal. 2005;41(5):1115-22.
[137] Liu L, Barber AH, Nuriel S, Wagner HD. Mechanical Properties of Functionalized Single-Walled Carbon-Nanotube/Poly(vinyl alcohol) Nanocomposites. Advanced Functional Materials. 2005;15(6):975-80.
[138] Liang J, Huang Y, Zhang L, Wang Y, Ma Y, Guo T, et al. Molecular-Level Dispersion of Graphene into Poly(vinyl alcohol) and Effective Reinforcement of their Nanocomposites. Advanced Functional Materials. 2009;19(14):2297-302.
[139] Menard KP. Dynamic mechanical analysis: a practical introduction: CRC; 2008.
[140] RamanathanT, Abdala AA, StankovichS, Dikin DA, Herrera Alonso M, Piner RD, et al. Functionalized graphene sheets for polymer nanocomposites. Nat Nano. 2008;3(6):327-31.
[141] Documentation PE. Characterization of LDPE Over a Large Frequency Range. 2007 [cited; Available from: http://www.perkinelmer.com/CMSResources/Images/44-74196APP_LDPECharacterization.pdf
[142] Kuilla T, Bhadra S, Yao D, Kim NH, Bose S, Lee JH. Recent advances in graphene based polymer composites. Progress in Polymer Science. 2010;35(11):1350-75.
[143] Zheng W, Lu X, Wong S-C. Electrical and mechanical properties of expanded graphite-reinforced high-density polyethylene. Journal of Applied Polymer Science. 2004;91(5):2781-8.
[144] Andrews R, Jacques D, Minot M, Rantell T. Fabrication of Carbon Multiwall Nanotube/Polymer Composites by Shear Mixing. Macromolecular Materials and Engineering. 2002;287(6):395-403.
[145] Guichon O, Séguéla R, David L, Vigier G. Influence of the molecular architecture of low-density polyethylene on the texture and mechanical properties of

blown films. Journal of Polymer Science Part B: Polymer Physics. 2003;41(4):327-40.
[146] Zhou T, Chen F, Tang C, Bai H, Zhang Q, Deng H, et al. The preparation of high performance and conductive poly (vinyl alcohol)/graphene nanocomposite via reducing graphite oxide with sodium hydrosulfite. Composites Science and Technology. 2011;71(9):1266-70.
[147] Zhao X, Zhang Q, Chen D, Lu P. Enhanced Mechanical Properties of Graphene-Based Poly(vinyl alcohol) Composites. Macromolecules. 2010;43(5):2357-63.
[148] Haque A, Shamsuzzoha M, Hussain F, Dean D. S2-glass/epoxy polymer nanocomposites: manufacturing, structures, thermal and mechanical properties. Journal of Composite Materials. 2003;37(20):1821-37.
[149] Jen MHR, Tseng YC, Wu CH. Manufacturing and mechanical response of nanocomposite laminates. Composites Science and Technology. 2005;65(5):775-9.
[150] Becker O, Varley R, Simon G. Use of layered silicates to supplementarily toughen high performance epoxy-carbon fiber composites. Journal of materials science letters. 2003;22(20):1411-4.
[151] Timmerman JF, Hayes BS, Seferis JC. Nanoclay reinforcement effects on the cryogenic microcracking of carbon fiber/epoxy composites. Composites Science and Technology. 2002;62(9):1249-58.
[152] Etienne S, Becker C, Ruch D, Grignard B, Cartigny G, Detrembleur C, et al. Effects of incorporation of modified silica nanoparticles on the mechanical and thermal properties of PMMA. Journal of thermal analysis and calorimetry. 2007;87(1):101-4.
[153] García N, Corrales T, Guzmán J, Tiemblo P. Understanding the role of nanosilica particle surfaces in the thermal degradation of nanosilica–poly (methyl methacrylate) solution-blended nanocomposites: From low to high silica concentration. Polymer degradation and stability. 2007;92(4):635-43.
[154] M. Cascione BF, M. Quaresimin, K. Schulte, M.H.G. Wichmann. Preparazione e caratterizzazione di nanocompositi a matrice epossidica. XXXIV Convegno Nazionale Associazione Italiana per l'Analisi delle Sollecitazioni. Politecnico di Milano 2005.
[155] Stojanovic D, Orlovic A, Markovic S, Radmilovic V, Uskokovic PS, Aleksic R. Nanosilica/PMMA composites obtained by the modification of silica nanoparticles in a supercritical carbon dioxide–ethanol mixture. Journal of Materials Science. 2009;44(23):6223-32.
[156] Finegan I, Tibbetts GG, Glasgow D, Ting JM, Lake M. Surface treatments for improving the mechanical properties of carbon nanofiber/thermoplastic composites. Journal of Materials Science. 2003;38(16):3485-90.
[157] Zou H, Wu S, Shen J. Polymer/silica nanocomposites: preparation, characterization, properties, and applications. ChemInform. 2008;39(52):no-no.
[158] Lai YH, Kuo M, Huang J, Chen M. On the PEEK composites reinforced by surface-modified nano-silica. Materials Science and Engineering: A. 2007;458(1):158-69.
[159] Kornmann X, Rees M, Thomann Y, Necola A, Barbezat M, Thomann R. Epoxy-layered silicate nanocomposites as matrix in glass fibre-reinforced composites. Composites Science and Technology. 2005;65(14):2259-68.
[160] Goertzen WK, Kessler MR. Dynamic mechanical analysis of fumed silica/cyanate ester nanocomposites. Composites Part A: Applied Science and Manufacturing. 2008;39(5):761-8.

[161] Nielsen LE. Dynamic mechanical properties of polymers filled with agglomerated particles. Journal of Polymer Science: Polymer Physics Edition. 1979;17(11):1897-901.
[162] McNally T, Pötschke P, Halley P, Murphy M, Martin D, Bell SEJ, et al. Polyethylene multiwalled carbon nanotube composites. Polymer. 2005;46(19):8222-32.
[163] Wei BQ, Vajtai R, Jung Y, Ward J, Zhang R, Ramanath G, et al. Microfabrication technology: Organized assembly of carbon nanotubes. Nature. 2002;416(6880):495-6.
[164] Agrawal S, Kumar A, Frederick MJ, Ramanath G. Hybrid Microstructures from Aligned Carbon Nanotubes and Silica Particles. Small. 2005;1(8-9):823-6.
[165] Zhang ZJ, Wei BQ, Ramanath G, Ajayan PM. Substrate-site selective growth of aligned carbon nanotubes. Applied Physics Letters. 2000;77(23):3764-6.
[166] Ago H, Nakamura K, Uehara N, Tsuji M. Roles of metal-support interaction in growth of single-and double-walled carbon nanotubes studied with diameter-controlled iron particles supported on MgO. The Journal of Physical Chemistry B. 2004;108(49):18908-15.
[167] Zhang X, Pei X, Zhang J, Wang Q. Effects of carbon fiber surface treatment on the friction and wear behavior of 2D woven carbon fabric/phenolic composites. Colloids and Surfaces A: Physicochemical and Engineering Aspects. 2009;339(1–3):7-12.
[168] Morgan RJ, Jurek RJ, Yen A, Donnellan T. Toughening procedures, processing and performance of bismaleimide-carbon fibre composites. Polymer. 1993;34(4):835-42.
[169] Sain M, Suhara P, Law S, Bouilloux A. Interface Modification and Mechanical Properties of Natural Fiber-Polyolefin Composite Products. Journal of Reinforced Plastics and Composites. 2005;24(2):121-30.
[170] Gassan J, Bledzki AK. Possibilities to Improve the Properties of Natural Fiber Reinforced Plastics by Fiber Modification – Jute Polypropylene Composites –. Applied Composite Materials. 2000;7(5-6):373-85.
[171] Hucker M, Bond I, Foreman A, Hudd J. Optimisation of hollow glass fibres and their composites. Advanced Composites Letters. 1999;8(4):181-9.
[172] Miyagawa H, Drzal LT. Thermo-physical and impact properties of epoxy nanocomposites reinforced by single-wall carbon nanotubes. Polymer. 2004;45(15):5163-70.
[173] Gou J, O'Braint S, Gu H, Song G. Damping augmentation of nanocomposites using carbon nanofiber paper. Journal of nanomaterials. 2006;2006.
[174] Mouritz AP, Leong KH, Herszberg I. A review of the effect of stitching on the in-plane mechanical properties of fibre-reinforced polymer composites. Composites Part A: Applied Science and Manufacturing. 1997;28(12):979-91.
[175] Laun HM. Rheological properties of aqueous polymer dispersions. Die Angewandte Makromolekulare Chemie. 1984;123(1):335-59.
[176] Hassan TA, Rangari VK, Jeelani S. Synthesis, processing and characterization of shear thickening fluid (STF) impregnated fabric composites. Materials Science and Engineering: A. 2010;527(12):2892-9.
[177] Lee YS, Wetzel ED, Wagner NJ. The ballistic impact characteristics of Kevlar® woven fabrics impregnated with a colloidal shear thickening fluid. Journal of Materials Science. 2003;38(13):2825-33.

[178] Decker MJ, Halbach CJ, Nam CH, Wagner NJ, Wetzel ED. Stab resistance of shear thickening fluid (STF)-treated fabrics. Composites Science and Technology. 2007;67(3–4):565-78.
[179] Lomakin E, Mossakovsky P, Bragov A, Lomunov A, Konstantinov A, Kolotnikov M, et al. Investigation of impact resistance of multilayered woven composite barrier impregnated with the shear thickening fluid. Archive of Applied Mechanics. 2011;81(12):2007-20.
[180] Fischer C, Braun SA, Bourban PE, Michaud V, Plummer CJG, Månson JAE. Dynamic properties of sandwich structures with integrated shear-thickening fluids. Smart Materials and Structures. 2006;15(5):1467.
[181] Soutrenon M, Michaud V. Structural damping using encapsulated shear thickening fluids. 2012:83410S-S.
[182] Picken SJ, Marissen R, Antonelli V, Jansen GW. DAMAGE TOLERANT COMPOSITE MATERIAL. WO Patent WO/2009/142,491 2009.
[183] Yiliu Liu ZWaXZ. Characterization of supramolecular polymers. Chem Soc Rev. 2012;41:5922–32.
[184] Bender JW, Wagner NJ. Optical measurement of the contributions of colloidal forces to the rheology of concentrated suspensions. Journal of Colloid and Interface Science. 1995;172(1):171-84.
[185] Maranzano BJ, Wagner NJ. Flow-small angle neutron scattering measurements of colloidal dispersion microstructure evolution through the shear thickening transition. The Journal of Chemical Physics. 2002;117(22):10291-302.
[186] Xianzhou Z, Weihua L, Gong XL. Study on magnetorheological shear thickening fluid. Smart Materials and Structures. 2008;17(1):015051.
[187] Lee YS, Wagner NJ. Rheological Properties and Small-Angle Neutron Scattering of a Shear Thickening, Nanoparticle Dispersion at High Shear Rates. Industrial & Engineering Chemistry Research. 2006;45(21):7015-24.
[188] Brown E, Forman NA, Orellana CS, Zhang H, Maynor BW, Betts DE, et al. Generality of shear thickening in dense suspensions. Nat Mater. 2010;9(3):220-4.
[189] Masoudi A, Madaah Hosseini HR, Shokrgozar MA, Ahmadi R, Oghabian MA. The effect of poly(ethylene glycol) coating on colloidal stability of superparamagnetic iron oxide nanoparticles as potential MRI contrast agent. International Journal of Pharmaceutics. 2012;433(1–2):129-41.
[190] Jiang W, Sun Y, Xu Y, Peng C, Gong X, Zhang Z. Shear-thickening behavior of polymethylmethacrylate particles suspensions in glycerine–water mixtures. Rheologica acta. 2010;49(11-12):1157-63.
[191] Wetzel ED, Lee YS, Egres RG, Kirkwood KM, Kirkwood JE, Wagner NJ. The Effect of Rheological Parameters on the Ballistic Properties of Shear Thickening Fluid (STF)-Kevlar Composites. AIP Conference Proceedings. 2004;712(1):288-93.
[192] Peng STJ, Landel RF. Rheological behavior of progressively shear thickening solutions. Journal of Applied Physics. 1981;52(10):5988-93.
[193] Choi GN, Krieger IM. Rheological studies on sterically stabilized model dispersions of uniform colloidal spheres: II. Steady-shear viscosity. Journal of Colloid and Interface Science. 1986;113(1):101-13.
[194] W.H. Boersma JL, HN Stein Shear Thickening (Dilatancy) in Concentrated Dispersions. AIChE Journal. 1990.
[195] Stickel JJ, Powell RL. Fluid mechanics and rheology of dense suspensions. Annu Rev Fluid Mech. 2005;37:129-49.

[196] Kang T, Hong K, Yoo M. Preparation and properties of fumed silica/Kevlar composite fabrics for application of stab resistant material. Fibers and Polymers. 2010;11(5):719-24.
[197] Maranzano BJ, Wagner NJ. The effects of particle size on reversible shear thickening of concentrated colloidal dispersions. The Journal of Chemical Physics. 2001;114(23):10514-27.
[198] Lu YP, Killian JW, Everstine GC. Vibrations of three layered damped sandwich plate composites. Journal of Sound and Vibration. 1979;64(1):63-71.
[199] Tadeu A, António J, Mateus D. Sound insulation provided by single and double panel walls—a comparison of analytical solutions versus experimental results. Applied Acoustics. 2004;65(1):15-29.
[200] Rogers CAaR, H. H. Shape Memory Alloy Reinforced Composites. Engineering Science Preprints. 1988;25.
[201] Angioni SL, Meo M, Foreman A. Impact damage resistance and damage suppression properties of shape memory alloys in hybrid composites—a review. Smart Materials and Structures. 2011;20(1):013001.
[202] Paine JSN, Rogers CA. The Response of SMA Hybrid Composite Materials to Low Velocity Impact. Journal of Intelligent Material Systems and Structures. 1994;5(4):530-5.
[203] Birman V, Chandrashekhara K, Sain S. An approach to optimization of shape memory alloy hybrid composite plates subjected to low-velocity impact. Composites Part B: Engineering. 1996;27(5):439-46.
[204] Khalili SMR, Shokuhfar A, Malekzadeh K, Ashenai Ghasemi F. Low-velocity impact response of active thin-walled hybrid composite structures embedded with SMA wires. Thin-Walled Structures. 2007;45(9):799-808.
[205] Tsoi KA, Stalmans R, Schrooten J, Wevers M, Mai Y-W. Impact damage behaviour of shape memory alloy composites. Materials Science and Engineering: A. 2003;342(1–2):207-15.
[206] Gao X, Huang M, Brinson LC. A multivariant micromechanical model for SMAs Part 1. Crystallographic issues for single crystal model. International Journal of Plasticity. 2000;16(10–11):1345-69.
[207] Hane KF, Shield TW. Symmetry and microstructure in martensites. Philosophical Magazine A. 1998;78(6):1215-52.
[208] Nayan N, Buravalla V, Ramamurty U. Effect of mechanical cycling on the stress–strain response of a martensitic Nitinol shape memory alloy. Materials Science and Engineering: A. 2009;525(1–2):60-7.
[209] Corran RSJ, Shadbolt PJ, Ruiz C. Impact loading of plates — An experimental investigation. International Journal of Impact Engineering. 1983;1(1):3-22.
[210] Abrate S. Impact on Composite Structures: Cambridge University Press; 2005.
[211] Aymerich F, Meili S. Ultrasonic evaluation of matrix damage in impacted composite laminates. Composites Part B: Engineering. 2000;31(1):1-6.
[212] Diamanti K, Soutis C. Structural health monitoring techniques for aircraft composite structures. Progress in Aerospace Sciences. 2010;46(8):342-52.
[213] Mili F, Necib B. Impact behavior of cross-ply laminated composite plates under low velocities. Composite Structures. 2001;51(3):237-44.
[214] Kin-tak L, Hang-yin L, Li-min Z. Low velocity impact on shape memory alloy stitched composite plates. Smart Materials and Structures. 2004;13(2):364.
[215] Meo M, Marulo F, Guida M, Russo S. Shape Memory Alloy Hybrid Composites for Improved Impact Properties for Aeronautical Applications. Composite Structures. 2012.

[216] Seguin JL, Bendahan M, Isalgue A, Esteve-Cano V, Carchano H, Torra V. Low temperature crystallised Ti-rich NiTi shape memory alloy films for microactuators. Sensors and Actuators A: Physical. 1999;74(1–3):65-9.
[217] Cui D, Song G, Li H. Modeling of the electrical resistance of shape memory alloy wires. Smart Materials and Structures. 2010;19(5):055019.
[218] Hideki N, Ryutaro O. Shape memory alloys as strain sensors in composites. Smart Materials and Structures. 2006;15(2):493.
[219] Schilling PJ, Karedla BR, Tatiparthi AK, Verges MA, Herrington PD. X-ray computed microtomography of internal damage in fiber reinforced polymer matrix composites. Composites Science and Technology. 2005;65(14):2071-8.
[220] Hung Y. Shearography for non-destructive evaluation of composite structures. Optics and lasers in engineering. 1996;24(2):161-82.
[221] Pickering S, Almond D. Matched excitation energy comparison of the pulse and lock-in thermography NDE techniques. NDT & E International. 2008;41(7):501-9.
[222] Carslaw HS, Jaeger JC. Conduction of heat in solids: Clarendon Press; 1959.
[223] Meola C, Carlomagno GM. Recent advances in the use of infrared thermography. Measurement Science and Technology. 2004;15(9):R27.
[224] Maldague X, Galmiche F, Ziadi A. Advances in pulsed phase thermography. Infrared Physics and Technology. 2002;43(3):175-81.
[225] Sakagami T, Kubo S. Applications of pulse heating thermography and lock-in thermography to quantitative nondestructive evaluations. Infrared Physics & Technology. 2002;43(3–5):211-8.
[226] Weritz F, Arndt R, Röllig M, Maierhofer C, Wiggenhauser H. Intestigation of concrete structures with pulse phase thermography. Materials and Structures. 2005;38(9):843-9.
[227] Grammatikos S, Kordatos E, Barkoula N, Matikas T, Paipetis A. Innovative non-destructive evaluation and damage characterisation of composite aerostructures using thermography. Plastics, Rubber and Composites. 2011;40(6-7):6-7.
[228] Avdelidis NP, Hawtin BC, Almond DP. Transient thermography in the assessment of defects of aircraft composites. NDT & E International. 2003;36(6):433-9.
[229] Okafor AC, Chandrashekhara K, Jiang YP. Delamination prediction in composite beams with built-in piezoelectric devices using modal analysis and neural network. Smart Materials and Structures. 1996;5(3):338.
[230] Zhou G, Sim LM. Damage detection and assessment in fibre-reinforced composite structures with embedded fibre optic sensors-review. Smart Materials and Structures. 2002;11(6):925.
[231] Di C, Gangbing S, Hongnan L. Modeling of the electrical resistance of shape memory alloy wires. Smart Materials and Structures. 2010;19(5):055019.
[232] Zi-xue Q, Xing-tian Y, Jiang Y, Costas S. Experimental research on strain monitoring in composite plates using embedded SMA wires. Smart Materials and Structures. 2006;15(4):1047.
[233] Maldague X. Theory and practice of infrared technology for nondestructive testing. 2001.
[234] Lau S, Almond D, Patel P. Transient thermal wave techniques for the evaluation of surface coatings. Journal of Physics D: Applied Physics. 2000;24(3):428.
[235] Petrenko V, Deresh L. System and method for an electrical de-icing coating. Google Patents 2004.

[236] MILLER C. ELECTRICALLY CONDUCTIVE EXOTHERMIC COATINGS. WO Patent 2,001,022,434 2001.
[237] [cited; Available from: http://www.kellyaerospace.com/

Appendix I

List of Abbreviations and Acronyms:

Acronym	*Definition*	*Page*
CFRP	Carbon Fibres Reinforced Polymers	10
PLLA	Poly L lactic acid	25
SHM	Structural Health Monitoring	26
CNT	Carbon Nanotubes	28
NDT	Non-Destructive Testing	28
SWCNT	single walled carbon nanotubes	36
MWCNT	multi walled carbon nanotubes	36
CVD	Chemical Vapour Deposition	38
DWCNT	Dual walled carbon nanotubes	38
FESEM	Field emission scanning electron microscope	38
SEM	Scanning electron microscopy	39
VACNTs	Vertically Aligned Carbon Nanotubes	40
PET	Polyethylene terephthalate	44
NDE	Non Destructive Evaluation	46
MEMS	Micro-Electro-Mechanical Systems	46
PFC	Piezoelectric fibres composites	48
IDE	Interdigitated electrodes	48
MFCs	Macro-fibres reinforced composite actuators	49
AFCs	Active Fibres Composites	49
GFRP	Glass Fibres Reinforced Polymers	50
SMART	*Stanford Multi-Actuator-Receiver Transduction Layer*	51
PE	Polyethylene	52
EIT	electric impedance tomographical	52
PZO	polyethylene oxide	52
FBG	Fibre Bragg Grating	53
AE	acoustic emission	55
EFPI	Extrinsic Fabry-Perot interferometers	55
SMA	Shape Memory Alloys	56
DCPD	dicyclopentadiene	56
NG	Natural Graphite	63
EG	Expanded Graphite	63
GNP	graphene nanoplatelets	64
LDPE	Low-Density Polyethylene	64
TEM	transmission electron microscopy	65
XRD	X-ray diffraction	65
DSC	Differential Scanning Calorimetry	70
PVA	Poly vinyl alcohol	71
DMA	Dynamic Mechanical Analysis	71

MD	machine direction	77
TD	Transverse direction	77
VA-RFI	*Vacuum Assisted Resin Film Infusion*	87
SPI	Spray Pressured Impregnation	91
PTFE	Polytetrafluoroethylene	100
STF	Shear Thickening Fluids	128
PEG	PolyEthylene Glycol	132
FFT	Fast Fourier Transform	139
NiTi	Nickel Titanium	156
TM	twinned configuration	158
DTM	detwinned configuration	158
SIM	stress-induced martensite	158
PPS	Polyphenylene Sulfide	161
LVI	Low velocity impact	162
IT	Infrared thermography	175
SHT	step-heating thermography	175
LT	Lock-in thermography	175
PT	pulsed thermography	175